A Thesis Submitted for the Degree of PhD at the University of Warwick

Permanent WRAP URL:

http://wrap.warwick.ac.uk/108298

Copyright and reuse:

This thesis is made available online and is protected by original copyright.

Please scroll down to view the document itself.

Please refer to the repository record for this item for information to help you to cite it.

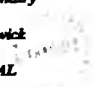Our policy information is available from the repository home page.

For more information, please contact the WRAP Team at: wrap@warwick.ac.uk

warwick.ac.uk/lib-publications

REDUCED STATE CONDUCTING POLYMERS

Vanessa Mary Eastwick-Field

A thesis submitted for

the degree of

Doctor of Philosophy

Department of Chemistry

University of Warwick

Coventry CV4 7AL

May 1991

To M and D

TABLE OF CONTENTS

LIST OF FIGURES

-vi-

LIST OF TABLES

ACKNOWLEDGEMENTS

DECLARATION

The work presented in this thesis was conducted by the author. Some of the results presented in chapter 8 were obtained in collaboration with Mr. M. Rabjons whilst under the supervision of the author. Where the work of other authors has been discussed this is clearly indicated.

This work was conducted in the chemistry departments at Warwick and Bristol Universities under the supervision of Dr. P. N. Bartlett and Dr. P. G. Pringle.

Signed *V. M. Edmunds Field*

SUMMARY

The work presented in this thesis is concerned with reduced state conducting polymers, and in particular with poly(pyridine).

The electroreductive polymerisation of 2,5-dibromopyridine based on either the $[Ni^{(0)}(PPh_3)_4]$ or $[Ni^{(0)}(bpy)_3(ClO_4)_2]$ systems was investigated. The results obtained via both routes are discussed in terms of their respective mechanisms. The initial steps of the polymerisation based on the latter system are analysed using a specially developed kinetic theory. Although the theory was designed specifically to better understand the mechanism of electrosynthesis of poly(pyridine), it has a broader usage for the electrochemist because it describes the limiting current responses of second order ECE reactions at RDEs.

The nature of poly(pyridine) prepared by both routes is investigated, and the results obtained are discussed in terms of their structural implications. Although the definitive nature of the polymers is still unclear, a particularly interesting possibility is that the polymers prepared from the $[Ni^{(0)}(bpy)_3(ClO_4)_2]/2,5-Br_2Py/TEAP/AN$ system are "pyridylonickel strings".

The electrosynthesis of poly(azines) using the $[Ni^{(0)}(bpy)_3(ClO_4)_2]$ route is reported, and demonstrates that this strategy can be successfully exploited in the preparation of novel reduced state conducting polymers.

Suggestions for further work forming an extension to this thesis are given in the final chapter.

CHAPTER 1

INTRODUCTION

In this introduction, we begin by briefly describing modified electrodes. In particular, organic conducting polymers, metal containing polymers and the conventional electropolymerisation of such electrode modifiers are discussed. We then describe the developments in organometallic chemistry which led to the reductive polymerisation of halogenated aryls. Finally the electroreduction of dihaloaromatics in the presence of nickel complexes is reviewed.

1.1 Modified electrodes

An electrode which has a thin film of material coated onto its surface is called a modified electrode. The most important feature of the film is that it prevents direct contact between the bulk electrolyte and the metal surface. Consequently, electron transfer between solution species and the electrode can only occur via mediation through the coat instead of by direct transfer to the metal's Fermi level. The nature of the coat confers new properties to the electrode, which depend upon its ability to mediate electron transfer, its mechanism of mediation and its interaction with solution species. The transport and kinetics of electrons and reactants at modified electrodes has been theoretically described by Savéant[1,2,3,4], Anson[5], Murray[6,7] and Albery[8,9]. Judicious choice of the coating material gives the electrochemist greater control over the selectivity and kinetics of electrochemical reactions.

The development of modified electrodes began in the early 1970's by Murray's group[10,11,12]. They covalently attached ligands to tin oxide electrodes via organosilane linkages. Intensive research into preparing and characterising the structure and nature of modified electrodes

followed Murray's first publication[10]. There are now many techniques used to fabricate modified electrodes. The four most common methods are:

1. Adsorption of the coat onto the electrode surface by either chemisorption or physiosorption.

2. Covalent bond formation between the electrode and the modifying material.

3. Plasma discharge, which causes deposition of the polymeric films onto an electrode surface by radical initiation of polymerisation.

4. Electrochemical deposition of the film onto the electrode surface.

There are advantages and disadvantages associated with each preparative method. For example, adsorption is very readily achieved, but often leads to uneven and poorly reproducible films. Conversely, plasma discharge produces consistently stable films, but requires the use of sophisticated equipment, and the resultant films are difficult to characterise. Probably the most satisfactory means of immobilising a film onto an electrode surface is by electrochemical deposition. This involves the coat being grown directly onto the electrode by either electrochemically induced precipitation of a preformed polymer or hydrolytically active monomer, or by electrochemical polymerisation of an electroactive monomer. In the latter method, the polymer-forming reaction and precipitation must occur more rapidly than the diffusion of the polymer away from the electrode into the bulk electrolyte. The rate at which the film is formed and the quantity of material in the film can often be controlled by varying the length of time and the potential at which the film-forming process is taking place. In this thesis, we are concerned with the electrochemical

polymerisation technique for preparing stable modified electrodes.

There are many electrode modifications reported in the literature. They range from simple monomer monolayers to highly complex multi-component polymeric multi-layers. A type of electrode coat which has been intensively studied is the conducting polymer. It is this type of modification, with particular reference to reduced state conduction and to metal-containing conducting polymers, that is discussed in the following sections.

1.2 Conducting polymers

Common materials at room temperature span a conductivity range of 10^{-14} σ^{-1} cm^{-1} to 10^6 σ^{-1} cm^{-1}. A good insulator, such as polyethylene, will lie at one extreme of the scale and a good conductor, such as copper, will lie at the other extreme. Organic polymeric materials are renowned for their inability to conduct electricity. It is commonly their insulating behaviour which accounts for most of the applications in the electronics and electrical industries. However, there is a growing number of organic polymers reported in the literature which do conduct electricity. Figure 1.1 illustrates the conductivity ranges of various materials.

The term "conducting polymer" is loosely applied to a wide range of materials which have many diverse properties. Conductivity may be an intrinsic property, as with poly(sulphur nitride)[13], $(SN)_x$, which was the first "non-metallic metal" and has a conductivity in the order of 10^3 σ^{-1} cm^{-1}. Alternatively, the addition of a conductive filler, such as carbon black, to an insulating polymer matrix produces modest conductivities of about 1 σ^{-1} cm^{-1}. A third type of conducting polymer displays marked increases in conductivity when exposed to oxidising, or reducing, agents. Accordingly, when an initially insulating material is progressively oxidized, or reduced, its conductivity changes from that of an insulator to that of a semiconductor, p- or n- type respectively, and on to that of a

Figure 1.1:

Conductivity ranges of various types of material.

$\log_{10}$ conductivity at 25°C

-20	-15	-10	-5	0	5	10

INSULATIVE   SEMI-CONDUCTIVE   METALLIC

polystyrene

$(SN)_x$

copper

polyethylene

additive conductor

CONDUCTING POLYMERS

poly(p-phenylene)*
poly(acetylene)*
poly(indole)*
poly(thiophene)*
poly(pyrrole)*
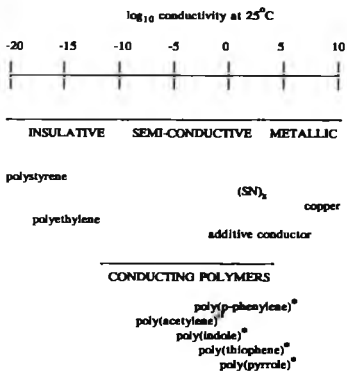
* when these polymers are in their oxidised states.

-4-

metal. The new conducting polymeric material retains overall neutrality by a process termed doping. The nature of the dopant is dependent on the method of oxidation or reduction. For example, if changes in the conductivity have been achieved using chemical oxidants or reductants, then the dopant is usually the corresponding reagent residue. However, electrochemically induced oxidation or reduction results in the appropriately charged electrolyte ion entering the new material as the dopant, as shown in the following equation:

Neutral insulating polymer ⟶ Ionic conducting polymer/counter ion composite

Conducting polymers of this type are all polyene polymers. The remaining discussion on conducting polymers will be confined to the latter type, but the reader's attention is drawn to references 14 to 19 for a more comprehensive survey of all conducting polymers.

1.2.1 Polyene conducting polymers

The chemical synthesis of polyene conducting polymers as amorphous insoluble powders was first reported many decades ago; for example, polyaniline[20], polypyrrole[21,22] and polyacetylene were reported in 1862, 1916 and 1955 respectively. However, it was not until 1968 when Dall ' Olio *et al.*[23] reported the electrochemical synthesis of polypyrrole, that widespread interest and concomitant understanding of these materials grew. Dall ' Olio *et al.* described the anodic oxidation of pyrrole which led to the precipitation of extended films that could be peeled off the electrode. Consequently, free standing, easily manageable, air stable films, which had electrical conductivities in the order of 10^2 Ω^{-1} cm^{-1}, were readily synthesized.

In this section, we describe the structure and conduction of polyene conducting polymers with particular reference to poly(pyridine).

1.2.1.1 Structural characterisation

Polyene conducting polymers can be divided into two structural types. These are linear polyenes and polyaromatic polyenes We are concerned with the latter which do not readily lend themselves to structural characterisation. They are usually non-crystalline, insoluble and decompose at high temperatures. Therefore much of our knowledge of the structure of these systems has had to be obtained from a variety of indirect measurements. Nevertheless, it is accepted that all polyaromatic conducting polymers consist of aromatic or heteroaromatic moieties. These units may be linked either directly, as in poly(1,4-phenylene), or via electron rich groups such as vinylene. A selection of polymers and their structures is given in figure 1.2.

The aromatic rings are linked together so that the oxidized or reduced polymer can configure an extensive conjugated π system along the polymer backbone between localised charges. For example, the conducting polymer poly(1,4-phenylene) is able to maintain an extensive conjugated π system on oxidation, whereas the insulating 1,3-coupled polymer cannot. This is schematically represented in figure 1.3.

The structure of conducting polymers is not as homogeneous as implied by figure 1.2. The fine detail still remains an area of dispute. The evidence resulting in the uncertainty about the definitive structures of these polymers has been extensively reviewed; in particular the reader's attention is drawn to references 24 to 27. Compared to many conducting polymers, the structural characterisation of poly(pyridine) is in its infancy. We believe that there are inconsistencies between our results presented in chapters 5 and 7 and those reported by other research groups. It is therefore pertinent to review the evidence reported in the literature.

Poly(pyridine) has been synthesised in two different ways. The first approach adopted by Yamamoto and co-workers[26-28] involved

Figure 1.2:

Selected polyene conducting polymers.
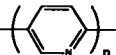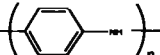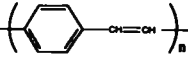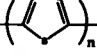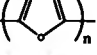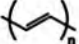
Name	Structure

Poly(phenylene)

Poly(pyridine)

Poly(analine)

Poly(phenylene vinylene)

Poly(pyrrole)

Poly(thiophene)

Poly(furan)

Poly(acetylene)

Figure 1.3:

Comparison of the ability of *para-* and *meta-* poly(phenylene) to configure
an extensive π conjugated system on oxidation.

Poly(1,4-phenylene)
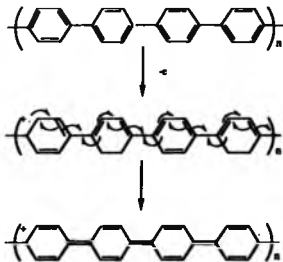
Poly(1,3-phenylene)
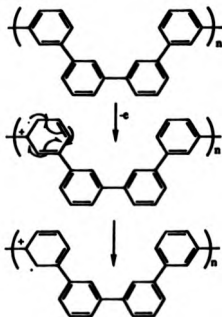
dehalogenation polycondensation of 2,5-dibromopyridine. The polymerisation required either catalytic quantities of nickel(II) in the presence of magnesium[26] or stoichiometric quantities of nickel(0)[27,28]. The purification of the polymers included techniques to ensure removal of any nickel. The natures of the resultant polymers were marginally dependent on the method of synthesis. However, on the whole they were orange/brown in colour, displayed high thermal stability, were soluble in formic and inorganic acids, had molecular weights in the region of 1.2×10^3 to 1.9×10^3 D, displayed $\pi-\pi^*$ electronic transitions (λ_{max} 370 nm formic acid, 380 nm KBr disc) and analysed reasonably well for the $-(C_5NH_3)-$ moiety although they showed some bromine was present. These results indicate that the polymer produced was 16-25 pyridyl units in length with bromine in the terminal position, figure 1.4.

Yamamoto also investigated the degree of depolarisation caused by light scattering[27] and the fluorescence properties of acidic solutions of the polymer[29]. The value of depolarisation was 0.33 and the solution showed a strong green fluorescence which suggests that the polymer had a rod-like structure with an extensive conjugated π system and mobile electrons along the polymer chain. No direct experimental evidence of the ability of the polymer to conduct electricity was reported.

The second approach to the synthesis of poly(pyridine), adopted by Schiavon *et al.*[30,31] involved nickel catalysed {[Ni(0)(PPh₃)₄][30] or [Ni(0)(bpy)₂][31]} electroreductive polymerisation of 2,5- and 2,6-dibromopyridine in acetonitrile solutions containing excess ligand and tetraalkylammonium perchlorate salt. The resultant polymers were precipitated onto the surface of the working electrode. They were investigated electrochemically as well as by the more usual characterisation techniques.

Electropolymerisation of 2,5-Br₂Py led to polymer modified

Figure 1.4:

Structure of poly(pyridine) proposed by Yamamoto *et al.*[27].
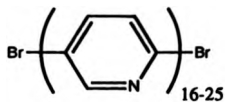
Figure 1.5:

Structure of untreated poly(pyridine) coordinated to $[Ni^{(II)}(L_n)(ClO_4)_{2n}]$ proposed by Schiavon *et al.*[30,31].
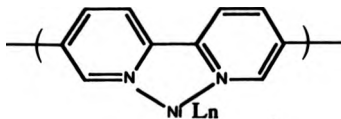
$Ln = (bpy)_2$ or $(PPh_3)_4$

electrodes whose cyclic voltammetric profiles were reported to show reversible cycles in the negative region whose peak height varied linearly with scan rate and involved a high capacitative current. These observations led Schiavon *et al.* to conclude that the electrode deposits were reduced state conducting polymers.

Removal of the electrode deposit yielded an orange solid which was insoluble in organic solvents, but soluble in concentrated hydrochloric acid. Schiavon *et al.* did not report the polymer's solubility in other acids, but it is probable that any reagent capable of protonating the ring nitrogen will allow dissolution. The IR spectra of the deposit (KBr disc) showed strong bands at 820 cm^{-1} indicative of a 1,4-disubstitution. Additional signals attributed to perchlorate ions and the nickel ligands were also present. UV-visible spectra revealed λ_{max} at 360nm assigned to π-π^* transition from an aromatic moiety with an extensive π conjugated system. Although a full elemental analysis of these deposits was not reported, atomic adsorption, mass spectra and relative IR absorbances of pyridyl/ligand led Schiavon *et al.* to conclude that the deposits were poly(2,5-pyridine) containing ligand (PPh_3 or bpy) complexes of nickel(II) perchlorate coordinated to the polymer. The authors suggested structures of the type shown in figure 1.5.

The extraction of nickel, perchlorate and PPh_3 or bpy was facilitated by treating the polymer deposit with EDTA buffered to pH 9.2 and washing with water and ethanol. The treated polymer was an orange/yellow solid which displayed IR and UV-visible spectra consistent with conjugated pyridyl rings. The signals attributed to ligand and perchlorate were absent in the EDTA treated polymer. Elemental analysis (C, H and N) showed reasonable agreement with the theoretical values for nickel-free poly(2,5-pyridine). Mass spectra recorded on the treated pyrolysed polymer gave signals corresponding to fragments containing 3 to 6 pyridyl moieties. Schiavon *et al.* concluded that the

-11-

pentamer was the dominant polymer length. The suggested chain length is inconsistent with the observation that the polymer has an extensive π conjugated system. It is more likely that pyrolysis of the polymer had caused chain fragmentation.

The electrochemical polymerisation of 2,6-Br_2Py undertaken by Schiavon et al.[30] was based on the $[Ni^{(0)}(PPh_3)_4]/PPh_3/TEAP$ system. The voltammetric response of the growth solution was typical of that displayed by the 2,5-Br_2Py system for the first cycle. Subsequent cycles showed a progressive decrease in charge consumed typical of an insulating film-forming process. The electrode was covered with a thin pale yellow coat. The response of these coated electrodes in background electrolyte was irreversible and led Schiavon et al. to conclude that they were electroinactive. The mass spectra reported for the pyrolysed films showed fragments containing 9 pyridyl moieties. The IR spectra showed a weak bond at 790 cm⁻¹ typical of meta-disubstituted pyridine, and the UV visible spectra displayed an absorption band with λ_{max} at 310 nm. The lower wavenumber compared to the para-disubstituted polymer is consistent with the lack of conjugation. A comparison between the 2,5- and 2,6- disubstituted pyridine provided confirmation that the meta natureof the monomer precludes the formation of a conducting polymer. This is due to the inability of the meta-polymer to configure an extensive π conjugated system on oxidation or reduction.

Table 1.1 summarises the reported characterisation results for poly(pyridine)

Table 1.1:

Summary of structural characterisation of purified nickel-free poly(pyridine) reported by Schiavon *et al.*[30,31] and Yamamoto *et al.*[26-28]

	PREPARATION				
	Chemical polymerisation		Electrochemical Polymerisation		
Transition Metal Catalyst	$NiCl_2(bpy)_2$, $NiBr_2(PPh_3)_2$ or $NiCl_2$ with Mg	$Ni^{(0)}L_n$ where L is cod, PPh_3	$Ni(PPh_3)_4$	$Ni(PPh_3)_4$	$Ni(bpy)_3(ClO_4)_2$
Monomer	$2,5\text{-}X_2Py$	$2,5\text{-}Br_2Py$	$2,5\text{-}Br_2Py$	$2,6\text{-}Br_2Py$	$2,5\text{-}Br_2Py$
Colour	brown orange	yellowish brown	orange yellow	pale yellow	orange
Solubility	acidic water	HCl and formic acid	conc HCl	—	conc HCl
UV, λ_{max}	—	370nm	360nm	310nm	360nm
IR	—	—	$825 cm^{-1}$	$790 cm^{-1}$	$820 cm^{-1}$
Molecular weight	—	$(1.2\text{-}1.9) \times 10^3$	—	—	—
% C	—	76.0	74.8	—	76.2
mass H	—	03.9	04.0	—	—
N	—	16.9	16.8	—	17.9
Br	—	00.6	—	—	—
Proposed Structure					

$$\{\bigcirc\}_n \quad \{\bigcirc\}_{n} \quad \{\bigcirc\}_n \quad \bigcirc\}_n \quad \{\bigcirc\text{-}\bigcirc\}_n$$

1.2.1.2 Conduction

It was predicted more than fifty years ago that extensive polyenes would have unusual electrical properties. Huckel proposed his π electron theory for unsaturated systems in 1931. Subsequently it was proposed that if the conjugated carbon-carbon bond lengths were equal, then the π-molecular orbitals would form a continuous band which would be half filled[34]. A π-electronic bond structure of this nature is akin to the bonding associated with metals, figure 1.6. In 1977 Shirakawa et al.[32] polymerised acetylene, and experimental observations began to confirm the theoretical predictions. The polymer displayed undoped conductivity in the range 10^{-8} to 10^{-5} Ω^{-1} cm^{-1}, which lies in the semiconductor regime. However, doping polyacetylene by oxidation or reduction increased the conductivity to metallic levels[33].

The charge carriers of polyene conducting polymers depend on whether the polymer has been oxidized or reduced and the degree of oxidation or reduction. Poly(acetylene) will be used to exemplify all the proposed carrier types.

At room temperature poly(acetylene) has a spin density corresponding to about 1 electron per 3000 carbons. The unpaired electron is believed to be located in the middle of the band gap between the bonding and anti-bonding levels. Thus the electron can be considered as a delocalised radical which is termed a neutral soliton.

The electrons most readily removed by oxidation will be those associated with the soliton. The next most readily removed will be those at the top of the π bonding level. Removal of the soliton electron creates a delocalised cation or positive soliton, whereas removal of a π bonding electron creates a delocalised radical cation or positive polaron. The removal of two electrons from the π bonding level may result in either the formation of two independent positive polarons or, if the spins of the two

-14-

Figure 1.6:

π-Electronic band structure for conjugated carbon-carbon bond systems.

| $-C=C-C=C-$ | Peierls Distortion | $=C=C=C=C=$ |

single and double
bond alternating

bond equality

INSULATIVE   SEMI-CONDUCTIVE   METALLIC
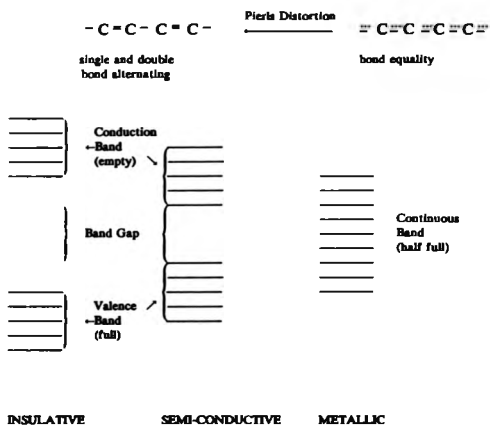
electrons combine, a delocalised dication or positive bipolaron. The bipolaron charges are fixed with respect to one another, for example in poly(pyrrole) they extend over approximately 4 rings. The formation of a bipolaron rather than a second polaron is confirmed by theoretical calculations and experimental observation. Most convincing are the quantitative energy considerations and the loss of ESR signals as the oxidation level of some polymers is increased[34,35]. The analogous negative species are found on reduction.

The removal or addition of electron(s) from a neutral polyene and the incorporation of counterions causes the polymer lattice to distort. The distortion involves the switching of the position of the carbon-carbon double and single bonds. Although this is an energetic transformation, it is compensated for by the lower ionisation energy of the distorted polymer. Figure 1.7 shows the nature and formation of the various charge carriers found in poly(acetylene).

Charge carriers are mobile under the influence of an electric field and thereby allow the polyene to conduct electricity. However, conductivity is a bulk phenomenon; the charge carriers must not be considered in isolation. Instead they should be thought of as being in close association with one another as well as with the charge balancing counter ions. There is also evidence that mobility exists between the polymer chains as well as along them.

Soliton species are only observed in systems which have symmetry equivalent to *trans-transoid* poly(acetylene) i.e. with two or more degenerate ground states. Cationic polaron species can be found in all types of conducting aromatic or heteroaromatic polymers which have non-degenerate ground states. For example, only positive polarons and bipolarons are observed in poly(pyrrole) and poly(thiophene). Interestingly, negative charge carriers have been much less studied than

Figure 1.7:

Charge carriers in conjugated polymers, illustrated for poly(acetylene).
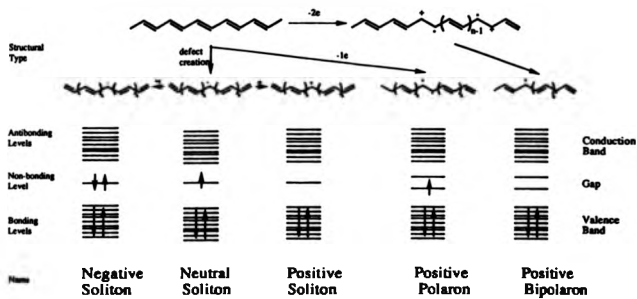
their positively charged equivalents. This is because, out of an estimated few thousand conducting polymers reported in the literature, only a few conduct in their reduced state. These include poly(acetylene)[36], poly(thiophene)[37,38], poly(naphthylene)[39], poly(furan)[40] and poly(pyridine)[26-31]. Poly(acetylene) has been extensively studied; negative soliton, polarons and bipolarons have all been cited as charge carriers. Poly(thiophene), poly(naphthylene) and poly(furan)[41,42], better known for conduction in their oxidized states[41-44], suffer from being unstable in their reduced forms. Consequently, only qualitative studies of the reduced forms have been reported. Poly(pyridine) is a stable reduced state conducting polymer. However, research has primarily been concerned with its preparation and structural characterisation. Therefore the type of charge carrier for reduced state polyaromatic conducting polymers is assumed to be the negative equivalent of the cationic species. In this thesis, we describe some characteristics of poly(pyridine) and report the synthesis of some novel reduced state conducting polymers, though investigations into their charge carrier type were limited.

The ability of poly(pyridine) to coordinate nickel is an unusual feature. Although there are many examples in the literature of metal-chelating-pendant groups attached covalently to a conducting polymer, the direct coordination of a metal to the conducting backbone has been reported only in the literature for poly(pyridine)[30,31]. The introduction of metals is reported to increase its ability to conduct electricity[43]. This is explained in terms of (1) an improved intermonomer orbital overlap resulting from the more diffuse metal d-orbitals and (2) an extension of the intermonomer conduction path by conjugation of the d-orbitals with the π electron system of the polymer.

In chapter 8 we report the synthesis of a novel conducting polymer also capable of coordinating metal ions directly to its π conjugated bonding system.

-18-

1.3 Electrodeposition of polyaromatic conducting polymers

A wide range of organic conducting polymers can be electrochemically deposited onto electrode surfaces. The polymer deposits are usually produced by the electrooxidation of the appropriate monomer in an electrolyte solution. The electrodepositions of poly(pyrroles)[24,44-50], poly(thiophenes)[51-55], poly(furans)[41,42], poly(indoles)[56-58], poly(anilines)[59-62] and poly(phenylenes)[63,64] are all achieved in this way.

Electrooxidative deposition is not universally successful. For example, electron deficient aromatic monomers tend to be difficult to oxidise. Consequently, pyridines, pyrimidines, pyrazines, pyrimidazine and pthalazines are all resistant to controlled electrooxidative polymerisation[65]. It is reasonable to propose that direct electroreduction of such monomers may facilitate polymer formation and electrode deposition. However, experimental evidence[66-68] shows that the reduced monomer species react with the solvent or electrolyte ions instead of forming carbon-carbon bonds leading to dimers, trimers and ultimately polymers.

Another approach to carbon-carbon bond formation widely reported in the literature involves the use of transition metal complexes[69-96]. One such type of reaction is the condensation of organic halides in the presence of either reducing agents and nickel compounds or nickel compounds alone. Nickel-catalysed electroreduction of dihaloaromatics, ArX_2, leads to the formation of polyaromatic polymers. Consequently this reaction pathway affords a new approach to preparing conducting polymers.

The work presented in this thesis is centred on nickel-catalysed electroreduction of aryl halides. Investigations into the reaction pathways and the resultant electrode deposits are reported in chapters 5, 7 and 8.

It is therefore relevant to review the current literature concerning aryl coupling in the presence of nickel compounds.

Semmelhack et al.[78] were the first to demonstrate the usefulness of nickel(0) in this respect. They described the reductive dimerisation of aromatic and vinylic halides catalysed by nickel(0)bis 1,5-cyclooctadiene, [Ni$^{(0)}$(cod)$_2$], according to scheme 1:

$$[Ni^{(0)}(cod)_2] \ + \ 2Ar\text{-}X \ \xrightarrow[40^\circ C]{DMF} \ Ar\text{-}Ar \ + \ Ni^{(II)}X_2 \ + \ 2cod$$
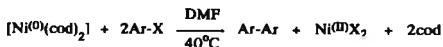
Scheme 1

During the 18 years succeeding Semmelhack's first publication, a broad mechanistic scheme for this type of reaction has not emerged. Indeed, the overall picture appears more complex with almost every publication. However, it is generally agreed that the first step of the coupling reaction is oxidative addition of the aryl halide to low valent nickel(0) species. The subsequent steps are still unclear. We will briefly describe oxidative addition and then review biaryl and polyaryl formation.

1.3.1 Oxidative addition reactions

Oxidative addition is a generic term used to designate, without mechanistic implication, a ubiquitous class of reactions in which the oxidation of a metal complex by an electrophile is accompanied by the concomitant increase in its coordination number. Applied to haloaryl complexes, ArX, oxidative addition converts a metal complex such as a divalent d^{10} complex (ML$_2$) to a d^8 organometal adduct:

$$ML_2(d^{10}) \ + \ ArX \ \longrightarrow \ M(Ar)(X)L_2(d^8)$$

Two types of mechanism have been proposed for this process, involving either concerted 2-charge equivalent transformations such as

3-centre addition and S_N2 displacements or multistep successions of 1-charge equivalent transformations involving paramagnetic intermediates.

1.3.2 Biaryl formation

The fate of the organonickel(II) adduct, $[ArNi^{(II)}XL_2]$ appears to be governed by a number of criteria. These include reaction temperature[79-81], solvent polarity[78,79,82,83], ligand type[84], presence or absence of excess ligand[81,82,84,85], presence or absence of excess alkyl or aryl halide[81,83,86-88] and the nature of aryl and halide moieties[78,83,89]. A further complication arises from the common usage of excess reductant (usually Zn or cathodic current) to promote the biaryl formation[90,91] and/or to generate the nickel(0) species[83,87-89,92,93] necessary for the initial oxidative addition step. Not surprisingly, with all these potential variables, many different reaction pathways have been postulated. The more plausible ones include:

1. A second oxidative addition of aryl halide followed by reductive elimination of biaryl, Ar-Ar, from a diaryl nickel(IV) species as shown in scheme 2:

$$Ar-\underset{\underset{L}{|}}{\overset{\overset{L}{|}}{Ni^{(II)}}}-X \ + \ ArX \longrightarrow [Ar-\underset{\underset{X}{|}}{\overset{\overset{Ar}{|}}{Ni^{(IV)}}}-X]^{2+} + 2L$$

$$[Ar-\underset{\underset{X}{|}}{\overset{\overset{Ar}{|}}{Ni^{(IV)}}}-X]^{2+} \longrightarrow Ar-Ar + [Ni^{(II)}X_2]$$
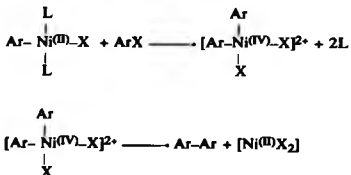
<p align="center">Scheme 2</p>

This reaction pathway was favoured by Semmelhack et al.[78]. It is

consistent with mechanisms proposed for other metal promoted couplings of organic halides[94], but has had little support in the more recent literature.

2. Reductive coupling of two aryl moieties in a diaryl nickel(II) species, $[Ni^{(II)}(Ar)_2L_2]$[81,82,84,88,89,93,95]. $[Ni^{(II)}L_2(Ar)_2]$ is formed by ligand exchange between two organonickel(II) halide adducts. This pathway generates nickel(0) species capable of further oxidative addition reactions shown in scheme 3:

$$2Ar-\overset{\overset{\displaystyle L}{|}}{\underset{\underset{\displaystyle L}{|}}{Ni^{(II)}}}-X \longrightarrow Ar-\overset{\overset{\displaystyle Ar}{|}}{\underset{\underset{\displaystyle L}{|}}{Ni^{(II)}}}-L + [Ni^{(II)}X_2L_2]$$

$$Ar-\overset{\overset{\displaystyle Ar}{|}}{\underset{\underset{\displaystyle L}{|}}{Ni^{(II)}}}-L \xrightarrow[\text{by RX or oxidation}]{\text{spontaneous or induced}} Ar-Ar + [Ni^{(0)}L_2]$$

$$[Ni^{(0)}L_2] + ArX \longrightarrow Ar-\overset{\overset{\displaystyle L}{|}}{\underset{\underset{\displaystyle L}{|}}{Ni^{(II)}}}-X \quad \text{etc}$$
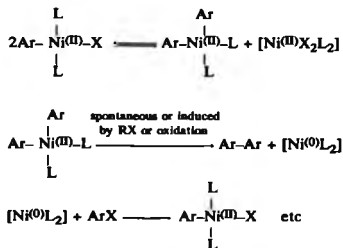
Scheme 3

The stability and lability of the organonickel(II) adduct is an important consideration in determining the intermediate steps of Ar_2 formation. The scheme requires the adduct to be unstable with respect to the diaryl- and dihalo- nickel(II) complexes under the appropriate reaction conditions. Therefore, ligand exchange can be militated against if the oxidative addition adduct is readily isolated and stable at the appropriate temperature and in the appropriate solvent. Unfortunately, many of the biaryl syntheses are all-in-one-pot reactions which masks this piece of mechanistic information. Nevertheless there is ample evidence for such ligand

-22-

exchange reactions. In particular, Nakamura and Otsuka[81] reported that the thermal decomposition (toluene, 80°C, 1hr) of equimolar mixtures of *trans*-chloro-bis(triphenylphosphine)phenyl nickel(II), [Ni(II)Cl(Ph)(PPh₃)₂] and *trans*-chloro-bis(triphenyl-phosphine)tolyl nickel(II), [Ni(II)Cl(MePh)(PPh₃)₂], yielded mixed biaryl products predicted by ligand exchange. The work by Meyer, Rollin and Perichon[88,89] on electroreductive heterocoupling of different substituted ArX (acetonitrile, 25°C) in the presence of 2'2-dipyridyl nickel(II) dibromide, [Ni(II)(Br)₂bpy], and bpy also supports a ligand exchange step.

The stability and configuration of the [Ni(II)L₂(Ar)₂] complex is also of key importance in this reaction scheme. Theoretical studies indicate that a *cis* arrangement is required for a concerted reductive elimination[96]. However, we are unaware of a [Ni(II)L₂(Ar)₂] species which has been characterised during Ar-Ar synthesis. This suggests these complexes are either difficult to handle or undergo spontaneous reductive elimination. There is evidence to suggest that they display one or other of these characteristics. Meyer, Rollin and Perichon[88] reported that spontaneous reductive elimination is favoured by [Ni(II)bpy(Ar)₂] complexes resulting from reactions between [Ni(0)(bpy)₂] and iodo-, bromo- and chloro-benzene, chloro-2-methyl benzene, chloromethyl benzene, 2-chlorothiophene or 2-chloroquinoline. These reactions are all reported to have greater than 75% Ar-Ar yields and regenerate the appropriate quantity of Ni(0) species.

The mechanism of spontaneous reductive elimination is unknown. However, several authors[84,88] have demonstrated that the addition of a reductive compound (e.g. EtI, EtBr, PhBr) to the reductive mixture enhances the rate of Ar-Ar formation. Consequently we postulate that any free ArX interacts with

-23-

$[Ni^{(II)}(Ar)_2]$ complex thereby stimulating the reductive elimination rather that simple first order thermal decomposition.

Some $[Ni^{(II)}(Ar)_2]$ complexes (where the aryl is alkylphenyl ether) are reported to be stable to spontaneous reductive elimination under oxygen free conditions[89]. The attempted electroreductive coupling of haloalkylphenyl ethers using $[Ni^{(II)}(Br)_2bpy]$ showed that (1) the potentiostatic charge fell to zero after the equivalent of 4 moles of electrons per mole of Ni(II) had been consumed, (2) no Ar-Ar had been produced and (3) a new reversible redox couple appeared at -1.5 V (SCE). These observations are consistent with the overall reaction:

$$2ArX + [Ni^{(II)}(Br)_2bpy] + 4e \longrightarrow [Ni^{(II)}(Ar)_2bpy] + 2X- + 2Br-$$

where the new redox couple is:

$$[Ni^{(II)}(Ar)_2bpy] + e \longrightarrow [Ni^{(I)}(Ar)_2bpy]^-$$

Quantitative yields of Ar-Ar and Ni(II) were obtained by either a positive potential excursion (0.2 V vs SCE) or exposure to oxygen. There is an obvious inconsistency between scheme 3 and these results. A maximum consumption of 4 electrons per nickel(II) does not account for the certain reduction of $[Ni^{(II)}X_2]^{2+}$ formed during the ligand exchange step. Exhaustive electrolysis of this type should theoretically consume 6 electrons per nickel(II): Smith and Kuo[95] reported similar observations for an equivalent set-up using $[Ni^{(II)}(phen)_3]^{2+}$ and alkylhalides but proposed the following overall

reaction:

$$[Ni^{(II)}(phen)_3]^{2+} + 2RBr + 4e \longrightarrow [Ni^{(0)}(R)_2(phen)_2] + 2Br^- + phen$$

$$[Ni^{(0)}(R)_2(phen)_2] + phen \longrightarrow [Ni^{(II)}(phen)_3]^{2+} + 2R^.$$
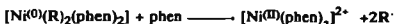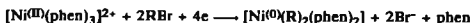
The credibility of this scheme is dubious as the formation of a neutral $[Ni^{(0)}(R)_2phen]$ complex is unlikely.

The formation of Ni(II) and the absence of polymeric material resulting from the anodically induced decomposition of $[Ni^{(II)}(Ar)_2bpy]$ is in direct contrast to the deposition of $[Ni^{(II)}(Ar')(Ar)(PEt_3)_2]$ reported by Alemark and Akemark[82]. They observed a one-electron oxidation followed by a fast irreversible chemical reaction producing Ar-Ar' and polymeric material. The proposed reaction pathway involves an equilibrium between the *cis*- and *trans*- phosphine complexes. The former undergoes oxidation to yield Ar-Ar', whereas oxidation of the latter produces aryl radicals causing polymer formation, scheme 4:

Scheme 4

-25-
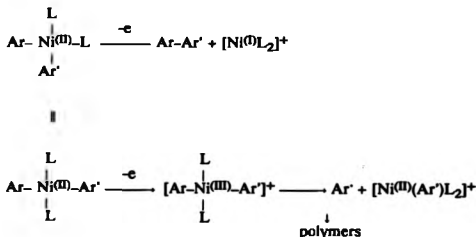
The difference between the two systems can be rationalised by considering the influence of the "innocent" ligands, PEt$_3$ and bpy. The bidentate ligand prevents an equilibrium between *cis* and *trans* biaryl nickel(II) isomers thereby barring the route to polymer formation for [Ni$^{(II)}$(Ar')(Ar)bpy]. The common oxidation states of nickel are zero, one , two and three. In the nickel phosphine complexes all these oxidation states are readily attainable electrochemically. However, only zero, two and three are common for nickel bpy complexes. Therefore 1 and 2 electron oxidations can be rationalised for the phosphine and bpy complexes respectively.

3. Simple homolysis followed by dimerisation of the aryl radicals, scheme 5:

$$Ar- \overset{\displaystyle L}{\underset{\displaystyle L}{\overset{|}{\underset{|}{Ni^{(III)}}}}}-X \longrightarrow Ar^\cdot + [Ni^{(I)}XL_2]$$

$$2Ar^\cdot \longrightarrow Ar-Ar$$
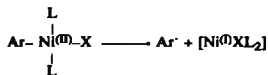
Scheme 5

Although this scheme was favoured in the early years of nickel catalysed haloaryl coupling, it has now lost support.

4. Intermolecular electron transfer between the organonickel(II) adduct and excess ArX evokes a mechanism involving aryl nickel(I) and (III) intermediates. An example of such a pathway is given in scheme 6:

$$\text{Ar–}\underset{\underset{\text{L}}{|}}{\overset{\overset{\text{L}}{|}}{\text{Ni(II)}}}\text{–X + ArX} \longrightarrow [\text{Ar–}\underset{\underset{\text{L}}{|}}{\overset{\overset{\text{L}}{|}}{\text{Ni(III)}}}\text{–X}]^+ + \text{ArX}^-$$

$$[\text{Ar–}\underset{\underset{\text{L}}{|}}{\overset{\overset{\text{L}}{|}}{\text{Ni(III)}}}\text{–X}]^+ + \text{Ar–}\underset{\underset{\text{L}}{|}}{\overset{\overset{\text{L}}{|}}{\text{Ni(II)}}}\text{–X} \longrightarrow [\text{Ar–}\underset{\underset{\text{Ar}}{|}}{\overset{\overset{\text{L}}{|}}{\text{Ni(III)}}}\text{–L}]^+ + [\text{Ni(II)(X)}_2]$$

$$\text{Ar–}\underset{\underset{\text{Ar}}{|}}{\overset{\overset{\text{L}}{|}}{\text{Ni(III)}}}\text{–L} \longrightarrow \text{Ar}_2 + [\text{Ni(I)L}_2]^+$$

$$[\text{Ni(I)L}_2]^+ + \text{ArX} \longrightarrow \text{Ar–}\underset{\underset{\text{L}}{|}}{\overset{\overset{\text{L}}{|}}{\text{Ni(III)}}}\text{–X} \quad \text{etc}$$
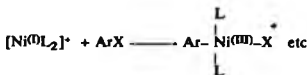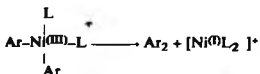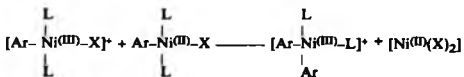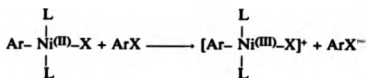
Scheme 6

Tsuo and Kochi[79] observed that *trans*-o-tolylbromo bis(triethlyphosphine) nickel(II) did not thermally decompose in toluene heated to 70°C for 20hrs. However, in the presence of tolylbromide, decomposition produced quantitative yields of bltolyl. Similar results have been reported for phenyl, chlorophenyl, anisyl, tolyl bromides and iodides. Identification of Ni(I) and (III) intermediates was not definitive, but scheme 6 satisfies many of their observations.

5. Reduction of organonickel(II) adducts evokes mechanisms involving arylnickel(I) and (0) intermediates of the type proposed in scheme 7:

$$
\begin{array}{c}
\text{L} \\
| \\
\text{Ar–Ni}^{(II)}\text{\_X} \\
| \\
\text{L}
\end{array}
$$

$$\downarrow \quad + \text{L, + e, - X}^-$$

$$
\begin{array}{c}
\text{L} \\
| \\
\text{Ar–Ni}^{(I)}\text{\_L} \\
| \\
\text{L}
\end{array}
$$

$$+ \text{L, + e} \quad \nearrow \qquad \searrow \quad + [\text{Ni}^{(I)}\text{ArL}_3] + \text{L}_2$$

$$+ [\text{Ni}^{(II)}\text{XArL}_2] \quad \nearrow \qquad \downarrow$$

$$\nearrow \qquad \downarrow$$

$$\downarrow \qquad \text{Ar}_2 + 2[\text{Ni}^{(0)}\text{L}_4]$$

$$\downarrow$$

$$[\text{Ni}^{(0)}\text{L}_4] + \text{Ar}_2 + \text{X}^-$$
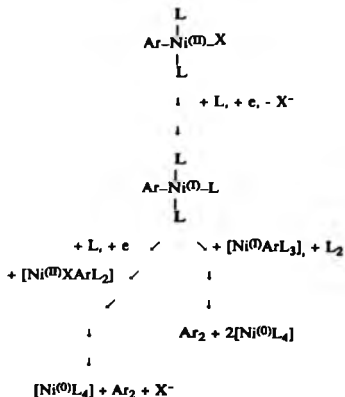
Scheme 7

Chemical synthesis of Ar-Ar using excess reductant has yielded little mechanistic information to either support or oppose scheme 7. This is because quantitative results on the consumption of reductant have either been inconclusive or not reported in the literature. Conversely, electrochemical studies have afforded a clean and easy way to determine the number of electrons involved in biaryl formation. Once again, the so called innocent ligand appears crucial in determining this number. Adducts containing phosphines undergo one- and two- electron reductions, whereas those containing bidentate ligands favour a two-electron reduction as described earlier.

Schiavon *et al.*[90,91] based their studies on electroreductive formation of Ar-Ar from electrolyte solutions containing TEAP, $[\text{Ni}^{(II)}(\text{ClO}_4)_2]$, PPh$_3$ and bromobenzene in the molar ratio 50:1:5:0 to 20

respectively. In the absence of bromobenzene, cyclic voltammetry shows Ni(II) is directly reduced in a two-electron irreversible process producing $[Ni^{(0)}(PPh_3)_4]$, ($E_{pc} = 1.3$ V, Ag/Ag^+ 0.1 mol dm^{-3}, AN). This species is oxidized in two successive one-electron processes[97]:

$$[Ni^{(0)}(PPh_3)_4] \xrightarrow{-e} [Ni^{(I)}(PPh_3)_4]^+ \qquad E_{pa} = -1.1V$$

$$[Ni^{(I)}(PPh_3)_4]^+ \xrightarrow[-2PPh_3]{-e} [Ni^{(II)}(PPh_3)_4(AN)]^{2+} \qquad E_{pa} = 0V$$
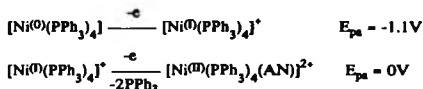
Stepwise addition of bromobenzene leaves the nickel(II) reduction peak unaltered while the associated anodic peaks concomitantly decrease and eventually disappear indicating the following oxidative addition reaction. Extension of the cathodic cycle reveals two new distorted reduction peaks. Traversing one or both of these, results in the restoration of the original anodic peaks in all instances except with a large excess of bromobenzene. Biphenyl and $[Ni^{(0)}(PPh_3)_4]$ formation is only associated with the two new reduction peaks as a result of the decomposition of the reduced species. The decomposition product $[Ni^{(0)}(PPh_3)_4]$ undergoes further oxidative addition with the remaining PhBr in accordance with scheme 7. Typical CV's and their assignments are given in figure 1.8. Similar results have been reported for other organohalides and preformed $trans$-$[Ni^{(II)}Br(Ph)(PPh_3)_2]$ in the presence of excess PPh_3.

The literature on biaryl formation involving nickel complexes presents a complicated and seemingly inconsistent picture. However, the following generalisations can be made:

1. The "innocent" ligand is central in determining the reaction pathway. Phosphine (PPh_3 or PEt_3) or a bidentate ligand (bpy or phen) have been employed almost exclusively.

Figure 1.8:

Cyclic voltammetric curves on Pt microelectrode in electrolyte containing
$[Ni^{(II)}(ClO_4)_2]$ (3 mmol dm^{-3}) (—), as above after the addition of BrPh
(300 mmol dm^{-3}) (— – —). Potentials with respect to Ag/Ag$^+$ (0.1 mol
dm^{-3}, AN). Scan rate 100 mV s^{-1}.
Reproduced from references 87 and 88.

Peak Assignment:

peak 1: $[Ni^{(II)}(PPh_3)_4(AN)]^{2+} \xrightarrow[2PPh_3]{2e} [Ni^{(0)}(PPh_3)_4]$

peak 2: $[Ni^{(II)}Br(Ph)(PPh_3)_2] \xrightarrow[PPh_3]{e} [Ni^{(I)}(Ph)(PPh_3)_3] + Br^-$

peak 3: $[Ni^{(I)}(Ph)(PPh_3)] \xrightarrow{e} [Ni^{(0)}(Ph)(PPh_3)]^-$

peak 4: $[Ni^{(0)}(PPh_3)_4] \xrightarrow{-e} [Ni^{(I)}(PPh_3)_4]^+$

peak 5: $[Ni^{(I)}(PPh_3)_4]^+ \xrightarrow{-e} [Ni^{(II)}(PPh_3)_2(AN)]^{2+}$
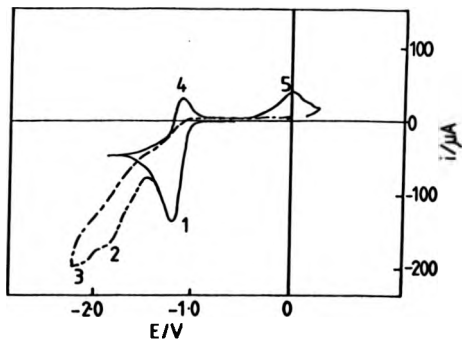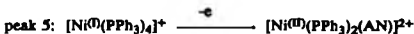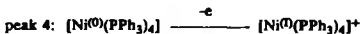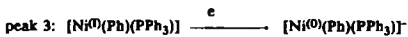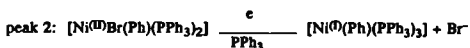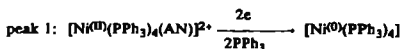
2. Organonickel(II) phosphine halide adducts are stable and readily isolated. They tend not to undergo either ligand exchange reactions or intermolecular electron transfer other than at elevated temperatures. At room temperature biaryl and nickel(0) species are the decomposition products of the adduct following one- and two-electron reductions.

3. Organonickel(II) bpy halide adducts are only produced *in situ* and undergo rapid ligand exchange yielding dihalo- and diaryl- nickel(II) species. The latter species decompose, either spontaneously or by anodic inducement, to yield biaryl and nickel(0) species. There are discrepancies between the observed and theoretical charges consumed during these electrosyntheses.

4. Excess reducing agent allows biaryl formation to become catalytic in all cases except when the diarylnickel(II)bpy species is stable to reductive decomposition.

5. Excess aryl halide tends to enhance the rate of biaryl formation, and in some cases is essential.

6. Polar solvents produce more satisfactory results than non-polar solvents.

The use of dihaloaryls, X-Ar-X, obviously increases the complexity of these reaction schemes. Oxidative addition can occur at either carbon-halogen bond, and the coupling reaction may produce a dihalodiaryl, X-Ar-Ar-X, capable of re-entering the reaction pathway leading to polyaryl formation.

1.3.3 Polyaryl formation

Polymerisation of diaryls under mild reaction conditions, (THF, 60°C, 4 to 15 hrs), was first reported by Yamamoto *et al.*[26] in 1978. They described the nickel-catalysed coupling reaction of the Grignard reagent of dibromoaryls according to the equation below:

$$X-Ar-X + Mg \xrightarrow{\text{Ni(II) catalyst}} X-(Ar)_{\text{n}}-X + nMgX_2$$

This approach was shown to be applicable to a wide variety of monomers and nickel(II) complexes. Subsequently they modified this approach to exclude Mg and used stoichiometric quantities of Ni(0) complexes[27]. Poly(pyridine) was prepared by both methods and has already been described in section 1.2.1.1.

Following Yamamoto *et al.'s* first publication, the interest in this area has been on nickel-catalysed electroreductive polymerisation of dihaloaromatics[30,31,37-39,89,98-102]. Table 1.2 lists the polyaryls prepared in this way and summaries their respective reaction conditions.

A survey of the literature shows that:

1. The most widely employed nickel catalysts were [Ni(II)Cl₂(dppe)], [Ni(II)(bpy)₃(ClO₄)₂] and [Ni(II)(ClO₄)₂] in the presence of at least 4 equivalents of PPh₃.

2. The dihaloaryls were almost exclusively the brominated species.

3. *In situ* generation of the oxidative addition adduct was commonly employed, but where the adduct was isolated and identified (elemental analysis), subsequent electropolymerisation yielded essentially the same results.

4. The use of GC or Pt working electrodes led to the

Table 1.2:

Summary of the reaction conditions for the preparation of polyarenes by nickel-catalysed reductive polymerisation of dihaloarenes
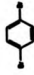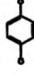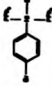
Polymer	Monomer	Nickel Complex	Solvent	Electrolyte	Working Electrode	Technique	Ref
poly(1,4-phenylene)		NiCl₂(dbbpy) or NiCl₂(dppe)	THF/HMPT	LiClO₄ or LiClO₄/MgBr	Hg pool	Electrolysis at -2.5 V	98,99
		NiCl₂(dppe)	THF/HMPT	LiClO₄/MgBr	Hg pool	Electrolysis at -2.5 V	99
		NiCl₂(dppe)	THF/HMPT	LiClO₄/MgBr	Hg pool	Electrolysis at -2.5 V	99
			AN	TBAP	Pt or GC	Electrolysis at -2.3 V	100

Table 1.2 continued
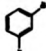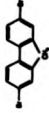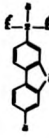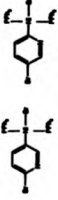
Polymer	Monomer	Nickel Complex	Solvent	Electrolyte	Working Electrode	Technique	Ref
poly(1,3-phenylene)	[structure]	NiCl₂(dppe)	THF/HMPT	LiClO₄/AgBr	Hg pool	Electrolysis at -2.5 V°	99
poly(2,7-fluorene)	[structure]	NiCl₂(dppe)	THF/HMPT	LiClO₄/AgBr	Hg pool	Electrolysis at -2.5 V°	99
	[structure]		AN	TBAP and ex PPh₃	Pt or GC	Repetitive CV 0 V to -2.85 V°, electrolysis at -1.8 V°	101
poly(2,5-pyridine)	[structure]	NiCl₂(dppe)	THF/HMPT	LiClO₄/AgBr	Hg pool	Electrolysis at -2.5 V°	99
	[structure]		AN	TBAP and ex PPh₃	Pt or GC	Repetitive CV 0 V to -1.8 V°-2.4 V°, electrolysis at -1.5 V°	30

Table 1.2 continued
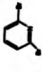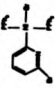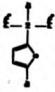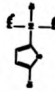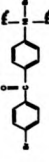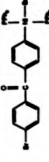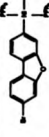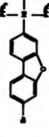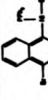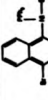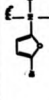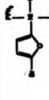
Polymer	Monomer	Nickel Complex	Solvent	Electrolyte	Working Electrode	Technique	Ref
poly(2,5-pyridine) cont.		Ni(bpy)$_3$(ClO$_4$)$_2$	AN	TEAP	GC	Repetitive CV 0 V to -2.3 V*, electrolysis at -1.7 V*	31
poly(2,6-pyridine)		NiCl$_2$(dppe)	THF/BMPT	LiClO$_4$/MgBr	Hg pool	Electrolysis at -2.5 V*	99
			AN	TBAP and or PPh$_3$	Pt or GC	Electrolysis at -1.5 V*	30
poly(2,5-thiophene)			AN	TBAP and or PPh$_3$	Micro GC or sheath	Electrolysis at -2.0 V*	37
			AN	TBAP	Pt, GC, GaAs or InP	Repetitive CV 0 V to -2.3 V*,2.2 V* Galvanostatically	38

Table 1.2 continued

Polymer	Monomer	Nickel Complex	Solvent	Electrolyte	Working Electrode	Technique	Ref
poly(4,4'-benzophenone)			AN	TBAP	GC	Electrolysis at -1.8 Va	102
poly(2,7-fluorenone)			AN	TBAP	GC	Electrolysis at -1.8 Va	102
poly(2,6-naphthylene)			AN	TBAP and ex PPh$_3$	GC	Electrolysis at -1.6 Va	39
poly(2,5-furan)			AN	TBAP	GC	Electrolysis at -2.0 Va	40

diphos = [(C$_6$H$_5$)$_2$P·CH$_2$]$_2$, dppe = 1,2-bis(diphenylphosphino)ethane, THF = tetrahydrofuran, HMPT = hexamethylphosphoric triamide, AN = acetonitrile, TBAP = tetrabutylammonium perchlorate, TEAP = tetraethylammonium perchlorate.
a Against Ag/Ag⁺ (AgClO$_4$, 0.1 mol dm⁻³, AN), b Against SCE, c monomer generated in situ by reductive electrolysis at -1.3V of Ni(ClO$_4$)$_2$ in the presence of 4 equivalents of PPh$_3$, followed by addition of 1 equivalent of dibromoarene and d monomer generated in situ by reductive electrolysis of [NiCl$_2$(PPh$_3$)$_2$] in the presence of large excess PPh$_3$, followed by addition of 1 equivalent of dibromoaryl.

precipitation of the polymer onto the electrode surface. The properties of the modified electrodes were unique to the polymer type. Table 1.3 summarises their electrochemical responses in background electrolyte.

5. Electroreductive polymerisation of dibromoaryls is a complementary technique to the more conventional electrooxidative polymerisation. It can produce some of the more common conducting polymers such as poly(thiophene) and poly(phenylene), but more interestingly it extends the range of conducting polymers to include those comprising electron deficient aromatic moieties. For example, it has been successfully used to electrodeposit poly(pyridine), poly(benzophenone) and poly(fluorene) which are unobtainable by anodic electrodeposition.

Our primary interest lies in reduced state conducting polymers with the potential ability to chelate transition metals. Poly(pyridine) is the only polymer reported in the literature which satisfies these two interests. In order to extend the number of such polymers we need to understand the characteristics of the monomer unit which allows reduced state conduction and chelation. A better insight into the electroreductive polymerisation mechanism is also fundamental to understanding this new class of materials.

There are two electrochemical routes to poly(pyridine)[30,31,99]. The first is based on nickel phosphine (PPh$_3$ or dppe)[30,99] and the second on nickel bpy[31]. The discussion on biaryl formation already suggests that these two routes will go via different mechanistic pathways. Indeed, Schiavon *et al.*[30] have proposed that the [Ni$^{(0)}$(PPh$_3$)$_4$] undergoes oxidative addition at the 2- and 5- pyridyl position to yield stable adducts, figure 1.9. A further two-electron reduction per adduct caused electrodeposition of poly(pyridine) according to the following equation but

Table 1.3:

Summary of the properties of electrodes modified by electroreductive polymerisation of dibromoarenes

Polymer	Solvent	Electrolyte	Cyclic voltammetric response	Comment	Ref
poly(1,4-phenylene)	AN	TBAP	Sharp reversible redox couples at -2.6 V[a] and 1.05 V[a]	Repetitive cycling leads to dissolution $i_p \propto$ Scan rate E_p° and ΔE_p independent of scan rate	99
poly(2,5-pyridine)	AN	TEAP	Sharp reversible redox couple centred at -2.15 V[b]	Reasonable stability towards repetitive cycling $i_p \propto$ Scan rate ΔE_p increases with every ten-fold increase in scan rate	30
	AN	TEAP	Sharp reversible redox couple centred at -2.30 V[b]		31

Table 1.3 continued

Polymer	Solvent	Electrolyte	Cyclic voltammetric response	Comment	Ref
poly(2,6-pyridine)	AN	TEAP	Irreversible cathodic couple centred at -2.6 V[a]	Cathodic excursion causes electroneutrality	30
poly(2,5-thiophene)	AN	TBAP	Reversible broad wave at 0.63 V[a] Irreversible wave at 1.5 V[a] Reversible wave at -2.14 V[a]	Anodic responses typical of a deposit produced by oxidative coupling of thiophene Cathodic wave unstable	37
poly(4,4'-benzo-phenone)	AN	TBAP	Reversible redox couple at -1.95 V[a] Irreversible cathodic peak at -2.60 V[a]	$i_p \propto$ scan rate for first cathodic excursion $E_{pa} - E_{pc} = 50$ mV Second cathodic peak causes electroneutrality	102
poly(2,7-fluorenone)	AN	TBAP	Reversible redox couples at -1.65 V[a] and -2.35 V[a] Irreversible peak at 1.7 V[a]	$i_p \propto$ scan rate $E_{pa} - E_{pc} = 100$ mV Anodic excursion causes electroneutrality	102

-39-

Table 1.3 continued

Polymer	Solvent	Electrolyte	Cyclic voltammetric response	Comment	Ref
poly(2,6-naph-thylene)	AN	TBAP	Reversible redox couples at -2.5 vs and 0.95 vs	Unstable to repetitive cycling	39
poly(2,7-fluorene)	AN	TBAP	Partially reversible reduction at -2.7 vs with associated oxidation waves at -2.5 and -1.1 V. Sharp reversible redox couple centred at 0.77 V	Unstable to repetitive cathodic cycling. ½ α scan rate. Large peak separation	101
poly(2,5-furan)	AN	TEAP	Partially reversible redox couple at -1.9 vs	Unstable to repetitive cycling	40

AN – acetonitrile, TBAP – tetrabutylammonium perchlorate, TEAP – tetraethylammonium perchlorate.
a Against Ag/Ag⁺ (AgClO₄, 0.1 mol dm⁻³, AN).
b Against SSCE

Figure 1.9:

Structure of intermediates produced during the electropolymerisation of 2,5-Br$_2$Py in the presence of [Ni$^{(0)}$(PPh$_3$)$_4$] proposed by Schiavon *et al.*[30].
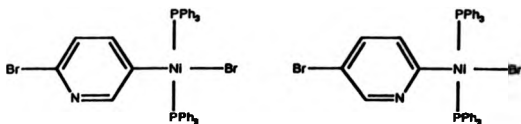
no further mechanistic information was reported.

$$[Ni^{(II)}(Br)(PyBr)(PPh_3)_2]+2e- \longrightarrow \frac{1}{n} -(Py)- + [Ni^{(0)}(PPh_3)_4] + 2Br-$$
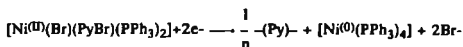
A low yield of polymer, whose stability was not always consistent, led Schiavon *et al.* and ourselves to investigate the electropolymerisation using $[Ni^{(II)}(bpy)_3(ClO_4)_2]$. Schiavon *et al.*[31] proposed a reaction pathway involving the formation of the adduct, $[Ni^{(II)}Br(PyBr)(bpy)]$. They proposed that the adduct had two simultaneous fates. The first was slow ligand exchange forming dipyridyl- and dibromo- nickel(II) species. The dipyridyl complexes subsequently underwent a two-electron reduction producing a polymer unit and regenerating $[Ni^{(0)}(bpy)_2]$. The overall reaction scheme and associated cyclic voltammetry is given in figure 1.10.

Schiavon *et al.* were unable to isolate and characterise the adduct by reacting 2,5-dibromopyridine with electrochemically prepared $[Ni^{(0)}(bpy)_2]$ because the polymer and Ni(II) complexes were directly obtained. From this observation, the authors inferred that $[Ni^{(0)}(bpy)_2]$ was able to reduce the organometallic adduct formed initially. However, their reaction mechanism takes no account of this. The cathodically induced elimination of Br-Py-Py-Br from $[Ni^{(II)}(PyBr)_2(bpy)]$ is inconsistent with the observation reported by Meyer *et al.*[88,89] for homocoupling of ArX species, (section 1.3.2).

In chapters 5 and 7 we describe our investigation into the electroreductive polymerisation of 2,5-dibromopyridine. Although a complete mechanistic stategy has not been derived, a promising kinetic model for the initial polymerisation steps for the $[Ni^{(II)}(bpy)_3(ClO_4)_2]/2,5-Br_2Py/TEAP$ system is proposed.

Figure 1.10:

First cyclic voltammetry recorded with a GC electrode in an AN solution containing TEAP (0.1 mol dm^{-3}). [Ni$^{(II)}$(bpy)$_3$(ClO$_4$)$_2$] (5 mmol dm^{-3}) and 2,5-Br$_2$Py (5 mmol dm^{-3}). Potentials with respect to Ag/Ag$^+$ (0.1 mol dm^{-3}, AN). Scan rate 100 mV s^{-1}.

Reproduced from reference 31.

$$[Ni^{(II)}(bpy)_3]^{2+}$$

↓ 2e, - bpy PEAK 1

$$[Ni^{(0)}(bpy)_2]$$

↓ 2,5-Br$_2$Py, - bpy

$$[Ni^{(II)}Br(PyBr)(bpy)]$$

bpy ⌒2e, bpy PEAK 1

[Ni$^{(II)}$(bpy)$_3$(Br)$_2$] + [Ni$^{(II)}$(PyBr)(bpy)]   [Ni$^{(0)}$(bpy)$_2$]+ 2Br$^-$ + –(Py)–

2e, bpy ↓ PEAK 2

$$[Ni^{(0)}(bpy)_2] + -(Py)- + Br^-$$
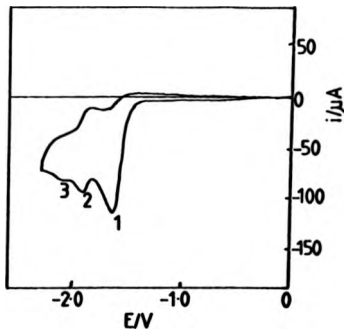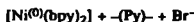
PEAK 3: Polymer reduction

-43-

1.4 Summary of the work presented in this thesis

In the next chapter all the organometallic syntheses and electrochemical and analytical techniques used during the course of this work are described.

In chapter 3, the products of the organometallic syntheses are presented and discussed.

In chapter 4, the electrochemistry of the starting materials is reported. Emphasis is placed on the results which contradict the current literature.

In chapter 5, the electrochemistry of the phosphine-containing organometallic adducts and their electrode deposits are reported. On the whole, these results are descibed qualitatively due to the problems encountered with reproducibility.

In chapter 6, a working theory is presented for an ECE reaction pathway at a RDE which accounts for the concentration polarisation of both reactants. This model is used in chapter 7 to explain the electroreductive polymerisation of 2,5-dibromopyridine in the presence of $[Ni^{(II)}(bpy)_3(ClO_4)_2]$. In this chapter we also present and discuss some of the properties of the resultant electrode deposits.

In the last chapter on the experimental work, the electrochemical synthesis and behaviour of novel reduced state conducting polymers are presented.

Finally in chapter 9, the work which could be undertaken as an extension to this thesis is outlined.

CHAPTER TWO

EXPERIMENTAL

The materials, apparatus, instrumentation and procedures used for the experimental work for this thesis are described in this chapter. The first section deals with the syntheses of the twenty organometallic complexes that have been investigated and with the instrumentation used to characterise them. Next the electrochemical reagents are described and in the final section the electrochemical apparatus and associated techniques are presented.

2.1 Organometallic syntheses and characterising instrumentation

In this section we begin with the source and quality of the solvents and starting materials. Next an outline of the procedures adopted for the synthesis of the organometallic complexes (I) to (XVIII) is given. The remaining section deals with the instrumentation.

2.1.1 Solvents and starting materials

All the solvents were reagent grade quality which were further purified by distillation over calcium hydride (acetonitrile, dichloromethane) or sodium benzophenone (benzene, toluene, diethylether, ethanol) under a nitrogen atmosphere. 2,5-dibromopyridine (2,5-Br$_2$Py), 2,5-dichloropyridine (2,5-Cl$_2$Py), 2-bromopyridine (2-BrPy), 3-bromopyridine (3-BrPy), 2,5-dibromothiophene (2,5-Br$_2$T), triphenylphosphine (PPh$_3$), 2,2-dipyridyl (bpy), were all obtained from Aldrich and used as received. 3,6-dibromopyridazine[105], 1,4-dibromophthalazine[105,106] and 2,3,5-tribromopyrazine[107,108] were all prepared by published procedures. Bis(1,5-cyclooctadiene)nickel(0), [Ni$^{(0)}$(cod)$_2$][109], tetrakis(triphenylphosphine) palladium(0),

$[Pd^{(0)}(PPh_3)_4]^{(110)}$, tetrakis(triphenylphosphine) platinum(0), $[Pt^{(0)}(PPh_3)_4]^{(111)}$, tetrakis(triethylphosphine) nickel(0), $[Ni(PEt_3)_4]^{(112)}$, tetrakis(triethylphosphine) palladium(0), $[Pd^{(0)}(PEt_3)_4]^{(113)}$, tetrakis(triethylphosphine) platinum(0), $[Pt^{(0)}(PEt_3)_4]^{(113)}$, and bis(2'2-dipyridyl) nickel(0), $[Ni^{(0)}(bpy)_2]^{(114)}$, were all prepared by literature methods. All remaining metal complexes were obtained from Johnson Matthey and used without further purification.

2.1.2 Organometallic syntheses

A number of the synthetic procedures are very similar, therefore where appropriate we have grouped together some of the complexes and described the synthesis of a typical member of that group.

2.1.2.1 Preparation of *trans*-(*P,N*)-bis[bromo(μ-5-bromopyridine-*C²,N*) (triphenylphosphine) nickel(II)], [I]

$[Ni^{(0)}(cod)_2]$ (1.02g, 3.71 mmol) in AN (80 cm³) was added to a stirred solution of PPh_3 (9.91g, 37.1 mmol) in AN (80 cm³). Immediately an orange solution and red precipitate formed. $2,5$-Br_2Py (0.95g, 4.01 mmol) in AN (5 cm³) was slowly added to the mixture which was then stirred for 3 h. The crude solid was filtered off then redissolved in CH_2Cl_2 (40 cm³). The resulting solution was filtered and then reduced to *ca.* 7 cm³. A dark orange solid was precipitated by dropwise addition of MeOH. The solid was filtered off, washed with Et_2O (40 cm³) and dried in vacuo over P_2O_5. The original filtrate was reduced to a minimum volume and more crude product was obtained by dropwise addition of MeOH. This solid was then recrystyallized as before to give a combined yield of 21%.

Elemental analysis calculated for $C_{46}H_{36}Br_4N_2P_4Ni_2$: C, 49.52; H, 3.25; N, 2.51; Br, 28.65; found: C, 49.32; H, 2.51; N, 2.58; Br, 25.54.

Crystals potentially suitable for X-ray diffraction were obtained from a slow evaporation of a saturated acetonitrile solution, which gave dark orange tablets. All bond lengths and angles and atomic co-ordinates are in appendix 3.1.

2.1.2.2 Preparation of *trans-(P,N)*-bis[bromo(μ-5-bromopyridine-*C²,N*)(triphenylphosphine) palladium(II)], [II], and *trans-(P,N)*-bis[chloro(μ-5-chloropyridine-*C²,N*)(triphenylphosphine) palladium(II)], [III]

These two complexes were synthesised using the same procedure. Complex (II) was prepared by treating a suspension of $[Pd^{(0)}(PPh_3)_4]$ (1.745g, 1.5 mmol) in toluene (25 cm^3) with 2,5-Br$_2$Py (0.511g, 2.11 mmol). The mixture was heated to reflux (95°C) for 4 h. The solid $[Pd^{(0)}(PPh_3)_4]$ dissolved and a cream coloured product began to precipitate within 30 min. After filtration, CH$_2$Cl$_2$ (15 cm^3) was added to the solid product to give a dark suspension which was then treated with fluorosil (0.5g). After filtration, MeOH (10 cm^3) was added to the clear yellow solution and the CH$_2$Cl$_2$ evaporated off until crystals formed. The crystals were filtered off and dried in vacuo over P$_2$O$_5$. The original filtrate was taken to dryness under reduced pressure to yield a yellow solid. The solid was dissolved in a minimum volume of CH$_2$Cl$_2$ (10 cm^3) and precipitated by the dropwise addition of Et$_2$O (20 cm^3). This solid was worked up as described above to give a combined yield of 64%. The yield for (III) was 71%.

Elemental analysis calculated for $C_{46}H_{36}Br_4N_2P_4Pd_2$: C, 45.62; H, 3.00; N, 2.31; Br, 26.39; found for (II): C, 45.33; H, 3.04; N, 2.12; Br, 24.34.

2.1.2.3 Preparation of *trans*-[bromo(5-bromopyridine-C^2,) bis(triphenylphosphine) platinum (II)], [IV], *trans*-[chloro(5-chloropyridine-C^2,) bis(triphenylphosphine) platinum (II)], [V]

These two complexes were synthesised using the same procedure. Complex (VI) was prepared by treating a suspension of $[Pt^{(0)}(PPh_3)_4]$ (0.800g, 0.643 mmol) in benzene (20 cm^3) with 2,5-Br$_2$Py (0.165g 0.695 mmol). The mixture was heated to reflux (110°C) for 24 h to give a yellow solution and a cream coloured precipitate. After filtration, the solid product was redissolved in a mixture of C_6H_6/CH_2Cl_2 (1:1 v/v) (7 cm^3), treated with activated charcoal and then filtered. Et$_2$O/n-hexane (3:1 v/v) (4 cm^3) was added to the clear pale yellow solution causing the product to precipitate. After filtration, the product was washed with Et$_2$O (2 x 5 cm^3) and dried in vacuo over P$_2$O$_5$. The original filtrate was evaporated to minimum volume under reduced pressure. Addition of Et$_2$O/n-hexane (3:1 v/v) (4 cm^3) caused precipitation of the crude product which was purified by recrystallisation from CH$_2$Cl$_2$/Et$_2$O to give a combined yield of 34%. The yield for (V) was 61%.

Elemental analysis calculated for $C_{41}H_{33}Br_2NP_2Pt$: C, 51.48; H, 3.48; N, 1.46; Br, 16.71; found (IV): C, 51.37; H, 3.58; N, 1.32; Br, 15.83.

Crystals of (IV) potentially suitable for X-ray diffraction were obtained from a slow evaporation of a saturated acetonitrile solution, which gave clear well formed blocks. All bond lengths and angles and atomic co-ordinates are in appendix 3.1.

2.1.2.4. Preparation of *trans*-[bromo(5-bromopyridine-C^2,) bis(triethylphosphine) nickel(II)], [VI], *trans*-[bromo(pyridine-C^3,) bis(triethylphosphine) nickel(II)], (VII) and *trans*-[bromo(5-bromothiophene-C^2,) bis(triethylphosphine) nickel(II)], [VIII]

These three nickel compounds were synthesised using the same procedure. Complex (VI) was prepared by treating a suspension of [Ni(0)(cod)$_2$] (0.413g, 1.5mmol) in pentane (4 cm^3) with PEt$_3$ (1.02 cm^3, 7 mmol). The [Ni(cod)$_2$] dissolved and a red solution and solid formed. 2,5-Br$_2$Py (0.355g, 1.5 mmol) was added to the mixture and stirred for 4 h to give a yellow precipitate and orange solution. The solution was filtered and the residue was washed with pentane (4 x 5 cm^3) and dried under reduced pressure for 8 h.

The yields for complexes (VI), (VII) and (VIII) were 65%, 55% and 62% respectively.

Elemental analysis calculated for $C_{17}H_{33}Br_2NP_2Ni$: C, 38.39; H, 6.25; N, 2.63; Br, 30.05; found for (VI): C, 38.35; H, 6.71; N, 2.64; Br, 30.48: Elemental analysis calculated for $C_{17}H_{34}BrNP_2Ni$: C, 45.07; H, 7.56; N, 3.09; Br, 17.64; found for (VII): C, 44.71; H, 7.64; N, 3.00; Br, 18.01: Elemental analysis calculated for $C_{16}H_{32}SP_2Ni$: C, 35.79; H, 6.01; Br, 29.76; found for (VIII): C, 36.06; H, 6.47; ; Br, 28.99.

2.1.2.5 Preparation of *trans*-[bromo(5-bromopyridine-C^2,) bis(triethylphosphine) palladium(II)], [IX], *trans*-[bromo(pyridine-C^2,) bis(triethylphosphine) palladium(II)], (X), *trans*-[bromo(pyridine-C^3,) bis(triethylphosphine) palladium(II)], (XI) and *trans*-[bromo(5-bromothiophene-C^2,) bis(triethylphosphine) palladium(II)], [XII]

These four palladium compounds were synthesised using the same procedure. Complex (IX) was prepared by adding [Pd(0)(PEt$_3$)$_4$] (0.475g, 0.820 mmol) in pentane (3 cm^3) to 2,5-Br$_2$Py (0.200 g, 0.844 mmol).

The mixture was stirred and the 2,5-Br$_2$Py dissolved and the solution changed colour from yellow to colourless. The solution was stirred vigoruosly for 5 min and a white solid precipitated. The solid was filtered off, washed with pentane (2 x 5 cm^3) and dried under reduced pressure for 2 h.

Elemental analysis calculated for C$_{17}$H$_{33}$Br$_2$NP$_2$Pd: C, 35.23; H, 5.74; N, 2.41; Br, 27.57; found for (IX): C, 38.35; H, 6.71; N, 2.64; Br, 30.48: Elemental analysis calculated for C$_{17}$H$_{34}$BrNP$_2$Pd: C, 40.78; H, 6.87; N, 2.80; Br, 15.96; found for (X): C, 40.82; H, 7.37; N, 2.81; Br, 16.65: found for (XI): C, 39.36; H, 7.41; N, 2.81; Br, 15.81: Elemental analysis calculated for C$_{16}$H$_{32}$SP$_2$Pd: C, 32.86; H, 5.52; Br, 27.33; found for (XII): C, 32.88; H, 6.03; Br, 26.55.

2.1.2.6 Preparation of *trans*-[bromo(5-bromopyridine-C^2,) bis(triethylphosphine) platinum(II)], [XIII]

A solution [Pt$^{(0)}$(PEt$_3$)$_4$] (0.113 g, 1.69 10^{-4} mol) in toluene (5 cm^3) was cooled to -78°C over a CO$_2$/acetone bath and treated with 2,5-Br$_2$Py (0.080 g, 3.38 x 10^{-4} mol). The reaction mixture was stirred for 3 h during which time it changed colour from pale yellow to orange. After warming to room temperature, the mixture was concentrated to a small volume and diluted with hexane to yield the crude product. The off white solid was filtered off, washed with toluene (5 cm^3) and dried under vacuo over P$_2$O$_5$ to give a yield of 35%.

Elemental analysis calculated for C$_{17}$H$_{33}$Br$_2$NP$_2$Pt: C, 30.55; H, 4.98; N, 2.10; found for (XIII): C, 30.56; H, 4.96; N, 2.01.

2.1.2.7 Preparation of _trans_-[bromo(pyridine-C^2,) bis(triethylphosphine) platinum(II)], [XIV],

A stirred solution of [$Pt^{(0)}(PEt_3)_4$] (0.253 g, 3.79 x 10^{-4} mol) in pentane (3 cm^3) was treated with 2-BrPy (0.036 cm^3, 3.79 x 10^{-4} mol) at -78°C. The reaction mixture was allowed to warm to room temperature and was stirred for a further 4 h. No colour change was observed and a ^{31}P-[^1H] n.m.r. of an aliquot of the reaction mixture suggested that some [$Pt^{(0)}(PEt_3)_4$] remained unreacted. Consequently excess 2-BrPy was added to the solution. After being stirred overnight the orange solution had changed to colourless. The solution was evaporated to a small volume under reduced pressure at 50°C and diluted with pentane. Precipitation of an off-white solid was achieved by vigorous stirring. The solid was filtered off, washed with pentane (2 cm^3) and dried under reduced pressure to give a yield of 42%.

Elemental analysis calculated for $C_{17}H_{33}Br_2NP_2Pt$: C, 34.64; H, 5.81; N, 2.38; Br; 13.56: found for (XIV): C, 34.76; H, 5.75; N, 2.31; Br; 14.01:

2.1.2.8 Preparation of _trans_-[bromo(pyridine-C^3,) bis(triethylphosphine) platinum(II)], [XV]

A stirred solution of [$Pt^{(0)}(PEt_3)_4$] (0.097 g, 1.45 10^{-4} mol) in pentane (2 cm^3) was treated with 3-BrPy (0.028 cm^3, 2.90 10^{-4} mol) at -78°C. The reaction mixture was allowed to warm to room temperature and was stirred overnight. The mixture was evaporated to dryness and the sticky off-white residue was redissolved in Et_2O (2 cm^3). Precipitation of the product was achieved by diluting with pentane (3 cm^3) followed by vigorous stirring. The precipitate was filtered off, washed with pentane (2 cm^3) and dried under reduced pressure. The yield was 46%.

Elemental analysis calculated for $C_{17}H_{33}Br_2NP_2Pt$: C, 34.64; H, 5.81; N, 2.38; Br; 13.56: found for (XV): C, 33.99; H, 5.80; N, 2.43; Br; 14.11.

2.1.2.9 Preparation of cis-[bromo(5-bromopyridine-C^2-)(2,2'-dipyridyl) nickel (II)], [XVI], cis-[bromo(pyridine-C^2-)(2,2'-dipyridyl) nickel (II)], [XVII], cis-[bromo(pyridine-C^3-)(2,2'-dipyridyl) nickel (II)], [XVIII]

These three nickel complexes were synthesised using the same procedure. Complex (XVI) was prepared by treating a stirred suspension of $[Ni^{(0)}(cod)_2]$ (1.160g, 4.22 mmol) in toluene (25 cm³) at 0°C with excess bpy (1.977g, 12.66 mmol). Immediately a dark purple solution formed which was stirred for 30 min. 2,5-Br_2Py (1.0g, 4.22 mmol) in toluene (10 cm³) was added to the reaction mixture which was allowed to warm to room temperature and stirred for a further 6 h. A dark brown solid was formed which was filtered off. The crude product was dissolved in a minimum volume of ethanol (25 cm³) and precipitated by dropwise addition of Et_2O (10 cm³). The solid was filtered off, washed with Et_2O (5 x 4 cm³) and dried in vacuo over P_2O_5.

The yields for complexes (XVI), (XVII) and (XVIII) were 78%, 56% and 35% respectively.

Elemental analysis calculated for $C_{15}H_{11}Br_2N_3Ni$: C, 39.93; H, 2.45; N, 9.30; Br, 35.37; found for (XVI): C, 43.15; H, 3.33 N, 9.50; Br, 31.00: Elemental analysis calculated for $C_{15}H_{12}BrN_3Ni$: C, 48.32; H, 3.25; N, 11.27; Br, 21.43; found for (XVII): C, 44.67; H, 3.76; N, 9.95; Br, 19.94: found for (XVII): C, 47.96; H, 3.78; N, 10.98; Br, 20.98.

2.1.3 Instrumentation

^1H n.m.r. spectra were obtained at either 100.62 MHz using a Bruker WH400 Fourier Transform spectrometer or 220 MHz using a Perkin-Elmer (Model R34) continuous wave spectrometer. The chemical shifts are quoted in ppm from TMS as the internal reference unless otherwise stated. $^{31}P-\{^1H\}$ n.m.r. spectra were obtained using a Bruker WH400 Fourier Transform spectrometer operating at 162 MHz. The chemical shifts are quoted in ppm from external 85% H_3PO_4.

Infrared spectra were recorded with a Perkin-Elmer (Model 580B) infrared spectrometer, or with a Perkin-Elmer (Model 1720X) Fourier Transform spectrometer, using either nujol mull thin films on NaCl plates or KBr discs.

Electronic spectra were recorded on either a Shimadzu (Model 365) spectrophotometer or a Philips (Model PU 8720 UV/VIS) scanning spectrophotometer in 1 cm^3 path length quartz cells.

Mass spectra were recorded using a Kratos (MS80) instrument fitted with a fast atom bombardment (F.A.B.) attachment. Mass spectra were simulated with a Hewlett-Packard 9845B minicomputer.

Atomic absorption experiments were carried out using a Varian Techtron (Model AA6) spectrometer. Typically, a stock solution containing the metal ion (Ni^{2+} 1001.2 μg cm^{-3}) was diluted to make a series of calibration samples. A calibration curve was then obtained from which the unknown metal ion concentration was calculated using:

$$\%M = \frac{cVM}{100m} \qquad (2.1)$$

where c = concentration found (μg cm^{-3}), V = volume of sample (cm^3), M

= mass of metal ion (Ni^{2+} is 58.71), and m = mass of sample in V cm^3 (g).

Crystal structures were determined from data collected with a Syntex $P2_1$ four circle diffractometer using graphite monochromated Mo-K radiation in the ω-2θ mode. Reflections were scanned around $K\alpha_1$-$K\alpha_2$ angles, with variable scan speeds (2-29° min^{-1}) and scan width +/- 0.5 (2θ). All data was taken at 20°C. Unit cell dimensions and standard deviations were obtained by linear square refinements on diffractometer angles for 15 automatically centred reflections. Reflections with $I/\sigma(I)>2$ were considered observed, and used in refinement, and corrected for Lorentz polarisation and absorption effects. Heavy atoms were located by Patterson interpretation, and light atoms were found on successive Fourier syntheses. Anisotropic temperature factors were used for all non-H atoms. Hydrogen atoms were given fixed isotropic temperature factors U = 0.007 $Å^2$. Those defined by molecular geometry were inserted at the calculated positions and not refined. Final refinement was on F by cascade least square methods refining [(Ia)-577 and (IV)-424 parameters]. A weighting scheme of the form ω + $1/[\sigma^2(F)$ = gF^2] (for g values see table 3.3) was used and shown to be satisfactory by a weighting analysis. Computing was with a SHELXTL PLUS[103] on a DEC Microvax II with scattering factors taken from International Tables[104]. All crystals were mounted on a fine quartz fibre using epoxy resin, then held in a grub screw. Specific data for each crystal is shown in table 3.3 and appendix 3.1.

2.2 Electrochemical reagents

All chemicals and solvents used for electrochemistry should be of high purity. The purification procedures are given below.

2.2.1 Solvents

The majority of the electrochemistry was carried out in nonaqueous solvents because they have a suitable potential window and dissolve the oxidative addition adducts.

-Acetonitrile, AN, (HPLC grade, Rathburn chemicals) was refluxed for at least 6 h over calcium hydride. It was either used immediately or stored over 3 Å molecular sieves.

-Dimethylsulphoxide, DMSO, (analytical grade, Fison) was stored over 4 Å molecular sieves for a week and then distilled under reduced pressure. It was used immediately.

-Dimethylformamide, DMF, (reagent grade, BDH) was allowed to stand over powdered BaO for a week followed by distillation over alumina powder.

2.2.2 Supporting electrolytes

Supporting electrolytes were used in 0.1 mol dm^{-3} concentration to ensure that the "iR drop" was minimised. Tetraalkylammonium perchlorate salts were preferred because they are the most resistant to cathodic decomposition and give small background currents in the negative potential region. The purification procedures are given below:

-Tetraethylammonium perchlorate, TEAP, (Fluka, purum) was recrystallised from water and dried under vacuum at 70°C for 24 h.

-Tetrabutlyammonium perchlorate, TBAP, (Fluka, purum) was

recrystallised from analytical grade ethanol and dried under vacuum at 100°C for 24 h in the dark. TBAP (Fluka, puriss) was used as received.

-Tetrabutylammonium bromide, TBABr, (Fluka, puriss) was only used in conjunction with TBAP as a means of varying the bromide concentration. It was used as received

-Tetraethylammonium tetrafluoroborate, TEAT, (Fluka, purum) was recrystallised from methanol-petroleum ether and dried under vacuum at 50°C for 24 h.

2.2.3 Miscellaneous reagents

-Triphenylphosphine, PPh_3, (Aldrich, 99%) was recrystallised from hexane and dried under vacuum at 65°C

-2'2-dipyridyl, bpy, (Aldrich, >99%) was used as received.

-2,5-dibromopyridine, $2,5-Br_2Py$,(Aldrich, >95%) and ferrocene, Fc, (Aldrich, reagent grade) were purified by sublimation under reduced pressure at 60°C and 80°C respectively. Fc was stored in the dark.

-Nickel (II) tris 2,2'-dipyridyl perchlorate, $[Ni^{(II)}(bpy)_3(ClO_4)_2]$, was prepared by adding a solution of bpy (Aldrich) (15.00g, 96 mmol) in ethanol (90 cm³) to a stirred solution of $[Ni^{(II)}(H_2O)_6(ClO_4)_2]$ (Johnson Matthey) (10.97 g, 30 mmol) in ethanol (40 cm³). A pale pink precipitate immediately formed. The mixture was filtered and the crude product was purified by recrystallization from water/ethanol. The product was dried under reduced pressure and stored in vacuo over P_2O_5.

-Iron (II) tris 2,2'-dipyridyl perchlorate, $[Fe^{(II)}(bpy)_3(ClO_4)_2]$ was prepared by adding an ethanolic solution of bpy (Aldrich) (7.47g, 47.8 mmol) to a stirred solution of $[Fe^{(II)}(H_2O)_6(ClO_4)_2]$, (Johnson Matthey) (5.44 g, 15 mmol) in ethanol (40 cm³). A deep red slurry formed. The

crude product was filtered off and redissolved in a minimum volume of nitromethane (40 cm^3). Precipitation of the product was caused by dropwise addition of ethanol. The product was filtered off, dried under reduced pressure and stored prior to use in vacuo over P_2O_5.

2.3 Electrochemical apparatus and associated techniques

In this section the electrochemical techniques and apparatus are presented. Many of the methods employed during the course of this work are universal and therefore do not warrant a detailed description here. The uninitiated reader is referred to references 115 to 117.

Plate 2.1 shows a typical set up of the electrochemical equipment.

2.3.1 The black boxes

The majority of the electrochemical experiments were controlled by commercially available electronics from Thompson Electrochem. The Ministat E-Series (model 251 28V/1A) comprises a three electrode type potentiostat, a galvanostat and a voltage source ($\pm$ 3V). This was used with a Miniscan (model MS1) triangular wave generator.

Ring-disc experiments were performed using in-house modular design electronics. The use of modular components enables construction of a number of types of control circuits suitable for different four electrode experiments. Typically the voltage of one working electrode was ramped whilst the other was maintained at a constant potential.

Voltage outputs were recorded on either an XY-t recorder (Gould series 6000) or a digital multimeter (Keithly, model 175).

2.3.2 Rotation equipment

Disc and ring-disc electrodes have an internal brass screw thread

Plate 2.1:

Typical experimental set up.
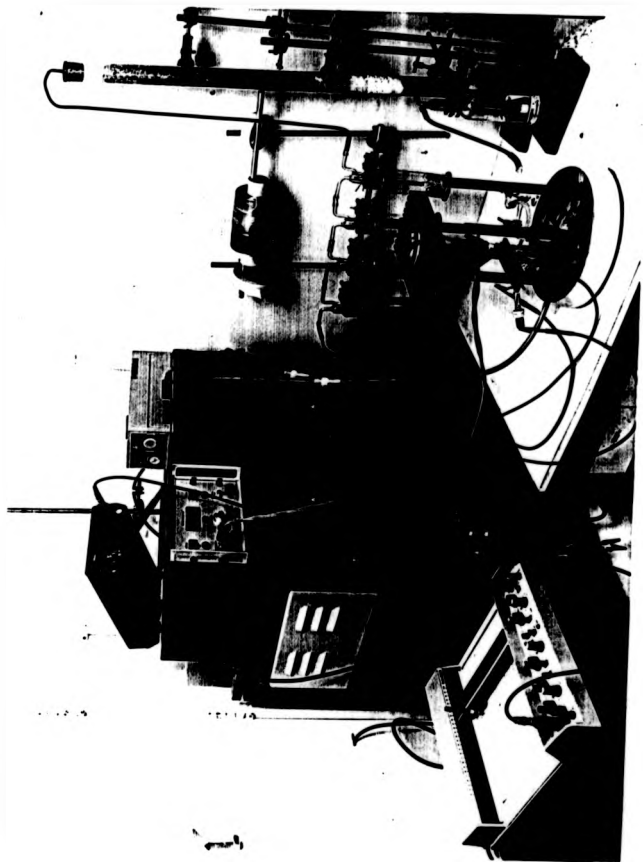
which allows them to be firmly contacted to the bearing block (Oxford Electrodes). The bearing block and electrode are rotated via a printed armature dc motor and motor controller (Oxford Electrodes). The rotation speed can be varied between 0 and 50 Hz ($\pm$ 0.01 Hz) using a slotted opto-switch connected to the motor drive shaft. A digital display of the rotation speed is continually updated.

2.3.3 Electrochemical cells

Two types of electrochemical cell were used. The choice of cell was a compromise between the volume of the sample available, and the importance of temperature control and/or rigorous oxygen exclusion from the sample solutions.

The majority of the work utilized water-jacketed, three-electrode pyrex cells which were divided into 2 compartments by a high porosity glass frit. The counter and working electrodes are positioned either side of the frit to prevent contamination by products of the counter electrode reactions. The cell design, figure 2.1, allows a stream of oxygen-free nitrogen or argon to bubble through the solution prior to an experiment, and to be passed over the solution during the course of an experiment.

Solutions were thermostatted at 25°C ($\pm$ 0.5°C) by the use of a water bath and circulator (Grant Instruments (Cambridge) Ltd. Model W141ZA). The solution volume of the cells was 15 - 25 cm^3.

Due to the expense of platinum and palladium, the use of small pyrex cells was preferred for solutions containing either precious metal. These cells are of a single compartment design in which the reference electrode is contacted to the bulk solution by means of a capillary. Thermostatic control was not possible with these small cells and rigorous oxygen exclusion was found to be less reliable.

-59-

Figure 2.1:

Schematic representation of a water-jacketed two compartment electrochemical cell.
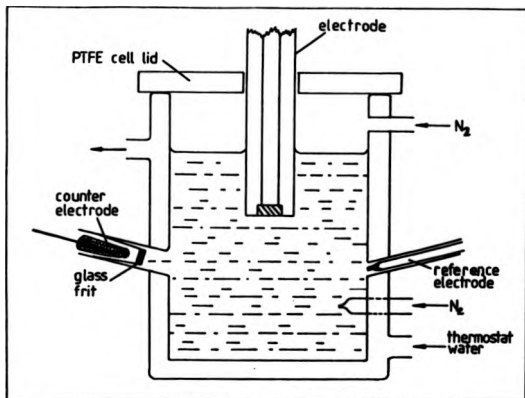
2.3.4 Electrodes

The majority of the work was carried out using platinum disc, glassy carbon disc and platinum-platinum ring-disc working electrodes. They were all supplied by Oxford Electrodes. Details are given in table 2.1.

On receipt from Oxford Electrodes and periodically thereafter, all the electrodes underwent a polishing regime using a purpose-built mechanical polishing device. Initially, they were polished with 25 micron aluminium oxide powder in a glycerol/water mixture. Subsequently, the electrodes were polished with 6, 3 and then 1 micron diamond lapping compound (Engis) mixed with Hyprez lubricating fluid (Engis). Prior to every experiment the electrodes were hand polished with a 1.0 and then 0.3 micron alumina (Banner Scientific) slurry in either water or AN. AN was preferred with experiments which involved reductive electrochemistry of nickel complexes because they were found to be sensitive to small quantities of water absorbed onto the electrode surface.

Table 2.1:

Disc and Ring-Disc Working Electrode

Marking	Type	Disc Area (cm^2)	Sheath Material
GC/V	RDE	0.200	KelF
Pt/KV	RDE	0.387	KelF
Pt/Pt/K	RRDE	0.127	KelF

Platinum and carbon fibre microelectrodes were also used as working electrodes. They were designed and constructed in-house to the design shown in figure 2.2. A fresh surface was obtained by slicing off a sliver at the end of the electrode using a sharp razor blade. On every occasion that a fresh electrode surface was exposed the limiting current, i_L (A), for the oxidation of ferrocene was recorded, and the new electrode area, A (cm^2), was calibrated according to the following equation[118]:

$$A = \frac{i_L^2 \pi}{16F^2 D^2 [Fc]_\infty^2} \qquad (2.2)$$

where F is the faraday, D is the diffusion coefficient of ferrocene in an AN solution containing 0.1 mol dm^{-3} TBAP (taken as 1.9×10^{-5} cm^2 s^{-1}[119]), and $[Fc]_\infty$ is the bulk concentration of ferrocene.

Strips of indium doped tin oxide (1 cm x 2 cm) were used as working electrodes in order that UV visible spectra of thin polymer films could be recorded. An external connection was achieved by painting silver conductive paint (RS Components) onto one end of the electrode and contacting this with a crocodile clip. The coated electrodes were throughly washed with AN and dried. The spectra were recorded using a Philips (Model PU 8720 UV/VIS) scanning spectrophotometer.

Counter electrodes for the larger cells were constructed of platinum gauze (ca. 2 cm^2) spot welded onto a length of platinum wire. A single length of platinum wire (diameter 0.5 mm) was used as the counter electrode in the small cells.

Potentials were measured with respect to a Ag/Ag+ (AgClO$_4$, 0.01 mol dm^{-3} in acetonitrile, 80 mV vs. Fc/Fc+) reference electrode except where aqueous solutions were employed, in which case a saturated calomel electrode (SCE) was used. Both reference electrodes were

Figure 2.2:

Design of home-made platinum and carbon fibre microelectrodes.

tinned copper wire

indium

heat shrink plastic

25μm Pt wire or 6·8μm carbon fibre
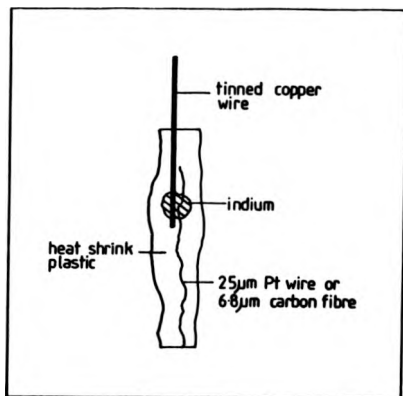
home-made and built to our design, figures 2.3 and 2.4. The potential of the calomel electrode was regularly checked against that of a commercial calomel electrode (Radiometer). A deviation of more than $\pm$ 5 mV was unacceptable and the electrode was repacked with calomel and retested. The potential of the Ag/Ag^+ electrode was checked against the half wave potential of ferrocene. During the course of this work it never deviated from 80 mV by more than $\pm$ 5 mV and the only maintenance required was to top up the $AgClO_4$ solution.

2.3.5 Deoxygenation of the solutions

Deoxygenation of the solutions was achieved by purging with high purity nitrogen or argon (BOC, white spot). The nitrogen had traces of oxygen removed by passage through 3 Dreschel bottles containing a caustic solution of anthraquinone-2-sulphate in contact with a zinc-mercury amalgam. The anthraquinone reagent is self-indicating, turning from deep red to yellow when exhausted. However during the course of this work the anthraquinone remained active. The treated nitrogen was then dried by passage through a column (1 m x 10 cm^2) containing self-indicating silica gel (Fisons), 3 and 4 Å active molecular sieves and sodium hydroxide pellets. The column was regularly repacked with fresh reagents.

The argon was used straight from the bottle or pretreated in the same manner as the nitrogen. Both procedures were found to provide adequate deoxygenation of solutions, but the former was preferred owing to its greater simplicity.

The nitrogen and argon were passed through a Dreschel bottle containing purified solvent, over activated molecular sieves, to presaturate the gas with the solvent being used. The molecular sieves were omitted for aqueous solutions.

-64-

Figure 2.3:

Design of the saturated calomel reference eletrode.
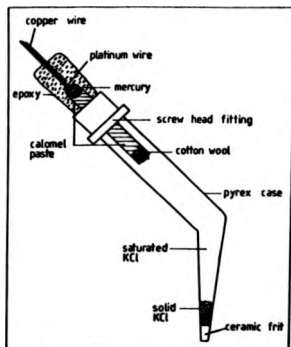
Figure 2.4:

Design of the Ag/Ag⁺ (AgClO₄, 0.01 mol dm⁻³, AN) reference electrode.
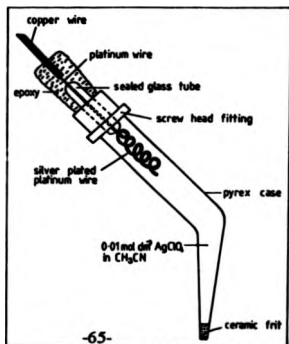
2.3.6 Miscellaneous

All glassware was soaked in Decon 90 (BDH), and rinsed several times with high purity water from a Whatman WR50 R0/Deioniser water purification system.

Molecular sieves were activated at 300°C in a sand bath under nitrogen.

A number of experiments involved electrode deposits that are particularly sensitive to air. These were undertaken in a glove bag filled with high purity argon (BOC, white spot).

Specular reflectance FTIR spectra were recorded using a Perkin-Elmer 1720XFTIR spectrophotometer modified with a specular reflectance accessory with a reflectance angle of 21° to the normal.

Scanning electron micrographs were recorded using a Stereoscan 90 manufactured by Cambridge Instuments.

EDAX were recorded using a S250 scanning electron microscope manufactured by Cambridge Instuments in conjunction with a LINK A10000 X-ray analyser.

Nickel was extracted from polymer films by soaking the coated electrodes in aqueous solutions of ethylene diaminotetraacetic acid (EDTA) (0.01 mol dm^{-3}) buffered to pH 9.5 for 30 min. The coated electrodes were then washed in water, ethanol and finally acetonitrile.

The thickness of the polymer films were recorded using a Talystep stylus manufactured by Rank Taylor Hobson.

CHAPTER 3

CHARACTERISATION OF COMPLEXES (I) TO (XVIII)

One of the aims of this project is to improve our understanding of the mechanisms for the electrosynthesis of poly(pyridine). It has been proposed[30,31] that the initial steps of the polymerisation processes involve the formation of the nickel(0) species ([Ni$^{(0)}$(PPh$_3$)$_4$] or [Ni$^{(0)}$(bpy)$_2$]) which then undergo an oxidative addition reaction with 2,5-Br$_2$Py. In neither case was the oxidative addition adduct isolated and characterised. In order to identify the adducts we attempted their chemical synthesis, isolation, characterisation and subsequent electrochemistry.

In chapter 2 we described the experimental procedures adopted for the synthesis of a number of adducts resulting from the oxidative addition of halopyridines to [M$^{(0)}$L$_{(4 \text{ or } 2)}$] (where M = Ni, Pd or Pt and L = PPh$_3$, PEt$_3$ or bpy). Complexes (I) and (XVI) result from the reaction of 2,5-Br$_2$Py with either [Ni$^{(0)}$(PPh$_3$)$_4$] or [Ni$^{(0)}$(bpy)$_2$] respectively. In this chapter we present and discuss the characterisation of the adducts and in chapters 5 and 7 we report their electrochemistry.

The complexes can be conveniently divided into two groups. The first group comprises those complexes containing phosphine ligands, (I) to (XV), and the second group comprises those complexes containing bpy ligands, (XVI) to (XVIII). We begin by considering the first group.

3.1 Characterisation of the phosphine containing complexes, (I) to (XV)

A review of the literature shows that [M$^{(0)}$L$_4$] (where M = Ni, Pd or Pt and L = PPh$_3$ or PEt$_3$) have frequently been used as the starting

materials for the preparation of organometallic compounds[79,119-132]. They have been shown to react readily with halogenated pyridines[125-132]. The relative rates of reaction are reported to be dependent on the particular halogen[123] and its ring position[122,131]. The rate increases as the halogen group is descended, and the reactivity of the pyridine at the C^2 position is appreciably higher than at the C^3 or C^4 positions.

The products of the reactions are organometallic adducts which maybe monomeric, dimeric or a mixture of the two as shown below:

and/or

and/or
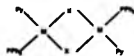
In all cases the adducts have been reported to be square planar and to have a *trans* configuration. Dimers have only been reported when M is either nickel or palladium. Isobe, Nakarmura and Kawaguchi[122] have reported the only examples of dimeric nickel adducts. They proposed that the bridging ligands were halides because the positions of infrared $\nu(\text{Ni-X})$ absorption bands were reasonable for bridging halides under a strong *trans* influence from $\underline{C}$-pyridyl ligands. All the dimeric palladium adducts have been assigned as $\underline{C,N}$-pyridyl bridged complexes[124,127,128,130,131].

The basis for the assignments arises from the unusual stability of the dimers to cleavage by donor ligands and the X-ray analysis of $[Pd^{(II)}Br(C_5H_4N\text{-}C^2)(PPh_3)]_2$ revealing that the 2-pyridyl ligands are bridging the two palladium atoms[124].

In this section we describe the properties of the phosphine containing oxidative addition adducts prepared in this project.

3.1.1 Complex (I)

Treatment of $[Ni(1,5\text{-cod})_2]$ with PPh_3 in acetonitrile generated a suspension of $[Ni^{(0)}(PPh_3)_4]$. Addition of $2,5\text{-Br}_2Py$ to the suspension yielded a red solid product. The $^{31}P\text{-}\{^1H\}$ n.m.r. spectroscopy of the red product shows two singlets located at 27.8 and 26.6 ppm in the ratio $ca.$ 20:1 respectively. Consequently we can infer that there are major and minor oxidative addition adducts, [(Ia) and (Ib) respectively] and that both adducts have a *trans* configuration with respect to the PPh_3 moieties. We have assumed that there is no accidental chemical shift equivalence between the $^{31}P\text{-}\{^1H\}$ n.m.r. signals of a *trans* complex with one of the signals of a *cis* complex. This is a reasonable assumption as there are no reported *cis* adducts resulting from analogous oxidative addition reactions between arylhalides and $[M^{(0)}L_4]$.

Oxidative addition at the C^5 position is ruled out for two reasons. First, the C^2 position is much more susceptible to oxidative addition than the C^5 position and second, the oxidative addition of 3-bromopyridine to any of the $[M^{(0)}L_4]$ species yield monomers rather than dimers[125]. Therefore we postulate that both adducts result from oxidative addition at the C^2 position.

The ratio of the $^{31}P\text{-}\{^1H\}$ n.m.r. signals is unaffected by the presence of up to ten fold excess of PPh_3; the only spectral change is the emergence of a signal at -4.4 ppm attributed to free PPh_3. Dinuclear

structures with bridging halides are quite common among nickel(II) complexes, however they are usually subject to cleavage by donor ligands. Since there are no changes in the ^{31}P-$\{^1H\}$ n.m.r. signals of the adducts as a result of PPh_3 addition we propose that the dimers are pyridyl bridged rather that bromo bridged. We can also infer from this observation that a monomer/dimer equilibrium of the type shown below cannot exist:

(Ia)
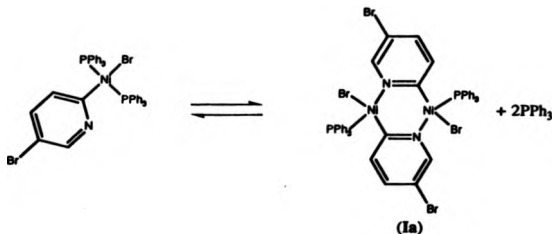
Therefore we are forced to conclude that both adducts are dimeric. Most likely the other *trans* adduct is (Ib).

The elemental analysis and the integrals of the ^1H n.m.r. signals reveal that the adducts are indeed exclusively dimeric in nature. The ^1H n.m.r. signals of the major and minor products either display a large degree of accidental chemical shift equivalence of the pyridyl protons, or the proton signals of the minor adduct are lost in the background noise, figure 3.1. Interestingly, the multiplicity of the pyridyl protons H^6 and H^4 can be rationalised by taking into account the additional coupling with the ^{31}P nucleus of the PPh_3 moiety *trans* to the Ni bonded heterocycle. A first order analysis gives $J^4(PH^6)$ and $J^3(PH^4)$ values of 2 and 3 Hz respectively. Further spectroscopic data are given in table 3.1.

(Ia) was recrystallised from AN and the structure was determined by
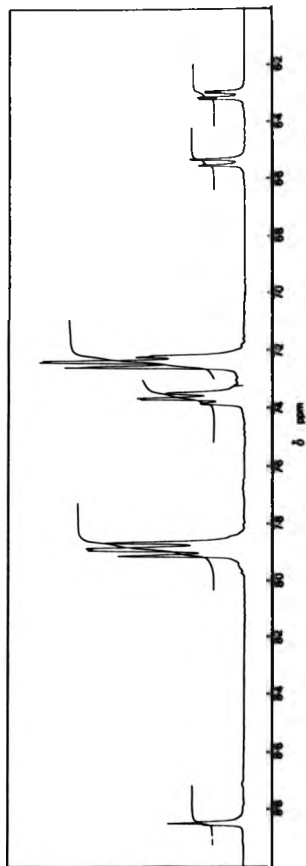
Figure 3.1:

1H n.m.r. spectrum of (I) in CDCl3

X-ray crystallography. It was found to be binuclear with the *trans* arrangement shown in figure 3.2. The structure of (Ia) closely resembles that reported for a similar palladium complex[124]. It contains square planar Ni bound to Br, C^2 of the pyridyl ring, PPh_3, and N of the other pyridyl ring. The $Ni_2C_2N_2$ ring is in boat form. Most dimensions are standard, but it is notable that the mean Ni-C distance (1.870 Å) is shorter than the overall mean (1.917 Å) obtained by Orpen *et al.*[134] for 18 nickel-aryl bonds. Further crystallographic data are given in table 3.3 and appendix 3.1.

Hence, we conclude that the reaction between 2,5-dibromopyridine and $[Ni^{(0)}(PPh_3)_4]$ yields the two binuclear complexes (Ia) and (Ib) according to the following equation:

$4[Ni^{(0)}(PPh_3)_4] + 4 (2,5\text{-}Br_2Py)$ ⟶

(Ia)

(Ib)

$+ 12 PPh_3$
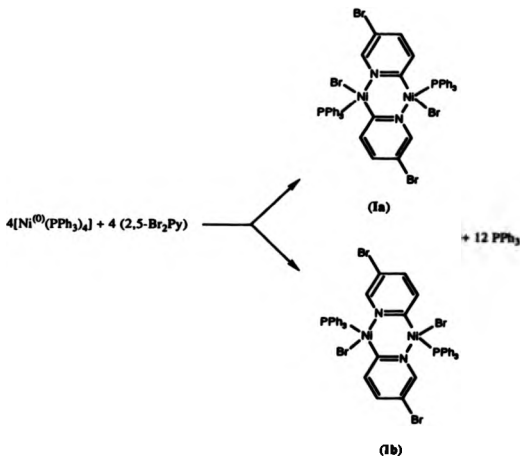
Structure of (Ia) as established by X-ray crystallography. H atoms omitted for clarity.
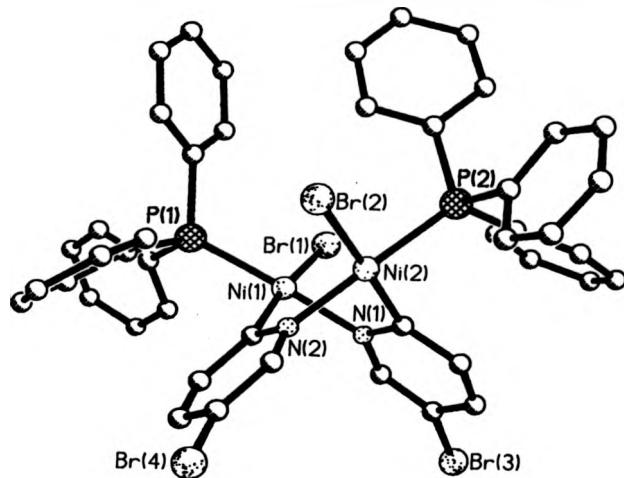
3.1.2 Complexes (II) and (III)

Treatment of $[Pd^{(0)}(PPh_3)_4]$ with 2,5-Br$_2$Py in toluene gave a pale yellow solid product, (II). The ^{31}P-(^1H) n.m.r. spectrum of (II) shows two singlets located at 29.7 and 22.0 ppm in the ratio *ca.* 10:1 respectively. Therefore we can infer that the yellow product is a mixture of two adducts, both of which have a *trans* configuration with respect to the PPh$_3$ moieties. Addition of 10 equivalents of PPh$_3$ to the mixture had no effect on the ratio or chemical shifts of the ^{31}P-(^1H) n.m.r. signals. Following the same rationale as for (I) we propose that both adducts are pyridyl bridged dimeric species.

The elemental analysis and the ^1H n.m.r. spectroscopy (II) are consistent with the formation of only dimeric adducts. The ^1H n.m.r. signals of the pyridyl protons are relatively broad and show a good degree of fine structure. This may be accounted for by accidental shift equivalence of the pyridyl protons of the two *trans* dinuclear species. The dinuclear structures (IIa) and (IIb), analogous to the nickel compounds (Ia) and (Ib) are assigned to the products:

(IIa)   (IIb)
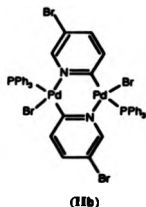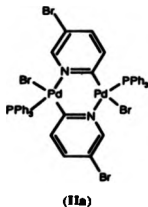
The crystal structure of a similar dipalladium complex has been reported[124].

Treatment of $[Pd^{(0)}(PPh_3)_4]$ with $2,5\text{-}Cl_2Py$ in toluene gave solid yellow products. The dinuclear structures (IIIa) and (IIIb), analogous to the palladium compounds (IIa) and (IIb) above, are assigned to the products. This is further supported by $^{31}P\text{-}\{^1H\}$ and ^1H n.m.r. spectroscopy. Spectroscopic data are given in tables 3.1 and 3.2.

3.1.3 Complexes (IV) and (V)

Addition of $2,5\text{-}Br_2Py$ to $[Pt^{(0)}(PPh_3)_4]$ in benzene gave a cream coloured solid, (IV). $^{31}P\text{-}\{^1H\}$ n.m.r. spectroscopy of the solid shows it is a single adduct which has a *trans* configuration. There is a single resonance at 21.9 ppm flanked by ^{195}Pt satellites with a $J^1(PtP)$ coupling constant of 3133 Hz. Elemental analysis and ^1H n.m.r. integral ratios reveal the adduct to be mononuclear. Interestingly, the low field H^6 proton resonance observed for the nickel and palladium complexes (I) to (IV) is absent, again confirming its different structure. In this case the H^6 resonance is masked by the resonances of the phenyl protons. Further spectroscopic data are given in tables 3.1 and 3.2.

(IV) was recrystallised from AN and the structure determined by X-ray crystallography. The structure was confirmed as the *trans* mononuclear isomer with the Pt bonded to the C^2 of the pyridyl ring, figure 3.3. As with (IIa) the Pt-C bond is somewhat short (2.013(8) Å), compared to the mean for 35 distances (2.049 Å) for platinum-(aryl) bonds[134]. Further crystallographic data is given in table 3.3 and appendix 3.1.

Addition of $2,5\text{-}Cl_2Py$ to $[Pt^{(0)}(PPh_3)_4]$ in benzene gave an off white solid, (V). By analogy with (IV) and from the $^{31}P\text{-}\{^1H\}$ and ^1H n.m.r. spectra (V) is assigned to the *trans* mononuclear adduct in which Pt is bonded to the C^2 position of the pyridyl ring.

Figure 3.3:

Structure of (**IV**) as established by X-ray crystallography. H atoms omitted for clarity.
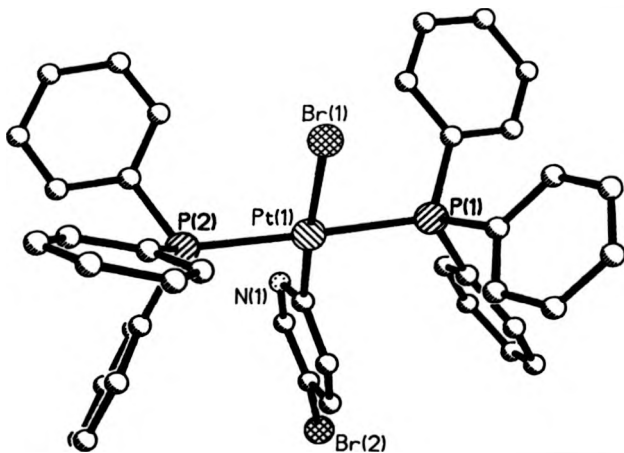
Table 3.1:

Summary of ^{31}P -$\{^{1}H\}$ n.m.r. data for complexes (I) to (V).

Compound	^{31}P-$\{^{1}H\}$ resonances major	minor	Integral ratio
(I)	27.8, s	26.6, s	20 : 1
(II)	29.7, s	22.0, s	1 : 7
(III)	30.1, s	27.5, s	1 : 10
(IV)	21.9, t $^{1}J(PtP) - 3132$	—	—
(V)	22.8, t $^{1}J(PtP) - 3159$	—	—

In $CDCl_3$; chemical shifts(δ) in ppm from external 85% H_3PO_4; coupling constants in Hz; s = singlet, t = triplet

Table 3.2:

Summary of ^{1}H n.m.r. data for complexes (I) to (V)

| Compound | Pyridyl ring proton | | | Phosphine protons | Integral ratio |
	H^3	H^4	H^6		
(I)	6.54, d $J^1(H^4H^3)$—11	6.30, dd $J^1(H^3H^4)$—11 $J^3(PH^4)$—4	8.85, m	7.19-7.92, m	2 : 2 : 2 : 15
(II)	6.60, d* $J^1(H^4H^3)$—11	6.45, d* $J^1(H^3H^4)$—11	8.71, s*	7.20-7.95, m	2 : 2 : 2 : 15
(III)	6.54, d* $J^1(H^4H^3)$—10	6.35, d* $J^1(H^3H^4)$—10	8.61, s*	7.21-7.86, m	2 : 2 : 2 : 15
(VI)	6.59, d $J^1(H^4H^3)$—6	6.44, d* $J^1(H^3H^4)$—6	●	7.35-7.86, m	1 : 1 : (1 + 30)
(V)	6.33, d $J^1(H^4H^3)$—5	6.20, d* $J^1(H^3H^4)$—5	●	7.30-7.80	1 : 1 : (1 + 30)

In CDCl$_3$; chemical shifts(δ) in ppm from TMS at 25°C; coupling constants in Hz;
s – singlet, d – doublet, dd – doublet of doublets, m – multiplet; * – fine splitting
observed; ● – masked by intense phenyl proton resonances;
proton labelling:
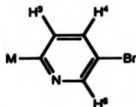
Table 3.3:

Crystallographic data for complexes (Ia) and (IV)

	(Ia)	(IV)
R.m.m	115.8	956.6
System	Triclinic	Triclinic
Space group	P1	P1
a/Å	12.743(8)	12.167(6)
b/Å	13.414(10)	12.746(8)
c/Å	16.758(14)	13.280(8)
α°	90.46(6)	90.53(8)
β°	120.43(6)	115.46(0)
γ°	105.727(6)	107.24(0)
U/Å³	2686(6)	1753(2)
ρ/g cm^{-3}	1.689	1.820
μ(Mo-K)/cm^{-1}	40.5	64.2
Unique reflections	5857	5953
Total reflection I/σ(I)$\leq$2.0	3352	4878
$2\theta_{max}$/min^{-1}	50	50
Range 2θ about $K_{\alpha 1}$-$K_{\alpha 2}$	±0.5	±0.5
Speed 2θ/min^{-1}	2-29	2-29
Dimensions/mm	0.10 x 0.34 x 0.60	0.19 x 0.18 0.23
Max/min transmission factors	0.44,0.71	0.78,0.47
Final R(R')	0.0776(0.076)	0.038(0.039)
Weighting (g)	0.0012	0.00086
Largest ± peaks on ΔF map/eÅ³	+0.76/-0.64	+1.11/-1.02

3.1.4 Characterisation of complexes (VI) to (VIII)

Treatment of a pentane solution of $[Ni^{(0)}(PEt_3)_4]$ with any one of 2,5-Br_2Py, 3-BrPy or 2,5-Br_2T in each case gave an orange/yellow solid product. All three products gave a single resonance located in the region $\delta = 11.0$ to 12.5 ppm in their ^{31}P-$\{^1H\}$ n.m.r. spectra which allows us to conclude that the products are of high isomeric purity and that the phosphorus atoms are in a mutually *trans* arrangement. Elemental analysis of the products, (VI), (VII) and (VIII), shows them to have the generalised empirical formulation of $[Ni^{(II)}Br(R)(PEt_3)_2]$ where R = 5-BrPy-C^2, Py-C^3 and 5-BrT-C^2 respectively. The mononuclear nature of all the complexes is determined from the ^1H n.m.r. integral ratios of the aryl to phosphine protons, illustrated for (VI) in figure 3.4. Once again we assume that in complexes (VI) and (VIII) oxidative addition has occurred exclusively at the C^2 position rather than the C^3 position. Further spectroscopic data is given in tables 3.4 and 3.5.

Hence, we conclude that the reactions between any one of 2,5-Br_2Py, 3-BrPy or 2,5-Br_2T and $[Ni^{(0)}(PEt_3)_4]$ yields a *trans* mononuclear complex.

3.1.5 Characterisation of complexes (IX) to (XII)

Treatment of a THF solution of $[Pd^{(0)}(PEt_3)_4]$ with any one of 2,5-Br_2Py, 2-BrPy, 3-BrPy or 2,5-Br_2T gave either a white or pale yellow solid product. ^{31}P-$\{^1H\}$ n.m.r. spectroscopy of the solids shows that they are of high isomeric purity and that the phosphorus atoms are in a mutually *trans* configuration because a single resonance is observed in each case. Elemental analysis of the isolated solids, (IX), (X), (XI) and (XII), shows them to have the generalised empirical formula of $[Pd^{(II)}Br(R)(PEt_3)_2]$ where R = 5-BrPy-C^2, Py-C^2, Py-C^3 and 5-BrT-C^2 respectively. The mononuclear nature of these complexes is confirmed from the ^1H n.m.r. integral ratios of the aryl to phosphine protons.

Figure 3.4:

^{1}H n.m.r. spectrum of complex (VI) in CDCl$_3$.
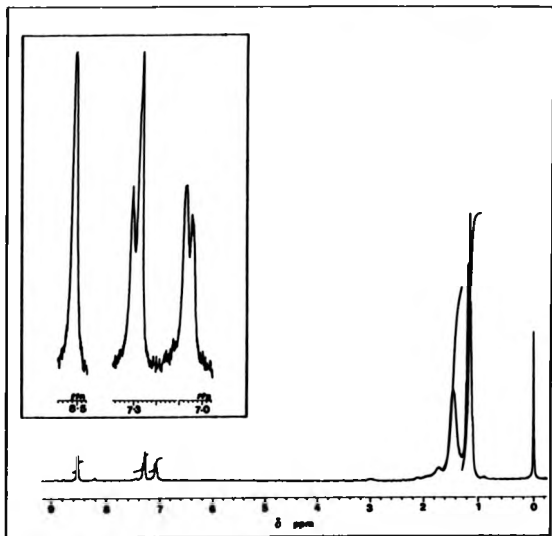
A different route affording complexes (X) and (XI) has been reported by Isobe *et al*.[125]. Their synthesis involved the treatment of diethylether solutions of the analogous PPh_3 complexes with PEt_3. They reported the exclusive formation of *trans*-mononuclear complexes. A comparison between the spectroscopic data obtained by Isobe *et al*.[125] and ourselves supports our structural assignment. In particular, the fact that the chemical shifts of the proton decoupled pyridyl carbons of (IX) more closely resembles those reported by Isobe *et al*.[125] for (X) rather than (XI), supports the assumption that oxidative addition has occurred exclusively at the C^2 position, figure 3.5. Further spectroscopic data is given in tables 3.4 and 3.5.

As with the analogous nickel complexes, we conclude that the reactions between any one of $2,5\text{-}Br_2Py$, 2-BrPy, 3-BrPy or $2,5\text{-}Br_2T$ and $[Pd^{(0)}(PEt_3)_4]$ yields a *trans* mononuclear complex.

3.1.6 Characterisation of complexes (XIII) to (XV)

Treatment of a pentane solution of $[Pt^{(0)}(PEt_3)_4]$ with any one of $2,5\text{-}Br_2Py$, 2-BrPy, or 3-BrPy resulted in a colour change from orange to colourless. Trituation of the colourless solutions yielded off-white solid products.

$^{31}P\text{-}\{^1H\}$ n.m.r. spectroscopy of (XIII) shows two resonances located at 11.9 and 12.5 ppm in the ratio of *ca.* 2:1 which are flanked by ^{195}Pt satellites with $J^1(PtP)$ coupling constants of 2632 and 2798 Hz respectively. From the magnitude of the coupling constants we can infer that the major and minor oxidative addition adducts, [(XIIIa) and (XIIIb) respectively] both have a *trans* configuration with respect to the PEt_3 moieties. Elemental analysis of (XIII) indicates the components of the mixture have the same empirical formula, $[Pd^{(II)}Br(R)(PEt_3)_2]$. ^1H n.m.r. spectroscopy of (XIII) confirms it to be a mixture and the integral ratios are consistent with both components being mononuclear. Consequently,

-82-

Figure 3.5:

^1H decoupled ^{13}C n.m.r. spectrum of (IX) in $CDCl_3$. The chemical shifts are given in ppm. The values in parenthesis are eqivalent chemical shifts for $[BrPd(Py-C^2)(PEt_3)_2]$ taken from reference 125.
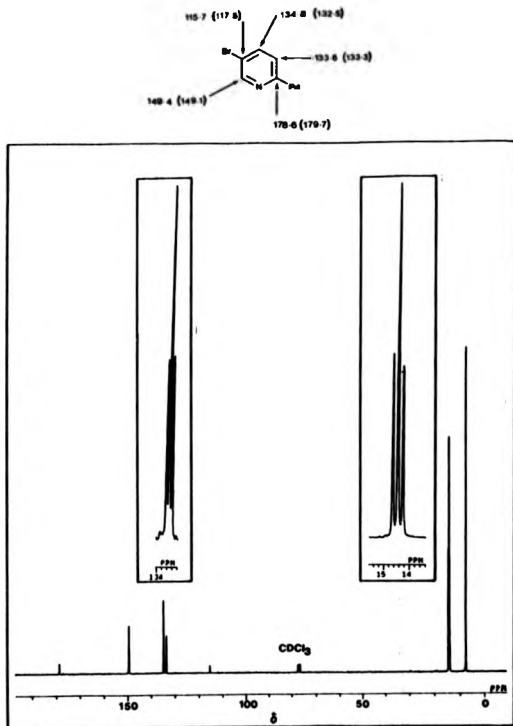
we conclude that the reaction between 2,5-Br$_2$Py and [Pt$^{(0)}$(PEt$_3$)$_4$] yields two *trans* mononuclear complexes according to the following equation:
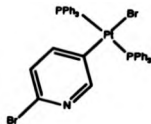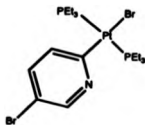
This is a somewhat surprising result as (XIII) is the only product in which oxidative addition has occurred at both the C^2 and C^5 positions and indicates that [Pt$^{(0)}$(PEt$_3$)$_4$] is a less selective nucleophile.

From the elemental analysis, the ^{31}P-{^{1}H} and ^{1}H n.m.r. spectroscopy and by comparison to the analogous nickel and palladium complexes, (XIV) and (XV) are assigned as the *trans*-mononuclear adducts. Further spectroscopic data are given in tables 3.4 and 3.5.

Table 3.4:

Summary of ^{31}P -{^1H} n.m.r. data for complexes (VI) to (XV)

Compound	^{31}P-{^1H} resonances		Integral ratio
	major	minor	
(VI), [NiBr(5-BrPy-C^2)(PEt$_3$)$_2$]	11.34, s	——	——
(VII), [NiBr(Py-C^3)(PEt$_3$)$_2$]	12.35, s	——	——
(VIII), [NiBr(5-BrT-C^2)(PEt$_3$)$_2$]	12.01, s	——	——
(IX), [PdBr(5-BrPy-C^2)(PEt$_3$)$_2$]	11.95, s	——	——
(X), [PdBr(Py-C^2)(PEt$_3$)$_2$]	11.61, s	——	——
(XI), [PdBr(Py-C^3)(PEt$_3$)$_2$]	12.61, s	——	——
(XII), [PdBr(5-BrT-C^2)(PEt$_3$)$_2$]	14.78, s	——	——
(XIII), [PtBr(5-BrPy-C^2)(PEt$_3$)$_2$]	11.87, t J(PtP)=2632 and 2798	12.52, t	2 : 1
(XIV), [PtBr(Py-C^2)(PEt$_3$)$_2$]	12.75, t J(PtP)=2861	——	——
(XV), [PtBr(Py-C^3)(PEt$_3$)$_2$]	12.21, t J(PtP)=2670	——	——

In CDCl$_3$; chemical shifts(δ) in ppm from external 85% H$_3$PO$_4$; coupling constants in Hz; s = singlet, t= triplet

Table 3.5:

Summary of ^{1}H n.m.r. data for complexes (VI) to (XV)

| Compound | Aryl ring protons | | | | Phosphine protons | Integral ratio |
	H3/2	H4	H5	H6		
(VI), [NiBr(5-BrPy-C2)(PEt3)2]	7.21, d, J(H4H3) - 10	7.10, d*, J(H3H4) - 10	—	8.52, s*	1.12 - 1.43	1.0:1.1:0.7:30
(VII), [NiBr(Py-C2)(PEt3)2]	8.41, s*	7.52, d*, J(H5H4) - 9	6.95, dd, J(H4H5) - 9, J(H6H5) - 7	8.08, dd, J(H5H6) - 7	1.10 - 1.60	0.8:0.9:30
(VIII), [NiBr(5-BrT-C2)(PEt3)2]	7.27, s*	6.34, s*	—	—	0.70 - 1.81	1.0:1.1:30
(IX), [PdBr(5-BrPy-C2)(PEt3)2]	7.27, dd*, J(H4H3) - 8, J(H6H3) - 2	7.12, d, J(H3H4) - 8	—	8.54, d*, J(H4H6) - 2	1.00 - 1.66	1.1:1.1:1.1:0.30
(X), [PdBr(Py-C2)(PEt3)2]	8.43, d*, J(H3H4) - 5	7.11, dd*, J(H3H4) - 5, J(H5H4) - 7	6.72, dd, J(H4H5) - 8, J(H6H5) - 7	7.19, d*, J(H5H6) - 8	1.00 - 1.71	1.2:1.1:1.1:1.0:30

Table 3.5 cont:

Compound	H³/²	Aryl ring protons H⁴	H⁵	H⁶	Phosphine protons	Integral ratio
(XI), [PdBr(Py-C⁶)(PEt₃)₂]	8.41, s*	7.52, d* J(H⁴H⁶) = 7	6.95, dd J(H⁴H⁵) = 7 J(H⁵H⁶) = 5	8.08, dd J(H⁵H⁶) = 5 J(H⁴H⁶) = 1	1.00 - 1.62	1.1:0.9:1.1:1.0:30
(XII), [PdBr(5-Br-Py-C⁶)(PEt₃)₂]	6.91, d J(H³H⁴) = 4	6.35, d J(H³H⁴) = 4	—	—	1.02 - 1.74	1.2:1.2:30
(XIII), [PdBr(5-Br-Py-C⁶)(PEt₃)₂] [PdBr(5-Br-Py-C⁶)(PEt₃)₂]		7.00 - 7.82, m*+		8.22, s* 8.42, s*	1.00 - 1.78	ca. 1.2:30
(XIV), [PdBr(Py-C⁶)(PEt₃)₂]	8.43, •	7.11, •	6.72, •	7.19, •	0.91 - 1.85	0.8:0.7:1.1:1.1.1:30
(XV), [PdBr(Py-C⁶)(PEt₃)₂]	8.50, s*+	7.59, d+ J(H⁴H⁵) = 8	6.87, dd J(H⁴H⁵) = 8 J(H⁵H⁶) = 5	8.05, d J(H⁵H⁶) = 5	1.00 - 1.80	1.3:1.1:1.0,0.7:30

In CDCl₃; chemical shifts(δ) in ppm from TMS at 25°C; coupling constants in Hz; s = singlet, d = doublet, dd = doublet of doublets, m = multiplet; * = fine splitting observed; • = broad resonance; + = Pt satellites observed. Proton labelling:
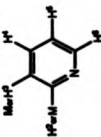
3.2 Characterisation of the bpy containing complexes, (XVI) to (XVIII)

As far as we are aware, there are no reports in the literature on the oxidative addition of halogenated pyridines to $[Ni^{(0)}(bpy)_2]$ other than by *in situ* electrochemical techniques[31]. The formulation of the adducts which are produced *in situ*, are suggested to be of the following type:
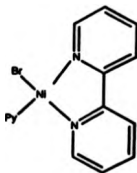
There have been several reports in the literature on the preparation of (aryl)(bpy)nickel(II) halide complexes from the action of bis(alky)(bpy)nickel(II) with aryl halides[133]. The stability of the products was reported to vary with the particular aryl halide employed. The iodide and bromide complexes were reported to be stable in air whereas the chloride analogue decomposes within a few hours to unidentified products. The relative stability of the complexes was reported to increase as the rotation of the aryl subsistent became more hindered, i.e. stability increases in the order p-tolyl < m-tolyl < o-tolyl. The stability of the complexes of the bulky ligands is likely to be steric, but Uchino *et al.*[133] have also suggested that restriction of rotation may favour the overlap of the nickel d-orbital with the aromatic π system thereby increasing the complexes stability.

In this section we report our investigations into the nature of products resulting from the action of $[Ni^{(0)}(bpy)_2]$ with 2,5-, 2- and 3-bromopyridines.

3.2.1 Complex (XVI)

Treatment of $[Ni^{(0)}(cod)_2]$ with bpy in toluene at 0 °C generated a dark purple solution of $[Ni^{(0)}(bpy)_2]$. Addition of 2,5-Br_2Py to this solution followed by warming to room temperature, yielded a solid brown product. The product is sparingly soluble in chloroform, but is readily soluble in DMSO. The ^1H n.m.r. of the complex in $CDCl_3$ shows that there are at least 6 low field resonances arising from aromatic protons, figure 3.6. From the integral ratios we propose that there is one bpy and one bromopyridine coordinated to the nickel(II). The resonances located at $\delta = 8.68$, 8.38, 7.81 and 7.31 ppm are assigned to the bpy protons and the those located at $\delta = 8.26$ and 7.93 ppm to the pyridyl protons. There should be another resonance arising from the pyridyl moiety, however we proposed that this signal is masked by the solvent signal, $\delta = 7.25$ ppm. It should be noted that the proton resonances are somewhat broad. The broadening is associated with the presence of a small quantity of paramagnetic nickel(II). The paramagnetic material may either be an impurity in the original sample or result from the coordination of the solvent to a proportion of the diamagnetic nickel(II) centres. The ^1H n.m.r. spectrum of (XVI) in $(CD_3)_2SO$ shows that all the resonances are very broad. We propose that the broadness is due to the formation of paramagnetic nickel(II) species resulting from solvent coordination.

The monomeric nature of the complex is evident from the F.A.B. mass spectrum, where a cluster of peaks is observed corresponding to the molecular ion, $[Ni^{(II)}Br(BrPy)(bpy)]^+$, figure 3.7. The electronic spectrum of (XVI) exhibits four absorption maxima located at 198, 246, 296 and 307 cm^{-1}. The latter signal is assigned to the charge transfer from the nickel d-orbitals to a vacant π orbital of bpy.

It is not possible to unequivocally determine the structure of (XVI)
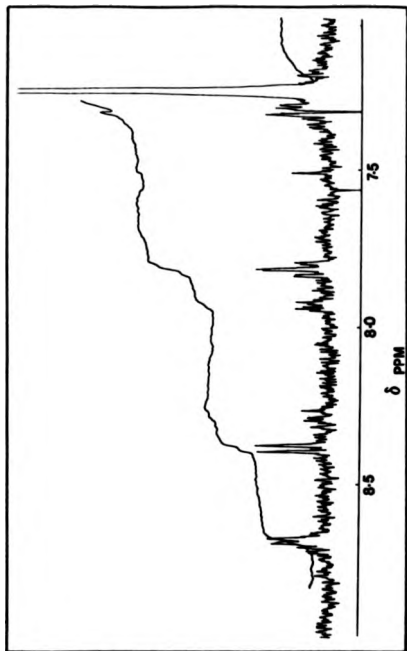
Figure 3.6:

^{1}H n.m.r. spectrum of (XVII) in CDCl$_3$

Figure 3.7:

F.A.B. mass spectrum of (XVI) in *m*-nitrobenzylalcohol matrix.
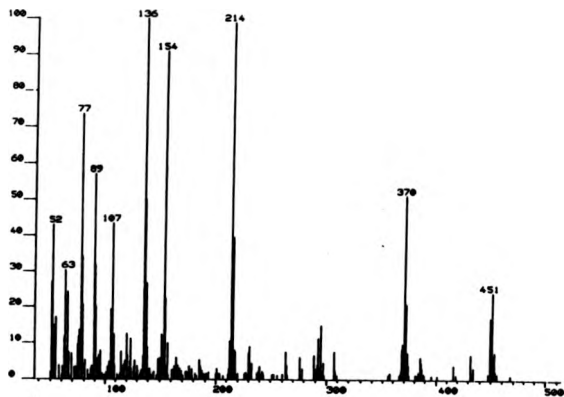
from our studies. This is because ^1H n.m.r. spectral interpretation was hampered by low solubility of the complex in $CDCl_3$ causing signal to noise problems, and by the formation of diamagnetic species in $(CD_3)_2SO$ causing broadening of the resonance signals. Nevertheless the results show the ratio of the bpy to bromopyridyl in (XVI) is 1 : 1. The F.A.B. mass spectrum shows the m/z^+ of the molecular ion to be consistent with an (aryl)(bpy)(bromo)nickel(II) adduct. The preferential position of oxidative addition cannot be determined from our studies, although by analogy with the phosphine complexes we propose that oxidative addition occurs exclusively at the C^2 position. Hence, we tentatively conclude that the reaction between 2,5-dibromopyridine and $[Ni^{(0)}(bpy)_2]$ yields a monomeric complex according to following equation:

$[Ni^{(0)}(bpy)_2] + 2,5-Br_2Py \longrightarrow$
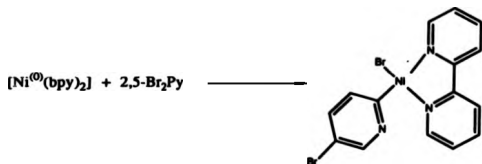
3.2.2 Complexes (XVII) and (XVIII)

The addition of either 2-BrPy or 3-BrPy to the dark purple solution produced by the treatment of $[Ni^{(0)}(cod)_2]$ with bpy in toluene at 0°C in each case yielded a dark brown precipitate on warming the mixture to room temperature. Elemental analysis (C, H, N and Br) for (XVII) and (XVIII) were in reasonable agreement with the formulation

-92-

[Ni$^{(II)}$Br(Py)(bpy)]. The ^{1}H n.m.r. studies of (XVII) and (XVIII) were uninformative as the resonances were very broad in all the solvents employed (CDCl$_3$, (CD$_3$)$_2$SO, CD$_3$CN, CD$_3$OD and CD$_3$NO$_2$). By analogy with (XVI), we tentatively assign (XVII) and (XVIII) to mononuclear adducts in which the Ni is bonded to the C^2 and C^3 of the pyridyl ring respectively:

3.3 List of complexes (I) to (XVIII)

Complex	Structure
(I)	*trans*-(_P_,_N_)-[NiBr(μ-5-BrC$_5$H$_3$N-_C_^{2})PPh$_3$]$_2$
(II)	*trans*-(_P_,_N_)-[PdBr(μ-5-BrC$_5$H$_3$N-_C_^{2})PPh$_3$]$_2$
(III)	*trans*-(_P_,_N_)-[PdCl(μ-5-ClC$_5$H$_3$N-_C_^{2})PPh$_3$]$_2$
(IV)	*trans*-[PtBr(5-BrC$_5$H$_3$N-_C_^{2})(PPh$_3$)$_2$]
(V)	*trans*-[PtCl(5-ClC$_5$H$_3$N-_C_^{2})(PPh$_3$)$_2$]
(VI)	*trans*-[NiBr(5-BrC$_5$H$_3$N-_C_^{2})(PEt$_3$)$_2$]
(VII)	*trans*-[NiBr(5-C$_5$H$_3$N-_C_^{3})(PEt$_3$)$_2$]
(VIII)	*trans*-[NiBr(5-BrC$_4$H$_2$S-_C_^{2})(PEt$_3$)$_2$]
(IX)	*trans*-[PdBr(5-BrC$_5$H$_3$N-_C_^{2})(PEt$_3$)$_2$]
(X)	*trans*-[PdBr(5-C$_5$H$_3$N-_C_^{2})(PEt$_3$)$_2$]
(XI)	*trans*-[PdBr(5-C$_5$H$_3$N-_C_^{3})(PEt$_3$)$_2$]
(XII)	*trans*-[PdBr(5-BrC$_4$H$_2$S-_C_^{2})(PEt$_3$)$_2$]
(XIII)	*trans*-[PtBr(5-BrC$_5$H$_3$N-_C_^{2})(PEt$_3$)$_2$]
(XIV)	*trans*-[PtBr(5-C$_5$H$_3$N-_C_^{2})(PEt$_3$)$_2$]
(XV)	*trans*-[PtBr(5-C$_5$H$_3$N-_C_^{3})(PEt$_3$)$_2$]
(XVI)	*cis*-[NiBr(5-BrC$_5$H$_3$N-_C_^{2})(bpy)]
(XVII)	*cis*-[NiBr(C$_5$H$_3$N-_C_^{2})(bpy)]
(XVIII)	*cis*-[NiBr(C$_5$H$_3$N-_C_^{3})(bpy)]

Appendix 3.1

Table A3(1):

Atomic coordinates (x 10^4) and equivalent isotropic displacement parameters (Å^2 x 10^3) for (Ia) and (IV).

(i) **(Ia):**

Atom	x	y	z	U(eq)
Br(1)	2214(2)	3422(1)	4285(1)	66(1)
Br(1)	3816(2)	2310(2)	1204(1)	75(1)
Br(3)	-2343(2)	2798(2)	2621(2)	110(1)
Br(4)	535(2)	-1498(2)	337(1)	103(1)
Ni(1)	1935(2)	2046(2)	3319(1)	39(1)
Ni(2)	2270(2)	2636(2)	1622(1)	41(1)
C1(11)	8892(9)	7420(9)	3191(6)	216(7)
C1(12)	9212(13)	5678(9)	4051(11)	356(14)
C1(13)	10596(8)	7765(10)	4582(8)	260(8)
C1(21)	8017(10)	9377(11)	1175(7)	245(9)
C1(22)	5815(14)	8382(10)	1236(8)	325(12)
C1(23)	6393(12)	10357(10)	897(11)	341(13)
P(1)	3242(4)	1422(3)	4058(2)	39(2)
P(2)	2904(4)	4300(3)	1490(3)	44(2)
N(1)	780(11)	2497(9)	2597(9)	48(7)
N(2)	1681(10)	1193(9)	1774(8)	42(6)
C(1)	949(14)	2804(11)	1842(9)	40(8)
C(2)	83(14)	3075(11)	1319(9)	36(7)
C(3)	-876(16)	3090(13)	1555(11)	53(9)
C(4)	-1034(15)	762(13)	2306(11)	55(9)
C(5)	-183(16)	2523(12)	2821(10)	49(9)
C(6)	1511(13)	920(12)	2541(10)	40(8)
C(7)	988(13)	-110(13)	2634(10)	47(8)
C(8)	698(14)	-840(12)	1974(11)	56(8)
C(9)	888(16)	-537(14)	1239(10)	63(10)
C(10)	1389(15)	494(13)	1144(10)	54(9)
C(101)	3460(14)	299(12)	3564(11)	47(8)
C(102)	3218(14)	-675(15)	3841(11)	59(9)
C(103)	3213(16)	-1527(14)	3395(14)	71(10)
C(104)	3497(20)	-1395(19)	2660(15)	76(14)
C(105)	3786(17)	-419(19)	2352(11)	76(11)
C(106)	3739(16)	424(13)	2819(11)	51(9)
C(111)	2848(14)	947(12)	5002(10)	45(8)
C(112)	1779(16)	794(14)	5057(11)	61(10)
C(113)	1453(16)	370(17)	5742(13)	82(11)

-94-

Table A3(1) cont.

Atom	x	y	z	U(eq)
C(114)	2191(23)	130(16)	6385(13)	86(12)
C(115)	3278(21)	319(14)	6353(10)	67(11)
C(116)	3617(15)	710(14)	5667(12)	64(9)
C(121)	4665(14)	2288(12)	4423(9)	40(8)
C(122)	5570(19)	2107(15)	4228(12)	67(10)
C(123)	6636(20)	2717(19)	4528(13)	79(12)
C(124)	6810(18)	3533(19)	5047(13)	82(12)
C(125)	5928(20)	3742(14)	5239(11)	79(10)
C(126)	4844(17)	3130(14)	4946(11)	72(10)
C(201)	3116(16)	4553(14)	454(10)	53(8)
C(202)	2506(17)	3819(15)	-163(11)	70(10)
C(203)	2595(23)	3973(24)	-962(16)	109(16)
C(204)	3190(28)	4852(26)	-1123(14)	108(18)
C(205)	3852(21)	5618(22)	-551(20)	115(17)
C(206)	3827(18)	5447(16)	268(13)	90(11)
C(211)	4194(14)	4943(13)	2228(10)	112(8)
C(212)	4555(16)	6046(15)	2335(13)	81(10)
C(213)	5494(25)	6515(18)	2899(17)	112(15)
C(214)	6096(24)	5904(27)	3362(13)	112(16)
C(215)	5748(20)	4924(24)	3267(14)	96(14)
C(216)	4085(19)	4370(15)	2705(11)	75(10)
C(221)	2026(14)	5075(12)	1670(10)	48(8)
C(222)	1841(15)	5189(14)	2436(11)	55(9)
C(223)	1088(19)	5626(16)	2602(13)	78(11)
C(224)	472(21)	6039(17)	2000(19)	102(15)
C(225)	620(19)	5969(15)	1219(15)	85(12)
C(226)	1402(17)	5486(12)	1035(11)	59(9)
C(1A)	9361(24)	6931(23)	4178(20)	165(21)
C(2A)	6627(29)	9217(26)	785(18)	158(21)

Table 3A(1) cont.

(ii) for (IV)

Atom	x	y	z	U(eq)
Pt(1)	1266.8(3)	2833.9(2)	2258.8(3)	31(1)
Br(1)	948.3(8)	774.1(6)	2165.0(9)	55(1)
Br(2)	1312.4(11)	8014.5(8)	2536.7(10)	78(2)
P(1)	-772(2)	2427(2)	2140(2)	36(1)
P(2)	3280.5(17)	3231.9(14)	2318.1(16)	33(1)
N(1)	1168(7)	4936(6)	1415(6)	56(4)
C(1)	1439(6)	4457(6)	2354(6)	35(3)
C(2)	1166(8)	6010(7)	1487(7)	51(4)
C(3)	1445(8)	6574(6)	2480(7)	48(4)
C(4)	1747(8)	6047(7)	3415(7)	52(4)
C(5)	1764(7)	5014(5)	3359(6)	34(3)
C(111)	090(7)	1681(6)	799(6)	41(3)
C(112)	-1898(7)	1106(7)	25(7)	51(4)
C(113)	-2929(3)	511(7)	-968(8)	66(5)
C(114)	-4159(2)	526(8)	-1251(9)	72(5)
C(115)	-4357(8)	1088(7)	-505(8)	60(4)
C(116)	-3347(9)	1675(8)	493(7)	52(4)
C(121)	1267(7)	3602(6)	2370(6)	37(3)
C(122)	-1574(7)	4243(7)	1530(7)	48(4)
C(123)	-1937(9)	5136(7)	1660(8)	62(5)
C(124)	-1980(9)	5407(8)	2634(9)	69(6)
C(125)	-1664(9)	4794(8)	3471(8)	65(5)
C(126)	-1296(8)	3893(7)	3379(7)	55(4)
C(131)	-962(7)	1592(6)	3188(6)	39(4)
C(132)	-1981(8)	613(7)	2096(8)	53(4)
C(133)	-2103(10)	40(8)	3759(11)	71(6)
C(134)	-1256(12)	443(9)	4867(10)	73(7)
C(135)	-240(11)	1406(9)	5156(9)	73(6)
C(136)	-70(8)	1962(7)	4312(8)	55(4)
C(211)	3179(7)	2954(6)	922(6)	39(3)
C(212)	4196(7)	3521(6)	673(7)	44(4)
C(213)	4135(8)	3239(7)	-351(7)	52(4)
C(214)	3084(8)	2410(7)	-1146(7)	50(4)
C(215)	2102(8)	1845(7)	-898(7)	55(4)
C(216)	2141(7)	2121(6)	120(7)	45(4)
C(221)	4375(7)	4660(6)	2850(6)	38(3)
C(222)	4138(8)	5491(6)	2199(8)	50(4)
C(223)	4966(10)	6582(7)	2632(9)	64(6)
C(224)	6033(10)	6816(7)	3694(8)	70(6)
C(225)	6242(9)	6051(7)	4315(8)	61(5)
C(226)	5425(7)	4936(6)	3919(7)	45(4)

Table 3A(1) cont.

(ii) for (IV)

Atom	x	y	z	U(eq)
C(231)	4276(7)	2443(5)	3171(6)	36(3)
C(232)	5299(7)	2349(7)	3023(7)	52(4)
C(233)	6075(8)	1817(7)	3711(9)	62(5)
C(234)	5860(9)	1371(7)	4567(8)	63(5)
C(235)	4857(10)	1479(8)	4750(8)	69(5)
C(236)	4051(8)	1998(6)	4028(7)	49(4)

Table 3A(2):

Bond lengths (Å) and angles (°).

(i) for (Ia)

Br(1)-Ni(1)	2.348(3)	Br(2)-Ni(2)	2.371(4)
Ni(1)-P(1)	2.212(5)	Ni(1)-N(1)	1.930(14)
Ni(1)-C(6)	1.870(16)	Ni(2)-P(2)	2.198(5)
Ni(2)-N(2)	1.918(11)	Ni(2)-C(1)	1.869(20)

Br(1)-Ni(1)-P(1)	94.2(1)	Br(1)-Ni(1)-N(1)	90.9(4)
P(1)-Ni(1)-N(1)	174.9(4)	Br(1)-Ni(1)-C(6)	172.4(5)
P(1)-Ni(1)-C(6)	91.1(5)	N(1)-Ni(1)-C(6)	83.9(6)
Br(2)-Ni(2)-P(2)	91.1(2)	Br(2)-Ni(2)-N(2)	91.2(5)
P(2)-Ni(2)-N(2)	177.4(5)	Br(2)-Ni(2)-C(1)	173.4(4)
P(2)-Ni(2)-C(1)	91.7(5)	N(2)-Ni(2)-C(1)	86.2(6)
Ni(1)-N(1)-C(1)	118.2(12)	Ni(1)-N(1)-C(5)	121.8(11)
Ni(2)-N(2)-C(6)	118.0(10)	Ni(2)-C(1)-N(1)	113.8(12)
Ni(1)-C(6)-N(2)	113.9(10)		

(ii) for (IV)

Pt(1)-Br(1)	2.531(2)	Pt(1)-P(1)	2.312(3)
Pt(1)-P(2)	2.316(3)	Pt(1)-C(1)	2.013(8)

Br(1)-Pt(1)-P(1)	88.1(1)	Br(1)-Pt(1)-P(2)	91.8(1)
P(1)-Pt(1)-P(2)	178.2(1)	Br(1)-Pt(1)-C(1)	176.9(2)

THE ELECTROCHEMISTRY OF THE STARTING MATERIALS

In this chapter we describe the electrochemistry of the various starting materials used during the course of this work.

4.1 Triphenylphosphine, PPh₃

In the electrochemical deposition of poly(pyridine) on GC based on the nickel/PPh₃/TBAP/AN system, it was found that the most satisfactory results were obtained from solutions containing excess PPh₃. Consequently, the electrochemistry of PPh₃ alone was investigated.

A cyclic voltammogram recorded at a GC electrode of an AN solution containing TBAP and PPh₃ shows three redox processes, figure 4.1. The CV has the same form as that previously reported in the literature[135]. The peaks are assigned by Schiavon *et al.* as an oxidation, peak A:

$$PPh_3 \longrightarrow PPh_3^{\cdot+} + e \qquad\qquad E_p = 1.77 \text{ V}$$

followed by a reduction, peak B:

$$PPh_3H^+ + e \longrightarrow PPh_3 + 1/2H_2 \qquad\qquad E_p = 0.14 \text{ V}$$
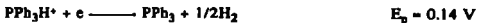
The hydrogen thus formed can be oxidised, peak C:

$$1/2H_2 \longrightarrow H^+ + e \qquad\qquad E_p = 0.43 \text{ V}$$

The species PPh_3H^+ is formed by the reaction of $PPh_3^{\cdot+}$ with traces of

Figure 4.1:

Cyclic voltammogram of PPh₃ (10 mmol dm⁻³) in an AN solution containing TBAP (0.1 mol dm⁻³) at GC/V. Potentials with respect to Ag/Ag⁺ (AgClO₄, 0.01 mol dm⁻³, AN). Scan rate = 100 mV s⁻¹.
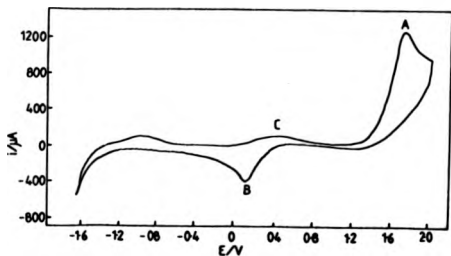
Figure 4.2:

Cyclic voltammogram of bpy (10 mmol dm⁻³) in an AN solution containing TBAP (0.1 mol dm⁻³) at GC/V. Potentials with respect to Ag/Ag⁺ (AgClO₄, 0.01 mol dm⁻³, AN). Scan rate = 50 mV s⁻¹.

water:

$$PPh_3^{\cdot +} + H_2O \longrightarrow PPh_3O + 2H^+ + e$$

$$PPh_3 + H^+ \longrightarrow PPh_3H^+$$
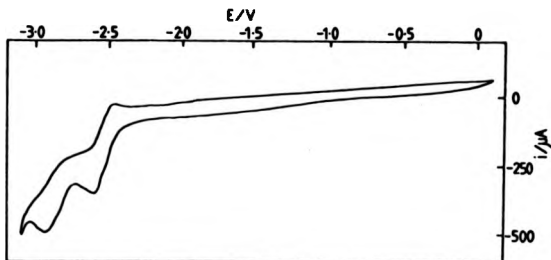
The reaction producing the voltammetric peaks B and C are due to reaction products formed from $PPh_3^{\cdot +}$. Consequently, B and C will be absent if peak A is not traversed and this is indeed found to be true. PPh_3 is resistant to reduction within the potential limits of the chosen background electrolyte (1.80 V to -3.00 V).

In order to avoid complications due to PPh_3 oxidation, solutions containing PPh_3 were not investigated above 0.0 V [Ag/Ag$^+$ (AgClO$_4$, 0.01 mol dm^{-3} in AN)].

4.2 2,2-Dipyridyl, bpy

The electrochemistry of $[Ni^{(II)}(bpy)_3]^{2+}$ plays a key role in the polymerisation mechanism reported in chapter 7. The reduction of $[Ni^{(II)}(bpy)_3]^{2+}$ leads to the loss of one or more of the bpy ligands. Therefore, in order to explain the electrochemistry of $[Ni^{(II)}(bpy)_3]^{2+}$ fully, it is necessary to understand the electrochemistry of bpy.

It has been reported in the literature that bpy undergoes two one-electron reductions in aprotic solvents[136]. The first reduction is reversible and results in the formation of the bpy radical anion:

$$bpy + e \longrightarrow bpy^{\cdot -}$$

The second reduction is quasi-reversible leading to the formation of the bpy dianion:

$$bpy^{\cdot -} + e \longrightarrow bpy^{2-}$$

Our own investigations accord with the literature. A typical cyclic voltammogram at a GC electrode in an AN solution containing bpy and TEAP is given in figure 4.2. It shows no oxidative electrochemistry and the two expected reductive peaks are located at E_{pc} = -2.60 and -2.94 V [Ag/Ag$^+$(AgClO$_4$, 0.01 mol dm^{-3} in AN)] .

4.3 Nickel (II) tris 2,2'-dipyridyl perchlorate, [Ni$^{(II)}$(bpy)$_3$(ClO$_4$)$_2$]

Several investigations into the electrochemistry of bpy-substituted transition metal complexes have been reported in the literature. Four of these studies were concerned with [Ni$^{(II)}$(bpy)$_3$(ClO$_4$)$_2$] in the same solvent system as that employed in our polymerisation experiments[136-139]. However, there are discrepancies between both the results and the authors' interpretation of the reductive electrochemistry of [Ni$^{(II)}$(bpy)$_3$(ClO$_4$)$_2$].

Tanaka and Sato[137] observed four polarographic waves for the reductive electrochemistry of [Ni$^{(II)}$(bpy)$_3$]$^{2+}$ on mercury in the presence of excess bpy. The ratio of the heights for the first and second reductions was reported to be 2:1, and the diffusion-current constant for the limiting current of the first wave was found to be approximately twice that of known one-electron reduction processes. In the absence of excess bpy the first reduction wave was complicated by a pre-wave. The height of the two waves at the more negative potentials was reported to increase as the concentration of excess bpy was also increased; however both waves were observed even in the absence of excess bpy. In the presence of excess bpy, Tanaka and Sato assigned the first wave to the two-electron reduction of [Ni$^{(II)}$(bpy)$_3$]$^{2+}$ to [Ni$^{(0)}$(bpy)$_3$] and the second wave to the reduction of [Ni$^{(0)}$(bpy)$_3$] to [Ni$^{(-I)}$(bpy)$_3$]$^-$. In the absence of excess bpy, it was suggested that some [Ni$^{(II)}$(bpy)$_3$]$^{2+}$ underwent loss of a ligand or ligands and the resultant [Ni$^{(II)}$(bpy)$_{3-n}$]$^{2+}$ was subsequently reduced to [Ni$^{(0)}$(bpy)$_{3-n}$] in the pre-wave.

Tanaka *et al*.[138] subsequently re-investigated the reductive electrochemistry of $[Ni^{(II)}(bpy)_3(ClO_4)]$ by studying the electron spin resonance spectra of the reduction products. They reported the formation of $[Ni^{(I)}(bpy)_3]^+$ and suggested the the first polarographic wave was indeed the summation of two one-electron reductions: $[Ni^{(II)}(bpy)_3]^{2+}$ to $[Ni^{(I)}(bpy)_3]^+$ followed by $[Ni^{(I)}(bpy)_3]^+$ to $[Ni^{(0)}(bpy)_3]$.

Prasad and Scaife[139] reported the following observations about the first cathodic redox couple of $[Ni^{(II)}(bpy)_3]^{2+}$. Firstly it had a peak separation of 60 mV at 100 mV s^{-1}, i_p/ν is constant and i_{pa}/i_{pc} is equal to unity. Secondly controlled exhaustive potential coulometry at -1.54 V (SCE) resulted in colour changes from pink to yellow to bright blue. The concomitant consumption of charge was reported to be equivalent to 1 electron per nickel. Thirdly the micro-analysis of the nickel product isolated from the controlled potential coulometry experiment was reported to be consistent with $[Ni^{(I)}(bpy)_2(ClO_4)]$. It should be noted that there was a discrepacy of 4% between the found and calculated carbon analysis and the authors reported only limited confidence in the purity of the isolated product. Prasad and Scaife concluded that $[Ni^{(II)}(bpy)_3]^{2+}$ is first reduced to $[Ni^{(I)}(bpy)_3]^+$ which then dissociates at a rate which is slow compared to the time scale of the voltammetry experiments to give $[Ni^{(I)}(bpy)_2]^+$ and free bpy.

Henne and Bartak[137] also investigated the cyclic voltammetry and controlled potential coulometry of $[Ni^{(II)}(bpy)_3]^{2+}$. They observed five redox processes at -1.26, -1.75, -1.96, -2.21 and -2.34 V (SCE) upon scanning in the cathodic direction from the rest potential. The couples were all reversible except the most negative which was quasi-reversible. The addition of bpy suppressed the small wave at -1.75 V and increased the wave at -2.21 V. They determined from controlled exhaustive potential coulometry that the wave at -1.26 V was a two-electron process. Henne and Bartak assigned the first reductive wave to the two-electron

reduction of $[Ni^{(II)}(bpy)_3]^{2+}$ to $[Ni^{(0)}(bpy)_3]$ and suggested that $[Ni^{(0)}(bpy)_3]$ subsequently eliminated a ligand or that the bpy ligands became unidentate. The second wave was attributed to the one-electron reduction of $[Ni^{(0)}(bpy)_2]$ followed by the homogeneous ligand solvent exchange reaction to give $[Ni^{(-I)}(bpy)AN]^-$ and free bpy. The third wave was assigned to the one-electron reduction of $[Ni^{(0)}(bpy)_2]$ to $[Ni^{(-I)}(bpy)_2]^-$. The fourth wave was assigned to the reduction of bpy itself and the fifth wave was assigned to the one-electron reduction of either $[Ni^{(-I)}(bpy)AN]^-$ or of $[Ni^{(-I)}(bpy)_2]^-$.

In order to understand the reductive polymerisation of 2,5-Br_2Py as promoted by $[Ni^{(II)}(bpy)_3(ClO_4)_2]$, it is important to eliminate any uncertainties about the electrochemistry of the nickel complex. In this section we present and discuss our findings on the electrochemistry of $[Ni^{(II)}(bpy)_3(ClO_4)_2]$ and compare them to those reported in the literature.

4.3.1 Determination of the number of electrons associated with each redox process of $[Ni^{(II)}(bpy)_3(ClO_4)_2]$

The cyclic voltammetry of $[Ni^{(II)}(bpy)_3(ClO_4)_2]$ is shown in figure 4.3. There are five redox processes A, B, C, D, and E at $E_{pa} = 1.5$ V and $E_{pc} = -1.65, -2.15, -2.40$ and -2.60 V respectively.

To determine the diffusion coefficient of $[Ni^{(II)}(bpy)_3]^{2+}$ in AN containing TEAP and hence the number of electrons associated with the $[Ni^{(II)}(bpy)_3]^{2+}$ redox processes, we employed a method recently discussed in the literature by Amatore et al.[140]. It is based on the combination of microelectrode voltammetry and chronoamperometry at a macroscopic electrode. First the diffusion controlled chronoamperometric response to a potential step for the redox process is analysed according to the Cottrell

Cyclic voltammogram of $[Ni^{(II)}(bpy)_3(ClO_4)_2]$ (5 mmol dm^{-3}) in an AN solution containing TEAP (0.1 mol dm^{-3}) at GC/V. Potentials with respect to Ag/Ag$^+$ (AgClO$_4$, 0.01 mol dm^{-3}, AN). Scan rate = 100mVs^{-1}.
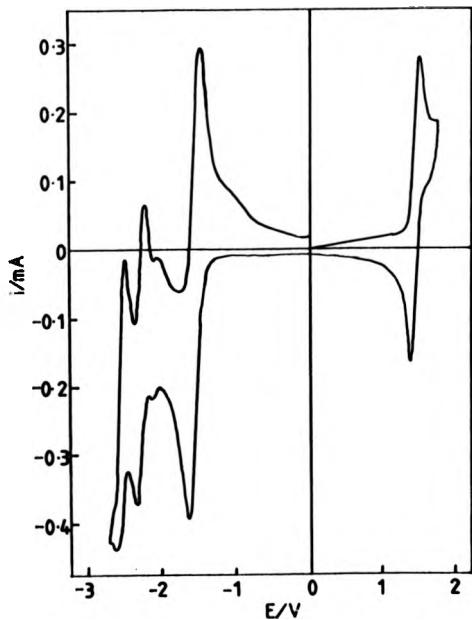
equation[140]:

$$i = \frac{nFAD^{1/2}p_\infty}{(\pi t)^{1/2}} \qquad (4.1)$$

where i is the current (A), n is the number of electrons involved in the electrode reaction, F is the faraday (C mol^{-1}), A is the area of the electrode (cm^2), D is the diffusion coefficient of P (cm^2 s^{-1}), p_∞ is the bulk concentration of P (mol cm^{-3}) and t is the time after the potential step (s). A plot of i against t$^{-1/2}$ yields a straight line passing through the origin whose gradient is given by $nFAD^{1/2}p_\infty\pi^{-1/2}$ and hence we can determine $nD^{1/2}$.

Second the diffusion controlled steady state currents, i_L, at a microelectrode over a range of p_∞ values are analysed according to the following equation[118]:

$$i_L = 4nFrDp_\infty \qquad (4.2)$$

where the notation is as previously stipulated and r is the radius of the microelectrode (cm). A plot of i_L against p_∞ will give a straight line whose gradient is given by 4nFrD. Consequently the quantity nD can be evaluated from this experiment.

Finally, n and D can be individually obtained from the experimentally determined quantities $nD^{1/2}$ and nD.

The oxidative process A and the reductive process B were both investigated in the manner described above. The chronoamperometric response for the potential step experiments are given in figure 4.4 and the corresponding Cottrell plots are given in figure 4.5. The steady state currents at a 25 μm diameter platinum microelectrode were recorded on a DVM, and the resultant plots are given in figure 4.6.

Figure 4.4:

Typical current-time curves at GC/V for an AN solution containing TEAP (0.1 mol dm^{-3}) and [Ni$^{(II)}$(bpy)$_3$(ClO$_4$)$_2$] (5 mmol dm^{-3}) for potential steps from 0.00 V to (a) 1.70 V and (b) -1.75 V. Potentials with respect to Ag/Ag$^+$ (AgClO$_4$, 0.01 mol dm^{-3}, AN).
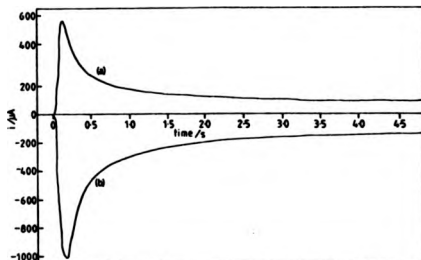
Figure 4.5:

Plot of i against t$^{-1/2}$ for the potential steps experiments shown in figure 4.4.
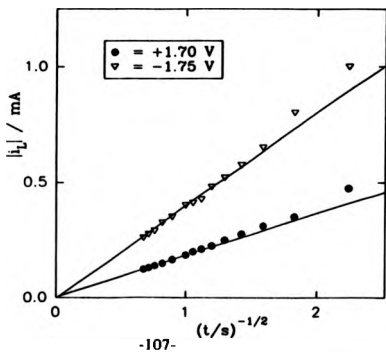
Figure 4.6:

Plot of the steady state current, i_L, against the concentration of $[Ni^{(II)}(bpy)_3(ClO_4)_2]$ in an AN solution containing TEAP (0.1 mol dm^{-3}) at a 25μ diameter platinum microelectrode held at (a) 1.70 V and (b) -1.80 V. Potentials with respect to Ag/Ag$^+$ (AgClO$_4$, 0.01 mol dm^{-3}, AN).

$[Ni(bpy)_3(ClO_4)_2]$ / mmol dm^{-3}
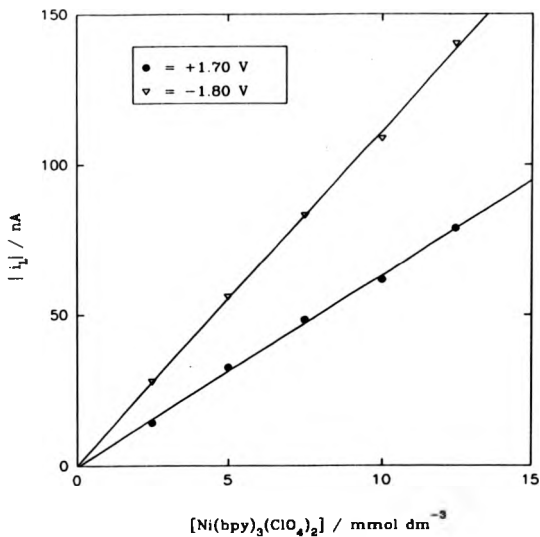
The results from these experiments are summarised in table 4.1:

Table 4.1:

Results from chronoamperometry and microelectrode voltammetry for redox processes A and B at 25°C

Redox Process	Potential Step, Microelectrode Potential (Ag/Ag⁺) /V	$nD^{1/2}$ ± 0.1 /cm s$^{-1/2}$	nD ± 0.1 x 10^{-5} /cm^2 s^{-1}	n ± 0.2	D ± 0.3 x 10^{-5} /cm^2 s^{-1}
A	0 to 1.7, 1.7	3.4 x 10^{-3}	1.3 x 10^{-5}	0.89	1.5 x 10^{-5}
B	0 to -1.8, -1.8	7.1 x 10^{-3}	2.3 x 10^{-5}	2.20	1.0 x 10^{-5}

It is pleasing to note that the two values obtained for the diffusion coefficient of $[Ni^{(II)}(bpy)_3]^{2+}$ in AN containing TEAP lie within experimental error of one another. The number of electrons associated with processes A and B are in good agreement with those obtained by controlled potential coulometry by Henne and Bartak[136]. Therefore, we can strongly dispute that a stable Ni(I) species is produced by the reductive process B as was proposed by Prasad and Scaife[139]. Instead, our results show that the $[Ni^{(II)}(bpy)_3]^{2+}$ undergoes a two-electron reduction to yield a Ni(0) species at B and a one-electron oxidation to give a Ni(III) species at A.

The number of electrons associated with processes C, D and E were determined using the chronoamperometric experiments alone and assuming the average value for the diffusion coefficient (1.25 x 10^{-5} cm^2 s^{-1}). The chronoamperometric responses and their corresponding Cottrell plots are given in figures 4.7 and 4.8 respectively. The results are summarised in table 4.2:

Figure 4.7:

Typical current-time curves for an AN solution containing TEAP (0.1 mol dm^{-3}) and [Ni$^{(II)}$(bpy)$_3$(ClO$_4$)$_2$] (5 mmol dm^{-3}) for potential steps from 0.00 V to (a) -2.20 V (b) -2.45 V and (c) -2.75 V at GC/V. Potentials with respect to Ag/Ag$^+$ (AgClO$_4$, 0.01 mol dm^{-3}, AN).
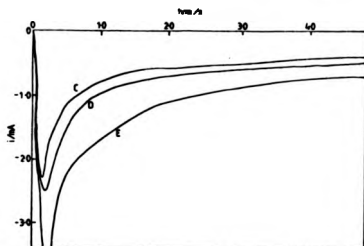
Figure 4.8:

Plot of I against t$^{-1/2}$ for the potential steps experiments shown in figure 4.7.
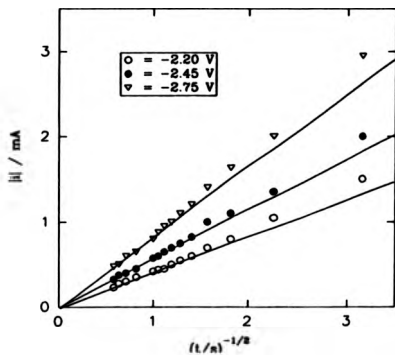
Table 4.2:

Results from chronoamperometry of processes C, D and E

Redox Process	Potential Step (Ag/Ag⁺) /V	n_T ± 0.2	n
C	0 to -2.20	2.18	0.18
D	0 to -2.45	3.00	0.82
E	0 to -2.75	4.33	1.33

n_T = total number of electrons associated with the cumulative electrode reactions

n = number of electrons associated with the individual electrode reactions

The number of electrons associated with the individual reductive processes C, D and E are all non-integer. Therefore the electrochemistry of the product of process B appears to be complicated by following homogeneous chemical reactions such as ligand loss and ligand-solvent exchange. A comparison between the CV's of the nickel complex in the presence and absence of a ten-fold excess bpy, figures 4.3 and 4.9, confirms that the ligand plays an active role in the overall electrochemistry of the nickel complex.

In order to understand the electrochemistry of $[Ni^{(II)}(bpy)_3]^{2+}$ we undertook extensive investigations. In the next section we present and discuss our proposed reaction scheme for the electrochemistry of $[Ni^{(II)}(bpy)_3]^{2+}$.

4.3.2 The reaction scheme

Figure 4.10 illustrates the reaction scheme and summaries the experimental results. The redox processes will be discussed sequentially in terms of their cyclic voltammetric, RDE and RRDE behaviour in the

Figure 4.9:

Cyclic voltammogram of $[Ni^{(II)}(bpy)_3(ClO_4)_2]$ (5 mmol dm^{-3}) in an AN solution containing bpy (0.05 mol dm^{-3}) and TEAP (0.1 mol dm^{-3}) recorded at Pt/KV. Potentials with respect to Ag/Ag$^+$ (AgClO$_4$, 0.01 mol dm^{-3}, AN). Scan rate = 100 mV s^{-1}.
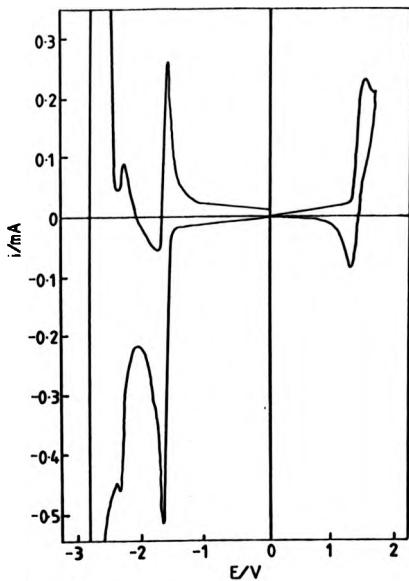
Figure 4.10

Proposed reaction scheme and summary of the electrochemistry of [Ni(bpy)$_3$](ClO$_4$)$_2$

(III)   [Ni^{III}(bpy)$_3$]$^{3+}$ $\underset{+AN}{\overset{-AN}{\rightleftharpoons}}$ Ni^{III}(bpy)$_2$AN$_2$$^{3+}$ + bpy

Quasi-reversible one-electron process   **A**

Combined CA and MV for the oxidation of [Ni^{III}(bpy)$_3$]$^{2+}$ gives n = 1, indicating a 1-electron oxidation yielding Ni(III).

CV shows single oxidation and reduction peaks. ΔE~ 60 mV and increases with ν; i_p increase with $\nu^{1/2}$ but are not proportional to it. Addition of excess bpy does not affect i_p, E_p or ΔE_p. These results are consistent with a quasi-reversible process.

RDE experiments show $i_L \propto W^{1/2}$, but is dependent on E. The i-E curves analyse according to equation (4.3) and give E° = 1.43 V, k_s = 1.2·10^{-3} cm s^{-1} and α_a = 0.28.

RDE shielding experiments detect two products of the reductive process B which can be reoxidized to two Ni(II) species which can be further oxidized to give two nickel(III) species. We propose that the nickel (III) species are [Ni^{III}(bpy)$_3$]$^{3+}$ and Ni^{III}(bpy)$_2$AN$_2$$^{3+}$.

(II)   [Ni^{II}(bpy)$_3$]$^{2+}$ $\underset{+AN}{\overset{-AN}{\rightleftharpoons}}$ [Ni^{II}(bpy)$_2$AN$_2$]$^{2+}$ + bpy

Two-electron EC process   **B**

Combined CA and MV for the reduction of [Ni^{II}(bpy)$_3$]$^{2+}$ gives n = 2, indicating a 2-electron reduction yielding Ni(0) species.

CV shows single reduction peak. E_{pc} shifts negatively with increasing ν. Reoxidation produces a well defined anodic peak with an associated shoulder. i_{pa}/i_{pc} increases with ν, but is always < 1. Addition of bpy positively shifts E_{pc} and suppresses the shoulder. These results are consistent with an EC process in which the following chemical reaction is altered by excess bpy. We propose that the shoulder is due to the reoxidation of [Ni^{0}(bpy)$_2$].

RDE experiments support CA and MV as Levich plots gives n = 2

RDE collection efficiency experiments show that the reduction products are all stable solution species.

RDE shielding experiments detect two disc products which yield two nickel(III) species. There is an unusual relationship between the ratio of the disc product and W. We explain this in terms of convective dilution affecting the position of the equilibrium between [Ni^{0}(bpy)$_3$] and [Ni^{0}(bpy)$_2$].

(C)

$$[Ni^{II}(bpy)_3] \xrightarrow{\text{fast}} [Ni^0(bpy)_2] + bpy \xrightarrow[\text{slow}]{\substack{\text{fast} \\ -AN \\ +AN}} [Ni^0(bpy)(AN)] + 2bpy$$

C
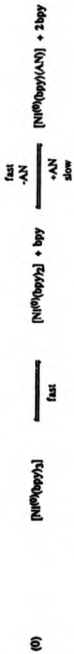
CA and MV gives n = 0.18 and 0.82 for processes C and D respectively indicating that their combined effect is the 1 electron reduction of the nickel(0) species.

CV shows process C < process D and that both are chemically reversible. Addition of excess bpy enhances D at the expense of C.

We propose that C is the reduction of $[Ni^{II}(bpy)(AN)]$ and D is the reduction of $[Ni^{II}(bpy)_2]$.

RDE experiments show that $i_c + i_D$ analyses according to the Levich equation whereas individually i_c and i_D give non-linear Levich plots. We explain this in terms of the ECE theory developed in chapter 6. We dismiss either process being due to the reduction of $[Ni^{II}(bpy)_3]$ because the relative proportions of i_c and i_D do not correspond with those recorded for the RDE shielding experiments at equivalent W.

D

$$[Ni^{(-I)}(bpy)_2]^- + bpy \xrightarrow[+AN]{-AN} [Ni^{(-I)}(bpy)(AN)]^- + 2bpy$$

(D)
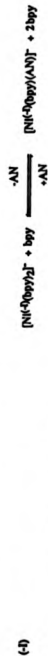
CA = chronoamperometry, MV = microelectrode voltammetry

presence and absence of excess bpy. We begin with the oxidative process A because it is the least complicated process.

4.3.2.1 Process A

Redox process A is unaltered by the presence of excess bpy. This implies that $[Ni^{(II)}(bpy)_3]^{2+}$ and its oxidation product, $[Ni^{(III)}(bpy)_3]^{3+}$, are both thermodynamically stable with respect to the ligand dissociated forms. This observation is consistent with the step-wise stability constants of $[Ni^{(III)}(bpy)_3]^{2+}$ and $[Ni^{(III)}(bpy)_3]^{3+(142)}$.

The electrochemical reversibility of process A was investigated by recording cyclic voltammogramms over a range of sweep rates, v, and polarograms over a range of rotation speeds, W.

Analysis of the CV's show that both the anodic and cathodic peak currents (i_{pa} and i_{pc}) increase with $v^{1/2}$ but are not proportional to it; the difference in the peak potentials, ΔE_p, is always greater than 60 mV and increases with increasing v; in addition the anodic peak potential, E_{pa}, shifts positively with increasing v. These observations are characteristic of a quasi-reversible system, that is, one in which the electron transfer rate is of comparable magnitude to the rate of mass transport. It should be noted that the iR drop between the reference and working electrodes could also account for the dependencies of i_p and E_p on v, however the electrochemistry of ferrocene in the same solvent-electrolyte system and at the same current density was found to have reversible v dependencies. We therefore rule out iR drop as an explaination of the behaviour for the nickel system.

The shape of the current-potential curves recorded at different rotation speeds for the redox process A is dependent on W, figure 4.11. This suggests that a kinetic step is involved in the electron transfer reaction which is consistent with the process being quasi-reversible. The

Figure 4.11:

Current-voltage curves recorded for the one-electron oxidation of
$[Ni^{(II)}(bpy)_3(ClO_4)_2]$ at GC/V in an AN solution containing
$[Ni^{(II)}(bpy)_3(ClO_4)_2]$ (5 mmol dm^{-3}) and TEAP (0.2 mol dm^{-3}). Potentials
with respect to Ag/Ag$^+$ (AgClO$_4$, 0.01 mol dm^{-3}, AN). Rotation speeds =
1, 4, 9, 16, 25, 36 and 49 Hz. Sweep rate = 10 mV s^{-1}.
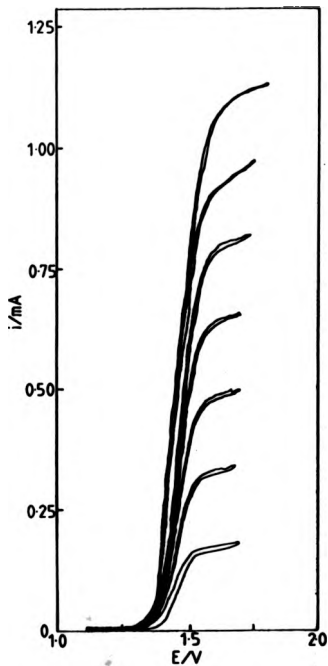
general i-E equation for a one-electron quasi-reversible reaction, where only the reduced form is present in the bulk solution is[143]:

$$\frac{nFAp_\infty}{i} = \frac{1}{k_f'} + \frac{(1 + k_b'/k_f')}{k_{D'(W-1)}W^{1/2}} \qquad (4.3)$$

where F is the faraday (C mol^{-1}), A is the electrode area (cm^2), p_∞ is the bulk concentration of the reduced species (mol cm^{-3}), k_f' and k_b' are the heterogeneous rate constants for the oxidative and reductive processes respectively (cm s^{-1}) and $k_{D'(W-1)}$ is the mass transport rate constant at 1 Hz and is given by:

$$k_{D'(W-1)} = 1.554D^{2/3}v^{-1/6} \qquad (4.4)$$

where D is the diffusion coefficient of the oxidized species (cm^2 s^{-1}) and v is the kinematic of viscosity of the electrolyte solution (cm^2 s^{-1}).

A graph of i^{-1} against $W^{-1/2}$ for data at different potentials gives a series of straight line plots whose gradients, M, and y-axis intercepts, C, are given by $[1 + (k_b'/k_f')]/k_{D'(W-1)}nFAp_\infty$ and $1/nFAp_\infty k_f'$ respectively, figure 4.12. The standard electrode potential, E^o, (V), the standard heterogeneous rate constant, k_s', (cm s^{-1}) and the transfer coefficient for the reduced species, α_o, for process A were determined from the gradients and intercepts of figure 4.12 according to the following procedure:

Let

$$\mathbf{\mathit{s}} = M - (k_{D'(W-1)}nFAp_\infty)^{-1} \qquad (4.5)$$

Figure 4.12:

Plots of the experimental data taken at potentials 1.450, 1.475, 1.500, 1.525 and 1.550 V from figure 4.11 according to equation (4.3).

and since

$$M = \frac{1 + k_b'/k_f'}{k_D'_{(W-1)}nFAp_\infty} \tag{4.6}$$

and
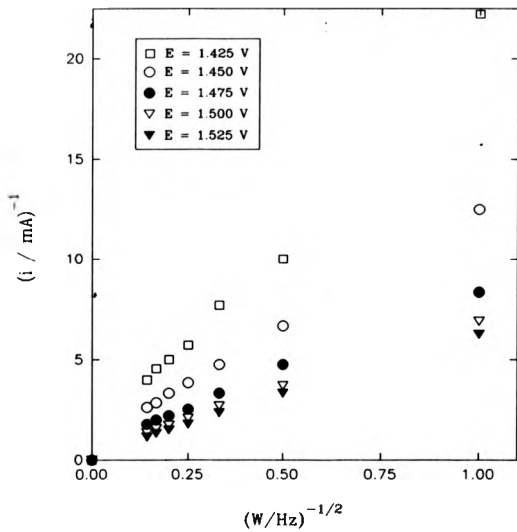
$$k_b'/k_f' = \exp[nF(E-E^o)/RT] \tag{4.7}$$

then substituting (4.6) and (4.7) into (4.5), rearranging and taking natural logs gives:

$$\ln\theta = \frac{nFE}{RT} - \frac{nFE^o}{RT} - \ln(k_D'_{(W-1)}nFAp_\infty) \tag{4.8}$$

A plot of $\ln\theta$ against E allows determination of E^o. From the intercept in figure 4.13, we obtain $E^o = 1.43$ V.

Now the intercepts of the original graph are given by:

$$C = 1/nFAp_\infty k_f' \tag{4.9}$$

and since:

$$k_f' = -k_o'\exp[\alpha_o nF(E-E^o)/RT] \tag{4.10}$$

then substituting of (4.10) into (4.9), rearranging and taking natural logs gives:

$$\ln C = -\ln(nFAp_\infty k_o') + \alpha_o F(E-E^o)/RT \tag{4.11}$$

A plot of $\ln C$ against E allows the determination of k_o' from the intercept

-118-

Figure 4.13:

Plot lnθ as a function of potential, E, according to equation (4.8).
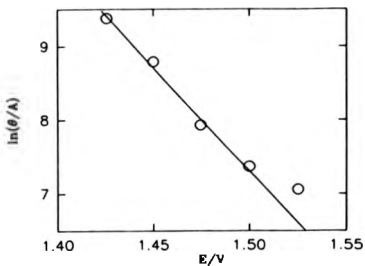
Figure 4.14:

Plot lnC as a function of potential, E, according to equation (4.11).
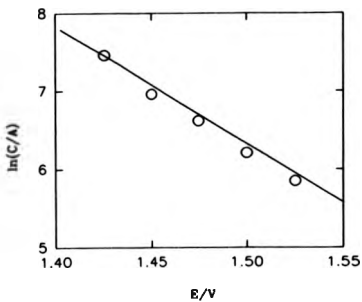
and of α_0 from the gradient, figure 4.14. The values for k_0' and α_0 were found to be 1.3×10^{-2} cm s^{-1} and 0.64 respectively.

In summary we find for redox process A:

$$[Ni^{(II)}(bpy)_3]^{2+} + e \xrightarrow{\quad k_0' = 1.3 \times 10^{-2} \text{ cm s}^{-1} \quad} [Ni^{(III)}(bpy)_3]^{3+} \qquad E^o = 1.43 \text{ V}$$

4.3.2.2 Process B

Redox process B is concerned with the two-electron reduction of $[Ni^{(II)}(bpy)_3]^{2+}$ and the reoxidation of the resultant nickel(0) species. We propose that $[Ni^{(II)}(bpy)_3]^{2+}$ is electrochemically reduced to $[Ni^{(0)}(bpy)_3]$ which then undergoes following homogeneous ligand loss and ligand-solvent exchange reactions in order to establish the following equilibria:

$$[Ni^{(0)}(bpy)_3] \xrightarrow{\quad\quad} [Ni^{(0)}(bpy)_2] + bpy \xrightarrow[+AN]{-AN} [Ni^{(0)}(bpy)AN] + 2bpy$$
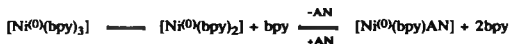
We further propose that the $[Ni^{(0)}(bpy)_3]$ and $[Ni^{(0)}(bpy)_2]$ are reoxidised to $[Ni^{(II)}(bpy)_3]^{2+}$ and $[Ni^{(II)}(bpy)_2]^{2+}$ respectively and that $[Ni^{(0)}(bpy)AN]$ is more difficult to reoxidise. Instead $[Ni^{(0)}(bpy)AN]$ recombines with bpy in order to maintain the thermodynamic equilibria at the electrode surface while $[Ni^{(0)}(bpy)_3]$ and $[Ni^{(0)}(bpy)_2]$ are reoxidised. The results from cyclic voltammetry, RDE and RRDE experiments allow us to postulate that the initial bpy loss is rapid; the replacement of bpy with AN is comparatively slow and that the recombination of bpy with $[Ni^{(0)}(bpy)AN]$ is rapid, i.e. the equilibrium in this case lies to the left hand side. Therefore process B can be represented by the following square scheme:

$$[Ni^{(II)}(bpy)_3]^{2+} \rightleftharpoons [Ni^{(II)}(bpy)_2]^{2+} + bpy$$

$$-2e \Big\Updownarrow +2e \qquad B \qquad -2e \Big\Updownarrow +2e$$

$$[Ni^{(0)}(bpy)_3] \underset{fast}{\overset{}{\rightleftharpoons}} [Ni^{(0)}(bpy)_2] + bpy \underset{+AN}{\overset{fast\ -AN}{\rightleftharpoons}} [Ni^{(0)}(bpy)AN] + 2bpy$$
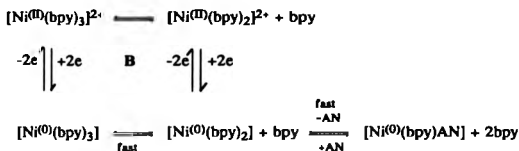
In the presence of a ten-fold excess of bpy, process B behaves like a simple reversible redox couple. This is because the additional bpy forces the equilibria to the left hand side thereby precluding the electrochemistry of either dissociated nickel species. This is exactly what we see, figure 4.9.

In the absence of excess bpy we observe a positive shift in the E_{pc} (+15 mV for every ten-fold reduction in bpy concentration) and the appearance of a small shoulder located on the positive side of the reoxidation peak. These observations can both be explained in terms of the square scheme. First, the positive shift in the position of E_{pc} is because the ligand dissociation reduces the concentration of $[Ni^{(0)}(bpy)_3]$ at the electrode surface when compared to that of the simple electron transfer reaction, and therefore in order to maintain a Nerstian equilibrium at the electrode surface there will be a positive shift in the peak potential, i.e. an EC mechanism. Second, the shoulder is attributed to the oxidation of $[Ni^{(0)}(bpy)_2]$ which forms by the loss of a bpy ligand from $[Ni^{(0)}(bpy)_3]$. This assignment is supported by the RDE and RRDE experiments described later.

No reoxidation of $[Ni^{(0)}(bpy)AN]$ is observed. This can be accounted for if we assume that $[Ni^{(0)}(bpy)AN]$ is the most difficult of the nickel(0) complexes to reoxidise and that it rapidly recombines with bpy in order to maintain thermodynamic equilibrium. Consequently as the $[Ni^{(0)}(bpy)_3]$ and $[Ni^{(0)}(bpy)_2]$ are reoxidised then $[Ni^{(0)}(bpy)AN]$ recombines with a free bpy thereby precluding its own reoxidation. A

consideration of the formal electron count on nickel and the back bonding ability of the ligands supports this rationale because the relative ease of oxidation of the three nickel(0) species will be $[Ni^{(0)}(bpy)_3] > [Ni^{(0)}(bpy)_2] > [Ni^{(0)}(bpy)AN]$.

The cyclic voltammetry of $[Ni^{(II)}(bpy)_3]^{2+}$ in the absence of excess bpy is affected by sweep rate. E_{pc} shifts in the negative direction with increasing v, and i_{pa}/i_{pc} increases with increasing v but is always less than one. These observations are as expected for an EC type process.

Polarograms recorded for process B at a RDE over a range of rotation speeds are given in figure 4.15. At the more negative potentials, < -1.4 V, a dark blue/purple material streams away from the RDE. An independent synthesis of $[Ni^{(0)}(bpy)_2]$ shows it to be a dark purple solid which further supports the view that $[Ni^{(0)}(bpy)_2]$ is a product of the reductive process B.

The relationship between the limiting current, i_L, and the rotation speed, W, is given by the Levich equation[144]:

$$i_L = \frac{1.554 nFAD^{2/3} p_\infty W^{1/2}}{v^{1/6}} \tag{4.12}$$

where the symbols have their usual meaning. A plot of i_L against $W^{1/2}$ yields a straight line passing through the origin, figure 4.16. The value for n determined from the gradient is 1.89 assuming D is 1.25×10^{-5} cm^2 s^{-1} and v is 3.29×10^{-3} cm^2 s^{-1}. It is pleasing that this value for n is consistent with the one obtained using the combined techniques of chronoamperometry and microelectrode voltammetry.

A series of experiments were attempted using the RRDE to study the products of the two-electron reduction of $[Ni^{(II)}(bpy)_3]^{2+}$. However, the ring poisoned readily at potentials less than approximately -2.2 V, so

Figure 4.15:

Current-voltage curves recorded for the two-electron reduction of $[Ni^{(II)}(bpy)_3(ClO_4)_2]$ (5 mmol dm^{-3}) in an AN solution containing TEAP (0.1 mol dm^{-3}) at the RDE GC/V. Potentials with respect to Ag/Ag^+ ($AgClO_4$, 0.01 mol dm^{-3}, AN). Rotation speeds = 1, 4, 9, 16, 25, and 36 Hz. Sweep rate = 10 mV s^{-1}.
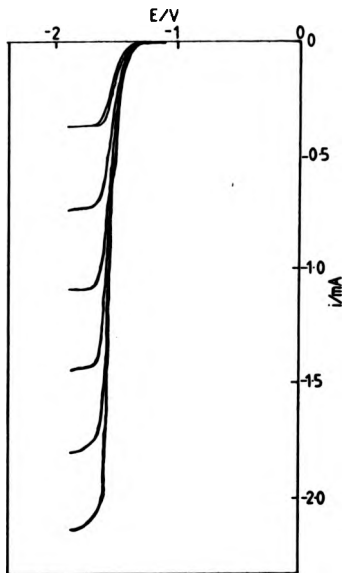
Figure 4.16:

Levich plot of the experimental data in figure 4.15.
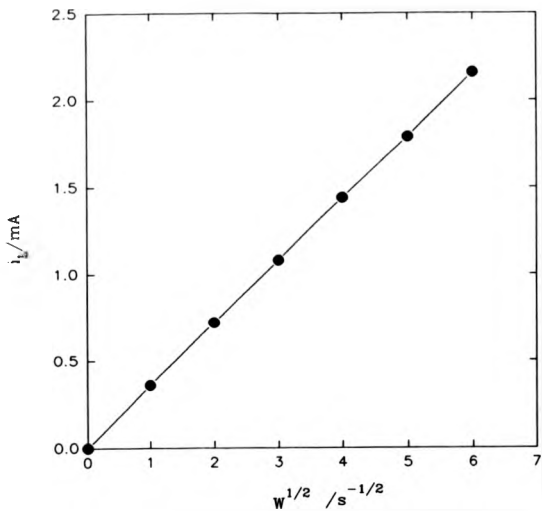
this technique was confined to the investigation of the oxidative electrochemistry of the products of process B. Initially, collection efficiency experiments were carried out to confirm that the products of process B were stable solution species. Under these circumstances the ratio of the ring and disc currents, i_R and i_D respectively, is given by[145]:

$$-N_o = \frac{i_R}{i_D} \qquad (4.13)$$

where N_o is the steady state collection efficiency which is calculated from the electrode geometry. The RRDE used for these experiments has a calculated N_o of 0.21 which compares well with an experimentally determined value of 0.20 using the known stable reversible redox couple, ferrocene. Typically the potential of the disc electrode, E_D, was swept between 0.0 and -2.0 V, and the ring potential, E_R, was held at -0.4 V. The ring and disc currents, were recorded as a function of disc potential as shown in figure 4.17. The ratio of the ring/disc currents is 0.19(8) which confirms that the disc products are not lost in non-faradaic processes such as adsorption or production of electroinactive species caused by a following chemical reaction.

Next, shielding experiments were carried out. Typically, the disc electrode was held at a potential corresponding to the limiting current plateau of process B, -1.8 V, and the ring potential, E_R, was scanned over the range +2.0 to -2.0 V. The ring current, i_R, was recorded as a function of E_R at different rotation rates. Figure 4.18 shows a typical ring polarogram at 9 Hz and compares it to a control polarogram recorded with the disc held at 0.0 V. Clearly there are two complexes produced at the disc which are then detected at the ring. The mass transport controlled reoxidation of the major species is at -1.6 V and that of the minor species is at -1.2 V.

Figure 4.17:

Disc and ring currents recorded as a function of disc potential for the two electron reduction of $[Ni^{(II)}(bpy)_3(ClO_4)_2]$ (5 mmol dm^{-3}) in an AN solution containing TEAP (0.1 mol dm^{-3}) at the RRDE Pt/Pt/T. Ring potential = -0.4 V. Potentials with respect to Ag/Ag$^+$ (AgClO$_4$, 0.01 mol dm^{-3}, AN). Rotation speed = 9 Hz. Sweep rate = 10 mV s^{-1}.
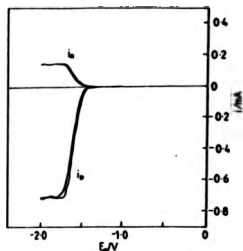
Figure 4.18:

Ring current-voltage curves recorded in an AN solution containing $[Ni^{(II)}(bpy)_3(ClO_4)_2]$ (5 mmol dm^{-3}) and TEAP (0.1 mol dm^{-3}) at the RRDE Pt/Pt/T. Disc potential: (a) -1.8 V and (b) 0.0 V. Potentials with respect to Ag/Ag$^+$ (AgClO$_4$, 0.01 mol dm^{-3}, AN). Rotation speed = 9 Hz. Sweep rate= 10 mV s^{-1}.

-126-
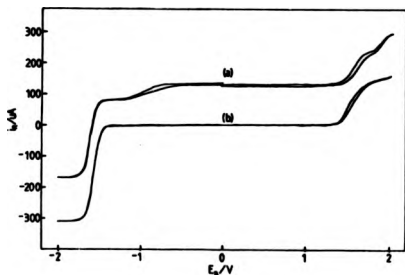
Now, according to our reaction scheme the major and minor disc products are $[Ni^{(0)}(bpy)_3]$ and $[Ni^{(0)}(bpy)_2]$ respectively. Consequently, addition of excess bpy to the electrolyte solution should cause the ring current assigned to the two-electron reoxidation of $[Ni^{(0)}(bpy)_3]$ to increase at the expense of that for $[Ni^{(0)}(bpy)_2]$. This is because the excess bpy suppresses the ligand dissociation reaction thereby preventing the formation of $[Ni^{(0)}(bpy)_2]$. This indeed is what we observe.

Interestingly, the ring current corresponding to the nickel(II)/(III) reoxidation is also split into two waves in the absence of excess bpy. The mass transport controlled reoxidation of the major species is at 1.8 V and that of the minor species is at 2.0 V. The relative height of each wave is the same as that for the two waves in the nickel(0)/(II) reoxidation waves. We propose that the major and minor waves are due to the one-electron oxidations of $[Ni^{(II)}(bpy)_3]^{2+}$ and $[Ni^{(II)}(bpy)_2]^{2+}$ to $[Ni^{(III)}(bpy)_3]^{3+}$ and $[Ni^{(III)}(bpy)_2]^{3+}$ respectively This assignment is supported by the suppression of the minor nickel(II)/(III) reoxidation wave by the addition of excess bpy. Consequently the following square scheme is proposed:

$$[Ni^{(III)}(bpy)_3]^{3+} \rightleftharpoons [Ni^{(III)}(bpy)_2]^{3+} + bpy$$

$$-e \updownarrow +e \qquad\qquad -e \updownarrow +e$$

$$[Ni^{(II)}(bpy)_3]^{2+} \rightleftharpoons [Ni^{(II)}(bpy)_2]^{2+} + bpy$$

We adopted a procedure described by Albery et al.[146] for studying first-, pseudo-first- and second- order homogeneous reactions following an electron transfer reaction at a RRDE. The experimental procedure for each case involves scanning the disc potential over the region where the reaction of interest is occurring whilst holding the ring potential at a value where a particular intermediate is oxidised or reduced. The ring

-127-

current is recorded as a function of the disc current at different potentials. Analysis of the experimental data depends on the reaction order.

This procedure was adopted to investigate the following two experimental modes:

Mode I

Disc: $[Ni^{(II)}(bpy)_3]^{2+} \longrightarrow [Ni^{(0)}(bpy)_3]$ $E_D = 0$ to -2.0 V

Solution: $[Ni^{(0)}(bpy)_3] \longrightarrow [Ni^{(0)}(bpy)_2] + bpy$

Ring: $\begin{cases} [Ni^{(0)}(bpy)_3] \longrightarrow [Ni^{(II)}(bpy)_3]^{2+} \\ [Ni^{(0)}(bpy)_2] \longrightarrow [Ni^{(II)}(bpy)_2]^{2+} \end{cases}$ $E_R = -0.4$ V
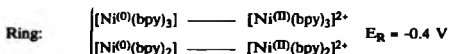
Mode II is the same as for mode I except that $E_R = -1.2$ V so that only $[Ni^{(0)}(bpy)_3]$ was reoxidised at the ring.

Figure 4.19 shows a typical i_R-i_D trace for mode I recorded at 36 Hz. The ring current increases linearly with the disc current and the gradient is equal to the steady state collection efficiency, N_o. The gradient is found to be independent of rotation speed. This result is as expected and confirms the previous observation that none of the disc products are lost in non-faradaic processes because all the nickel is either $[Ni^{(0)}(bpy)_3]$ or $[Ni^{(0)}(bpy)_2]$. No kinetic information can be extracted from this result, but it confirms that all the nickel is either as $[Ni^{(0)}(bpy)_3]$ or $[Ni^{(0)}(bpy)_2]$.

Figure 4.20 shows a typical series of i_R-i_D traces for mode II recorded over a range of rotation speeds. Table 4.3 summaries the data from these traces. The shape of the traces immediately allows us to eliminate simple first- or pseudo-first- order homogeneous reaction kinetics. This is because they would both produce linear traces whose

-128-

Figure 4.19:

Ring current-disc current curves recorded for the two-electron reduction of [Ni(II)(bpy)$_3$(ClO$_4$)$_2$] (5 mmol dm^{-3}) in an AN solution containing TEAP (0.1 mol dm^{-3}) at the RRDE Pt/Pt/T. Ring potential = -0.4 V. Disc potential scanned over the range -1.0 to -2.0 V. Rotation speed = 36 Hz. Sweep rate = 10 mV s^{-1}. Potentials with respect to Ag/Ag$^+$ (AgClO$_4$, 0.01 mol dm^{-3}, AN).
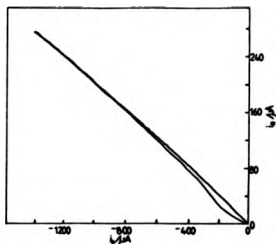
Figure 4.20:

Ring current-disc current curves recorded for the two-electron reduction of [Ni(II)(bpy)$_3$(ClO$_4$)$_2$] (5 mmol dm^{-3}) in an AN solution containing TEAP (0.1 mol dm^{-3}) at the RRDE Pt/Pt/T. Ring potential = -1.2 V. Disc potential scanned over the range -1.0 to -2.0 V. Rotations speed = 1, 4, 9, 16, 25, 36 and 49 Hz. Sweep rate = 10 mV s^{-1}. Potentials with respect to Ag/Ag$^+$ (AgClO$_4$, 0.01 mol dm^{-3}, AN).
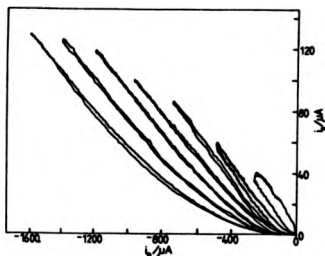
gradients would increase with increasing rotation speed[146]. This is a somewhat surprising result as the reaction scheme suggests that we should observe first-order kinetics. Instead, the shape of the i_R-i_D responses suggests second order reaction kinetics[146]. In view of the composition of the solution, this is not very likely because other than AN or TEAP there is ostensibly nothing with which the disc product can react. Reaction with either AN or TEAP would produce classic pseudo-first order reaction kinetics. There may be small amounts of water or dissolved oxygen in the electrolyte solution which are reacting with the disc products. However, addition of small quantities of water or oxygen produced such dramatic changes to the i_R-i_D traces, (figures 4.21 and 4.22) that we can conclude that neither could cause the typical responses.

Table 4.3:

Table of data taken from figure 4.20

Rotation Rate (Hz)	Gradient of Linear Portion of i_R-i_D trace	Intercept on y axis by Linear Extrapolation
1	0.160	400
4	0.130	305
9	0.142	237
16	0.138	175
25	0.136	130
36	0.133	57
49	0.136	27

Figure 4.21:

Ring current-disc current curves recorded under the same conditions described in legend to figure 4.19 following the addition of water (0.5 mM) to the electrolyte solution. Rotation speed = 9 Hz.
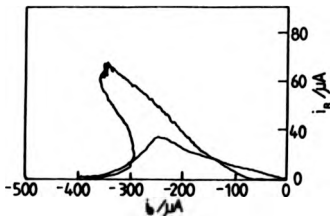
Figure 4.22:

Ring current-disc current curves recorded under the same conditions described in legend to figure 4.19 using an air saturated electrolyte solution Rotation speed = 9 Hz.
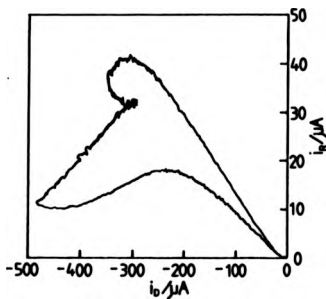
The experimental i_R-i_D traces were analysed for second order homogeneous reaction kinetics according to the method of Albery[146]. For the RRDE Pt/Pt/K pairs of values of N' and i_D'/M used for this analysis are given in appendix 4.1. Lines of gradient N' are drawn on the i_R-i_D curves and the value of i_D where these constructed lines cross the curves is read off, $i_{D_{Obs}}$. Each $i_{D_{Obs}}$ value is then plotted against the value of i_D'/M corresponding to that particular N', figure 4.23.

Typical plots of $i_{D_{Obs}}$ against i_D'/M for a second order homogeneous reaction are linear and can be extrapolated through the origin. The gradient of each plot is M for each rotation speed. Any deviation of the points tends to be towards the x-axis. Deviation is most common at high rotation speeds and low disc currents. Obviously our data does not conform to this regime so we can conclude that simple second order reaction kinetics cannot explain our data.

Finally we investigated the relationship between rotation speed and the relative quantities of $[Ni^{(0)}(bpy)_3]$ and $[Ni^{(0)}(bpy)_2]$ detected at the ring. Increasing W decreases the time taken to transport the disc products to the ring. Consequently, high rotation speeds favour the detection of the unstable species, whereas low rotation speeds favour the detection of the products of the unstable species. In this case, $[Ni^{(0)}(bpy)_3]$ loses a bpy ligand and is therefore expected increasingly to dominate the ring current as W is increased, whereas $[Ni^{(0)}(bpy)_2]$ is expected to be more dominant at low W. The data in table 4.4 shows that the reverse effect is observed. This apparent anomally with the proposed reaction scheme can be explained in terms of the unusual effect convective dilution has on the position of the equilibrium between $[Ni^{(0)}(bpy)_3]$ and its dissociation products, $[Ni^{(0)}(bpy)_2]$ and bpy.

Plot of the observed disc current taken from the experimental data in figure 4.20 as a function of the calculated values of i_D'/M.
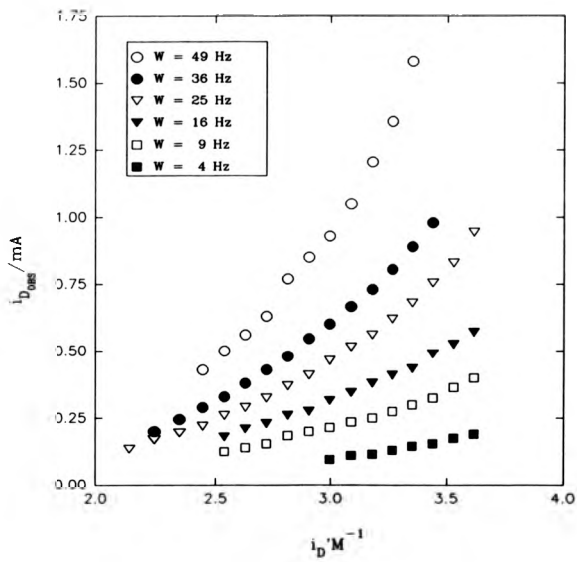
Table 4.4:

Table of ring crrents corresponding to the reoxidation of the disc products of process B recorded at Pt/Pt/K for an AN solution containing $[Ni^{(II)}(bpy)_3(ClO_4)_2]$ (5 mmol dm^{-3}) and TEAP (0.1 mol dm^{-3})

	Rotation Speed /Hz				
	1	4	9	16	25
Ring current due to oxidation of both disc products (μA)	95	180	273	363	465
Ring current due to oxidation of minor disc product (μA)	15	30	53	78	100
Ring current due to oxidation of major disc product (μA)	80	150	220	285	365
Ratio of major to minor ring currents	5.3	5.0	4.2	3.7	3.7

Now, a RDE acts like a pump, drawing solution towards it from the bulk and flinging it out centrifugally close to the disc surface. A species generated at the disc will be diluted by this pump action as it is flung towards the ring. Obviously, the faster the rotation speed the greater the convective dilution. Ordinarily, convective dilution simply results in a constant fraction of the disc products being collected at the ring. However, in this case, it has a more complex influence because the disc products are related by the following equilibrium:

$$[Ni^{(0)}(bpy)_3] \overset{K}{\rightleftharpoons} [Ni^{(0)}(bpy)_2] + bpy$$

where K is the equilibrium constant, (mol dm^{-3}). Although dilution will affect each species equally the equilibrium will also be upset. In order to

-134-

counter the influence of dilution and restore the thermodynamic equilibrium, more of the $[Ni^{(0)}(bpy)_3]$ must undergo the ligand dissociation reaction. Since convective dilution increases with rotation speed its influence will become more dominant at high W therefore the equilibrium position will increasingly favour the formation of $[Ni^{(0)}(bpy)_2]$ and [bpy]. It should be noted that in order for convective dilution to affect the relative proportions of the disc products detected at the ring, we must assume the ligand dissociation reaction is fast.

In conclusion, we propose that there are two factors which have a conflicting influence on the relationship between W and the relative amounts of $[Ni^{(0)}(bpy)_3]$ and $[Ni^{(0)}(bpy)_2]$ detected at the ring. The experimental results show that the influence of convective dilution is dominant.

Returning to the Albery analysis, and bearing in mind that the homogeneous chemical reaction following the two-electron reduction of $[Ni^{(II)}(bpy)_3]^{2+}$ is complicated by convective dilution, it is reasonable that our i_R-i_D data would not conform to the classical analysis for a first order EC process. This is because the Albery analysis does not account for the unusual effect convective dilution has on the position of the equilibrium between $[Ni^{(0)}(bpy)_3]$ and $[Ni^{(0)}(bpy)_2]$ + bpy. Consequently, the i_R-i_D data does not rule out our reaction scheme, instead it supports the hypothesis that the ring current responses are complicated by convective dilution.

4.3.2.3 Processes C and D

We have already surmised that the two-electron reduction of $[Ni^{(II)}(bpy)_3]^{2+}$ leads to the formation of three nickel(0) species. Therefore any subsequent reductive electrochemistry must account for the fate of these three complexes. We propose that processes C and D correspond to the one-electron reductions of $[Ni^{(0)}(bpy)AN]$ and

-135-

$[Ni^{(0)}(bpy)_2]$ respectively and that $[Ni^{(0)}(bpy)_3]$ is resistant to further reduction. Instead $[Ni^{(0)}(bpy)_3]$ rapidly undergoes bpy dissociation to maintain thermodynamic equilibrium as $[Ni^{(0)}(bpy)AN]$ and $[Ni^{(0)}(bpy)_2]$ are reduced at the electrode surface. The relative ease of reduction of the three nickel(0) complexes is predicted to be $[Ni^{(0)}(bpy)AN] > [Ni^{(0)}(bpy)_2] > [Ni^{(0)}(bpy)_3]$. This trend is based on the formal electron count of the nickel in each complex and the back bonding abilities of bpy and AN. Our proposed reaction scheme conforms to this trend.

Henne and Bartak[136] assign C and D to the one-electron reductions of $[Ni^{(0)}(bpy)_2]$ and $[Ni^{(0)}(bpy)_3]$ respectively. We have rejected this assignment because it predicts that the relative amounts reduced in processes C and D must match those oxidised at the ring. Our results conclusively show that this is not the case. Therefore we must introduce an additional product of the reductive process B which is more readily reduced, but more resistant to reoxidation than $[Ni^{(0)}(bpy)_2]$. $[Ni^{(0)}(bpy)AN]$ fits these criteria.

The reduction and following reoxidation of $[Ni^{(0)}(bpy)_2]$ and $[Ni^{(0)}(bpy)AN]$ can be represented by the following square scheme:

$$[Ni^{(0)}(bpy)_3] \underset{fast}{\rightleftharpoons} [Ni^{(0)}(bpy)_2] + bpy \underset{\substack{+AN \\ slow}}{\overset{\substack{fast \\ -AN}}{\rightleftharpoons}} [Ni^{(0)}(bpy)AN] + 2bpy$$

$$D \; {-e \atop +e} \Big\updownarrow \qquad\qquad\qquad C \; {-e \atop +e} \Big\updownarrow$$

$$[Ni^{(-I)}(bpy)_2]^- + bpy \longrightarrow [Ni^{(-I)}(bpy)AN]^- + 2bpy$$
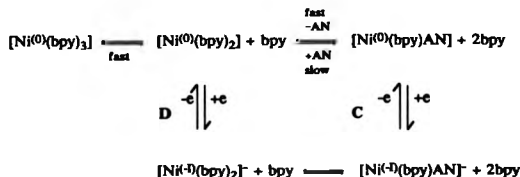
The chronoamperometry results discussed earlier indicated that $[Ni^{(0)}(bpy)AN]$ is a minor product of the reductive process C since it accounts for only 18% of the nickel(0) to nickel(-I) reduction. The

-136-

remaining 82% of the nickel(0) is reduced in process D. The cyclic voltammetry qualitatively supports the chronoamperometry because the peak heights of the redox couple C are considerably smaller than those of process D. However this technique yielded little mechanistic information because it proved difficult to determine accurate values for i_p and E_p.

The addition of bpy to the electrolyte solution affects the relative peak heights of redox processes C and D. An increase in bpy concentration suppresses, and eventually eliminates, C, while simultaneously, D gradually increases to a finite size. This is as expected because the additional bpy forces the equilibrium between $[Ni^{(0)}(bpy)_2]$ and $[Ni^{(0)}(bpy)AN] + bpy$ to the left hand side thereby precluding any $[Ni^{(0)}(bpy)AN]$ electrochemistry.

The relationship between processes C and D was more fully investigated using a RDE. This is because we found that the current contributions of the two electrode reactions were most easily distinguished using this technique. A typical polarogram recorded over the potential region 0.0 to -2.7 V is shown in figure 4.24. The data presented in table 4.5 is taken from similar polarograms recorded at different rotation speeds.

Current-voltage curves recorded of $[Ni^{(II)}(bpy)_3(ClO_4)_2]$ (5 mmol dm^{-3}) in an AN solution containing TEAP (0.1 mol dm^{-3}) at the RDE Pt/KV. Rotation speed = 36 Hz. Sweep rate = 20 mV s^{-1}. Potentials with respect to Ag/Ag$^+$ (AgClO$_4$, 0.01 mol dm^{-3}, AN).
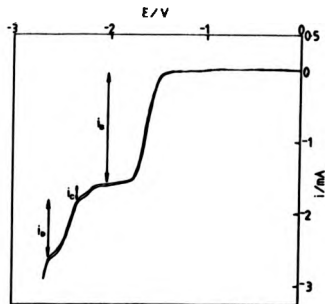
Figure 4.25:

Levich plots of the experimental data in table 4.5.
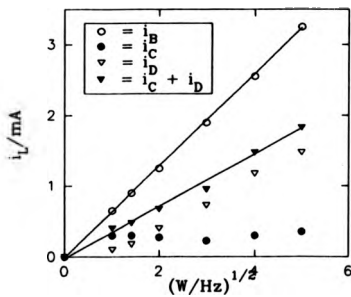
Table 4.5:

Table of limiting current contributions for the reductive processes B, C
and D recorded at Pt/KV for an AN solution containing
$[Ni^{(II)}(bpy)_3(ClO_4)_2]$ (4.5 mmol dm^{-3}) and TEAP (0.1 mol dm^{-3})

Rotation Speed /Hz	I_B (μA)	I_C (μA)	I_D (μA)	$I_C + I_D$ (μA)
1	650	300	100	400
2	900	300	175	475
4	1250	275	400	675
9	1900	225	725	950
16	2550	300	1175	1475
25	3250	350	1475	1825

Analysis of these data according to the Levich equation shows that
the reductive process B, and the combined currents for processes C and D
yield straight line plots passing through the origin with gradients of 6.55
x 10^{-4} and 3.55 x 10^{-4} A s$^{1/2}$ respectively, figure 4.25. The ratio of the
slopes is 1.85. If we assume that the diffusion coefficients of
$[Ni^{(II)}(bpy)_3]^{2+}$, $[Ni^{(0)}(bpy)_2]$ and $[Ni^{(0)}(bpy)AN]$ are the same, then the
ratio of the slopes would be 2 because B is assigned to a two-electron
reduction and C plus D to a one-electron reduction. The discrepancy
between these values is probably due to the smaller diffusion coefficients
of $[Ni^{(0)}(bpy)_2]$ and $[Ni^{(0)}(bpy)AN]$ reflecting their smaller size.

Individual Levich plots of I_C and I_D are both non-linear, figure 4.25.
This implies that the currents I_C and I_D are under kinetic control as well
as mass transport control. At slow rotation speeds the reduction of
$[Ni^{(0)}(bpy)AN]$ to $[Ni^{(-I)}(bpy)AN]^-$ is the dominant process, whereas at

-139-

fast rotation speeds the reduction of $[Ni^{(0)}(bpy)_2]$ to $[Ni^{(-I)}(bpy)_2]^-$ dominates. These observations can be readily interpreted in terms of our reaction scheme: When the electrode is held at a potential corresponding to the current plateau of process C we postulate the following four-step reaction sequence:

$$[Ni^{(II)}(bpy)_3]^{2+} + 2e \rightleftharpoons [Ni^{(0)}(bpy)_3]$$

$$[Ni^{(0)}(bpy)_3] \xrightarrow{fast} [Ni^{(0)}(bpy)_2] + bpy$$

$$[Ni^{(0)}(bpy)_2] + AN \underset{slow}{\overset{k}{\rightleftharpoons}} [Ni^{(0)}(bpy)AN] + bpy$$

$$[Ni^{(0)}(bpy)AN] + e \rightleftharpoons [Ni^{(-I)}(bpy)AN]^-$$
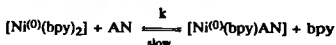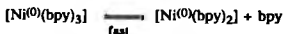
The first two steps involve the electrochemical reduction of $[Ni^{(II)}(bpy)_3]^{2+}$ forming a 20-electron nickel(0) complex which rapidly loses a bpy ligand to give an 18-electron complex. The third step is a ligand exchange reaction which results in the replacement of a bpy by AN. The final step involves the one-electron reduction of the ligand exchange product. We assume that the first bpy loss occurs significantly faster than the following ligand exchange reaction and in the absence of excess bpy we treat it as irreversible. Consequently, this reaction sequence may be regarded as an ECE process whose rate determining step is step 3. The overall rate constant, k, is pseudo-first order because the AN is obviously in large excess.

At slow rotation speeds, more of the $[Ni^{(0)}(bpy)AN]$ will have formed in the diffusion layer than at faster rotation speeds. This means that the slower the rotation speed the greater the relative current contribution from the fourth step in the reaction sequence. Now, if the electrode potential is extended in the negative direction so that the

current plateau corresponding to i_D is encountered, then the $[Ni^{(0)}(bpy)_2]$ which did not have time to undergo the ligand exchange reaction, will be reduced. The current corresponding to the reduction of $[Ni^{(0)}(bpy)_2]$ will therefore increase relative to the current contribution from the reduction of $[Ni^{(0)}(bpy)AN]$ as the rotation speed is increased.

The theory necessary to describe the total limiting current at plateau C has been derived in chapter 6. It is a special case of the second order ECE analysis at a RDE in which one of the reactants is in large excess and corresponds to case I of the theory. The pertinent equations are:

$$i_L = \frac{nFADp_\infty}{X_D}\left(1+\frac{\pi}{3}\right) \qquad (6.45)$$

$$X_D = 0.643\nu^{1/6}D^{1/3}W^{-1/2} \qquad (4.14)$$

and

$$\pi = \frac{kX_D^2}{D} \qquad (6.16)$$

where in this case p_∞ is the bulk concentration of $[Ni^{(II)}(bpy)_3(ClO_4)_2]$, and $i_L = i_B + i_C$.

In the derivation of equation (6.45) we have assumed that n was the same in both steps. In order to account for the number of electrons in the first and second chemical steps being 2 and 1 respectively we need to make a trivial extension to get to the following equation:

$$i_L = \frac{nFADp_\infty}{X_D}\left(2+\frac{kX_D^2}{3D}\right) \qquad (4.15)$$

-141-

Combining equations (4.14) and (4.15) and rearranging gives:

$$\frac{i_L}{W^{1/2}} = \frac{3.108FAD^{2/3}p_{\infty}}{v^{1/6}} + \frac{0.214FAD^{1/3}v^{1/6}kp_{\infty}}{W} \quad (4.16)$$

A plot of $i_L W^{-1/2}$ against W^{-1}, figure 4.26, allows the rate constant, k, to be determined from the gradient as 0.7 ± 0.1 s^{-1} assuming D to be 1.25×10^{-6} cm^2 s^{-1} and v to be 3.29×10^{-3} cm^2 s^{-1}. The intercept on the y-axis is an experimentally determined point as it is the Levich gradient for the reductive process B, $6.5 \times 10^{-4} \pm 0.2 \times 10^{-4}$ A $s^{1/2}$. At low rotation speeds the points tend to deviate from the line. This is because the theory for case I has assumed that $kX_D^2/D \ll 1$, but at low rotation speeds $kX_D^2/D \rightarrow 1$. Therefore at low W, the boundary between cases I and III is being crossed. In terms of the chemistry this means that very little $[Ni^{(0)}(bpy)_2]$ is able to cross the diffusion layer without undergoing the ligand exchange reaction.

Our attempts to investigate processes C and D using the RRDE were frustrated by rapid poisoning of the ring.

4.3.2.4 Process E

The addition of bpy to the electrolyte solution causes the charge associated with the redox couple E to increase dramatically. This observation and the position of the couple confirms that it is due to the reduction of bpy:

$$bpy + e \rightleftharpoons bpy^-$$

The presence of free bpy confirms that at least some of the products of the reductive processes B, C and/or D undergo ligand loss. The chronoamperometric results show that approximately $1\frac{1}{4}$ bpy are lost per nickel if we assume that the diffusion coefficient of bpy is of the

Plots of the experimental data in table 4.5 according to equation (4.16).
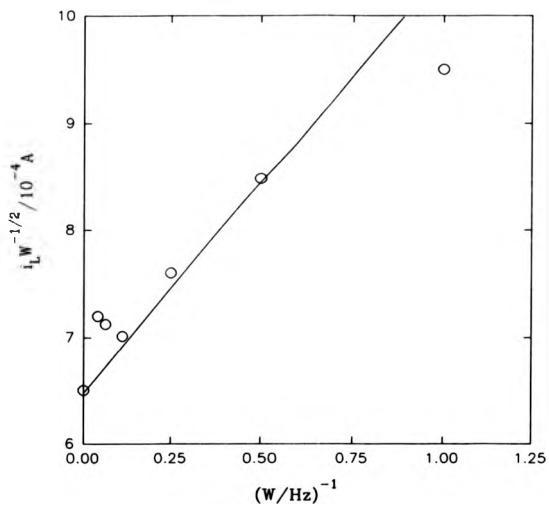
same order as that of $[Ni^{(II)}(bpy)_3(ClO_4)_2]$. This is consistent with the proposal that most of the nickel(-I) has lost one bpy ligand, $[Ni^{(-I)}(bpy)_2]^-$, and that the remaining nickel(-I) has lost two bpys, $[Ni^{(-I)}(bpy)AN]^-$.

4.3.3 Summary

A comparison between our results with those reported in the literature allows us to draw the following conclusions:

1. Prasad and Scaife[139] are incorrect in their assignment of process B to a one-electron reduction. The formation of a stable nickel(I) can be rejected based on our chronoamperometry, microelectrode voltammetry and RDE experiments. All clearly indicate that process B is a two-electron reduction leading to the formation of a stable solution free nickel(0) species.

2. Tanaka *et al.*[137,138] propose that there is a pre-wave associated with process B which is due to the reduction of $[Ni^{(II)}(bpy)_2]^{2+}$ which has formed from the ligand dissociation of $[Ni^{(II)}(bpy)_3]^{2+}$. We observed no equivalent pre-wave in the presence, or absence, of excess bpy although the foot of the CV and the polarogram of process B are notably sharp. The one-electron oxidation of $[Ni^{(II)}(bpy)_3]^{2+}$ is a simple quasi-reversible process of a single solution species. Therefore we must contradict Tanaka *et al.* and conclude that only $[Ni^{(II)}(bpy)_3]^{2+}$ undergoes a two-electron reduction in process B.

3. Tanaka *et al.* have assigned process D to the one-electron reduction of $[Ni^{(0)}(bpy)_3]$. We reject this assignment based on our RRDE studies. These show that there are three nickel(0) complexes resulting from the reduction of $[Ni^{(II)}(bpy)_3]^{2+}$. The resistance of $[Ni^{(0)}(bpy)_3]$ to further reduction and its relative ease of oxidation compared to the other nickel(0) complexes immediately allows us to assign process D to the reduction of $[Ni^{(0)}(bpy)_2]$.

4. The cyclic voltammetry reported by Henne and Bartak[136] and that observed by ourselves is the same. However, our interpretation of the electrochemistry is slightly different because we have the advantage of RDE and RRDE studies as well. In particular we prefer the assignment of process C and D to the one-electron reductions of $[Ni^{(0)}(bpy)AN]$ and $[Ni^{(0)}(bpy)_2]$ respectively.

4.4 Aromatic Bromides

The electrochemical polymerisations of 2,5-dibromopyridine, 3,6-dibromopyridazine, 1,4-dibromophthalazine and 2,3,5-tribromo-pyrazine are presented in chapters seven and eight. We propose that the polymerisation processes involve the *in situ* generation of $[Ni^{(0)}(bpy)_2]$ followed by the oxidative addition of the brominated monomer to the nickel(0) species. In order to minimise the complexity of the polymerisation processes and ensure that the oxidative addition reactions are possible, the electrosyntheses should be undertaken at potentials where $[Ni^{(0)}(bpy)_2]$ is generated at the electrode surface and the brominated monomer is electroinactive.

In this section we begin by summarising the generally accepted mechanisms for the electroreduction of aromatic halides. We then present our brief investigations into the reductive electrochemistry of the brominated monomers in order to determine the cathodic limits for the electropolymerisations.

A survey of the literatures shows that electrochemical reduction of aromatic halides in aprotic solvents results in the cleavage of the carbon-halogen bond in a two-stage process[147-149]:

$$ArX + e^- \longrightarrow ArX^-$$
$$ArX^- \longrightarrow Ar^{\cdot} + X^-$$

The neutral radical thus formed then has a number of possible fates. It may undergo either an electrode or solution reduction:

Electrode: $Ar^{\cdot} + e^{-} \longrightarrow Ar^{-}$

Solution: $Ar^{\cdot} + ArX^{-} \longrightarrow Ar^{-} + ArX$
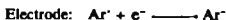
leading to the formation of the aromatic anion. This anion is then protonated by either the solvent, residual water or the quaternary ammonium cation of the supporting electrolyte:

$$Ar^{-} + \begin{cases} SH \\ H_2O \\ R_3N^{+}\text{-}CH_2R' \end{cases} \longrightarrow Ar\,H + \begin{cases} S^{-} \\ OH^{-} \\ R_3N^{+}\text{-}C^{-}HR' \end{cases}$$
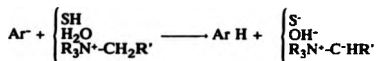
Alternatively $Ar^{\cdot}$ may abstract a hydrogen atom directly from the solvent and the solvent radical thus formed is then further reduced to the solvent conjugated based:

$$Ar^{\cdot} + SH \longrightarrow ArH + S^{\cdot}$$
$$S^{\cdot} + e^{-} \longrightarrow S^{-}$$

All these possibilities lead to the main reduction process appearing as a two-electron irreversible wave.

Cyclic voltammograms recorded at a glassy carbon electrode of AN solutions containing TEAP and any one of 2,5-dibromopyridine or 3,6-dibromopyridazine or 1,4-dibromophthalazine or 2,3,5-tribromopyrazine are given in figure 4.27(a), (b), (c) and (d) respectively. The CVs have a number of common features: Firstly, the first reduction wave encountered on the first cathodic scan is chemically irreversible for all the brominated monomers. By comparison with the literature, we assign the first irreversible reduction wave to the apparent two-electron reduction of

Figure 4.27

Cyclic voltammograms of an AN solution containing TEAP (0.1 mol dm^{-3}) and (a) 2,5-dibromopyridine (1 mmol dm^{-3}) recorded at GC/V, (b) 3,6-dibromopyridazine (2 mmol dm^{-3}) recorded at GC/V (c) 1,4-dibromophthalazine (5 mmol dm^{-3}) recorded at Pt/KV and (d) 2,3,5-tribromopyrazine (4.3 mmol dm^{-3}) recorded at Pt/KV. Potentials with respect to Ag/Ag^+ (AgClO$_4$, 0.01 mol dm^{-3}, AN). Sweep rate = 100 mV s^{-1}.
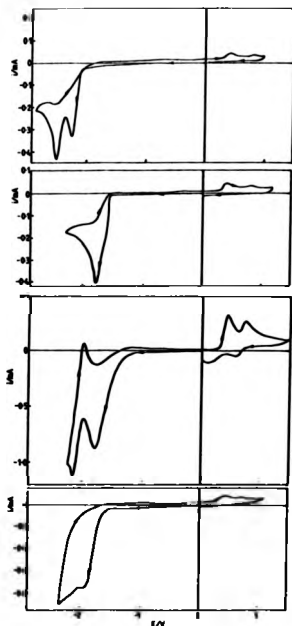
the brominated monomer resulting in the formation of the protonated monomer and the liberation of bromide. Secondly, $i_{Pc}/v^{1/2}$ is constant for the first reduction wave, and according to the Randles-Sevcik equation[150] and assuming that n = 2 in all cases, we calculate that the diffusion coefficients of the brominated monomers are of approximately the same magnitude. The position of E_{Pc} for this reduction wave varies from one brominated species to the next. Thirdly, there are two oxidation processes observed in the subsequent anodic scan which are located at E_{Pa} = 0.42 and 0.80 V irrespective of the actual brominated monomer. These peaks can be attributed to the oxidation of a solution product of the first irreversible reduction wave which is common to all four brominated species. The position and shape of these two waves are typical of the response of Br^-. Indeed the addition of TEABr to the electrolyte solution enhances both waves. In accordance with the literature[150] we assign the peaks as follows:

$$3Br^- \longrightarrow Br_3^- + 2e^- \qquad\qquad E_{Pa} = 0.42 \text{ V}$$

$$2Br_3^- \longrightarrow 3Br_2 + 2e^- \qquad\qquad E_{Pa} = 0.80 \text{ V}$$

The salient features of the CVs are summarised in table 4.6.

Table 4.6:

Summary of the CV data of 2,5-dibromopyridine or 3,6-dibromopyridazine or 1,4-dibromophthalazine or 2,3,5-tribromopyrazine

Brominated Monomer[a]	E_{p_c} of 1st reduction wave[c] /V	E_{p_c} of 2nd reduction wave[c] /V	E_{p_a}'s of oxidation waves /V	Diffusion coefficient[b] /cm^2 s^{-1}
2,5-Br$_2$Py	-2.27	-2.52	0.42, 0.80	4.98 x 10^{-6}
3,6-Br$_2$Pdz	-1.82	—	0.43, 0.81	5.79 x 10^{-6}
1,4-Br$_2$Phz	-1.84	-2.20	0.38, 0.77	3.24 x 10^{-6}
2,3,5-Br$_3$Pz	-2.00	-2.25	0.42, 0.80	—

[a] 2,5-Br$_2$Py = 2,5-dibromopyridine, 3,6-Br$_2$Pdz = 3,6-dibromopyridazine, 1,4-Br$_2$Phz = 1,4-dibromophthalazine and 2,3,5-Br$_2$Pz = 2,3,5-tribromopyrazine

[b] calculated assuming n = 2

[c] Potentials with respect to Ag/Ag$^+$ (AgClO$_4$, 0.01 mol dm^{-3}, AN). Scan rate = 100 mV s^{-1}.

Appendix 4.1

The calculated values for N' and i_D'/M for the RRDE Pt/Pt/K are given in the following table:

N'	i_D'/M
0.0020	1.8344
0.0059	1.9432
0.0105	2.0480
0.0157	2.1499
0.0211	2.2494
0.0267	2.3470
0.0323	2.4430
0.0379	2.5376
0.0436	2.6311
0.0492	2.7237
0.0547	2.8153
0.0602	2.9063
0.0656	2.9966
0.0709	3.0863
0.0761	3.1755
0.0813	3.2643
0.0863	3.3526
0.0913	3.4406
0.0962	3.5282
0.1010	3.6155

CHAPTER 5

THE NICKEL-PHOSPHINE CATALYSED ELECTROCHEMICAL SYNTHESIS OF PPY

5.1 Introduction

In this chapter we concentrate on the electroreductive deposition of poly(2,5-pyridine), PPy, based on the $[Ni^{(0)}(PPh_3)_4]/2,5$-Br$_2$Py/PPh$_3$/ TBAP system first proposed by Schiavon et al.[30]. Although a general description of their electrosynthesis was given in section 1.3, it is now appropriate to examine it in more detail.

Schiavon et al. prepared a stock solution of anhydrous $[Ni^{(II)}(AN)_6](ClO_4)_2]$ from a sacrificial nickel electrode in an AN solution containing 0.1 mol dm^{-3} TBAP. Reductive electrolysis of the stock solution after the addition of ten equivalents of PPh$_3$ produced a solution of $[Ni^{(0)}(PPh_3)_4]$. It was suggested that the addition of one equivalent 2,5-Br$_2$Py to the $[Ni^{(0)}(PPh_3)_4]$ solution gave either or both of the organometallic intermediates (A) and (B), figure 5.1, although these were not isolated or characterised. Deposition of PPy on the working electrode was achieved by a reductive potential step or by repetitive cyclic voltammetry in solution containing (A) and/or (B) in the presence of excess PPh$_3$.

In this chapter we report the preparation of PPy by two methods. The first method closely follows Schiavon's all-in-one-pot synthesis. The experimental changes were minor and undertaken for simplicity. The second method involved the electroreductive polymerisation of the pre-prepared dinuclear organonickel complexes, (Ia,b). These two

Figure 5.1:

The structures of the organonickel polymer precursors proposed by
Schiavon et al.[30].
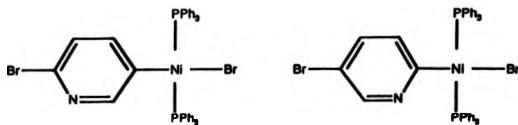
Figure 5.2:

Structure of metallised conducting polymers.
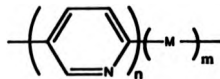
methods allow for easy comparison between the electroreductive polymerisation reported in the literature, method 1, and the electroreductive polymerisation of (I), method 2.

Bis(aryl) metal complexes increase in stability towards reductive elimination as the transition metal triad Ni, Pd and Pt is descended. Consequently, it was of interest to investigate whether the palladium and platinum analogues of the nickel complexes would produce polymers of the type shown in figure 5.2. The success of preparing such metallised polymers appears feasible because the coupling of aryl halides using Pd(0) complexes is known[152,153], although less widely reported than with Ni(0) complexes. For example, Torri *et al.*[152] reported that [Pd$^{(0)}$(PPh$_3$)$_4$] acts as an efficient catalyst for the electroreductive coupling of aryl halides. They proposed the following reaction scheme although the mechanism was not clarified:

$$Pd^{(0)} + R\text{-}X \longrightarrow R\text{-}Pd^{(II)}\text{-}X$$

$$R\text{-}Pd^{(II)}\text{-}X + R\text{-}X + 2e \longrightarrow \left[R\text{-}\overset{\overset{\displaystyle R}{|}}{\underset{\underset{\displaystyle X}{|}}{Pd^{(II)}}}\text{-}X \right]^{2-}$$

$$\left[R\text{-}\overset{\overset{\displaystyle R}{|}}{\underset{\underset{\displaystyle X}{|}}{Pd^{(II)}}}\text{-}X \right]^{2-} \longrightarrow Pd^{(0)} + R\text{-}R + 2X^-$$
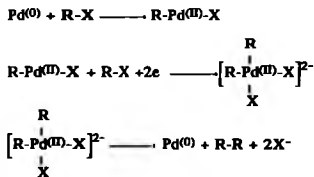
In section 5.5 we report the electrochemistry of complexes (II) and (IV) which are the palladium and platinum analogues of the organonickel polymer precursor (I).

5.2 All-in-one-pot electrochemical synthesis of the organonickel polymer precursors.

Controlled reductive electrolysis of AN solutions containing $[Ni^{(II)}(DMSO)_6][ClO_4]_2$ (5 mmol dm^{-3}), PPh$_3$ (0.05 mol dm^{-3}) and TEAP (0.1 mol dm^{-3}) caused the solution to change colour from pale blue to red. Addition of 2,5-Br$_2$Py (5 mmol dm^{-3}) resulted in a further colour change from red to orange/red. The colour changes arise from the following sequence of reactions[97]:

$$[Ni^{(II)}(DMSO)_6]^{2+} \xrightarrow[\text{AN}]{\text{excess PPh}_3} [Ni^{(II)}(PPh_3)_4(AN)_2]^{2+} + 6DMSO$$
$$\text{pale blue}$$

$$[Ni^{(II)}(PPh_3)_4(AN)_2]^{2+} + 2e \longrightarrow [Ni^{(0)}(PPh_3)_4]$$
$$\text{red}$$

$$[Ni^{(0)}(PPh_3)_4] + 2,5\text{-Br}_2\text{Py} \longrightarrow \text{Organonickel polymer precursors}$$
$$\text{orange/red}$$
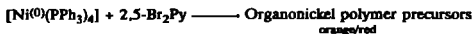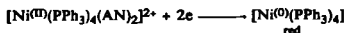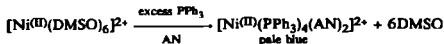
Electrochemical polymerizations were attempted using these freshly prepared orange/red solutions.

5.3 Electrochemical synthesis of PPy

We begin by comparing the electrochemistry of the dinuclear Ni complexes (Ia,b) with the behaviour found for a mixture of electrochemically generated $[Ni^{(0)}(PPh_3)_4]$ and 2,5-dibromopyridine as described in section 5.2. Figures 5.3 (a) and (b) show repetitive cyclic voltammograms recorded at a platinum electrode for the two systems. In both cases we observe an increase in charge passed with each successive cycle consistent with the progressive deposition of an electroactive material on the electrode surface. Film growth is observed at potentials below -1.2 V. After a few cycles (ca. 10) yellow films are easily visible

Figure 5.3:

Cyclic voltammograms for the nickel system recorded at Pt/KT in AN containing TEAP (0.1 mol dm^{-3}) and PPh$_3$ (10 mmol dm^{-3}): a) dinuclear nickel complexes (Ia,b) (10 mmol dm^{-3}) ; b) Ni(0) generated *in situ* from exhaustive electrolysis of [Ni$^{(II)}$(DMSO)$_6$][ClO$_4$]$_2$ (1 mmol dm^{-3}) followed by addition of 2,5-Br^{2}Py (1 mmol dm^{-3}). Potentials with respect to Ag/Ag$^+$ (AgClO$_4$, 0.01 mol dm^{-3}, AN). Sweep rate = 200 mV s^{-1}.
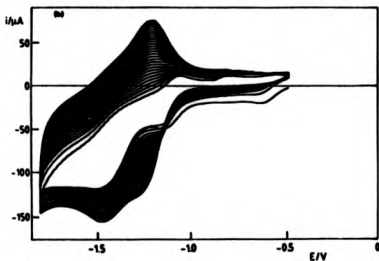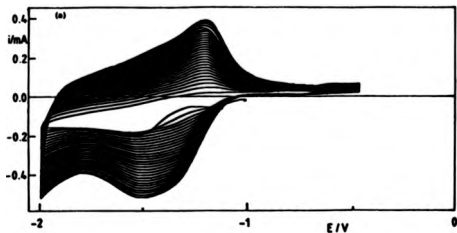
on the electrode surface. The similarity in the behaviour observed for the electrochemistry of the dinuclear Ni complexes (Ia,b) and for the reactive intermediate generated *in situ* in our experiments and in those of Schiavon *et al.* strongly suggests that (Ia,b) is the common intermediate in all three polymerizations.

On extending the cathodic switching potential to -2.35 V, a second redox wave is observed which also increases with each successive cycle. At potentials more cathodic than -1.6 V the polymeric films are orange or orange-brown depending on the film thickness. At potentials positive of -1.2 V the polymer films change colour to yellow; a similar change is observed on exposure to oxygen.

Films can also be grown by stepping the potential of the electrode from - 0.5 V to potentials between - 1.2 V and - 2.4 V. The most smooth and reproducible films are prepared by potential steps to - 1.8 V at a stationary electrode in millimolar solutions of (Ia,b). These growth conditions were preferred for subsequent studies.

Exhaustive electrolysis (until the current dropped to 5% of its original value) of the dinuclear nickel complexes (Ia,b) to form a polymeric deposit at a large area platinum gauze held at - 1.8 V in a stirred solution showed that one mole of electrons was required per mole of nickel. This is consistent with the following stoichiometry for the overall reaction:

$$(Ia,b) + 2e \longrightarrow PPy + 2\ Ni(I) + 4\ Br^-$$

Addition of a five-fold excess of 2,5-dibromopyridine did not alter the stoichiometry of the polymerisation showing that the nickel(I) is unable to undergo oxidative addition with the excess 2,5-dibromopyridine; this may be because the nickel is bound to, or trapped within, the

-156-

polymer. Our results are not consistent with the suggestion of Schiavon et al.[30] that the reduction involves two electrons per nickel centre to generate Ni(0). A mechanism for the formation of the polymer, consistent with our results, is shown in the following scheme:
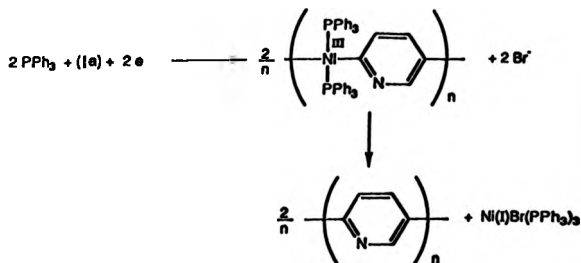
We postulate the involvement of an organonickel(III) polymer which undergoes reductive elimination of PPy. Organonickel(III) intermediates are common in phosphine-nickel(0) catalysed coupling of aryl bromides[153].

The peak current of the first reduction wave observed in the cyclic voltammetry of the dinuclear nickel complex at a clean platinum electrode is proportional to the square root of the sweep rate, figure 5.4. This is as expected for a diffusion controlled process. The diffusion coefficient of the nickel complex can be determined from the gradient of the graph in figure 5.4 according to the Randle-Sevčik equation[151]:

$$\left| i_P \right| = 0.4463 n F A \left(\frac{nF}{RT} \right)^{1/2} c_\infty D^{1/2} v^{1/2} \qquad (5.1)$$

Figure 5.4:

Sweep rate dependence of i_{pc} for the first reduction wave observed for complex (I) (5 mmol dm^{-3}) in an AN solution containing TEAP (0.1 mol dm^{-3}) at Pt/KV.
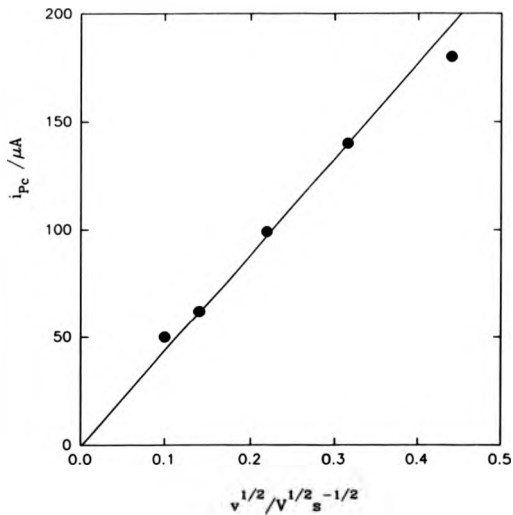
The notation has its usual meaning. Now, assuming that the reduction is a two-electron process, we calculate the diffusion coefficient to be 3.2×10^{-7} cm^2 s^{-1}.

5.4 Electrochemistry and properties of the polymer films

The electrochemistry of the coated electrodes was investigated in deoxygenated AN solutions containing TEAP. It should be noted that the coated electrodes were transferred in air from the growth solutions to the background electrolyte solutions and no measures were taken to avoid the exposure of the pristine films to oxygen.

In background electrolyte the coated electrodes show two broad cathodic peaks (i) and (ii) which merge for the thicker films (> 0.50 C cm^{-2}), figure 5.5. The peak currents for both processes increase linearly with sweep rate as expected for a surface confined redox species. The corresponding anodic peaks (iii) and (iv) are less well resolved but are distinct for thin films (< 0.15 C cm^{-2}). At potentials less than - 2.7 V the films dissolve and orange material can be seen streaming away from the electrode. At potentials greater than 1.7 V the films come away from the electrode in flakes.

Nickel and PPh$_3$ were extracted from the films by soaking in EDTA (0.01 mol dm^{-3} aqueous solution buffered to pH 9.2) for 1/2 h, followed by washing in water, ethanol and finally acetonitrile. The treated films show significantly different cyclic voltammetry in background electrolyte, figure 5.6. Comparison with figure 5.5 shows that peaks (i) and (iv) are no longer present and that peaks (ii) and (iii) are much sharper ($E_{P_{1/2}}$ = -2.29 V; ΔE_P = 0.36 V; i_P/v constant). The original form of the cyclic voltammetry can be restored by soaking the film in a solution of 1 mmol dm^{-3} [Ni^{II}(DMSO)$_6$][ClO$_4$]$_2$ containing 10 mmol dm^{-3} PPh$_3$ in acetonitrile for 1/2 h. Typically removal and subsequent replacement of the Ni leads to ca. 50% reduction in the redox capacity of the film. A

Figure 5.5:

Cyclic voltammogram of the as-grown polymer film recorded at Pt/KV in
AN containing TEAP (0.1 mol dm^{-3}). Potentials with respect to Ag/Ag$^+$
(AgClO$_4$, 0.01 mol dm^{-3}, AN). Sweep rate = 200 mV s^{-1}.
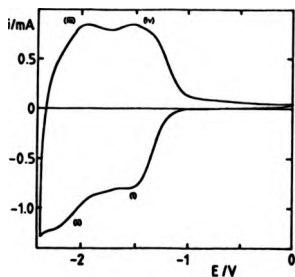
Figure 5.6:

Cyclic voltammogram of an EDTA treated polymer film recorded at
Pt/KV in AN containing TEAP (0.1 mol dm^{-3}). Potentials with respect
to Ag/Ag$^+$ (AgClO$_4$, 0.01 mol dm^{-3}, AN). Sweep rate = 200 mV s^{-1}.
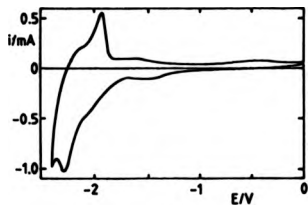
possible explanation for the loss in redox capacity is that the films slowly dissolve during the washing and soaking processes. Based on these observations we conclude that the redox activity around - 1.35 V (peaks (i) and (iv)) is associated with Ni bound within the polymer film and that this Ni can be removed and replaced within the film. The redox activity around - 2.29 V (peaks (ii) and (iii)) is associated with oxidation and reduction of the polymer itself and occurs in the presence and absence of bound Ni.

The ability of PPy to coordinate nickel will directly reflect the linkage and orientation of adjacent pyridyl moieties. There are three possible linkages between adjacent pyridyls, they are C^2-C^5, C^2-C^2 and C^5-C^5. The former linkage can exist to the exclusion of the others, whereas the latter two linkages must coexist. There are two possible orientations of adjacent pyridyls depending on whether the ring nitrogens are on the same or different sides of the polymer chain. Figure 5.7 (a-d) illustrates some of the possible positions of the pyridyl units with respect to one another. Clearly the only linkage and orientation of the pyridyl moieties capable of strongly coordinating metal ions is shown in figure 5.7 (a). Consequently we postulate that PPy synthesised from the nickel-phosphine system must contain an appreciable amount of C^2-C^2/C^5-C^5 linked pyridyls in which the ring nitrogens lie on the same side of the polymer chain in order to account for its ability to coordinate nickel.

Specular reflectance FTIR spectra of the film coated Pt electrodes, figure 5.8, show bands corresponding to the presence of aromatic rings at 1468, 1439 and 837 cm^{-1}, the latter being consistent with 1,4-disubstitution of the pyridine ring[155a]. The presence of PPh$_3$ in the as-grown films is also confirmed by absorptions at 1098, 738 and 697 cm^{-1} which are noticeably absent for the EDTA treated films. The intensity of the bands attributable to TEA$^+$ and ClO$_4^-$ from the

Figure 5.7:

Possible structures of PPy: (a) C^2-C^2/C^5-C^5 linkages with ring nitrogens same side, (b) C^2-C^2/C^5-C^5 linkages with ring nitrogens opposite sides, (c) C^2-C^5 linkages with ring nitrogens same side and (d) C^2-C^5 linkages with ring nitrogens opposite sides.
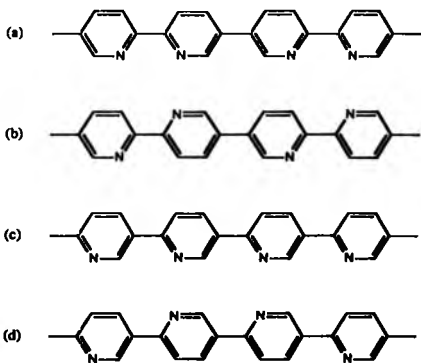
Specular reflectance FTIR spectrum of the as-grown film on a platinum electrode removed from the growth solution at -1.8 V.
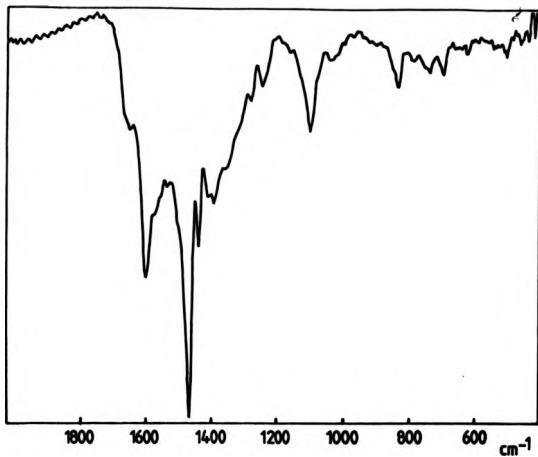
background electrolyte varies with the oxidation state of the film. For the reduced film (removed from solution at - 1.8 V) there are strong bands due to TEA+ (1098 cm⁻¹); for the oxidized film (removed from solution at - 0.5 V) there are strong bands due to ClO_4^- (620 and 1098 cm⁻¹). In both cases residual absorption due to the other counter ion is also observed. The absorption band centred at 1098 cm⁻¹ is broad because PPh_3, TEA+ and ClO_4^- all absorb in this region.

The UV-visible spectra of treated polymer deposits on indium-doped tin oxide electrodes display an absorption maximum at λ = 373 nm. We assign this to the $\pi \rightarrow \pi^*$ transition of the pyridyl moieties. Compared to the equivalent adsorption for pryridine (λ_{max} = 260 nm) there is a large bathochromic shift which is caused by the extended conjugation of the pyridyl moieties in the polymer[155b].

5.5 Electrochemistry of complexes (II) and (IV)

Figure 5.9 shows a cyclic voltammogram for the dinuclear Pd complexes (II). On the first anodic cycle starting from 0.0 V there are two irreversible oxidations at 0.44 and 1.08 V. On the cathodic cycle there are four irreversible reductions. The first of these at -1.66 V is associated with a solution product of the oxidation at 0.44 V. The remaining three reductions at -2.04, -2.40 and -2.68 V are associated with the Pd complexes (II) and are present on an initial cathodic sweep from 0.0 V (not shown). Associated with the irreversible reduction of (II) at -2.04 V there are two oxidation processes of solution products in the subsequent anodic scan at -0.46 and 0.72 V. The oxidations at 0.44 and 1.08 V appear to be associated with the oxidation of the Br⁻ and are not present in the electrochemistry of the analogous chloro compound, (III). Analysis of the variation of peak height with square root of the sweep rate for the main reduction peak at -2.04 V gives a diffusion coefficient of 3.2×10^{-7} cm² s⁻¹ assuming n = 2. This agrees with our

-164-

Figure 5.9:

Cyclic voltammogram of the dinuclear palladium complexes (IIa,b), (5 mmol dm^{-3}), recorded on GC/V in DMF containing TEAP (0.1 mol dm^{-3}). Potentials with respect to Ag/Ag$^+$ (AgClO$_4$, 0.01 mol dm^{-3}, AN). Sweep rate = 50 mV s^{-1}.
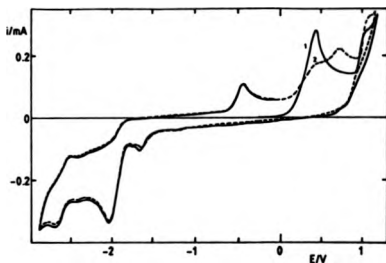
Figure 5.10:

Cyclic voltammogram of the platinum complexes (IV), (5 mmol dm^{-3}), recorded on GC/V in DMF containing TEAP (0.1 mol dm^{-3}). Potentials with respect to Ag/Ag$^+$ (AgClO$_4$, 0.01 mol dm^{-3}, AN). Sweep rate = 50 mV s^{-1}.
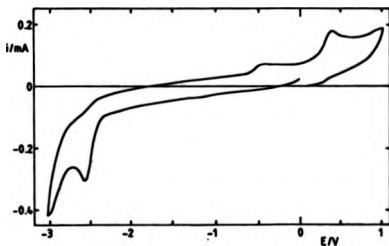
result for the corresponding nickel compound. On repetitive cycling through the reduction peak at -2.04 V, with and without a ten-fold excess of PPh$_3$, the current slowly decays and a thin visible film is deposited at the electrode. However there is no evidence for any electrochemical activity of this film in background electrolyte.

Figure 5.10 shows the cyclic voltammogram for the mononuclear platinum complex (IV). There are two irreversible reductions at - 2.58 and -3.00 V. On the subsequent anodic scan there are two oxidations at -0.48 and 0.40 V associated with the oxidation of solution products formed from the reduction of (IV). Analysis of the variation of the peak height with the square root of the sweep rate for the main reduction peak at -2.58 V gives a diffusion coefficient of 2.1 x 10^{-7} cm^2 s^{-1}, assuming n = 2. Repetitive cycling through the reduction peak, with and without an added ten-fold excess of PPh$_3$, provided no evidence for the formation of a film at the electrode surface.

We also investigated the electrochemistry of the two other groups of palladium and platinum complexes in our attempts to electrosynthesis metallised conducting polymers. The first group were the chloro analogues, [(III) and (V)], and the second group were the PEt$_3$ analogues, [(IX), (XIII)]. In both cases no electrodeposition was observed.

5.6 Conclusions

The electrochemical reduction of (I) in the presence of excess PPh$_3$ at -1.8 V leads to the deposition of polymeric films on the surface of the working electrode. These films are indistinguishable by infra-red spectroscopy, UV-visible spectroscopy and electrochemistry from those formed by the *in situ* generation of nickel(0) in the presence of excess PPh$_3$ and 2,5-Br$_2$Py. From these results it can be concluded that the dinuclear organonickel complex (Ia,b) is the stable intermediate in both polymerisation processes. In (Ia,b) the nickel is bonded exclusively to the

C^2 position of the pyridyl moiety. Consequently we dismiss the proposal of Schiavon *et al.* that the stable intermediates are mononuclear in which the oxidative addition has taken place at either the C^2 or C^5 positions.

In accordance with the results reported by the Italian group, the as-grown polymer films display reduced state conductivity. They are also able to chelate nickel ions, which can be removed and replaced by soaking in solutions of EDTA and $[Ni(PPh_3)_4(AN)_2]$ respectively. We propose that the polymers ability to chelate nickel ions is because the nitrogens of the pyridyl moieties lie on the same side of the polymer chain and that the linkages are predominately C^2-C^2 and C^5-C^5.

The stability of the polymer films to repeated cyclic voltammetry is poor. Therefore we curtailed our investigations into this system in favour of the $[Ni^{(II)}(bpy)_3(ClO_4)_2]/2,5$-$Br_2Py/AN/TEAP$ system reported in chapter 7.

CHAPTER 6

THEORETICAL ANALYSIS OF A SECOND ORDER ECE PROCESS AT A RDE

6.1 Introduction

In this chapter a generalised theoretical treatment of second order ECE processes under mass transport control at a RDE is presented. The theory has been developed to describe the initial stages of the electrochemical polymerisation of 2,5-Br_2Py in the presence of $[Ni^{(III)}(bpy)_3(ClO_4)_2]$, but is generally applicable to other examples of this type.

6.1.1 Second order ECE mechanism

A second order ECE mechanism may be written as:

$$\text{Electrode:} \quad P \underset{+ne}{\overset{-ne}{\rule{1cm}{0.4pt}}} Q \qquad E_i^{\circ} \qquad \text{(i)}$$

$$\text{Solution:} \quad Q + R \xrightarrow{k_2} S \qquad \text{(ii)}$$

$$\text{Electrode:} \quad S \underset{+ne}{\overset{-ne}{\rule{1cm}{0.4pt}}} T \qquad E_{iii}^{\circ} \qquad \text{(iii)}$$
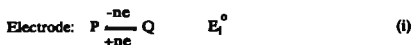
where k_2 is the second order homogeneous rate constant and n is the number of electrons transferred in steps (i) and (iii).

The product, Q, of the first electron transfer is not electroactive in the potential region where P is reduced. Instead it undergoes a chemical reaction with R to produce an electroactive product, S. S undergoes a

-168-

second electron transfer in the final step of the mechanism.

A generalised theoretical treatment of second order ECE processes at a RDE has not been reported in the literature. However, first order ECE mechanisms, pseudo first order ECE mechanisms, DISP1 mechanisms and second order EC' mechanisms have all been described. In the next subsection we describe the literature pertinent to our theory.

6.1.2 DISP1, EC' and other ECE mechanisms

Malachesky, Marcoux and Adams[156] were the first group to report a theoretical treatment of a first order ECE reaction mechanism at a RDE. Their theory was based upon the combination of results from the classic hydrodynamic studies by Levich[144] and an equation derived from the chronoamperometric treatment of the ECE process at a stationary electrode[157]. Due to the incongruous linkage of steady state and time dependent situations the theory was a poor approximation to the truth. A more rigorous treatment by Karp[158] led to the following equation for the limiting current, i_L, for a first order ECE mechanism:

$$i_L = \frac{nFADp_\infty}{X_D}\left(\frac{2 - \tanh[X_D/(D/k)^{1/2}]}{X_D/(D/k)^{1/2}} \right) \qquad (6.1)$$

More recently, a different theoretical approach taken by Compton et al.[159] led to the derivation of the expression (6.2). It first appeared with a typographical error, but is shown here in its corrected form[160]:

$$i_L = \frac{nFADp_\infty}{X_D}\left(2 - \frac{(D/k)^{1/2}}{X_D} \right) \qquad (6.2)$$

In both expressions X_D is the diffusion layer thickness, D is the

-169-

diffusion coefficient of P and Q (assumed to be of similar magnitude), F is the faraday, A is the area of the RDE, k is the first order homogeneous rate constant and the bulk concentration of P is denoted p_∞. Digital simulation of the mechanism has also been reported in the literature[161-163] and shows good agreement with (6.1) and (6.2).

ECE mechanisms in which another substrate, R, is involved in the chemical step have only been described for special cases[163-165]. Commonly, the substrate R is present at a much higher concentration than Q so that the kinetic step (ii) may be taken as pseudo first order. Under these conditions the homogeneous rate constant becomes: $k = k_2 r_\infty$. Equation (6.1) and (6.2) can therefore be used to determine the pseudo first order rate constant. Feldberg et al.[164] reported digital simulation of a second order ECE dimerisation reaction at a RDE. For this case, step (ii) of the mechanism becomes:

$$\text{Solution:} \quad Q + Q \xrightarrow{\ k\ } S \qquad\qquad (iv)$$

This simplifies the theory because it avoids tackling the problem of concentration polarisation of both species P and R. Our analysis for the second order ECE mechanism is valid for all relative concentrations of the two species.

Compton et al.[167] and Fletcher et al.[168] respectively have studied the RDE voltammetry and the steady state limiting currents at a microelectrode for reactions with the following mechanism:

$$\text{Electrode:} \quad P \underset{+ne}{\overset{-ne}{\rightleftharpoons}} Q \qquad E_v^o \qquad\qquad (v)$$

$$\text{Solution:} \quad Q + R \xrightarrow{\ k_2\ } S + P \qquad\qquad (vi)$$

$$\text{Electrode:} \quad P \underset{+ne}{\overset{-ne}{\rightleftharpoons}} Q \qquad E^o_{vii} \qquad \qquad \text{(vii)}$$
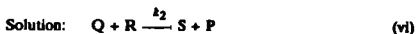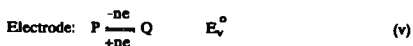
Although there are similarities with the second-order ECE mechanism, this mechanism is correctly defined as EC*

Another type of mechanism involving two electron transfers can be represented by the following reaction scheme:

$$\text{Electrode:} \quad P \underset{+ne}{\overset{-ne}{\rightleftharpoons}} Q \qquad E^o_{viii} \qquad \qquad \text{(viii)}$$

$$\text{Solution:} \quad Q \overset{k}{\longrightarrow} S \qquad \qquad \text{(ix)}$$

$$\text{Solution:} \quad Q + S \longrightarrow P + T \qquad \qquad \text{(x)}$$

where the second electron transfer takes place homogeneously via disproportionation, step (x), and the overall rate is determined by step (ix). This mechanism is described as DISP1. Traditionally it has been difficult to discriminate between ECE and DISP1 mechanisms by conventional electrochemical techniques[169]. However, more recently Compton et al.[170,171] have devised two separate analyses which attempt to distinguish between these two mechanistic pathways. The first analysis demonstrates that ECE and DISP1 mechanisms give different chronoamperometric responses arising from potential step experiments at a RDE. Similarly, the second analysis shows that the two mechanisms produce different current-voltage curves at a RDE. However, in both analyses the theoretical difference is small and will probably lie within experimental error for all but idealised systems. Consequently it should be emphasised that although the following theory has been devised for ECE reactions, it is unlikely that the theory can discriminate against DISP1 mechanisms.

6.2 The theoretical model

A generalised second order ECE mechanism is defined by reactions (i), (ii) and (iii). In the model presented here, figure 6.1, it is assumed that $E_{iii} < E_i$; so that the potentials at which P is converted to Q also strongly favours the formation of T in reaction (iii). The "Levich approximation" has also been assumed such that a stagnant layer, whose thickness, X_D, is determined by the rotation speed, lies immediately adjacent to the electrode. At distances $< X_D$ from the electrode, mass transport is entirely diffusion controlled and at distances $> X_D$, mass transport is wholly convective. This approximation simplifies the solution of the mass transport equations because only diffusion, rather than a combination of convection and diffusion, need be considered.

The equations describing the combination of diffusion and homogeneous chemistry for the steady state second order ECE system at a RDE are:

$$D \frac{d^2p}{dx^2} = 0 \tag{6.3}$$

$$D \frac{d^2q}{dx^2} - k_2qr = 0 \tag{6.4}$$

$$D \frac{d^2r}{dx^2} - k_2qr = 0 \tag{6.5}$$

$$D \frac{d^2s}{dx^2} + k_2qr = 0 \tag{6.6}$$

$$D \frac{d^2t}{dx^2} = 0 \tag{6.7}$$

where we have assumed that $D = D_P = D_Q = D_R = D_S = D_T$ and that only

-172-

Figure 6.1

General scheme for second order ECE reactions at a RDE.

| Electrode | Diffusion Layer | Bulk Solution |

$E > E_{(i)}$

$ne-$

$E > E_{(iii)}$

$ne-$

P ⟵〜〜〜 P $[P] = p_\infty$

Q ⟶ R $[R] = r_\infty$

S ⟵ S ⟶

T

x_D
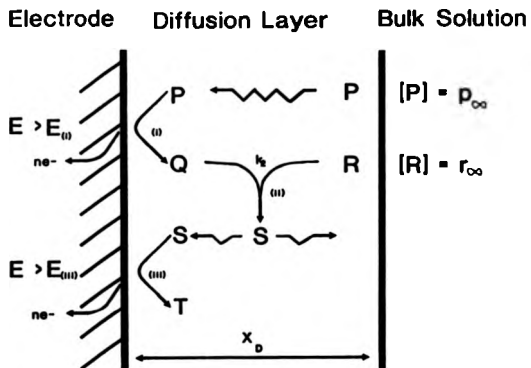
P and R are present in the bulk solution. The convention of using lower case letters to denote the concentrations of the various species is adopted and x is the distance from the electrode. Subscripts associated with the lower case letters denote the distance from the electrode surface. The boundary conditions for a potential corresponding to the limiting current, i_L, are:

$$p = 0; \quad \frac{dq}{dx} = -\frac{dp}{dx}; \quad \frac{dr}{dx} = 0 \text{ and } s = 0 \text{ at } x = 0$$

and

$$p = p_\infty; q = 0; r = r_\infty \text{ and } s = 0 \text{ at } x = X_D$$

Now the observed limiting current, i_L, at the RDE [area A] is the sum of the current contributions from steps (i) and (iii):

$$i_L = i_{(i)} + i_{(iii)} \tag{6.8}$$

Applying Fick's first law (6.8) becomes:

$$\frac{i_L}{nFA} = D\frac{dp}{dx}\bigg|_{x=0} + D\frac{ds}{dx}\bigg|_{x=0} \tag{6.9}$$

where n is the number of electrons transferred in each step and F is the faraday. The boundary conditions at the electrode surface in combination with expression (6.3) gives:

$$\frac{i_L}{nFA} = D\frac{p_\infty}{X_D} + D\frac{ds}{dx}\bigg|_{x=0} \tag{6.10}$$

The term X_D is given by[172]:

$$X_D = 0.643W^{-1/2}\nu^{1/6}D^{1/3} \tag{6.11}$$

where W is the rotation speed (Hz) and ν is the kinematic viscosity (cm^2 s^{-1}) of the solution.

If we introduce the following dimensionless variables:

$$u = \frac{q}{p_\infty}\,; \quad v = \frac{r}{r_\infty}\,; \quad w = \frac{s}{p_\infty}\,; \quad \text{and} \quad \chi = \frac{x}{X_D}$$

then equations (6.4), (6.5) and (6.6) respectively become:

$$\frac{d^2u}{d\chi^2} - \kappa uv = 0 \tag{6.12}$$

$$\frac{d^2v}{d\chi^2} - \kappa uv\gamma = 0 \tag{6.13}$$

$$\frac{d^2w}{d\chi^2} + \kappa uv = 0 \tag{6.14}$$

where γ reflects the balance between the original solution species:

$$\gamma = \frac{p_\infty}{r_\infty} \tag{6.15}$$

and κ reflects the balance between homogeneous kinetics and diffusion:

$$\kappa = \frac{k_2 X_D^2 r_\infty}{D} \tag{6.16}$$

When $\kappa \gg 1$ then the reaction between Q and S is much faster than the time taken for Q to cross the diffusion layer into the bulk solution.

Therefore all of Q is captured by S within the diffusion layer. Conversely, when $\varepsilon \ll 1$ then Q diffuses across the diffusion layer more rapidly than it reacts with S resulting in the majority of Q escaping into the bulk solution.

The dimensionless boundary conditions are:

$$\frac{dv}{d\chi} = 0; \quad \frac{du}{d\chi} = -1 \text{ and } w = 0 \text{ at } \chi = 0$$

and

$$u = 0; \quad v = 1; \quad w = 0 \text{ at } \chi = 1$$

Now in terms of dimensionless variables, equation (6.10) can be converted to the form:

$$\frac{i_L}{nFA} = D \frac{p_\infty}{X_D} \left(1 + \frac{dw}{d\chi} \Big|_{\chi = 0} \right) \tag{6.17}$$

Hence the problem is reduced to evaluating the term $dw/d\chi\big|_{\chi = 0}$. Combining equations (6.13) and (6.14) yields the following second order differential equation:

$$\frac{d^2 (v + w_y)}{d\chi^2} = 0 \tag{6.18}$$

This has solutions of the form:

$$v + w_y = A\chi + B \tag{6.19}$$

-176-

where

$$\frac{dv}{d\chi} + \gamma \frac{dw}{d\chi} = A \tag{6.20}$$

Substitution from the dimensionless boundary conditions leads to the expression:

$$\frac{dw}{d\chi}\bigg|_{\chi = 0} = \frac{1 - v_o}{\gamma} \tag{6.21}$$

Similarly, combining equations (6.12) and (6.14), solving by integration, followed by the substitution of the boundary conditions leads to the expression:

$$\frac{dw}{d\chi}\bigg|_{\chi = 0} = 1 - u_o \tag{6.22}$$

Thus given either v_o or u_o we can obtain an expression for i_L using (6.21) or (6.22) and (6.18). A number of approximate solutions for v_o and u_o are determined in the following subsections. The solutions depend on the magnitude of κ and/or the product of $\kappa\gamma$. The values of κ and $\kappa\gamma$ chosen for this theoretical treatment are conveniently represented in terms of a case diagram, figure 6.2.

6.2.1 Region 1: $\kappa \ll 1$

In this situation the homogeneous chemical reaction is slow compared to the rate of diffusion away from the electrode surface. Consequently Q may escape from the reaction layer before reacting with

This picture shows the regions considered to develop the solutions for the theoretical model of second order ECE reactions at a RDE.

Fast kinetics

Large excess R

Large excess P

Slow kinetics

Key			
Region 1(a)	▮	Region 2(b)	▮
Region 1(b)	▮	Region 3(a)	▮
Region 2(a)	▮	Region 3(b)	▮
Case boundaries	▬		
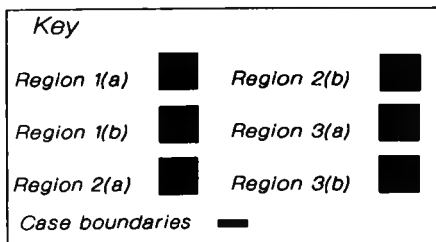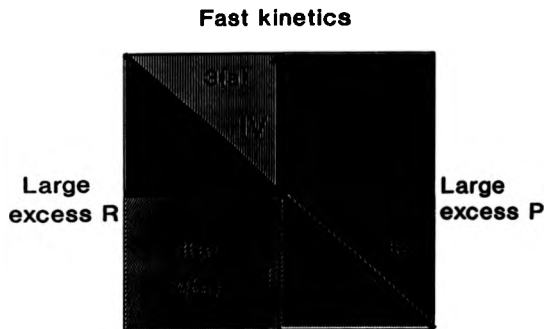
R. Under these circumstances equation (6.12) becomes:

$$\frac{d^2u}{d\chi^2} = 0 \qquad (6.23)$$

and on integration:

$$u = 1 - \chi \qquad (6.24)$$

Combining equations (6.24) and (6.13) produces the following equation:

$$\frac{d^2v}{d\zeta^2} - \kappa\gamma\nu\zeta = 0 \qquad (6.25)$$

where $\zeta = 1 - \chi$. Equation (6.25) has solutions in terms of Airy functions[173]; $A_i(z)$, $B_i(z)$:

Let $\psi = (\kappa\gamma)^{1/3}$ $\qquad (6.26)$

then $v = A_1 A_i(\psi\zeta) + B_1 B_i(\psi\zeta)$ $\qquad (6.27)$

where A_1 and B_1 are constants which are determined by applying the appropriate boundary conditions such that:

$$A_1 = \frac{1}{A_i(0) - [B_i(0)A_i'(\psi) / B_i'(\psi)]} \qquad (6.28)$$

$$B_1 = - \frac{A_1 A_i'(\psi)}{B_i'(\psi)} \qquad (6.29)$$

where A_i' and B_i' are the differentials of the Airy functions. Hence

equation (6.27) is converted to the following form:

$$v = \frac{B_i'(\psi)A_i(\psi\zeta) - A_i'(\psi)B_i(\psi\zeta)}{B_i'(\psi)A_i(0) - A_i'(\psi)B_i(0)}$$ (6.30)

Now when $\zeta = 1$, $(\chi = 0)$, the expression (6.30) transforms to :

$$v_o = \frac{B_i'(\psi)A_i(\psi) - A_i'(\psi)B_i(\psi)}{B_i'(\psi)A_i(0) - A_i'(\psi)B_i(0)}$$ (6.31)

and using the Wronskian[174] relationship:

$$W[A_i(z),B_i(z)] = A_i(z)B_i'(z) - A_i'(z)B_i(z) = \pi^{-1}$$ (6.32)

equation (6.31) becomes:

$$v_o = \frac{1}{\pi}\left(\frac{1}{B_i'(\psi)A_i(0) - A_i'(\psi)B_i(0)}\right)$$ (6.33)

Substitution of (6.33) and (6.26) into (6.21) gives the full expression for all the relative concentrations of P and R when $x < 1$:

$$\frac{dw}{d\chi}\bigg|_{\chi = 0} = \frac{1}{\gamma}\left(1 - \frac{1}{\pi(B_i'(\psi)A_i(0) - A_i'(\psi)B_i(0))}\right)$$ (6.34)

Equation (6.34) is quite complex, however it can be simplified in the following manner:

Given that[173]:

$$B_i'(\psi)A_i(0) - A_i'(\psi)B_i(0)$$
$$= \sqrt{3}c_1[c_1 f'(\psi) + c_2 g'(\psi)] - \sqrt{3}c_1[c_1 f'(\psi) - c_2 g'(\psi)]$$ (6.35)

-180-

$$= 2\sqrt{3}c_1c_2g'(\psi) \qquad (6.36)$$

where:

$$c_1 = A_i(0) = B_i(0)/\sqrt{3} \qquad (6.37)$$

and

$$c_2 = A_i'(0) = B_i'(0)/\sqrt{3} \qquad (6.38)$$

then using the Wronskian relationship, it can readily be shown that:

$$2\sqrt{3}c_1c_2 = \pi^{-1} \qquad (6.39)$$

and hence:

$$B_i'(\psi)A_i(0) - A_i'(\psi)B_i(0) = \pi^{-1}g'(\psi) \qquad (6.40)$$

The series expansion for $g'(\psi)$ is given by:

$$g'(\psi) = 1 + \frac{1}{3}\psi^3 + \frac{1}{72}\psi^6 + \ldots\ldots \qquad (6.41)$$

Now for both large and small values of ψ the later terms of the expansion may be ignored because for $\psi < 1$ the higher terms are small and for $\psi > 1$, $1/g'(\psi)$ is small in the final expression. Therefore taking the first two terms of (6.41) and substituting (6.39) into (6.37) converts (6.40) into the following form:

$$B_i'(\psi)A_i(0) - A_i'(\psi)B_i(0) = \pi^{-1}(1 + \frac{1}{3}\psi^3) \qquad (6.42)$$

Finally, substitution of (6.42) into (6.33) gives an expression for v_o which

may then be inserted into (6.21) to yield an expression for $dw/d\chi\big|_{\chi\,=\,0}$ when $\kappa \ll 1$:

$$\frac{dw}{d\chi}\bigg|_{\chi\,=\,0} \simeq \frac{1}{\gamma}\left(\frac{\psi^3}{3+\psi^3}\right) \tag{6.43}$$

This is a good approximation for (6.34) with an error of < 8% in all cases as shown in figure 6.3.

Equation (6.43) has two limiting forms. These are when $\psi < 1$ and when $\psi > 1$ which are denoted regions 1(a) and 1(b) respectively. First if $\psi < 1$ and therefore from equation (6.26) $(\kappa\gamma)^{1/3} < 1$, then:

$$\frac{dw}{d\chi}\bigg|_{\chi\,=\,0} \simeq \frac{\kappa}{3} \tag{6.44}$$

and hence the limiting current for $\kappa \ll 1$, $\psi < 1$ is:

$$\frac{i_L}{nFA} = \frac{Dp_\infty}{X_D}\left(1+\frac{\kappa}{3}\right) \tag{6.45}$$

We will call this solution Case I.

Second, if ψ is large then by inspection equation (6.43) simplifies to:

$$\frac{dw}{d\chi}\bigg|_{\chi\,=\,0} \simeq \frac{1}{\gamma} \tag{6.46}$$

and therefore the limiting current for $\kappa \ll 1$, $\psi > 1$ is:

$$\frac{i_L}{nFA} = \frac{Dp_\infty}{X_D}\left(1+\frac{1}{\gamma}\right) \tag{6.47}$$

-182-

Figure 6.3:

Graph showing comparative plots of equations (6.34), (6.43), (6.44) and (6.46).
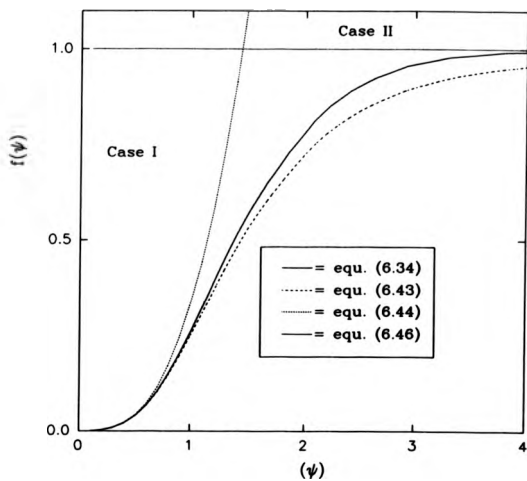
We will call this case II.

6.2.2 Region 2: $xy \ll 1$

We will now consider the behaviour when $xy \ll 1$. Under these circumstances equation (6.13) becomes:

$$\frac{d^2v}{d\chi^2} = 0 \qquad (6.48)$$

which integrates immediately to give:

$$v = C\chi + D \qquad (6.49)$$

where C and D are constants. From the boundary conditions, $C = 0$, $D = 1$ and so $v = 1$. In this region the concentration of R within the diffusion layer is equal to that of the bulk concentration r_∞. This is the pseudo first order case since there is no concentration polarisation of R. Substitution of $v = 1$ into (6.12) allows it to be converted to the form:

$$\frac{d^2u}{d\chi^2} - xu = 0 \qquad (6.50)$$

Equation (6.50) has the general solution:

$$u = A_2\sinh(\chi\sqrt{x}) + B_2\cosh(\chi\sqrt{x}) \qquad (6.51)$$

then:

$$\frac{du}{d\chi} = A_2\sqrt{x}\cosh(\chi\sqrt{x}) + B_2\sqrt{x}\sinh(\chi\sqrt{x}) \qquad (6.52)$$

It can be seen from the appropriate boundary conditions that:

$$0 = A_2 \sinh\sqrt{\varepsilon} + B_2 \cosh\sqrt{\varepsilon} \tag{6.53}$$

and

$$-1 = A_2\sqrt{\varepsilon} \tag{6.54}$$

therefore:

$$A_2 = \frac{-1}{\sqrt{\varepsilon}} \tag{6.55}$$

and

$$B_2 = \frac{1}{\sqrt{\varepsilon}}(\tanh\sqrt{\varepsilon}) \tag{6.56}$$

Substitution of u_o into equation (6.22) gives the full expression for region 2:

$$\frac{dw_2}{d\chi}\bigg|_{\chi=0} = 1 - \frac{\tanh\sqrt{\varepsilon}}{\sqrt{\varepsilon}} \tag{6.57}$$

This solution can be further simplified if we consider two situations. Firstly when $\varepsilon \gg 1$ and secondly when $\varepsilon \ll 1$.

6.2.2.1 Region 2(a): $\kappa \gg 1$

When $\kappa \gg 1$, $\tanh\sqrt{\kappa} \to 1$, therefore (6.57) approximates to the following expression:

$$\frac{dw}{d\chi} \simeq 1 - \frac{1}{\sqrt{\kappa}} \tag{6.58}$$

The limiting current for $\kappa y \ll 1$, $\kappa \gg 1$ is therefore:

$$\frac{i_L}{nFA} = \frac{Dp_\infty}{X_D}\left(2 - \frac{1}{\sqrt{\kappa}}\right) \tag{6.59}$$

We will call this case III.

It is pleasing to note that equation (6.59), which describes i_L in the presence of a large excess of R i.e. pseudo first order kinetics, is equivalent to the expressions (6.1) and (6.2) proposed respectively by Karp and Compton *et al.* for a first order ECE process.

6.2.2.2 Region 2(b): $\kappa \ll 1$

When $\kappa \ll 1$, the later terms of the Maclaurian expansion of $\tanh\sqrt{\kappa}$ may be ignored to produce the following close approximation:

$$\tanh\sqrt{\kappa} = \sqrt{\kappa} - \frac{(\sqrt{\kappa})^3}{3} \tag{6.60}$$

Substitution of this value into (6.57) yields the following simple expression:

$$\left.\frac{dw}{d\chi}\right|_{\chi=0} = \frac{\kappa}{3} \tag{6.44}$$

As required (since $\varepsilon \ll 1$) this agrees with region 1(a) above so the limiting current is given by (6.45).

6.2.3 Region 3: $\varepsilon > 1$

Finally we must consider the behaviour when $\varepsilon > 1$. Under these circumstances the kinetics are fast compared to the diffusion of P away from the electrode. This region has been divided into two different approximations; firstly when $\gamma < 1$ ($r_\infty > p_\infty$) so no Q can escape, and secondly when $\gamma > 1$ ($r_\infty < p_\infty$) so some Q escapes to react in the bulk solution.

6.2.3.1 Region 3(a): $\gamma < 1$

Since in this case $r_\infty > p_\infty$, we assume that over a thin reaction layer close to the electrode $v = v_o$. Consequently equation (6.12) becomes:

$$\frac{d^2u}{d\chi^2} - \varepsilon u v_o = 0 \tag{6.61}$$

Taking the relevant boundary condition we then obtain the following solution:

$$u = u_o \exp[-\sqrt{(\varepsilon v_o)}\chi] \tag{6.62}$$

so that:

$$\frac{du}{d\chi} = -\sqrt{(\varepsilon v_o)}u_o \exp[-\sqrt{(\varepsilon v_o)}\chi] \tag{6.63}$$

However from the boundary conditions at $\chi = 0$, $du/d\chi\big|_{\chi = 0} = -1$, then:

$$\sqrt{(\varepsilon v_o)}u_o = 1 \tag{6.64}$$

-187-

In the steady state we must balance the flux of Q across the diffusion layer by the flux of R entering the diffusion layer so:

$$\frac{du}{d\chi}\bigg|_{\chi=0} = -\frac{dv}{d\chi}\bigg|_{\chi=0} \tag{6.65}$$

but if we have a thin reaction layer at the electrode surface we can write:

$$\frac{dv}{d\chi}\bigg|_{\chi=0} = -\frac{1-v_0}{\gamma} \tag{6.66}$$

and since a boundary condition is $du/d\chi|_{\chi=0} = -1$, then:

$$v_0 = 1 - \gamma \tag{6.67}$$

Combining equations (6.67) and (6.64) followed by substitution into equation (6.22) gives:

$$\frac{dw}{d\chi}\bigg|_{\chi=0} = 1 - \frac{i}{\sqrt{(\kappa(1-\gamma))}} \tag{6.68}$$

The limiting current for $\gamma < 1$ and $\kappa > 1$ is therefore:

$$\frac{i_L}{nFA} = \frac{Dp_\infty}{X_D}\left(2 - \frac{1}{\sqrt{(\kappa(1-\gamma))}}\right) \tag{6.69}$$

We will call this case IV.

It is satisfying to note that when $\gamma \ll 1$, equation (6.68) approximates to equation (6.58). This indicates that regions 2(a) and

-188-

3(a) are compatible along the $xy = 1$ boundary.

6.2.3.2 Region 3(b): $y > 1, x > 1$

Under these conditions the reaction between R and Q is fast and the two species react together in a thin reaction zone located at a distance x_o from the electrode. This is like a titration so the fluxes of Q and R must balance in the steady state such that:

$$D \frac{dq}{dx} = -D \frac{dr}{dx} \tag{6.70}$$

Converting to the dimensionless parameters and rearranging gives:

$$\frac{du}{d\chi} = -\frac{1}{y} \frac{dv}{d\chi} \tag{6.71}$$

Now if χ_o is the location of the reaction zone within the diffusion layer then:

$$\frac{du}{d\chi}\bigg|_{\chi = \chi_o} = -1 \tag{6.72}$$

and

$$\frac{dv}{d\chi}\bigg|_{\chi = \chi_o} = \frac{1}{1 - \chi_o} \tag{6.73}$$

Substituting (6.73) and (6.72) into (6.71) and rearranging gives:

$$\chi_o = 1 - \frac{1}{y} \tag{6.74}$$

So when $y = 1$, $\chi_\bullet = \chi_0 = 0$ and when $y \to \infty$, $\chi_\bullet \to 1$, the product of the chemical step, S, is produced at $\chi_\bullet$ and diffuses away from this plane so that in steady state the flux of Q is balanced by the fluxes of S to the electrode and away into the bulk solution. We then have:

$$D\frac{dq}{d\chi} = \frac{Ds_\bullet}{x_\bullet} + \frac{Ds_\bullet}{x_D - x_\bullet} \tag{6.75}$$

Converting to dimensionless parameters, applying the boundary condition $du/d\chi\big|_{\chi=0} = -1$ and rearranging gives:

$$w_\bullet = \chi_\bullet(1 - \chi_\bullet) \tag{6.76}$$

Finally, combining equations (6.76), (6.74) and since $dw/d\chi\big|_{\chi=0} = w_\bullet/\chi_\bullet$ leads to:

$$\frac{dw}{d\chi}\bigg|_{\chi=0} = \frac{1}{y} \tag{6.46}$$

This expression is identical to that derived for region 1(b). Consequently the limiting current is given by (6.46).

The model is now complete for all values of ϵ and y.

6.3 The chemistry and concentration profiles of each case

The purpose of this section is to help the reader understand, in a qualitative manner, the actual chemistry occurring close to the electrode surface for each case of the theoretical model. In particular, the effect of the ratio between the kinetics of the chemical step, $k_2 r_\infty$, and the rate of the diffusion, D/X_D^2, will be highlighted. Similar emphasis will be placed upon the effect of the ratio of the concentrations of the two initial solution species, P and R. This approach has been adopted because both of these parameters are under experimental control. The former ratio is affected by the rotation speed of the RDE. The faster the rotation speed the more dominant the diffusion term. The latter term is obviously controlled by altering the relative bulk concentrations of P and R. Consequently, we can move between all the cases by varying W, p_∞ or r_∞ as illustrated in figure 6.4.

Experimentally there may be restrictions on the ability to move between the cases. This is because the rotation rate is not infinitely variable and P and R are not infinitely soluble. The electrochemical reduction of P to Q in the first step of the reaction scheme sets up the same steady state concentration profile for each case. Consequently, the ensuing discussion will be concerned only with the fate of Q and the resultant formation of S.

6.3.1 Case 1: $x \ll 1$, $xy < 1$

In this case, $x \ll 1$ implies that the kinetics of the homogeneous chemical step are slow compared to the rate of diffusion. Consequently, the diffusion of Q through the distance X_D is faster than its reaction with P. This means that a large proportion of Q will escape into the bulk of the solution prior to the chemical step. This case also demands that when the bulk concentration of P is greater than that of R, the kinetics of the chemical step are always too slow to consume all of R in the diffusion

Figure 6.4:

ECE case diagram showing how the parameters p_∞, r_∞ and W need to be altered to move between the different cases.
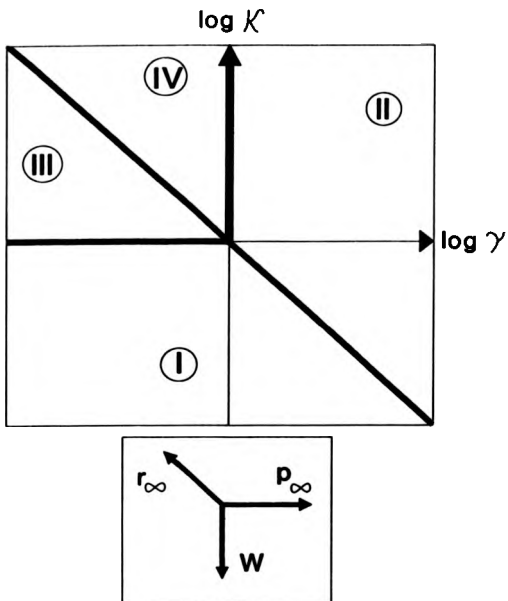
layer. If this latter criterion is violated, by reducing W or increasing p_∞, then the boundary between case I and II will be crossed.

The boundary between case I and case III can be crossed by increasing the time Q takes to cross the diffusion layer to such an extent that it is all consumed by R. This is achieved by either reducing the rotation rate or increasing the bulk concentration of R, for solutions in which $r_\infty > p_\infty$.

6.3.2 Case II: $\gamma > 1$; $\kappa\gamma > 1$

In this case, $\gamma > 1$ simply implies that the bulk concentration of P is always greater than that of R. The second restriction, $\kappa\gamma > 1$, demands that the kinetics of the reaction between Q and R are fast enough to ensure that all of Q is destroyed somewhere within the diffusion layer. The boundary between case II and case I can be traversed by increasing the rotation speed to the point where the diffusion layer is so thin that Q does not have time to react with R before it escapes into the bulk solution. It is also possible to move from case II into case I by increasing the bulk concentration of P provided that the chemical step is slow compared to the rate of diffusion.

6.3.3 Case III: $\kappa > 1$; $\kappa\gamma < 1$ and Case IV: $\gamma < 1$; $\kappa\gamma > 1$

The processes occurring within the diffusion layer of cases III and IV are very similar. In both cases, the conditions stipulate that the bulk concentration of R is always greater than that of P, i.e. $\gamma < 1$, and that the kinetics of the homogeneous chemical step are fast compared to the time taken for Q to diffuse the distance X_D, i.e. $\kappa > 1$. Consequently, all of Q reacts rapidly with R within the diffusion layer. The difference between the two cases arises from the relative magnitudes of γ and κ. Case III demands that $\kappa\gamma < 1$. Therefore the chemical step in case III can be said to be pseudo first order because the kinetics of the chemical step are not

fast enough to deplete the quantity of R within the diffusion layer. However, case IV demands that $\eta > 1$, which implies that the kinetics of the chemical step are always rapid enough to affect the concentration of R. Obviously the boundary between these two cases can be crossed by altering the magnitude of η.

The boundary can be crossed from case III to case I either by increasing the rotation rate so that X_D becomes sufficiently thin for Q to diffuse across it prior to the chemical step, or by decreasing the bulk concentration of R to such an extent that Q once again is able to escape into the bulk solution prior to the chemical step. Finally, it is possible to move from case IV into case II by increasing the bulk concentration of P such that $p_\infty > r_\infty$.

Idealised concentration profiles for the species Q, R, and S are illustrated for each case in figure 6.5.

Figure 6.5:

Plots of the concentration profiles of Q, R, and S as a function of distance normal to the electrode surface for cases I, II, III and IV.
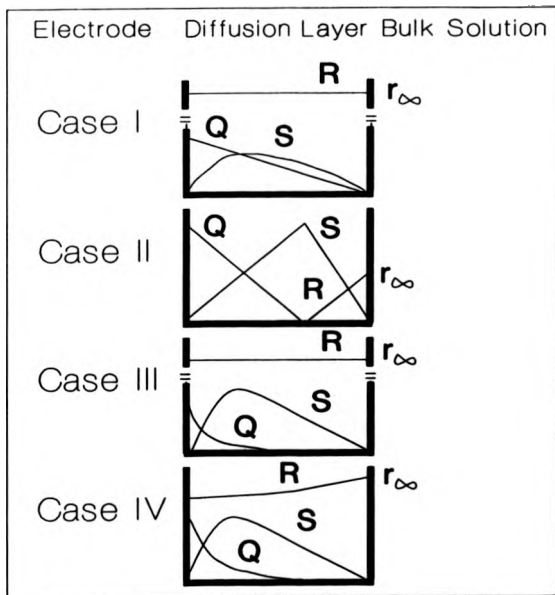
6.4 Treatment of limiting current responses of ECE reaction schemes according to this theory

In this chapter, we have derived equations for the limiting currents for ECE reaction regimes. These are collected together below:

CASE	LIMITING CURRENT	EQU. NO.
I	$\dfrac{i_L}{nFA} = \dfrac{Dp_\infty}{X_D}\left(1 + \dfrac{\kappa}{3}\right)$	(6.45)
II	$\dfrac{i_L}{nFA} = \dfrac{Dp_\infty}{X_D}\left(1 + \dfrac{1}{\gamma}\right)$	(6.47)
III	$\dfrac{i_L}{nFA} = \dfrac{Dp_\infty}{X_D}\left(2 - \dfrac{1}{\sqrt{\kappa}}\right)$	(6.59)
IV	$\dfrac{i_L}{nFA} = \dfrac{Dp_\infty}{X_D}\left(2 - \dfrac{1}{\sqrt{(\kappa(1 - \gamma))}}\right)$	(6.69)

Typically the limiting current is recorded as a function of W, p_∞ or r_∞. Consequently, it is helpful to rearrange these expressions so as to yield straight line relationships. These relationships are summarised in tables 6.1, 6.2 and 6.3 after substituting for X_D from (6.11), for κ from (6.16) and (6.11) and for γ from (6.15).

Table 6.1:

Table of terms of the straight line equation used to analyse an ECE reaction in which the limiting current is recorded as a function of the rotation speed with constant bulk concentrations of P and R.

CASE	Y AXIS	X AXIS	GRADIENT[a]	INTERCEPT[a] ON Y AXIS	EQU. NO.
I	$\dfrac{i_L}{W^{1/2}}$	$\dfrac{1}{W}$	$0.214nFAp_{\infty}r_{\infty}k_2 v^{1/6}D^{1/3}$	$\dfrac{1.554nFAp_{\infty}D^{2/3}}{v^{1/6}}$	(6.77)
II	i_L	$W^{1/2}$	$\dfrac{1.554nFAD^{2/3}(p_{\infty}+i_{\infty})}{v^{1/6}}$	0	(6.78)
III	$\dfrac{i_L}{W^{1/2}}$	$W^{1/2}$	$\dfrac{-2.419nFAp_{\infty}D^{5/6}}{k_2^{1/2}v^{2/6}r_{\infty}^{1/2}}$	$\dfrac{3.110nFAp_{\infty}D^{2/3}}{v^{1/6}}$	(6.79)
IV	$\dfrac{i_L}{W^{1/2}}$	$W^{1/2}$	$\dfrac{-2.419nFAp_{\infty}D^{5/6}}{k_2^{1/2}v^{2/6}(r_{\infty}-p_{\infty})^{1/2}}$	$\dfrac{3.110nFAp_{\infty}D^{2/3}}{v^{1/6}}$	(6.80)

[a] for W in Hz

Table 6.2:

Table of terms of the straight line equation used to analyse an ECE reaction in which the limiting current is recorded as a function of the bulk concentration of P with all other parameters constant.

CASE	Y AXIS	X AXIS	GRADIENT[a]	INTERCEPT[a] ON Y AXIS	EQU NO.
I	i_L	p_∞	$nFA\left(\dfrac{1.554D^{2/3}W^{1/2}}{\nu^{1/6}} + \dfrac{0.214r_\infty k_2\nu^{1/6}D^{1/3}}{W^{1/2}}\right)$	0	(6.81)
II	i_L	p_∞	$\dfrac{1.554nFAD^{2/3}W^{1/2}}{\nu^{1/6}}$	$\dfrac{1.554nFAD^{2/3}W^{1/2}r_\infty}{\nu^{1/6}}$	(6.82)
III	i_L	p_∞	$\left(\dfrac{1.554nFAD^{2/3}W^{1/2}}{\nu^{1/6}}\right)\left(1 - \dfrac{1.554D^{1/6}W^{1/2}}{k_2\nu^{1/2}r_\infty^{1/2}}\right)$	0	(6.83)
IV	$\dfrac{i_L}{p_\infty}$	$\dfrac{1}{(r_\infty - p_\infty)^{1/2}}$	$\dfrac{2.419nFAD^{5/6}W}{k_2^{1/2}\nu^{2/6}}$	$\dfrac{3.110nFAD^{2/3}W^{1/2}}{\nu^{1/6}}$	(6.84)

[a] for W in Hz

Table 6.3:

Table of terms of the straight line equation used to analyse an ECE reaction in which the limiting current is recorded as a function of the bulk concentration of R with all other parameters constant.

CASE	Y AXIS	X AXIS	GRADIENT[a]	INTERCEPT[a] ON Y AXIS	EQU NO.
I	i_L	r_∞	$\dfrac{0.214nFAD^{1/3}\nu^{1/6}k_2 p_\infty}{W^{1/2}}$	$\dfrac{1.554nFAD^{2/3}W^{1/2}p_\infty}{\nu^{1/6}}$	(6.85)
II	i_L	r_∞	$\dfrac{1.554nFAD^{2/3}W^{1/2}}{\nu^{1/6}}$	$\dfrac{1.554nFAD^{2/3}W^{1/2}p_\infty}{\nu^{1/6}}$	(6.86)
III	i_L	$\dfrac{1}{r_\infty^{1/2}}$	$\dfrac{2.419nFAD^{5/6}p_\infty}{k_2^{1/2}\nu^{2/6}}$	$\dfrac{3.110nFAD^{2/3}W^{1/2}p_\infty}{\nu^{1/6}}$	(6.87)
IV	i_L	$\dfrac{1}{(r_\infty - p_\infty)^{1/2}}$	$\dfrac{2.419nFAD^{5/6}p_\infty}{k_2^{1/2}\nu^{2/6}}$	$\dfrac{3.110nFAD^{2/3}W^{1/2}p_\infty}{\nu^{1/6}}$	(6.88)

[a] for W in Hz

6.5 Summary of the theoretical model

This theoretical model accounts for the limiting current at a RDE for a generalised ECE reaction scheme. The model is applicable to a wide range of relative concentrations of the initial solution species P and R. It is also valid for a broad range of homogeneous rate constants and diffusion rates.

It is apparent that there are four different cases arising from this analysis. The expressions derived for the limiting currents for each case, and the relationship between the cases is conveniently represented by way of a case diagram, figure 6.6. The parameters which are easily varied experimentally are p_∞, r_∞, and W. The alteration of one or more of these parameters moves the reaction scheme from one case to another. In order to determine where within the case diagram the reaction is occurring experimental data should be treated as described in section 6.4. There is a single kinetic parameter which can be evaluated from this treatment. It is the second order homogeneous rate constant k_2. It should be noted that k_2 cannot be evaluated from data lying within case II because this corresponds to a titration between P and R.

In chapter 7 the limiting current responses for the initial stages of the electrodeposition of poly(pyridine) are analysed using the model presented in this chapter.

Figure 6.6

Case diagram for the second order ECE reaction showing approximate expressions for the i_L in each case.

The bold lines show the case boundaries.
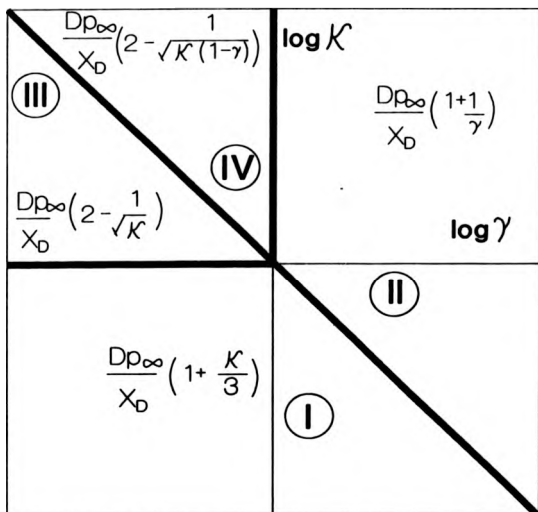
THE ELECTROCHEMICAL SYNTHESIS AND PROPERTIES OF NICKEL-2'2-DIPYRIDYL CATALYSED PPY

7.1 Introduction

In chapter 5, we described the electrochemical synthesis and deposition of PPy from electrolyte solutions containing excess PPh_3 and the dinuclear nickel complex, (I). The electrode deposits were unstable towards repetitive potential cycling which meant that further investigations into their properties proved unreliable. However, during the course of this work, Schiavon et al.[31] reported the electrosynthesis of PPy based on a $Ni^{(II)}/bpy/2,5-Br_2Py$ system (see section 1.3.3). We adopted a similar strategy which led to improved reproducibility and stability of the electrode deposits. This chapter is concerned with the properties and electrochemical synthesis of PPy prepared from $2,5-Br_2Py$ in the presence of $[Ni^{(II)}(bpy)_3(ClO_4)_2]$.

We begin by describing the optimum conditions for the electroreductive polymerisation of $2,5-Br_2Py$ in the presence of $[Ni^{(II)}(bpy)_3(ClO_4)_2]$. Next, the effect of the relative concentrations of the two reactants on the charge associated with the polymerisation is presented and discussed in terms of the reactant stoichiometry. This leads us to propose a reaction pathway describing the initial steps of the electroreductive polymerisation process. Following this, the proposed reaction pathway is tested in two ways. First, by analysing the limiting current responses at a RDE under the optimum polymerisation conditions. This analysis uses the specially formulated kinetic model

presented in the previous chapter. Second, by comparing the electrochemistry of a complex (XVI) with that of 2,5-Br$_2$Py in the presence of [Ni$^{(II)}$(bpy)$_3$(ClO$_4$)$_2$]. In the last section of this chapter, the properties of the electrode deposits are reported.

7.2 Optimum conditions for the electrochemical synthesis of PPy

In order to establish optimum conditions for electrodeposition, it is necessary to have a set of criteria which the electrode deposit should fulfil. Typically, the eventual application of the electrode deposit determines these criteria. However, in this case, there was no special application in mind, so the criteria we chose were broad and somewhat subjective. They were that:

1. the polymer was to be adherent to the electrode surface,

2. the polymer film was to be uniform to the naked eye,

3. the modified electrode was to be stable to repetitive cyclic voltammetry in electrolyte solutions following an initial breaking in period,

4. the polymerisation and polymer responses were to be reproducible.

Based on similar electroreductive polymerisation processes reported in the literature[30,31,37-40,99,101,102], AN and a tetraalkylammonium perchlorate (TEAP) were chosen as solvent and background electrolyte respectively. The potential window for AN solutions containing TEAP (0.1 mol dm^{-3}) is 1.90 V to -2.90 V [Ag/Ag$^+$ (AgClO$_4$, 0.01 mol dm^{-3} in AN)].

Mechanisms reported in the literature for nickel catalysed carbon-carbon bond formation between arylhalides all invoke oxidative

addition of the arylhalide to a low valent nickel (0) species. Therefore, for this electropolymerisation to be possible, $[Ni^{(0)}(bpy)_2]$ must be generated at the electrode surface and $2,5\text{-}Br_2Py$ must be electroinactive. The electrochemistry of $[Ni^{(II)}(bpy)_3(ClO_4)_2]$ and $2,5\text{-}Br_2Py$ (sections 4.3 and 4.4 respectively) indicate that suitable potentials for the electrosynthesis of PPy lie within the range -1.45 to -2.15 V [Ag/Ag^+ ($AgClO_4$, 0.01 mol dm^{-3} in AN)].

We found that the electrodeposition of PPy is relatively insensitive to the growth potential. It may be grown by either sweeping the potential back and forth over a potential range whose lower limit lies within -1.50 and -2.15 V and whose upper limit lies within -1.40 V to 0.0 V; or by stepping the potential from the solution's resting potential (-0.4 V) to a potential lying within the range -1.50 to -2.15 V. The former method produced the best electrode coats when the lower limit was -1.80 V (potentials more negative than this tended to give uneven deposits) and the upper limit was -1.25 V (potentials more positive than this produced films which were unstable to repetitive cyclic voltammetry). The latter potentiostatic method gave the best results when the stepped potential was -1.8 V and this was the preferred method owing to its greater experimental simplicity. Figures 7.1 and 7.2 show the typical growth responses.

Rigorous exclusion of oxygen from the growth solution was found to be essential. This is likely to be due to the reaction of the electrochemically generated $[Ni^{(0)}(bpy)_3]$ with oxygen inhibiting the initiation of the polymerisation reaction.

The electrodeposition of PPy was found to be insensitive to the reactant concentrations. PPy was successfully grown from test solutions containing equimolar concentrations of $[Ni^{(II)}(bpy)_3(ClO_4)_2]$ and $2,5\text{-}Br_2Py$ in the range 0.25 to 50 mmol dm^{-3}. The reactant

Figure 7.1

Forty successive cyclic voltammograms of an AN solution containing [Ni$^{(II)}$(bpy)$_3$(ClO$_4$)$_2$] (5 mmol dm^{-3}), 2,5-Br$_2$Py (5 mmol dm^{-3}) and TEAP (0.1 mol dm^{-3}) at GC/V. Potentials with respect to Ag/Ag$^+$ (0.01 mol dm^{-3}, AgClO$_4$ in AN). Sweep rate = 100 mV s^{-1}.
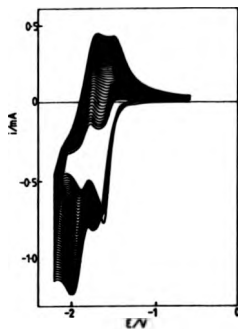
Figure 7.2:

Typical current-time curves at GC/V for an AN solution containing TEAP (0.1 mol dm^{-3}), [Ni$^{(II)}$(bpy)$_3$(ClO$_4$)$_2$] (5 mmol dm^{-3}) and 2,5-Br$_2$Py (5 mmol dm^{-3}) for a potential step from -0.4 V to -1.8 V. Potentials with respect to Ag/Ag$^+$ (0.01 mol dm^{-3}, AgClO$_4$ in AN).
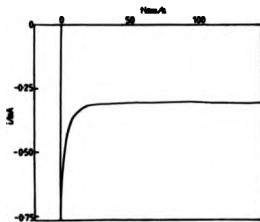
concentration for the majority of the experiments were each arbitrarily chosen to be 5 mmol dm^{-3}.

It was found that PPy could be successfully deposited onto platinum, glassy carbon, carbon fibres, gold and indium-doped tin oxide coated glass slides.

7.3 The effect of reactant concentration on polymerisation

The effect of varying the concentrations of $[Ni^{(II)}(bpy)_3(ClO_4)_2]$ and 2,5-Br$_2$Py in the growth solution on the charge passed during polymerisation at a stationary electrode was studied. Initially, a series of current-time transients were recorded for potential steps from -0.4 to -1.8 V in electrolyte solutions containing a fixed concentration of $[Ni^{(II)}(bpy)_3(ClO_4)_2]$ (5, 10 or 20 mmol dm^{-3}) and a range of 2,5-Br$_2$Py concentrations (0 to 45 mmol dm^{-3}). The charge passed during the first twenty seconds of each polymerisation was determined from the area under the i-t curves. Figure 7.3 shows the plots of the charge as a function of 2,5-Br$_2$Py concentration at each $[Ni^{(II)}(bpy)_3(ClO_4)_2]$ concentration. Each plot has two regions: a linear rise followed by a plateau. The intercept on the y axis, the gradients of the linear rise and the position of the shoulder between the two regions for each plot are summarised in the table 7.1:

Figure 7.3:

Plots of the charge passed over a period of 20 s following a potential step from -0.4 V to -1.8 V at GC/V against bulk concentration of 2,5-Br$_2$Py for AN solutions containing TEAP (0.1 mol dm^{-3}) and [Ni$^{(II)}$(bpy)$_3$(ClO$_4$)$_2$]: (a) 5 mmol dm^{-3}, (b) 10 mmol dm^{-3} and (c) 20 mmol dm^{-3}. Potentials with respect to Ag/Ag$^+$ (0.01 mol dm^{-3}, AgClO$_4$ in AN).
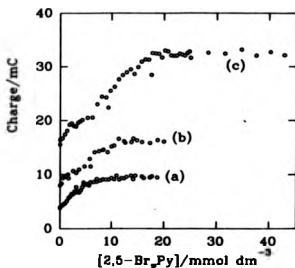
Figure 7.4:

Plots of the charge passed over a period of 20 s following a potential step from -0.4 V to -1.8 V at GC/V against bulk concentration of [Ni$^{(II)}$(bpy)$_3$(ClO$_4$)$_2$] for AN solutions containing TEAP (0.1 mol dm^{-3}) and 2,5-Br$_2$Py: (a) 5 mmol dm^{-3}, (b) 10 mmol dm^{-3} and (c) 20 mmol dm^{-3}. Potentials with respect to Ag/Ag$^+$ (0.01 mol dm^{-3}, AgClO$_4$ in AN).
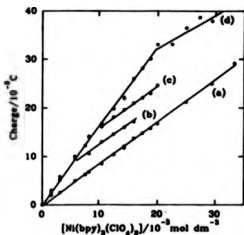
Table 7.1:

Summary of data in figure 7.3 for potential steps from -0.4 V to -1.8 V

		$[Ni^{(II)}(bpy)_3(ClO_4)_2]$ /mmol dm^{-3}		
		5	10	20
Intercept /mC		4.3 ± 0.5	7.5 ± 0.5	16.5 ± 0.5
Gradient of Linear Rise /C mol^{-1} dm^3		0.89 ± 0.05	0.85 ± 0.05	0.88 ± 0.05
Position of Dog Leg	[2,5Br$_2$Py] /mmol dm^{-3}	5.0 ± 0.5	10 ± 1	19 ± 1
	Charge /mC	8.5 ± 1	15.5 ± 1	32 ± 1

The intercept on the y-axis corresponds to the total charge consumed over a period of twenty seconds for the two-electron diffusion controlled reduction of $[Ni^{(II)}(bpy)_3]^{2+}$. Addition of 2,5-Br$_2$Py to the solution initially causes a charge increase which is directly proportional to the combined bulk concentrations of $[Ni^{(II)}(bpy)_3(ClO_4)]$ and 2,5-Br$_2$Py. The proportionality constant is approximately unity. Now, since 2,5-Br$_2$Py was shown to be electroinactive at -1.8 V (section 4.4) then a reaction scheme which accounts for the increase in charge must be invoked. There is ample evidence in the literature to suggest that 2,5-Br$_2$Py will undergo a chemical reaction with the electrogenerated nickel(0) species forming an oxidative addition adduct[30,31,37-40,99,101,102]. The adduct must then undergo a further two-electron reduction to account for the charge passed.

The charge becomes independent of any further addition of 2,5-Br$_2$Py when its bulk concentration exceeds that of the nickel complex.

This implies that each nickel zero species can only react with one dibromoaromatic during the polymerisation process. Any excess 2,5-Br$_2$Py remains unreacted. At the plateau the amount of charge has doubled compared to its value for [Ni$^{(II)}$(bpy)$_3$(ClO$_4$)$_2$] alone. This supports our proposal that the reductive polymerisation is a four-electron process.

The complementary set of current-time transients were recorded for growth solutions containing a range of [Ni$^{(II)}$(bpy)$_3$(ClO$_4$)$_2$] concentrations (0 to 35 mmol dm^{-3}) at fixed concentrations of 2,5-Br$_2$Py (0, 5, 10 or 20 mmol dm^{-3}). Figure 7.4 shows the plots of the charge consumed during the first twenty seconds immediately following the potential step as a function of [Ni$^{(II)}$(bpy)$_3$(ClO$_4$)$_2$] concentration at each 2,5-Br$_2$Py concentration. The salient features of the plots are summarised in table 7.2:

Table 7.2:

Summary of data in figure 7.4 for potential steps from –0.4 V to –1.8 V

		[2,5-Br$_2$Py] /mmol dm^{-3}			
		0	5	10	20
Gradient of 1st Linear Rise /C mol^{-1} dm^3		0.86 ± 0.02	←— 1.63 ± 0.05 —→		
Gradient of 2nd Linear Rise /C mol^{-1} dm^3		—	0.87 ± 0.02	0.88 ± 0.02	0.89 ± 0.02
Position of Dog Leg	[Ni(bpy)$_3$(ClO$_4$)$_2$] /mmol dm^{-3}	—	5.5 ± 0.5	10.0 ± 1	19.5 ± 1
	Charge /mC	—	8.5 ± 1	16.0 ± 1	31.5 ± 1

-209-

A straight line plot passing through the origin was obtained for the control solutions in which there was no 2,5-Br$_2$Py. This is as expected for a redox process under diffusion control. It represents the charge passed for the two-electron reduction [Ni$^{(II)}$(bpy)$_3$]$^{2+}$.

Plots (b), (c) and (d) have two distinct regions. The first region corresponds to solutions in which the bulk concentration of the nickel complex is less than that of the 2,5-Br$_2$Py. In this region the charge increase is twice that of plot (a). Therefore we can infer that the charge passed is equivalent to four electrons per nickel.

The transition to the next region occurs when the reactant concentrations are equal and the charge is double that of the control solution at the equivalent [Ni$^{(II)}$(bpy)$_3$(ClO$_4$)$_2$] concentration. At this point there is just enough of the nickel complex being reduced at the electrode surface to react with all the available 2,5-Br$_2$Py. The product of this reaction then undergoes a further two-electron reduction to account for the charge doubling. Addition of more of the nickel complex results in a second linear rise whose gradient is equal to that of plot (a). This is consistent with the excess [Ni$^{(II)}$(bpy)$_3$(ClO$_4$)$_2$] only undergoing a two-electron reduction because there is no unreacted 2,5-Br$_2$Py available for the following chemical reaction.

The results from both series of experiments are consistent. It can be concluded that the polymerisation process has an overall stoichiometry of 1 to 1 for the reactants and that a maximum of four electrons per nickel are consumed. Based on these conclusions, we propose that the initial steps of the polymerisation can be represented by the following

reaction scheme:

Electrode: $[Ni^{(II)}(bpy)_3]^{2+} \xrightarrow{2e} [Ni^{(0)}(bpy)_3]$

Solution: $[Ni^{(0)}(bpy)_3] \xrightarrow{k_a} [Ni^{(0)}(bpy)_2] + bpy$

Solution: $[Ni^{(0)}(bpy)_2] + 2,5\text{-}Br_2Py \xrightarrow{k_b} [BrNi^{(II)}(BrPy)(bpy)] +$

$$bpy$$

Electrode: $[BrNi^{(0)}(BrPy)(bpy)] \xrightarrow{2e} \longrightarrow \longrightarrow polymer$
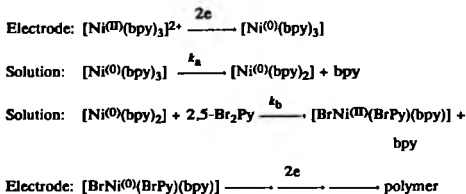
This reaction scheme is an ECCE process whose overall rate will be determined by the slowest chemical step. This means that it can be treated as an ECE type mechanism in which the chemical step is represented by:

Solution: $[Ni^{(0)}(bpy)_3] + 2,5\text{-}Br_2Py \xrightarrow{k_2} [BrNi^{(II)}(BrPy)(bpy)] +$

$$2bpy$$
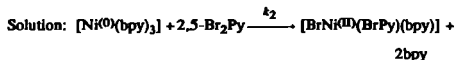
An alternative reaction scheme which also accounts for the observed stoichiometry and charge consumption may be represented as follows:

Electrode: $2[Ni^{(II)}(bpy)_3]^{2+} \xrightarrow{4e} 2[Ni^{(0)}(bpy)_3]$

Solution: $[Ni^{(0)}(bpy)_3] + 2,5\text{-}Br_2Py \xrightarrow{k_2} [BrNi^{(II)}(BrPy)(bpy)] +$

$$2bpy$$

Solution: $[BrNi^{(II)}(BrPy)(bpy)] + [Ni^{(0)}(bpy)_3] \xrightarrow{k_c}$

$$BrNi^{(0)}(BrPy)(bpy)] + [Ni^{(II)}(bpy)_3]^{2+}$$

Solution: $BrNi^{(0)}(BrPy)(bpy)] \longrightarrow \longrightarrow \longrightarrow polymer$

-211-
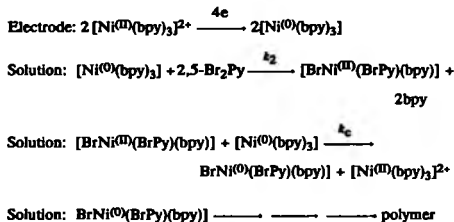
This is a DISP process. There are potentially two possible mechanisms depending on whether the first- or second- chemical step is rate determining; these are denoted DISP1 and DISP2 respectively. Since the polymerisation reaction is first order with respect to nickel then the only alternative to the ECE mechanism is the DISP1 mechanism. Discrimination between ECE and DISP1 reactions using electrochemical techniques requires accuracies which are almost unattainable in practice. Consequently, although we have analysed the initial stages of the polymerisation reaction on the theory developed in chapter 6 for a second order ECE process, we cannot rule out DISP1 as a possible mechanism.

7.4 Current responses at a RDE for PPy growth solutions

In the previous section we postulated that the initial stages of the nickel/bpy catalysed electroreductive polymerisation of 2,5-Br_2Py conforms to an ECE type mechanism. In this section, the proposed mechanism is tested by analysing the limiting current responses for the polymerisation at a RDE using the theory developed in chapter 6.

The theory describes the limiting current responses of the following ECE reaction scheme.
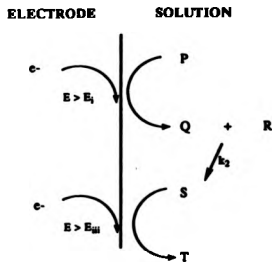
where the electrode is held at a potential which ensures that the reduction of P and S are entirely mass transport controlled.

In terms of our polymerisation, P and R are the reactants $[Ni^{(II)}(bpy)_3]^{2+}$ and 2,5-Br$_2$Py respectively; Q is the reduced form of P, $[Ni^{(0)}(bpy)_3]$; S is the oxidative addition adduct, $[BrNi^{(II)}(BrPy)(bpy)]$, and T is the reduced form of S, $[BrNi^{(0)}(BrPy)(bpy)]^{2-}$. The rate constant, k_2, describes the homogeneous chemical reaction(s) between $[Ni^{(0)}(bpy)_3]$ and 2,5-Br$_2$Py leading to the formation of the adduct.

7.4.1 Experimental constraints on moving around the case diagram

Returning to the theoretical model presented in chapter 6, and in particular to figure 6.3, it can be seen that there are 4 different cases for the ECE system. It is theoretically possible to move between the cases by varying the bulk concentration of either $[Ni^{(II)}(bpy)_3(ClO_4)_2]$, p_∞, or 2,5-Br$_2$Py, r_∞, or by varying the rotation speed, W.

In this system, both reactants are very soluble in the chosen electrolyte solution. This means that the ratio of the reactant concentrations, γ, can be varied over a wide range. An examination of the case diagram in figure 6.3 reveals that altering the bulk concentration of the nickel complex (from 1×10^{-6} to 40×10^{-6} mol cm^{-3}) will move us in a direction horizontal to the logγ axis.

Movement in the vertical direction of the case diagram is achieved by altering the value of ϵ. ϵ reflects the balance between the homogeneous kinetics and diffusion and is given by:

$$\epsilon = \frac{0.413 \nu^{2/6} k_2 r_\infty}{D^{1/3}W} \qquad (7.1)$$

where ν is the kinematic viscosity of acetonitrile (3.29×10^{-3} cm^2 s^{-1})[175],

D is the diffusion coefficient of the solution species (1.25×10^{-5} cm^2 s^{-1}), k_2 is the homogeneous rate constant (mol^{-1} cm^3 s^{-1}). r_∞ is the bulk concentration of 2,5-Br$_2$Py (from 1×10^{-6} to 40×10^{-6} mol cm^{-3}) and W is the rotation speed (1 to 49 Hz).

Examination of equation (7.1) shows that x is dependent on the experimental parameters W and r_∞. The effect of changing W will be to move us vertically in a direction parallel to the log$x$ axis of the case diagram. The effect of changing r_∞ will move us in a direction parallel to the $x \propto 1/y$ axis. The compound effect of r_∞ on the direction of movement within the case diagram is because it is proportional to x and inversely proportional to y.

In this system, the limits of the experimental parameters are known. There is only one unknown quantity, namely k_2. Consequently, the outer boundary of the case diagram, which should encompass all the experimental data, can be determined in terms of k_2, figure 7.5. It is apparent from figure 7.5 that the accessible cases are dependent on the actual value of k_2.

In the following section we describe the experimental conditions and treatment of the data used to record the limiting current responses suitable for analysis using the ECE theory.

7.4.2 Experimental conditions and data treatment

In order to apply the theory to the current responses of the polymerisation, it was first necessary to determine the potential at which the electrode reactions were entirely mass transport controlled. It has been suggested by Schiavon et al.[31] and confirmed by our own studies (section 7.5), that the electroreduction of [BrNi$^{(II)}$(BrPy)(bpy)] will be entirely mass transport controlled at all potentials where the two-electron reduction of [Ni$^{(II)}$(bpy)$_3$]$^{2+}$ is also entirely mass transport controlled.

-214-

Figure 7.5:

The modified ECE case diagram showing the boundary which encompasses all the experimental data, —. The boundary was calculated knowing that p_{∞} and r_{∞} were varied between 1×10^{-6} and 40×10^{-6} mol cm^{-3} and W was varied between 1 and 49 Hz. The hatched areas within this boundary represent the relative positions of the experiments carried out to test whether the polymerisation process conforms to the ECE theory. The boundaries separating the 4 different cases are represented by —.

Key

Expt 1   Expt 3

Expt 2   Expt 4
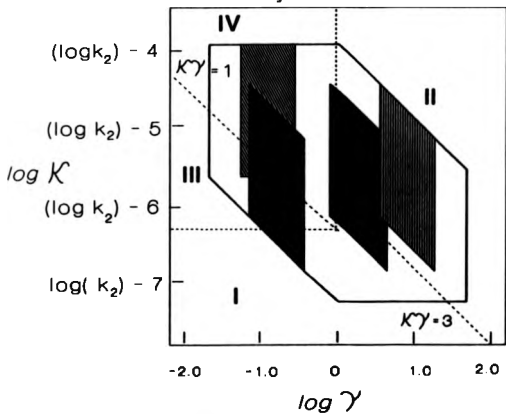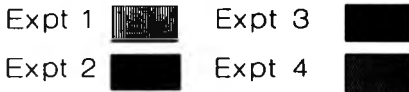
Figure 7.6 shows a typical polarogram of a growth solution and compares it to the two-electron reduction of $[Ni^{(II)}(bpy)_3]^{2+}$. It can be seen that a suitable potential for the RDE studies is -1.9 V [Ag/Ag$^+$(AgClO$_4$, 0.01 mol dm^{-3} in AN)].

The shape of the current-time response is affected by the deposition of PPy onto the electrode surface. The amount of deposit depends on p_∞, r_∞ and W. To ensure that the data analysed was not complicated by the changing properties of the electrode surface, the current responses were extrapolated back to zero time to give $i_{L,t=0}$, figure 7.7. Inevitably the extrapolation introduces errors into the $i_{L,t=0}$ values. The magnitude of the errors increase with increasing W and decreasing p_∞/r_∞ and therefore the data becomes more imprecise or scattered as W or r_∞ are increased. However in all cases we estimate that the error was less than 10% and in most cases less than 5%.

Once a suitable potential had been established, the current-time responses were recorded as a function of W, p_∞ and r_∞. The measurements were made as follows: freshly polished GC/V was rotated at the desired speed and the potential was stepped to -1.8 V in a thoroughly deoxygenated electrolyte solution containing the desired concentrations of P and R. Typically, a set of experiments involved recording $i_{L,t=0}$ over the entire range of W for a series of concentrations of one reactant while the concentration of the other reactant was held constant. The transients were very reproducible; we estimate that the variation between transients recorded under identical conditions is less than 5%. The relative position of each set of experiments was chosen so that all the accessible cases within the case diagram could be tested, figure 7.5.

Figure 7.6:

Typical current-voltage curves at the RDE GC/V in AN solutions containing TEAP (0.1 mol dm^{-3}) and either (a) [Ni$^{(II)}$(bpy)$_3$(ClO$_4$)$_2$] (1 mmol dm^{-3}) or (b) [Ni$^{(II)}$(bpy)$_3$(ClO$_4$)$_2$] (1 mmol dm^{-3}) and 2,5-Br$_2$Py (1 mmol dm^{-3}). Potentials with respect to Ag/Ag$^+$ (0.01 mol dm^{-3}, AgClO$_4$ in AN). Rotation speed = 16 Hz. Sweep rate = 20 mV s^{-1}.
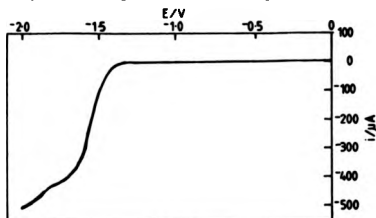
Figure 7.7:

Typical current-time curve at the RDE GC/V for an AN solution containing TEAP (0.1 mol dm^{-3}), [Ni$^{(II)}$(bpy)$_3$(ClO$_4$)$_2$] (40 mmol dm^{-3}) and 2,5-Br$_2$Py (12.5 mmol dm^{-3}) for a potential step from -0.4 V to -1.8 V. Potentials with respect to Ag/Ag$^+$ (0.01 mol dm^{-3}, AgClO$_4$ in AN). Rotation speed = 9 Hz. The current is extrapolated back to zero time in order to determine the limiting current for the polymerisation process at a clean electrode surface, $i_{L,t=0}$.
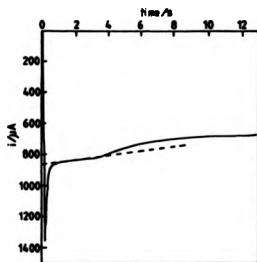
7.4.3 Analysis of $i_{L,t=0}$ using the theoretical model

In this section the effect of changing the experimental parameters on $i_{L,t=0}$ is presented and analysed in terms of the theoretical model. As we shall see, the results demonstrate that the value of k_2 for this system allows us to reach all four cases within the experimental constraints of W, p_∞ and r_∞.

7.4.3.1 Experiment 1

Let us first consider the situation for the dependence of $i_{L,t=0}$ on W where $p_\infty = 40 \times 10^{-6}$ mol cm^{-3} and r_∞ is varied from 2.5×10^{-6} to 12.5×10^{-6} mol cm^{-3}, experiment 1, figure 7.5. The data was analysed for case II by plotting $i_{L,t=0}$ against $W^{1/2}$ according to equation (6.78):

$$i_L = \frac{1.554 nFAD^{2/3}(p_\infty + r_\infty)W^{1/2}}{\nu^{1/6}} \qquad (6.78)$$

The theory predicts that this plot passes through the origin and has a gradient proportional to the sum of the reactant concentrations, $p_\infty + r_\infty$. Figure 7.8 shows that the data fit for case II is good. Table 7.3 shows that there is close agreement between the theoretical and experimental gradients of these plots.

Figure 7.8:

Plots of $i_{L,t=0}$ recorded at different rotation speeds (1 to 49 Hz) for polymerisation solutions containing $[Ni^{(II)}(bpy)_3(ClO_4)_2]$ (40 mmol dm^{-3}) and 2,5-Br$_2$Py (12.5, 10.0. 7.5, 5.0, 2.5 and 0.0 mmol dm^{-3}) according to equation (6.78).
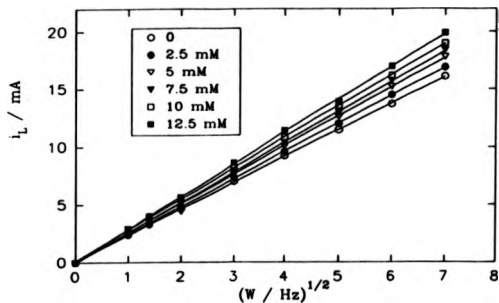
Figure 7.9:

Plots of the experimental data in table 7.3 according to equation (7.2).
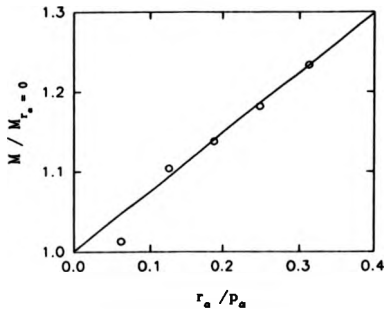
Table 7.3:

Comparison of the theoretical and experimental gradients of the case II plots in figure 7.8.

$[Ni(bpy)_3(ClO_4)_2]$ /mol cm^{-3}	$[2,5-Br_2Py]$ /mol cm^{-3}	Gradient /A s$^{-1/2}$ Theoretical	Experimental
40×10^{-6}	0	——	2.31×10^{-3}
40×10^{-6}	2.5×10^{-6}	2.42×10^{-3}	2.73×10^{-3}
40×10^{-6}	5.0×10^{-6}	2.54×10^{-3}	2.54×10^{-3}
40×10^{-6}	7.5×10^{-6}	2.65×10^{-3}	2.63×10^{-3}
40×10^{-6}	10.0×10^{-6}	2.77×10^{-3}	2.73×10^{-3}
40×10^{-6}	12.5×10^{-6}	2.88×10^{-3}	2.85×10^{-3}

The validity of the assumption that the diffusion coefficients of P, R and S are equal, can be tested by plotting $M/M_{r\infty \, = \, 0}$ against r_∞/p_∞ according to equation (7.2):

$$\frac{M}{M_{r\infty \, = \, 0}} = 1 + \frac{r_\infty}{p_\infty} \qquad (7.2)$$

where M and $M_{r\infty \, = \, 0}$ are the slopes of the plots in figure 7.8 in the presence and absence of 2,5-Br$_2$Py respectively. Now, assuming that $D_P = D_R = D_S$ then the theory predicts that both the gradient and intercept should be unity. However, figure 7.9 shows that although the intercept is 1.0 ± 0.1, the gradient is 0.75 ± 0.05 which indicates that our assumption is not wholly valid. Modification of equation (7.2) (appendix 7.1) to account for different diffusion coefficients is readily achieved:

$$\frac{M}{M_{r\infty=0}} = 2 - \left(\frac{D_R}{D_S}\right)^{1/3} + \left(\frac{D_R}{D_P}\right)\left(\frac{D_P}{D_S}\right)^{1/3} \frac{r_\infty}{p_\infty} \qquad (7.3)$$

Since the intercept is $\simeq 1$ we can infer that $D_R \simeq D_S$. Similarly, since the gradient is $\simeq 0.75$ and $D_P = 7.16 \times 10^{-6}$ cm^2 s^{-1}, then D_R and $D_S \simeq 4.65 \times 10^{-6}$ cm^2 s^{-1}. It is pleasing that these values are in good agreement with those determined independently and given in sections 4.4 and 7.5 ($D_R = 4.98 \times 10^{-6}$ and $D_S = 3.58 \times 10^{-6}$ cm^2 s^{-1}).

We can conclude that when the bulk concentration of $[Ni^{(II)}(bpy)_3(ClO_4)_2]$ is fixed at 40×10^{-6} mol cm^{-3} and that of 2,5-Br$_2$Py is varied between 2.5×10^{-6} and 12.5×10^{-6} mol cm^{-3}, then the initial steps of the polymerisation reaction are fully described by the ECE theory for case II over the entire rotation speed range, 1 to 49 Hz.

Qualitatively these results indicate that all the $[Ni^{(0)}(bpy)_3]$ produced at the electrode surface is destroyed within the diffusion layer by a fast homogeneous chemical reaction with 2,5-Br$_2$Py. Increasing the rotation speed does not result in the boundary between case II and I being crossed. This is because the maximum rotation speed cannot reduce the thickness of the diffusion layer sufficiently to enable some of the $[Ni^{(0)}(bpy)_3]$ to escape into the bulk solution. Consequently, we cannot obtain any kinetic information, k_2, from this data.

7.4.3.2 Experiment 2

Let us now consider the situation where the concentration of $p_\infty = 10 \times 10^{-6}$ mol cm^{-3} and r_∞ and W are varied as before, experiment 2, figure 7.5. This has moved us towards the central region of the case diagram.

Once again the experimental data was analysed for case II according to equation (6.78). Figure 7.10 shows that at low rotation

Figure 7.10:

Plots of $i_{L, t \to 0}$ recorded at different rotation speeds (1 to 49 Hz) for polymerisation solutions containing $[Ni^{(II)}(bpy)_3(ClO_4)_2]$ (10 mmol dm^{-3}) and 2,5-Br$_2$Py (7.5, 5.0 and 2.5 mmol dm^{-3}) according to equation (6.78).

Figure 7.11:

Plots of $i_{L, t \to 0}$ recorded at rotation speeds 25, 36 and 49 Hz for polymerisation solutions containing $[Ni^{(II)}(bpy)_3(ClO_4)_2]$ (10 mmol dm^{-3}) and 2,5-Br$_2$Py (7.5, 5.0 and 2.5 mmol dm^{-3}) according to equation (6.77).
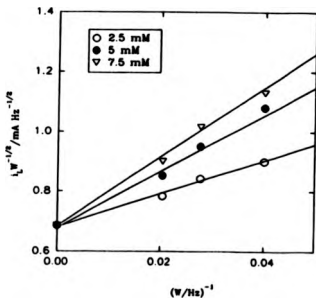
speeds (1- 16 Hz) where r_∞ is 2.5 x 10^{-6}, 5.0 x 10^{-6} and 7.5 x 10^{-6} mol cm^{-3}, the plots are linear and pass through the origin. The slopes of the linear portions are in good agreement with the theoretical gradients, table 7.4:

Table 7.4:

Comparison of the theoretical and experimental gradients of the linear portions of the case II plots in figure 7.9

[Ni(bpy)$_3$(ClO$_4$)$_2$] /mol cm^{-3}	[2,5-Br$_2$Py] /mol cm^{-3}	Gradient Case II /A s$^{-1/2}$ Theoretical	Experimental
10 x 10^{-6}	0	————	6.85 x 10^{-4}
10 x 10^{-6}	2.5 x 10^{-6}	8.56 x 10^{-4}	9.00 x 10^{-4}
10 x 10^{-6}	5.0 x 10^{-6}	10.28 x 10^{-4}	11.50 x 10^{-4}
10 x 10^{-6}	7.5 x 10^{-6}	12.00 x 10^{-4}	13.50 x 10^{-4}

At high rotation speeds, the case II plots bend towards the x-axis because the limiting currents are smaller than predicted by case II. This probably arises because some of the [Ni$^{(0)}$(bpy)$_3$] produced at the electrode surface escapes from the diffusion layer before reacting with 2,5-Br$_2$Py. This means that at high rotation speeds (25 to 49 Hz) we begin to enter case I.

The experimental data recorded at high rotation speeds (25 to 49 Hz) were analysed for case I by plotting $i_{L,t=0}W^{-1/2}$ against W^{-1} according to equation (6.77).

$$\frac{i_L}{W^{1/2}} = \frac{0.214nFAD^{1/3}\nu^{1/6}k_2 r_\infty p_\infty}{W} + \frac{1.554nFAD^{2/3}p_\infty}{\nu^{1/6}} \quad (6.77)$$

Figure 7.11 shows that this data conforms to case I. The plots are linear and all intersect the y-axis at approximately 6.85×10^{-4} A $s^{1/2}$. The intercept is an experimentally determined point as it corresponds to the Levich gradient of the test solution in the absence of 2,5-Br$_2$Py. A value of k_2 can be determined from each plot given that n = 2, F = 96485 C mol^{-1}, A = 0.2 cm^2, D = 1.25×10^{-5} cm ^{2} s^{-1}, ν = 3.29×10^{-3} cm ^{2} s^{-1} and p_∞ = 10×10^{-6} mol cm^{-3}. The slopes and their corresponding homogeneous rate constants are presented in table 7.5:

Table 7.5:

Gradients and homogeneous rate constants determined from the case I plots given in figure 7.10

[Ni(bpy)$_3$(ClO$_4$)$_2$] /mol cm^{-3}	[2,5-Br$_2$Py] /mol cm^{-3}	Gradient /A s$^{-1/2}$	k_2 /mol^{-1} cm^3 s^{-1}
10×10^{-6}	2.5×10^{-6}	5.3×10^{-3}	2.8×10^6
10×10^{-6}	5.0×10^{-6}	8.6×10^{-3}	2.3×10^6
10×10^{-6}	7.5×10^{-6}	11.6×10^{-3}	2.1×10^6

We can conclude that when p_∞ = 10×10^{-6} mol cm^{-3}, r_∞ lies between 2.5×10^{-6} and 7.5×10^{-6} mol cm^{-3} and W < 16 Hz, then the diffusion layer is so thick that none of the [Ni$^{(0)}$(bpy)$_3$] produced at the electrode surface can escape into the bulk solution. However, as the rotation speed is increased, W > 25 Hz, and the diffusion layer concomitantly decreases in thickness, then some of the nickel (0) is able to cross the diffusion layer without being "caught" by 2,5-Br$_2$Py. The change over from the former to the latter situation corresponds to crossing the boundary from case II to case I. Analysis of the data lying within case I allows the homogeneous rate constant to be determined; the

average value is 2.4×10^6 mol^{-1} cm^3 s^{-1}.

The limiting current responses described by case I have also been analysed as a function of 2,5-Br$_2$Py concentration according to equation (6.85):

$$I_L = \frac{0.214nFAD^{1/3}\nu^{1/6}k_2 r_\infty p_\infty}{W^{1/2}} + \frac{1.554nFAD^{2/3}p_\infty W^{1/2}}{\nu^{1/6}} \quad (6.85)$$

Figure 7.12 shows that these plots are linear. The intercepts on the y axis are experimentally determined points and correspond to the product of the square root of the rotation speed and the Levich gradient of the test solution in the absence of any 2,5-Br$_2$Py. Again k_2 can be evaluated from the gradient of each plot. The average value is 1.9×10^6 mol^{-1} cm^3 s^{-1} which agrees well with the previously determined values.

It is also pleasing to note that the data recorded for the test solutions containing 10.0×10^{-6} and 12.5×10^{-6} mol cm^{-3} 2,5-Br$_2$Py does not conform to either case I or case II even at low rotation speeds. This is as expected because the theory predicts that when log$\gamma \leq 0$, then the experimental conditions no longer conform with the criteria for cases I or II.

7.4.3.3 Experiment 3

Let us consider the situation where p_∞ is altered to 1.0×10^{-6} mol cm^{-3}, and r_∞ and W are varied as usual, experiment 3, figure 7.5. The theory predicts that we are on the left hand side of the case diagram, and the value of k_2 (calculated in section 7.4.3.2) places us in case I when W is fast and r_∞ is low; in case IV when W is slow for all values of r_∞ and in case III for the other combinations of W and r_∞.

We initially analysed the current responses for case I by plotting $I_{L,t=0}W^{-1/2}$ against W^{-1} according to equation (6.77):

-225-

Plots of $i_{L,t=0}$ recorded at rotation speeds 16, 25, 36 and 49 Hz for polymerisation solutions containing $[Ni^{(II)}(bpy)_3(ClO_4)_2]$ (10 mmol dm^{-3}) and $2,5\text{-}Br_2Py$ (7.5, 5.0 and 2.5 mmol dm^{-3}) according to equation (6.85).

$[2,5Br_2Py]/mmol\ dm^{-3}$
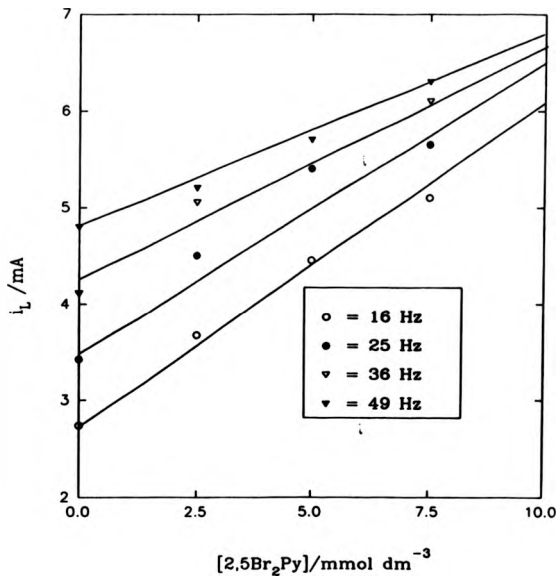
$$\frac{i_L}{W^{1/2}} = \frac{0.214nFAD^{1/3}v^{1/6}k_2r_\infty p_\infty}{W} + \frac{1.554nFAD^{2/3}p_\infty}{v^{1/6}} \quad (6.77)$$

Figure 7.13 shows that the data fit for case I is only good when $W > 16$ Hz and $r_\infty < 5.0 \times 10^{-6}$ mol cm^{-3}. Values of k_2 obtained from the linear portion of these plots are collected together in table 7.6.

Next, the limiting current responses were analysed for cases III and IV by plotting $i_{L,t\to 0}W^{-1/2}$ against $W^{1/2}$ according to equations (6.79) and (6.80) respectively:

$$\frac{i_L}{W^{1/2}} = \frac{-2.419nFAD^{5/6}p_\infty W^{1/2}}{k_2^{1/2}v^{2/6}r_\infty^{1/2}} + \frac{3.110nFAD^{2/3}p_\infty}{v^{1/6}} \quad (6.79)$$

$$\frac{i_L}{W^{1/2}} = \frac{-2.419nFAD^{5/6}p_\infty W^{1/2}}{k_2^{1/2}v^{2/6}(r_\infty - p_\infty)^{1/2}} + \frac{3.110nFAD^{2/3}p_\infty}{v^{1/6}} \quad (6.80)$$

Figure 7.14 shows that these plots are linear for low values of W and high values of r_∞. The intercept on the y-axis is an experimentally determined point as it corresponds to twice the Levich gradient of the test solution in the absence of 2,5-Br$_2$Py.

Ideally, equations relating $i_{L,t\to 0}$ to W for cases III and IV allow discrimination between the two cases. However, experimental error prevents realistic discrimination, so we have presented the homogeneous rate constants determined from the linear portion of each plot in figure 7.14 as a range rather than a single value, table 7.6.

Plots of $i_{L-1} - 0$ recorded at different rotation speeds (1 to 49 Hz) for polymerisation solutions containing $[Ni^{(II)}(bpy)_3(ClO_4)_2]$ (1 mmol dm^{-3}) and 2,5-Br_2Py (12.5, 10.0. 7.5, 5.0, 2.5 and 0.0 mmol dm^{-3}) according to equation (6.77). The insert shows the expanded region of the plots corresponding to high rotation speeds (25, 36 and 49 Hz) and low 2,5-Br_2Py concentrations (2.5 and 5.0 mmol dm^{-3}).
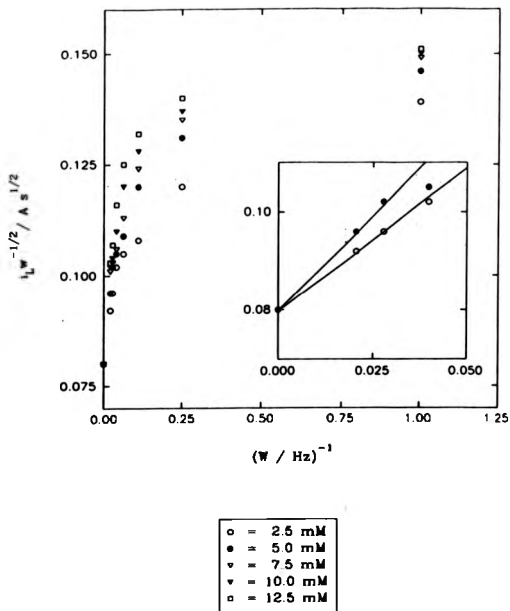
Plots of $i_{I_{t}^{-1} = 0}$ recorded at different rotation speeds (1 to 49 Hz) for polymerisation solutions containing $[Ni^{(II)}(bpy)_3(ClO_4)_2]$ (1 mmol dm^{-3}) and 2,5-Br_2Py (12.5, 10.0, 7.5, 5.0, 2.5 and 0.0 mmol dm^{-3}) according to equations (6.79) and (6.80).
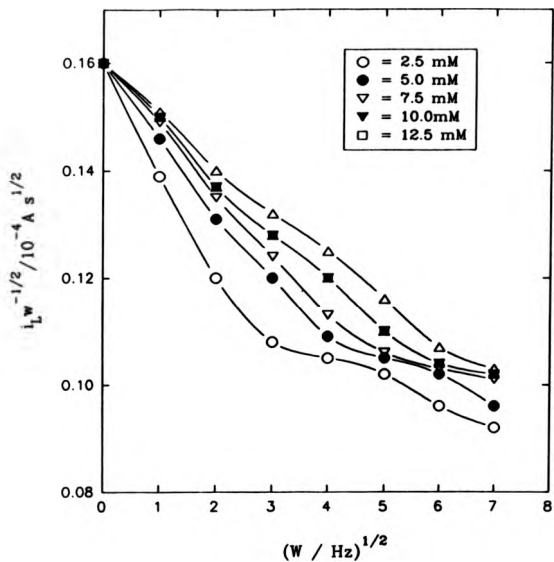
Table 7.6:

Gradients and homogeneous rate constants Ootained from the linear
portion of plots 7.13 and 7.14

$[Ni(bpy)_3(ClO_4)_2]$	$[2,5\text{-}Br_2Py]$	Gradient		k_2
		Case II	Case III/IV	
/mol cm^{-3}	/mol cm^{-3}	/A s$^{1/2}$	/A	/mol^{-1}cm^{-3}s^{-1}
1×10^{-6}	2.5×10^{-6}	5.4×10^{-4}	———	2.9×10^{6}
1×10^{-6}	5.0×10^{-6}	7.5×10^{-4}	———	2.1×10^{6}
1×10^{-6}	7.5×10^{-6}	———	12.5×10^{-6}	$(2.3\text{-}2.6) \times 10^{6}$
1×10^{-6}	10.0×10^{-6}	———	10.8×10^{-6}	$(2.3\text{-}2.5) \times 10^{6}$
1×10^{-6}	12.5×10^{-6}	———	9.0×10^{-6}	$(2.6\text{-}2.8) \times 10^{6}$

Once again, $i_{L,t=0}$ can also be analysed as a function of r_∞. This is
illustrated for cases I and IV for $W = 49$ Hz, $r_\infty < 7.5 \times 10^{-6}$ mol cm^{-3}
and $W = 1$ Hz, $0 \leq r_\infty < 12.5 \times 10^{-6}$ mol cm^{-3} in figures 7.15 and 7.16
respectively. The value of k_2 determined from the gradients of the case I
and case IV plots are 2.0×10^{6} and 3.2×10^{6} mol^{-1} cm^{3} s^{-1} respectively.

We can conclude from the results of experiment 3 that when $p_\infty = 1
\times 10^{-6}$ mol cm^{-3}, $W \geq 16$ Hz and $r_\infty < 5 \times 10^{-6}$ mol cm^{-3} then some of
the $[Ni^{(0)}(bpy)_3]$ produced at the electrode surface can escape into the
bulk solution. Consequently $i_{L,t=0}$ is described by the theory appropriate
to case I. The effect of decreasing the rotation rate or increasing the bulk
concentration of $2,5\text{-}Br_2Py$ is to prevent any of the $[Ni^{(0)}(bpy)_3]$ crossing
the diffusion layer without undergoing oxidative addition with the addend.
This results in $i_{L,t=0}$ increasing as we cross the boundary from case I into
case III and then IV.

Figure 7.15:

Plots of $i_{L,t=0}$ recorded at 49 Hz for polymerisation solutions containing $[Ni^{(II)}(bpy)_3(ClO_4)_2]$ (1 mmol dm^{-3}) and 2,5-Br$_2$Py (7.5, 5.0, 2.5 and 0 mmol dm^{-3}) according to equation (6.85).
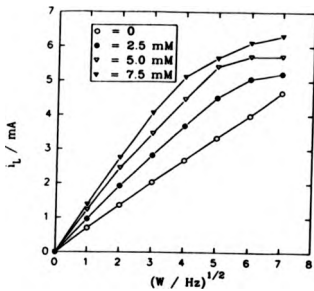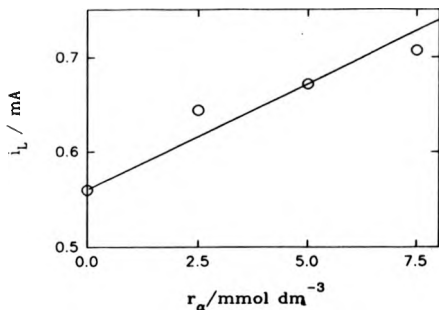

Figure 7.16:

Plots of $i_{L,t=0}$ recorded at 1 Hz for polymerisation solutions containing $[Ni^{(II)}(bpy)_3(ClO_4)_2]$ (1 mmol dm^{-3}) and 2,5-Br$_2$Py (12.5, 10.0, 7.5, 5.0, 2.5 and 0 mmol dm^{-3}) according to equation (6.88).
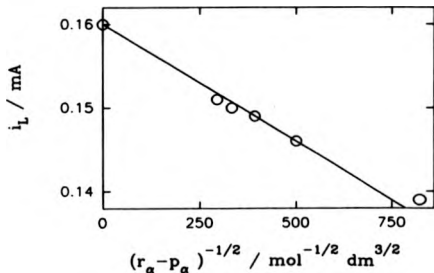
7.4.3.4 Experiment 4

The final experiment examined the dependence of $i_{L,t=0}$ on W where $r_\infty = 40 \times 10^{-6}$ mol cm^{-3} and p_∞ is varied from 2.5×10^{-6} to 12.5×10^{-6} mol cm^{-3}. This places us in the top left hand region of the case diagram, figure 7.5. The limiting current responses were analysed as a function of rotation speed according to equation (6.80). Figure 7.17 shows the variation of $i_{L,t=0}W^{-1/2}$ with $W^{1/2}$; the symbols represent the experimental data, and the lines are computer generated using a non-linear least squares curve-fitting routine (Jandel, Sigma Plot 4.0). A single two-parameter fit for $i_{L,t=0}$ was performed (homogeneous rate constant and diffusion coefficient) for all the experimental data according to the following equation:

$$\frac{i_L}{W^{1/2}} = \frac{Ap_\infty W^{1/2}}{(r_\infty - p_\infty)^{1/2}} + Bp_\infty \qquad (7.4)$$

where
$$A = \frac{-2.419nFAD^{5/6}}{k_2^{1/2}\nu^{1/3}}$$

and
$$B = \frac{3.110nFAD^{2/3}}{\nu^{1/6}}$$

Table 7.7 summarises the computer generated results for parameters A and B.

Plots of $i_{L,t=0}$ recorded at different rotation speeds (1 to 49 Hz) for polymerisation solutions containing 2,5-Br$_2$Py (40 mmol dm^{-3}) and [Ni$^{(II)}$(bpy)$_3$(ClO$_4$)$_2$] (12.5, 10.0, 7.5, 5.0 and 2.5 mmol dm^{-3}) according to equation (6.80).
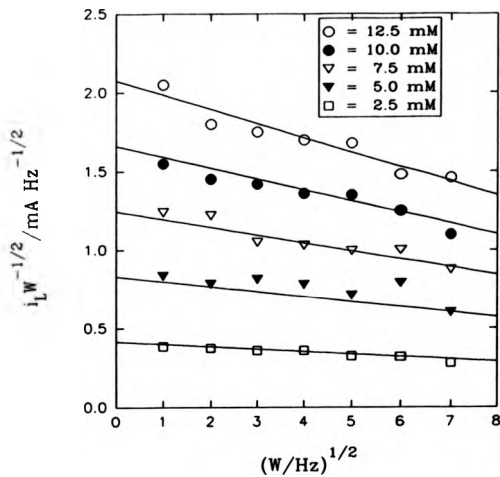
Table 7.7:

Computer generated data for parameters A and B

Parameter	A $/\text{A mol}^{-1/2} \text{cm}^{3/2}$	B $/\text{A s}^{1/2} \text{mol}^{-1} \text{cm}^3$
Value	-3.79×10^{-2}	1.66×10^2
S.D.	2.9×10^{-3}	2.4
C.V.	7.7	1.4

S.D. is the standard deviation and C.V. is defined as the standard
deviation divided by the parameter value and expressed as a percentage.

Given that $n = 2$, $F = 96485$ C mol^{-1}, $A = 0.2$ cm^2 and $v = 3.29 \times 10^3$ cm^2 s^{-1}, we calculate the diffusion coefficient and homogeneous rate constant from parameters A and B to be 1.23×10^{-5} cm^2 s^{-1} and 1.80×10^6 mol^{-1} cm^3 s^{-1} respectively. These values compare very favourably to values obtained in experiments 1, 2 and 3.

The experimental data was also analysed as a function of p_∞ according to equation (6.84). Figure 7.18 shows the behaviour of $i_{L,t=0} p_\infty / (r_\infty - p_\infty)^{-1/2}$: the symbols represent the experimental data and the lines are computer generated using the curve fitting routine. A single two-parameter fit was performed for all the experimental data according to the following equation:

$$\frac{i_L}{p_\infty} = \frac{AW}{(r_\infty - p_\infty)^{1/2}} + BW^{1/2} \qquad (7.5)$$

where A and B are defined as before.

Figure 7.18:

Plots of $i_{L,t=0}$ recorded at different rotation speeds (1 to 49 Hz) for polymerisation solutions containing 2,5-Br$_2$Py (40 mmol dm^{-3}) and [Ni$^{(II)}$(bpy)$_3$(ClO$_4$)$_2$] (12.5, 10.0. 7.5, 5.0 and 2.5 mmol dm^{-3}) according to equation (6.84).
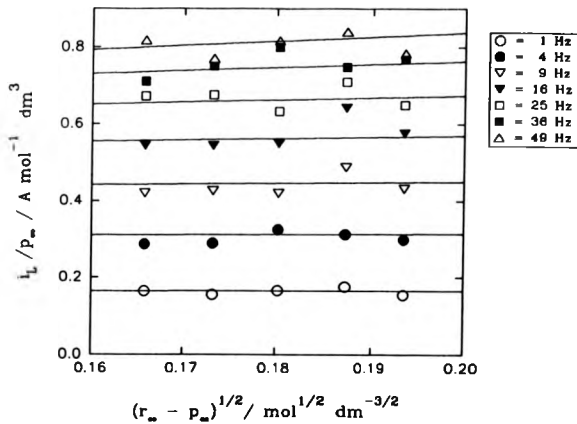
Table 7.8 summarises the computer generated results for parameters A and B.

Table 7.8:

Computer generated data for parameters A and B

Parameter	A /A mol$^{-1/2}$ cm$^{3/2}$	B /A s$^{1/2}$ mol^{-1} cm^3
Value	-3.41×10^{-2}	1.72×10^2
S.D.	3.9×10^{-3}	4.0
C.V.	8.7	2.3

S.D. is the standard deviation and C.V. is defined as the standard
deviation divided by the parameter value and expressed as a percentage.

We calculate k_2 and D from parameters A and B to be 2.22×10^6 mol^{-1} cm^3 s^{-1} and 1.29×10^{-5} cm^2 s^{-1} respectively.

We can conclude from experiment 4 that when $r_{os} = 40 \times 10^{-6}$ mol cm^{-3}, and 2.5×10^{-6} mol cm$^{-3} \leq p_{os} \leq 12.5 \times 10^{-6}$ mol cm^{-3} and W is varied between 1 and 49 Hz then the homogeneous kinetics are fast enough to prevent any $[Ni^{(0)}(bpy)_3]$ escaping from the diffusion layer.

7.4.4 Comparison of results from experiments 1, 2, 3 and 4.

In section 7.4.3 we described a number of experiments which moved us around the case diagram from one case to the next. This procedure provides a rigorous method of testing whether the initial steps of the polymerisation mechanism conform to the ECE theory presented in chapter 6. The agreement between the experimental data and theory is good for each set of results. However, it should be stressed that another

-236-

criterion must also be satisfied if the ECE theory is to be accepted as the model for the initial steps of the polymerisation process. The criterion is that the different experiments are consistent with one another as well as internally consistent. We have assessed the inter-consistency of the experiments in two ways. First we have collected together the values of k_2 obtained by analysing each set of experimental data using the ECE theory. These are presented in table 7.9. It is apparent that the values of k_2 show excellent agreement with one another.

Table 7.9:

Average values obtained from experiments 1, 2, 3 and 4 for the second order rate constant for the reaction between 2,5-Br$_2$Py and [Ni$^{(0)}$(bpy)$_2$]

	SECOND ORDER HOMOGENEOUS RATE CONSTANT, k_2 (10^3 dm^3 mol^{-1} s^{-1})						
Expt.	1	2		3			4
Case	II	I	II	I	III/IV	IV	
Vary W	-	2.4 $\pm$ 0.4	-	2.5 $\pm$ 0.4	2.5 $\pm$ 0.3	1.8 $\pm$ 0.2	
Vary p$_\infty$	-	1.9 $\pm$ 0.2	-	2.0 $\pm$ 0.2	3.2 $\pm$ 0.4	-	
Vary r$_\infty$	-	-	-	-	-	2.0 $\pm$ 0.9	

Second where possible we have combined, analysed and compared the data from different experiments on the same graphical plots. Equation (7.6) has been derived by from equations (6.43), (6.27), (6.18),(6.16) and (6.12) and is a good approximation for cases I and II:

$$\gamma\left(\frac{i_L - 1}{i_L'}\right) = \frac{p_\infty}{W}\left(\frac{k_2 \nu^{2/6} D^{-1/3}}{0.138 + p_\infty k_2 \nu^{2/6} W^{-1} D^{-1/3}}\right) \qquad (7.6)$$

-237-

where i_L' is the limiting current when $r_\infty = 0$.

All the data lying within cases I and II has been analysed according to equation (7.6), figure 7.19. The points on the graph represent experimental data. The solid line is drawn according to equation (7.7), which is a modified version of equation (6.43) and which accounts for the different values of the diffusion coefficients of P, Q and R.

$$f(\psi) = \left(\frac{0.75 \, \psi^3}{3 + 0.75 \, \psi^3} \right) \qquad (7.7)$$

Although there is some scatter of the experimental points due to the imprecise nature of the data, it can be seen that experiments 1, 2, and 3 are consistent with one another and the theory.

Equation (7.8) has been been derived from equations (6.57), (6.18) and (6.16) and represents a good approximation for cases I and III:

$$\frac{i_{L,t=0}}{i_L'} = 2 - \frac{\tanh\sqrt{(0.413 \psi^{2/6} k_2 r_\infty W^{-1} D^{-1/3})}}{\sqrt{(0.413 \psi^{2/6} k_2 r_\infty W^{-1} D^{-1/3})}} \qquad (7.8)$$

All the data lying within cases I and III has been analysed according to equation (7.8), figure 7.20. The points on the graph represent the experimental data and the solid line is a computer generated curve (Jandel, sigma plot 4.0). A single parameter fit for $i_{L,t=0}/i_L$' was performed (homogeneous rate constant) for all the experimental data according to the following equation:

$$\frac{i_{L,t=0}}{i_L'} = 2 - \frac{\tanh\sqrt{(Z r_\infty W^{-1})}}{\sqrt{(Z r_\infty W^{-1})}} \qquad (7.9)$$

-238-

Figure 7.19:

Plots of $i_{L, t = 0}$ from experiments 1, 2 and 3 which lie within cases 1 and II according to equation (7.6). The solid line is draw according to equation (7.7). The inset shows the expanded region of the plot corresponding to low values of $p_a W^{-1}$.
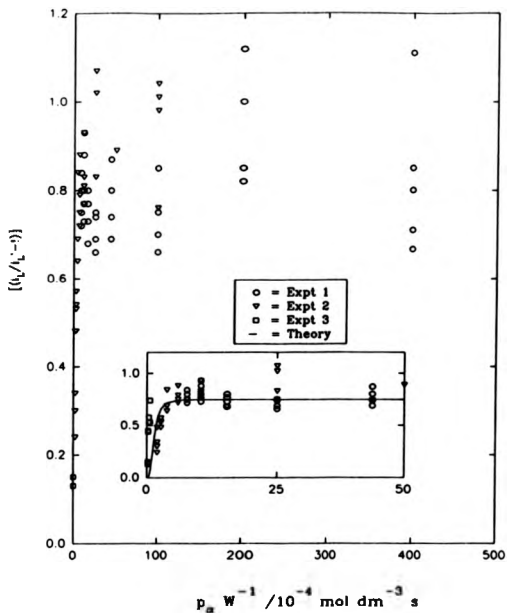
Figure 7.20:

Plots of $i_{L,t=0}$ from experiments 2, 3 and 4 which lie within cases I and III according to equation (7.8). The solid line is a computer generated fit according to equation (7.9). The inset shows the expanded region of the plot corresponding to low values of $r_\alpha W^{-1}$.
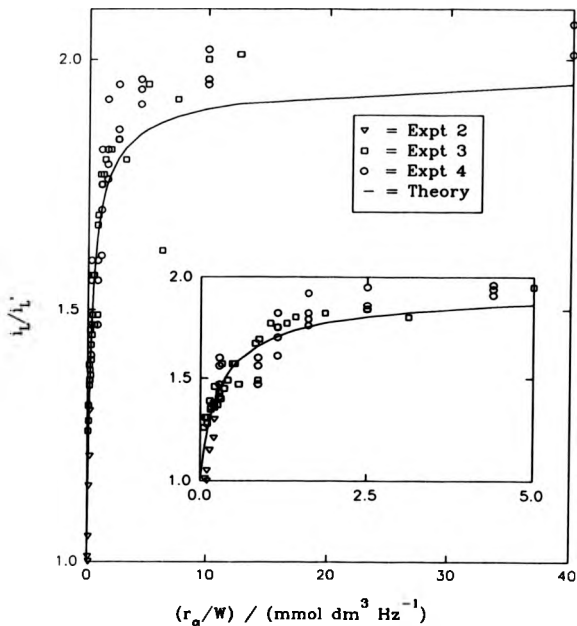
where

$$Z = 0.413 v^{2/6} k_2 D^{-1/3}$$

The computer generated value for Z is 10.22×10^6 mol^{-1} cm^3 s^{-1} and the standard deviation and C.V.% are 0.79 and 7.8% respectively. Given that $v = 3.29 \times 10^{-3}$ cm^2 s^{-1} and $D = 1.25 \times 10^{-5}$ cm^2 s^{-1}, we can calculate the homogeneous rate constant from parameter Z to be $3.8(6) \times 10^6$ mol^{-1} cm^3 s^{-1}. This value shows good agreement with those determined from the independent analysis of the data in figure 7.20. We can therefore conclude that the results obtained from experiments 2, 3 and 4 compare favourably with one another and the theory.

7.4.5 Conclusions

The results from experiments 1, 2, 3 and 4 all mutually support the hypothesis that the initial steps of the electrochemical polymerisation of 2,5-Br$_2$Py in the presence of $[Ni^{(II)}(bpy)_3(ClO_4)_2]$ can be treated according to the theory developed in chapter 6 for second order ECE mechanisms.

7.5 Electroreductive polymerisation of [BrNi$^{(II)}$(BrPy)(bpy)]

In chapters 2 and 3 we described the chemical synthesis, isolation and characterisation of [Ni$^{(II)}$Br(PyBr)(bpy)], (XVI). Earlier in this chapter we postulated that the electrosynthesis of PPy from 2,5-Br$_2$Py/[Ni$^{(II)}$(bpy)$_3$]$^{2+}$ is an ECE process in which the chemical step leads to the formation of (XVI) and its subsequent two-electron reduction results in the deposition of polymer films on the electrode surface. If these postulates are correct, then the two-electron reduction of the pre-prepared complex (XVI) should lead to the formation of comparable electrode deposits. In this section we report the electrochemistry of (XVI) and compare it to the 2,5-Br$_2$Py/[Ni$^{(II)}$(bpy)$_3$]$^{2+}$ system.

We begin by comparing the repetitive cyclic voltammograms for the two systems, figures 7.1 and 7.21. In the (XVI) system there is one reduction- and one oxidation- wave, whereas we observe two reduction- and two oxidation- waves over the same potential range (-0.5 to -2.2 V) for the 2,5-Br$_2$Py/[Ni$^{(II)}$(bpy)$_3$]$^{2+}$ system. This is as expected because in the latter system there are two electrochemical steps:

step 1:   ([Ni$^{(II)}$(bpy)$_3$]$^{2+}$ $\longrightarrow$ [Ni$^{(0)}$(bpy)$_3$]

step 2:   [Ni$^{(II)}$Br(PyBr)(bpy)] $\longrightarrow$ [Ni$^{(0)}$Br(PyBr)(bpy)])
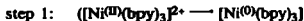
which lead to polymer deposition whereas the former system cuts out the first step.

A comparison between the first reduction waves of (XVI) and [Ni(bpy)$_3$]$^{2+}$ show that the E_{p_c}'s are both -1.6 V. This is consistent with the suggestion made by Schiavon *et al.*[31] that the oxidative addition adduct would be at least as easy to reduce as the parent nickel complex. At a freshly polished electrode, the peak current for this reductive process varies linearly with the square root of the sweep rate, figure 7.22. The

Figure 7.21:

Thirty successive cyclic voltammograms of an AN solution containing
[Ni$^{(II)}$Br(PyBr)(bpy)] (3 mmol dm^{-3}) and TEAP (0.1 mol dm^{-3}) at GC/V.
Potentials with respect to Ag/Ag+ (0.01 mol dm^{-3}, AgClO$_4$ in AN).
Sweep rate = 100 mV s^{-1}.
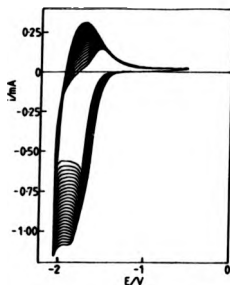
Figure 7.22:

Sweep rate dependence of i$_{pc}$ for the first reductive wave of complex
(XVI) (3 mmol dm^{-3}) in an AN solution containing TEAP (0.1 mol dm^{-3})
at Pt/KV.
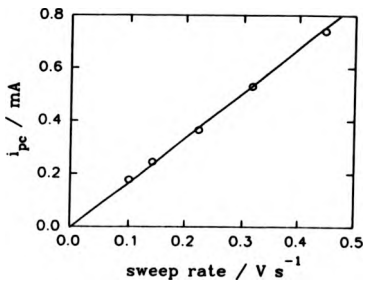
diffusion coefficient is determined from the gradient of the graph to be 3.6×10^{-6} cm^2 s^{-1} assuming the reduction is a two-electron process and the kinematic viscosity of the electrolyte solution is 3.29×10^{-3} cm^2 s^{-1}. Repeated potential cycling of the (XVI) complex causes a cathodic shift in this peak presumably due to a concomitant increase in the overpotential required to reduce the complex as the electrode surface is altered by polymer deposition.

In both cases we observe an increase in the charge passed with each successive cycle consistent with the progressive deposition of an electroactive film. The fact that complex (XVI) alone is capable of producing polymer films supports our proposals that the stoichiometry of the reactants in the 2,5-Br$_2$Py/[Ni$^{(II)}$(bpy)$_3$]$^{2+}$ system is 1 : 1. The increase in charge from one cycle to the next is more pronounced with the (XVI) system, from which it can be inferred that the polymer film is being deposited at a faster rate. Indeed, after < 10 cycles orange films are easily visible on the electrode surface. The difference in the rate of electrodeposition can be attributed to the different number of steps leading to polymer formation. In the 2,5-Br$_2$Py/[Ni$^{(II)}$(bpy)$_3$]$^{2+}$ system there is at least an extra reductive process and a following chemical reaction, which can only act to increase the probability of material produced at the electrode diffusing away into the bulk solution, thereby decreasing the efficiency of the deposition.

As with the 2,5-Br$_2$Py/[Ni$^{(II)}$(bpy)$_3$]$^{2+}$ system, films can be grown by stepping the potential of the electrode to potentials more negative than -1.4 V for the (XVI) system. The relative amount of charge consumed during the first 20 s of electropolymerisation at -1.8 V for 2,5-Br$_2$Py/[Ni$^{(II)}$(bpy)$_3$]$^{2+}$ and for (XVI) is *ca.* 2 : 1 respectively. This is a very pleasing result as it supports the proposal that the second electrochemical step of the ECE mechanism is a two-electron reduction.

In background electrolyte the cyclic voltammetry of polymer films grown from either system is very similar. In particular, the EDTA treated films were indistinguishable. We conclude that the electrode deposits are fundamentally the same, although the coordination sphere of the nickel within the films will vary since in the $2,5$-Br_2Py/$[Ni^{(II)}(bpy)_3]^{2+}$ system there will be more bpy available for coordination. Investigations into the properties of the deposits are presented in section 7.6.

We can conclude that the electrochemistry of the growth solutions containing (XVI) and that of the resultant electrode deposits are consistent with our proposed reaction scheme for the initial stages of the polymerisation of PPy from $2,5$-Br_2Py in the presence of $[Ni(bpy)_3]^{2+}$. In particular, the fact that the electrosyntheses of PPy from either complex (XVI) or $2,5$-Br_2Py/$[Ni^{(II)}(bpy)_3]^{2+}$ yield electrode deposits whose electrochemistry, FTIR and UV-visible spectra are very similar, strongly suggests that (XVI) is common to both reaction pathways. This in turn accords with the proposed reactant stoichiometry of the polymerisation process since the ratio of nickel to pyridyl in (XVI) is also 1 to 1. The electropolymerisation of (XVI) requires two electrons per nickel. Again this agrees with the postulated ECE mechanism in which each electrochemical step consumes two electrons.

In order to reconcile the stoichiometry with the number of electrons consumed and those required for bond formation we can invoke two possible fates for the nickel which depend on the stability of the *in situ* generated "Py-Ni^{(II)}-Py" type species. These are represented schematically below:

Scheme I
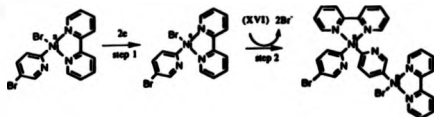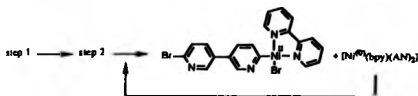
Scheme II

The second scheme can be dismissed because the addition of excess 2,5-Br$_2$Py to the growth solution does not increase the total charge consumed. An increase in charge would be expected because the Ni(0), generated by the spontaneous reductive elimination, would react with any excess 2,5-Br$_2$Py leading to the formation of more (XVI) which in turn would re-enter the reaction scheme and consume a further two electrons. Consequently as this effect is not observed the nickel must be in an oxidation state inappropriate for oxidative addition, i.e. Ni(II). Hence the nickel appears to be an integral part of the polymer backbone forming an "organometallic string". This would be a very novel polymer. In the next section we describe our investigations into the nature of the polymer deposits which add credence to, although not definite confirmation of, this structure.

7.6 Characterization and Properties of the Electrode Deposits

In this section we present and discuss our investigations into the nature of the films prepared from the [Ni(bpy)$_3$(ClO$_4$)$_2$]/ 2,5-Br$_2$Py/TEAP/AN system. Typically polymer films were grown potentiostatically at -1.8 V from electrolyte solutions containing equimolar quantities of [Ni(bpy)$_3$(ClO$_4$)$_2$] and 2,5-Br$_2$Py (1 - 10 mmol dm^{-3}).

7.6.1 Cyclic Voltammetry

The cyclic voltammetry of the polymer films in AN containing TEAP (0.1 mol dm^{-3}) depends on the treatment of the coated electrodes.

A typical response of a coated electrode which has only been handled under oxygen-free conditions is given in figure, 7.23 (a). There are two broad cathodic peaks (A) and (C) with corresponding anodic peaks (B) and (D). Both redox processes are very stable to repeated potential cycling between -0.5 and -2.4 V and the i$_p$'s increase linearly with sweep rate as expected for surface confined redox processes. The films are orange or orange/brown (depending on thickness) at potentials more cathodic than -1.5 V; at more positive potentials the polymers change colour to yellow. Increasing the anodic switching potential to +0.2 V reveals an irreversible anodic peak, (E), figure 7.23 (b). Traversing (E) results in the gradual loss of peaks (A) and (B) and the sharpening and stabilising of peaks (C) and (D), figure 7.23 (c).

It should be noted that rigorous exclusion of oxygen was difficult to achieve and only the use of an Ar-filled glove bag led to polymer films which reliably gave stable (A)/(B) traces.

The initial response of a film which has been exposed to oxygen has the same form as one from which oxygen has been excluded. However, repeated cyclic voltammetry results in the loss of peaks (A) and (B) and the sharpening and stabilising of peaks (C) and (D), figure 7.23 (d). The stable (C)/(D) couple has the following characteristics: $E_{p_{1/2}}$ = 2.10 V; ΔE_p = 0.25 V; i$_p$/v is constant.

Nickel and bpy were extracted from the films by soaking in EDTA (0.01 mol dm^{-3} aqueous solution buffered to pH 9.2) for 1/2 h, followed by washing with water and AN. The success of this process was confirmed by atomic absorption and EDAX. The cyclic voltammetry of the EDTA

Figure 7.23:

Cyclic voltammograms of polymer coated GC/V in AN solutions containing TEAP (0.1 mol dm^{-3}). The polymer films were grown potentiostatically at -1.8 V for *ca* 3 min in an Ar-filled glove bag in AN solutions containing [Ni$^{(II)}$(bpy)$_3$(ClO$_4$)$_2$] (5 mmol dm^{-3}), 2,5-Br$_2$Py (5 mmol dm^{-3}) and TEAP (0.1 mol dm^{-3}). The films were treated as follows (a) pristine i.e. rigorous exclusion of oxygen, (b) — first and — 3rd anodic excursions of the pristine film, (c) 10th anodic excursion of pristine film, (d) successive potential cycles of a film which has been exposed to the air and (e) EDTA treated. Potentials with respect to Ag/Ag$^+$ (0.01 mol dm^{-3}, AgClO$_4$ in AN). Sweep rate 50 mV s^{-1}.
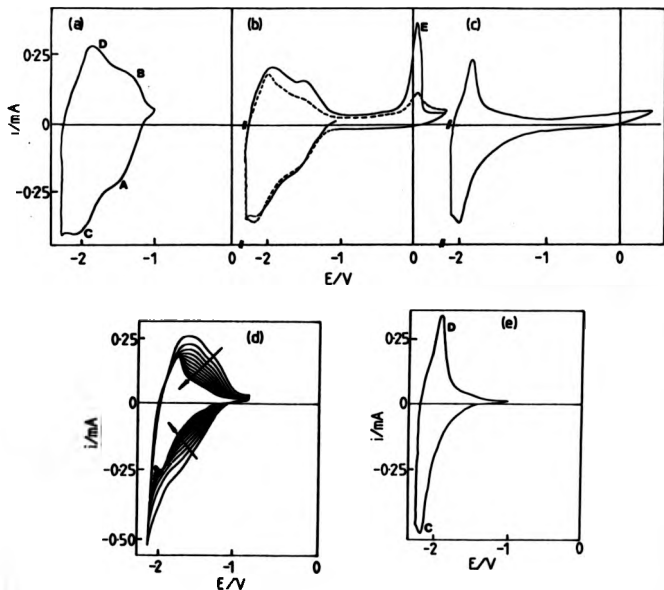
treated films shows only peaks (C) and (D) which are stable to repeated cyclic voltammetry and have the following characteristics: $E_{P_{1/2}} = 2.10$ V; $\Delta E_P = 0.270$ V; i_P/ν is constant, figure 7.23 (e).

Based on these observations we propose that the redox activity around -1.50 V (peaks (A) and (B)) is associated with nickel within the polymer film. The redox activity around -2.10 V ((C) and (D)) is associated with the oxidation and reduction of the polymer itself and occurs in the presence and absence of bound nickel.

Pristine films, i.e. those which have not been exposed to oxygen or anodic potentials, show minimal loss in redox activity during prolonged cyclic voltammetry (upto 1 h). Therefore, we conclude that the nickel must be tightly held within the polymer. Exposure of the films to oxygen or anodic potentials must alter the association between the nickel and the polymer because we observe the gradual loss of redox activity assigned to the nickel. These observations are similar to those reported by Meyer, Rollin and Perichon[89] for the electroreductive coupling of haloanisoles using [Ni(Br)(Br)(bpy)$_2$] as the catalyst. They suggest that an oxidant (oxygen or an anodic potential) promotes elimination of nickel from the stable diarylnickel complex initially formed during the electroreduction. The yields of diaryl are reported to be almost quantitative. By analogy, we propose that the pristine films comprise repeating -(NiPy)- units in which the coordination sphere of the nickel is satisfied by bpy and AN. Exposure of the films to oxygen or anodic potentials similarly causes the elimination of nickel and the formation of PPy. Initially the nickel remains trapped within the film, but is expelled during potential cycling.

Integration of the current-time curve enclosing by each redox process observed during the cyclic voltammetry allows us to determine the number of electrons associated with the oxidation/reduction of each component of the film and with the oxidative process leading to the

-249-

eventual expulsion of nickel from the film. A series of films were grown potentiostatically for 5 min. The pristine films were then cycled in background electrolyte between the limits -2.3 V and -1.2 V and the the total charge enclosed by the trace was determined once the trace had stabilised (ca. 5 cycles). The films were then treated with oxygen, EDTA or oxidising potentials, returned to the background electrolyte and cycled as before until stable. The total charge enclosed by the stable trace was again determined. The average results for three films are summarised in table 7.10.

Table 7.10:

Summary of charges associated with redox process observed in the cyclic voltammetry of the pristine, oxygen exposed and EDTA treated PPy films.

Treatment of the polymer	Charge /mC		
	Nickel/Pyridyl Moieties[a]	Pyridyl Moieties[a]	Anodic[b]
Exposed to O_2	0.117	0.051	----
Taken to Anodic Potentials	0.098	0.044	0.053
Treated with EDTA	0.100	0.043	----

[a] Half of the total charge enclosed by CV, adjusted for background charge.
[b] Summed charge under peak (E) for consecutive cycles until no peak was observed, adjusted for background charge.

Let us first consider the data corresponding to the pristine polymer films which are then electrochemically oxidised: If we assume that the charge enclosed under successive oxidation peaks at 0.08 V, peak E, corresponds to the following process:

$$\left(\text{Ni}^{(II)}\text{Py}\right)_n \xrightarrow{-2e} \text{Ni}^{(II)} + \left(\text{Py}\right)_n \qquad \text{Peak E}$$
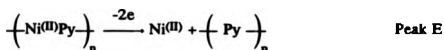
then the same quantity of charge, (ie 0.053 C) must be associated with each of the redox processes centred at -1.50 V, peaks A and B:

$$\left(\text{Ni}^{(II)}\text{Py}\right) \xrightarrow[+2e]{-2e} \left(\text{Ni}^{(0)}\text{Py}\right) \qquad \text{Peaks A, B}$$
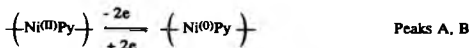
assuming that the nickel within the films cycles between the oxidation states (II) and (0) and that the ratio of nickel to pyridyl is 1:1. The charge associated with each of the redox process centred at -2.10 V, peaks C and D, is determined by simple subtraction to be 0.045 C. This is equivalent to a charge of 1.70 electrons per pristine polymer unit in its fully reduced state:

$$\left(\text{Ni}^{(0)}\text{Py}\right) \xrightarrow[+\ 0.045/0.027\ e]{-\ 0.045/0.027\ e} \left(\text{Ni}^{(0)}\text{Py}\right)^{-1.70} \qquad \text{Peaks C, D}$$
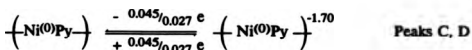
Next we will consider the data corresponding to the pristine polymer films which are then treated with EDTA. The total charge corresponding to redox processes A/B and C/D is 0.100 C for the pristine films. From our previous calculations we know that the nickel within the polymer films accounts for a $0.053/0.098^{th}$ of the total charge i.e. 0.054 C and the pyridyls account for a $0.045/0.098^{th}$ of the total charge i.e. 0.046 C. The charge associated with the oxidation or reduction of the pyridyl moeities in the EDTA treated films is 0.043 C. Therefore we calculate the charge per pyridyl unit of the fully reduced EDTA treated polymer films to be 1.59 electrons.

A similar methodology applied to the data corresponding to the

pristine polymer films which are then exposed to oxygen, leads to a value for the charge per pyridyl unit of the fully reduced oxygen exposed polymer films of 1.61 electrons. It is pleasing that the two values determined for the charge on the pyridyl moieties show excellent agreement.

There have been no similar investigations into the charge per monomer unit of reduced state conducting polymers reported in the literature. However poly(pyrrole), poly(1-methylpyrrole) and poly(3-methylpyrrole) are all reported to have a charge of +0.25 electrons per pyrrole unit when fully oxidised[176]. By comparison these results would suggest that poly(2,5-pyridine) is highly charged in its conducting state.

We propose that the structures of, and the relationship between, the pristine (oxidised and reduced forms), electrochemically oxidised (> 0 V) and the EDTA treated polymer films can be summarised by the following reaction scheme:
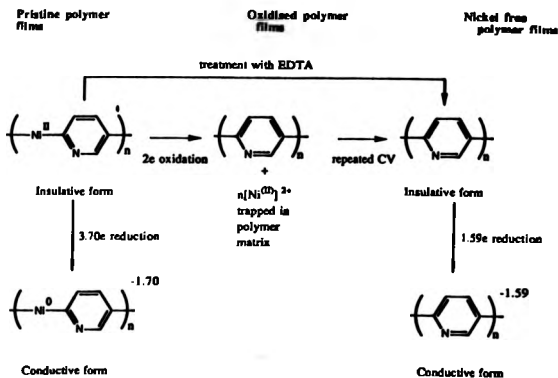
7.6.2 Growth Charge, Cyclic Voltammetric Charge and Film Thickness

The thickness of a conducting polymer film is usually directly related to both the charge passed during electrodeposition and the charge required to reduce fully or oxidise fully the polymer film according to equations (7.12) and (7.13) respectively:

$$t = \frac{VQ'L}{n'FA} \qquad (7.12)$$

and

$$t = \frac{VQL}{nFA} \qquad (7.13)$$

where t is the thickness of the polymer film (cm) and V is the volume of the polymer repeat unit (estimated by using known or approximate bond lengths of $[Ni^{(II)}(bpy)_2]^{2+}$ to be 4.82×10^{-20} cm^3), Q' and Q are the growth charge and the oxidation or reduction charge of the polymer film (mC) respectively, L is Avagadro's number, n' and n are the electrons required per monomer unit for deposition and oxidation or reduction respectively, F is the faraday and A is the geometric area of the electrode (cm^2).

In this section the relationship between charge and measured thickness of pristine PPy/Ni is presented and used to estimate the number of monolayers of polymer laid down in terms of charge per unit area.

Polymer films were deposited potentiostatically over a range of growth times on Pt flags (1 cm^2) which were half covered with a low temperature melting wax. The coated electrodes were then cycled in background electrolyte as usual and the total charge associated with the reduction/oxidation of the film was recorded. The wax was dissolved off by stirring in toluene (15 min) to expose the bare electrode-polymer step.

-253-

The height of the step was measured using a Talystep stylus. Table 7.11 summaries these results:

Table 7.11:

Summary of the data for polymer films grown potentiostatically at -1.8 V for different lengths of time in AN solutions containing TEAP (0.1 mol dm^{-3}), [Ni$^{(II)}$(bpy)$_3$(ClO$_4$)$_2$] (5 mmol dm^{-3}) and 2,5-Br$_2$Py (5 mmol dm^{-3}) on Pt flags.

Growth Time /s	Growth Charge /mC cm^{-2} ± 5	Charge to reduce or oxidise polymer /mC cm^{-2} ± 0.5	Measured thickness /μm ± 0.005
150	130	7.5	1.280
200	155	9.5	1.460
350	190	10.0	1.920
500	250	13.0	2.220
780	335	22.5	3.075
880	365	24.5	3.250

The charge related to either the reduction or oxidation of the oxygen exposed polymer film was calculated by measuring the total charge enclosed by the redox processes adjusting for background charge and dividing by 2.

Figure 7.24 clearly shows that there is a linear relationship between film thickness and either charge consumed during electrodepsition or charge associated with the reduction/oxidation of the polymer film. The gradients of the plots allows us to determine that the conversion factor (CF) between charge and thickness to be 9.2 ± 0.5 nm mC^{-1} cm^2 and 0.16 ± 0.05 nm mC^{-1} cm^2 for electrodeposition and the full reduction or oxidation of the polymer respectively.

Plot of data given in table 7.11. The inset is a rescaled portion of the graph to show more clearly the relationship between film thickness and the charge required to oxidise or reduce the polymer film.
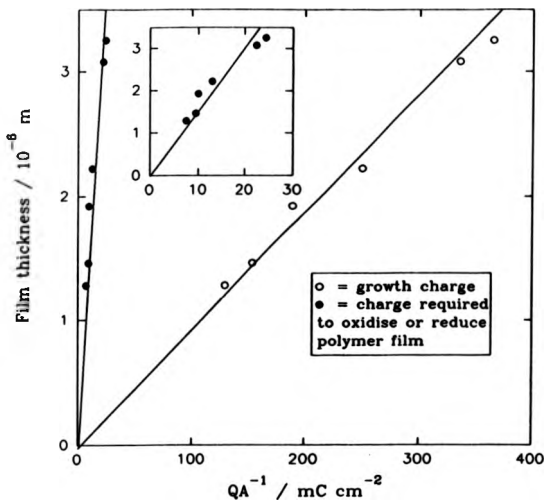
For an ideal system the difference in the conversion factors should only reflect the difference in the number of electrons involved in the deposition of a single monomer unit compared to the number of electrons required to reduce or oxidise a single monomer unit. In this case we know that the electrosynthesis is a 4-electron process (see section 7.3) and that either oxidation or reduction of the polymer requires 3.6 electrons per monomer unit (see section 7.6.1) so the ratio of the conversion factors should be 1 : 0.9 rather than *ca* 1 : 0.06. In order to account for this discrepancy we propose that the deposition is less than 10% efficient. We observe a change in colour of the growth solution from pale pink to orange during prolonged electrolysis which may be due to soluble oligomers which have failed to precipitate onto the electrode surface. Qualitatively this supports the proposal that the electrodeposition is an inefficient process.

Based on the charge required to oxidise or reduce the polymer, another conversion factor (CF') which relates the charge to equivalent monolayers can be estimated using equation 7.14:

$$CF' = \frac{A \times 10^2}{Q t V^{1/3}} \qquad (7.14)$$

For pristine polymer films CF' is 10.3 monolayers mC^{-1} cm^2. Therefore a typical polymer film is several hundred monolayers thick.

7.6.3 Elemental analysis, EDAX, UV-visible spectroscopy, FTIR spectroscopy, ^1H nmr spectroscopy and SEM

Conducting polymers are usually difficult to characterise because they tend to be insoluble and to pyrolyse at high temperatures. Consequently the techniques available to probe the nature of a conducting polymer tend to be limited to indirect, surface and electrochemical

analyses. PPy is soluble in acids so we were able to include some of the more classical characterisation techniques.

In order to prepare large enough quantities of the polymer for analysis, a glassy carbon tablet of surface area $ca.$ 25 cm^2 (a gift from David Hart (Feckenham) Ltd.) was used as the working electrode and the growth solutions typically contained 25 mmol dm^{-3} [Ni(bpy)$_3$(ClO$_4$)$_2$] and 2,5-Br$_2$Py. The polymer films were removed from the underlying electrode by holding the electrode at an anodic potential, 1.2 V, such that the films peeled off. These oxidised films were then filtered off and either washed in AN and water or treated with EDTA prior to drying under reduced pressure. This technique inherently changes the nature of the pristine films and will probably lead to the incorporation of anions (perchlorate and/or bromide) which act to maintain the overall charge neutrality of the polymer/nickel mixture. However this method avoids complications resulting from oxygen reacting with the pristine polymer films (see section 7.6.1).

Table 7.12 compares the theoretical (calculated for the stuctures illustrated in the reaction scheme in section 7.6.1) and measured elemental analyses of the oxidised and EDTA treated polymer films.

Table 7.12:

Elemental analysis of the polymer films

Polymer			C	H	N	Ni	Over
Oxidised[a]	Theory[b]	% Mass	48.51	3.32	12.51	8.78	26.69
		molar ratio	4.5	3.7	1	0.17	——
	Found	% Mass	48.12	3.41	12.87	10.59	25.01
		Molar ratio	4.4	3.9	1	0.21	——
EDTA treated	Theory[b]	% Mass	77.91	3.91	18.18	0	0
		Molar ratio	5	3	1	0	0
	Found	% Mass	65.24	3.80	15.90	——	15.06
		Molar ratio	4.8	3.3	1	0	——

[a] In calculating the theoretical % masses we have assumed that there must be two charge compensating anions (taken to be perchlorate and Br-) per nickel trapped within the oxidised film.

[b] Calculation of the theoretical % mass has assumed infinite chain length

A comparison between the calculated and found molar ratios for C : H : N supports the proposed structure of the electrochemically oxidised polymer deposit. However the relative number of moles of nickel within the films is more than the predicted value. A possible explanation for this discrepancy is that some of the nickel trapped within the film coordinates to the nitrogen of the polymer pyridyl units rather than to bpy thereby increasing the percentage mass of nickel in the polymer film.

The theoretical and found molar ratios of C : H : N of the films treated with EDTA compare favourably. This is consistent with pyridyl being the polymer repeat unit. The difference between the theoretical and found % masses for treated films probably arises because the calculated value does not account for polymer chain end groups. If we assume that bromines are the chain terminators, then the average polymer is 12

pyridyl units long. It is pleasing that this value is of the same order as that reported by Yamamoto *et al.*[27] for chemically synthesised PPy.

EDAX studies of polymer coated platinum flags confirm that nickel is present in the polymer matrix. These studies also demonstrate that the treatment of the polymer films with EDTA is an effective way of removing the metal. Figure 7.25 shows a typical EDAX spectrum of the untreated polymer coated platinum flags.

The treated and untreated polymers are moderately soluble in dilute inorganic acids. Typically they produce slightly cloudy orange solutions in dilute acids which on filtering through a 0.02 μm mesh give clear orange solutions. Dissolution is probably due to protonation of the nitrogen in the pyridyl rings and the cloudiness is probably due to the longer polymer chains remaining unsolvated. ^{1}H n.m.r. spectroscopy was carried out on filtered solutions of the polymers in DCl/D$_2$O (3:10 v/v) using TSP as the internal reference. The ^{1}H n.m.r. spectra of the EDTA treated polymer show that there are a multitude of low field resonances (8.2 to 9.9 ppm) which we assign to the polymer pyridyl protons, (figure 7.26). All aromatic protons are shifted to low field due to the deshielding caused by the so-called ring current effect. Interestingly, in this case the resonances are shifted further down field than those of free bpy which indicates a greater degree of deshielding. This would be expected for a highly conjugated system and therefore supports the proposal that the films consist of conjugated pyridyl chains. The untreated, but oxygen exposed, polymer deposit gives similar ^{1}H n.m.r. spectra except the resonance signals are broader. The broadening can be attributed to either the presence of paramagnetic nickel or the rapid exchange of the ligands coordinating to the nickel. Further stuctural information using ^{1}H n.m.r. spectroscopy requires more sophisticated experiments such as COSY which are outside the scope of this project.

Figure 7.25:

EDAX spectrum of an untreated polymer coated Pt flag.
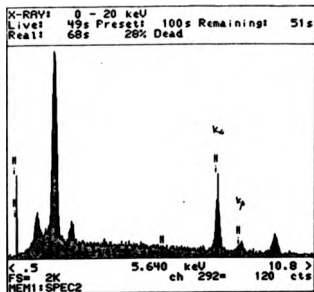
Figure 7.26:

^{1}H n.m.r. spectrum of the EDTA treated polymer material in DCl/D$_2$O (3:10 v/v) with added free bpy at 400 MHz. Absorption at δ 7.2 is due to water and the doublets and triplets at δ 8.46, 8.73, 9.00 and 9.21 are due to the free bpy.
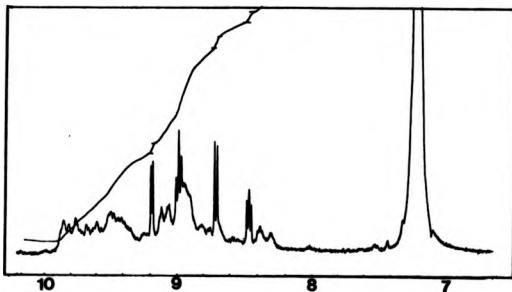
In the UV-visible spectra of treated polymer deposits on indium doped tin oxide electrodes, the $\pi \rightarrow \pi^*$ absorption band is in the region 375 - 385 nm (figure 7.27), whereas the equivalent absorptions band for bpy and pyridine are located between 275 - 285 and 255 - 265 nm respectively[154b]. The bathochromic shifts from pyridine to bpy to polymer correlate with the increase in the number of conjugated pryidyl units. It is pleasing that this result further supports the proposed nature of the electrode deposits.

Specular reflectance FTIR spectra of treated polymer coated Pt electrodes show bands corresponding to the presence of aromatic rings. The broad absorption at 3000 cm⁻¹ is due to the aromatic C-H stretch; the sharp bands at 1584 and 1456 cm⁻¹ are due to ring vibrations and the absorption at 830 cm⁻¹ is consistent with a C-H out of plane stretch for 1,4-disubstituted pyridyl rings[177], figure 7.28. Once again these observations confirm that the polymer deposits contain conjugated pyridyl units.

Pt flags were coated with different amounts of polymer by altering the potentiostatic growth time (15-900 s). Scanning electron micrographs of the electrode deposits show the polymer surface to have a "cauliflower-type" appearence, plate 7.1. Growth times of less than 60 s lead to incomplete electrode coverage, and we observe individual "clumps" of polymer. In accordance with the literature, we propose that each clump arises from a nucleation point.

7.6.4 CO insertion, Metal Ion Chelation and the Electrochemistry of Complexes (XVII) and (XVIII)

The series of experiments described in the previous section clearly indicate that the oxidised and nickel-free polymers contain conjugated pyridyl units. However, they give no definitive evidence that nickel is covalently bonded to the pyridyl units in the as-grown polymers, or that

Figure 7.27:

UV-visible spectrum of an EDTA treated polymer coated indium-doped tin oxide electrode.
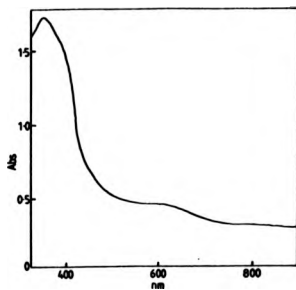
Figure 7.28:

FTIR spectrum of EDTA treated polymer coated Pt/KV.
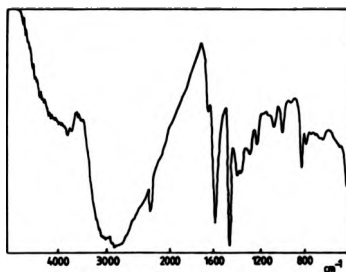
Plate 7.1

Scanning electron microgragh of a platinum flag coated with an as grown polymer film. The film was grown potentiostatically at -1.8 V for 300 s from an AN solution containing $[Ni^{(II)}(bpy)_3(ClO_4)_2]$ (5 mmol dm^{-3}), 2,5-Br$_2$Py (5 mmol dm^{-3}) and TEAP (0.1 mol dm^{-3}). Magnification = x 108K.

the bonding between the pyridyl units is C_2-C_5. In an attempt to clarify these points we investigated the susceptibility of the pristine polymers to CO insertion, the coordinating ability of the nickel-free polymer toward transition metal ions and the electroreduction of the analogous [Ni$^{(II)}$Br(Py)(bpy)] complexes, (XVII) and (XVIII).

It is known that CO can insert into or replace the nickel-carbon bonds[178]. Therefore potentially we might expect CO to react with pristine polymer films leading to the formation of carbonyls in the polymer chain. This reaction was investigated by bubbling carbon monoxide through acetonitrile containing pristine polymer coated Pt electrodes (1 h). The electrodes were then removed, rinsed with fresh solvent and dried. Specular reflectance FTIR spectra of the CO treated coated electrodes were recorded. Although considerable care was taken to prevent exposure of the polymer deposits to air, the FTIR spectra were very similar to those obtained with air oxidised polymers deposits. There were no appreciable absorption bands which could indicate insertion of CO into the polymer chains. This is a disappointing result, but nevertheless does not rule out the proposed formulation of the as-grown polymer.

The orientation of the pryidyl units of the nickel-free polymer will dictate its ability to chelate metal ions as previously discussed in section 5.4. The proposed polymerisation mechanism and structure of the pristine polymer militates against the formation of a polymer capable of strongly coordinating metal ions, i.e. poly(2,2'-dipyridyl). In particular it is difficult to envisage a mechanism in which nickel elimination from the pristine polymer does not result in C_2 to C_5 linkage of adjacent pyridyls.

We attempted to coordinate divalent metal ions (Ni, Fe, Co, and Cu) to EDTA treated coated electrodes in two ways. First, the coated electrodes were simply soaked in AN solutions containing TEAP (0.1

mol dm-3) and any one of $[M^{(II)}(H_2O)_6][ClO_4]_2$ or $[M^{(II)}(DMSO)_6][ClO_4]_2$ or $[M^{(II)}(bpy)_3(ClO_4)_2]$ (10 mmol dm^{-3}). The electrodes were then briefly washed in electrolyte and any changes in their cyclic voltammetry were recorded. The second method involved cycling the potential of the coated electrodes repeatedly between the limits 0 to -2.4 V in solutions with the same composition as described for the first method. Again the electrodes were then washed in electrolyte and any changes in their cyclic voltammetry were recorded.

The cyclic voltammetry of the polymer coated electrodes which had been soaked or cycled in the AN/TEAP/$[M^{(II)}(H_2O)_6]^{2+}$ solutions was altered. In every case a new broad redox couple at -1.45 V was observed and the polymer redox couple centred at -2.10 V had broadened, figure 7.29 (a), (b) and (c). It was also observed that the films became patchy if the electrodes were left in the hexaaquametal (II) perchlorate solutions for prolonged lengths of time (>2 h).

Initially these observations seemed to present us with a number of anomalies. First, the changes in the cyclic voltammetry are independent of the actual $[M^{(II)}(H_2O)_6][ClO_4]_2$ complex and bore no relationship to the electrochemistry of known $M^{(II)}$ pyridyl-, bpy- or terpy- type complexes. Second, since DMSO is a better leaving group than H_2O, we would expect the polymer to pick up the metal ions more readily from the solutions containing the anhydrous metal salts. Instead the reverse effect is observed. Finally, the deterioration of the polymer films was only observed when the electrodes were left in the solutions containing hexaaquametal (II) ions. We believe that these apparent anomalies arise because in aprotic solvents all the hexaaquametal (II) ions investigated are acidic and liberate protons[179]:

$$[M^{(II)}(H_2O)_6]^{2+} \longrightarrow [M^{(II)}(H_2O)_5(OH)]^+ + H^+$$

$$[M^{(II)}(H_2O)_5(OH)]^+ \longrightarrow [M^{(II)}(H_2O)_4(OH)_2] + H^+ \text{ etc}$$
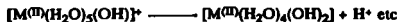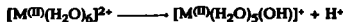
Figure 7.29:

Cyclic voltammograms of polymer coated GC/V in AN solutions containing TEAP (0.1 mol dm^{-3}). The polymer films were grown potentiostatically at -1.8 V in AN solutions containing [Ni$^{(II)}$(bpy)$_3$(ClO$_4$)$_2$] (5 mmol dm^{-3}), 2,5-Br$_2$Py (5 mmol dm^{-3}) and TEAP (0.1 mol dm^{-3}). The films were all treated with EDTA then soaked for *ca.* 2 h in AN solutions containing TEAP (0.1 mol dm^{-3}) and (a) [Ni$^{(II)}$(H$_2$O)$_6$](ClO$_4$)$_2$ (10 mmol dm^{-3}) (b) [Fe$^{(II)}$(H$_2$O)$_6$](ClO$_4$)$_2$ (10 mmol dm^{-3}) and (c) [Co$^{(II)}$(H$_2$O)$_6$](ClO$_4$)$_2$ (10 mmol dm^{-3}) Potentials with respect to Ag/Ag$^+$ (0.01 mol dm^{-3}, AgClO$_4$ in AN). Sweep rate 50 mV s^{-1}.
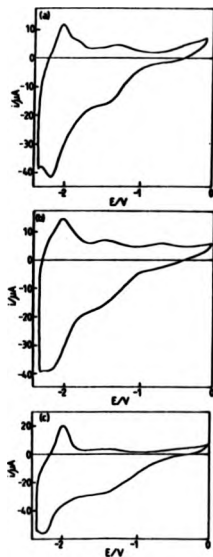
The liberation of the H⁺ will be aided by the basic character of the polymer as the protons will be mopped up by the pyridyl nitrogens in the polymer chains. We propose that the changes in the cyclic voltammetry are due to protonation of the polymer. This explains why the same changes are induced by all the hexaaquametal (II) ions and why no effect is seen with the equivalent DMSO complexes. We postulate that the patchiness of the films results from the increased solubility of the protonated polymers causing gradual dissolution. The hypothesis that the changes are due to an acidity effect rather than to coordination of the metals, is further supported by the fact that dipping the electrodes into a basic solution regenerates the original form of the cyclic voltammograms.

The changes in the cyclic voltammetry of the polymer coated electrodes which had been soaked or cycled in either AN/TEAP/$[M^{(II)}(bpy)_3]^{2+}$ or AN/TEAP/$[M^{(II)}(DMSO)_6]^{2+}$ solutions were negligible or lost after the first few potential sweeps in background electrolyte. Consequently it can be inferred that very few metal ions have coordinated to the polymer. This supports the proposal that the pyridyls in the nickel-free polymer are C^2-C^5 linked.

Interestingly, the behaviour of this polymer towards $Ni^{(II)}$ is notably different to that of PPy prepared via the Ni/PPh$_3$/2,5-Br$_2$Py system. The latter polymer irreversibly coordinates the metal ions and the cyclic voltammetry changes dramatically. However, in this case the polymer appears unable to chelate either metal ion and any changes are only transitory. We can tentively conclude that these nominally identical electrode deposits have markedly different chelating ability. This may reflect different polymerisation mechanisms which in turn result in the former having a repeat 2,2'-dipyridyl polymer unit and in the latter having the 2,5-Py as the repeat unit.

In section 7.5 we proposed that there are two possible reaction

schemes for the electropolymerisation of [BrNi(PyBr)(bpy)]. The preferred scheme leads to the formation of "organonickel strings" whereas the alternative scheme leads to the formation of PPy with coordinated nickel. By analogy, the electroreduction of the pre-prepared oxidative addition adduct of 2-BrPy to [Ni$^{(0)}$(bpy)$_2$] (figure 7.30a) may lead to the formation of either dipyridyl Ni(II) complexes (scheme I) or the synthesis of free dipyridyl and Ni(0) (scheme II). The reductive electrochemistry of this adduct, (XVII) was investigated by cyclic voltammetry and potential step.

Figure 7.31 shows the first cyclic voltammogram of (XVII) in electrolyte solution. We observe three chemically reversible reduction processes centred at E_{pc} = -1.5, -2.14 and -2.34 V. By comparison with the reduction potentials of [Ni$^{(II)}$(bpy)$_3$]$^{2+}$ and [Ni$^{(II)}$Br(PyBr)(bpy)], we propose that the first reduction process corresponds to the two-electron reduction of [BrNi$^{(II)}$(Py)(bpy)] yielding the Ni(0) species. Repeated cyclic voltammetry between the solution's resting potential and -1.8 V sees the loss of this reduction wave with the concomitant deposition of a pale yellow film onto the electrode surface. Thus we conclude that the reduction of (XVII) leads to the deposition of an insulating film. Potential steps to -1.8 V also result in a pale yellow film forming on the electrode surface. EDAX spectra of Pt flags, which have been coated with this electrode deposit and then thoroughly washed in AN, show that nickel is present on the electrode surface.

Figure 7.32(a) and (b) show cyclic voltammograms of the coated electrodes in background electrolyte. A broad, ill-defined, irreversible oxidation wave located around 1.4 V is observed on the first anodic potential sweep. Subsequent potential sweeps show neither reductive nor oxidative electroactivity and the pale yellow film is no longer visible on the electrode surface. Thus we can conclude that the oxidation has destroyed the electrode deposit. If the initial potential excursion is

Figure 7.30:

Structures of (a) (XVII) and (b) (XVIII).

(a)   (b)
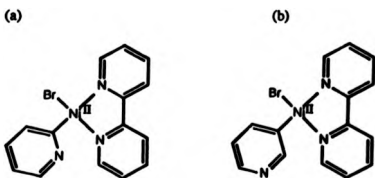
Figure 7.31:

Cyclic voltammogram of an AN solution containing (XVII) (5 mmol dm^{-3}) and TEAP (0.1 mol dm^{-3}) at GC/V. Potentials with respect to Ag/Ag$^+$ (0.01 mol dm^{-3}, AgClO$_4$ in AN). Sweep rate – 50 mV s^{-1}.
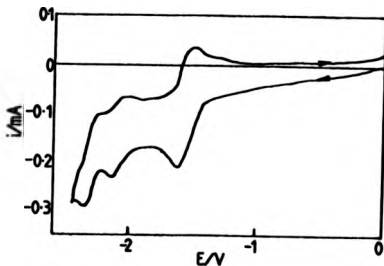
Figure 7.32:

Cyclic voltammograms of coated GC/V in AN solutions containing
TEAP (0.1 mol dm^{-3}) showing the initial potential excursion in (a) anodic
direction and (b) cathodic direction. The electrodes were coated
potentiostatically at -1.8 V in AN solutions TEAP (0.1 mol dm^{-3}) and
(XVII) (5 mmol dm^{-3}). The growth charge $ca.$ 17 mC. Potentials with
respect to Ag/Ag$^+$ (0.01 mol dm^{-3}, AgClO$_4$ in AN). Sweep rate = 50
mV s^{-1}.
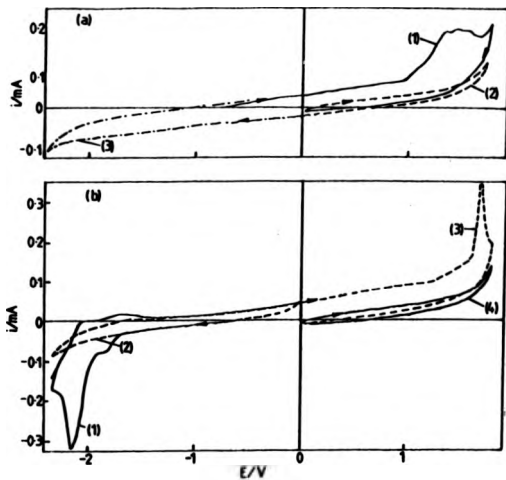
negative, then a sharp reduction wave with an associated shoulder at E_{Pc} = -2.16 V is observed on the first cycle. Subsequent cathodic cycles show no electroactivity. However, on sweeping positively, a sharp irreversible wave at E_{Pa} = 1.7 V is observed on the first cycle. The charge under the waves located at E_P = 1.7 and -2.16 is the same.

The electrochemistry of the analogous oxidation addition adduct resulting from the reaction between 3-BrPy and [Ni$^{(0)}$(bpy)$_2$], [(XVIII)] (figure 7.30b) was also investigated. The electrochemistry of (XVIII) is very similar to that of (XVII), although (XVIII) is only sparingly soluble in AN (< 1 mmol dm^{-3}). Cyclic voltammograms of (XVIII) have the same form as those of (XVII) and once again potential steps to -1.8 V lead to the deposition of thin insulating films on the surface of the working electrode.

We conclude that the reduction of both (XVII) and (XVIII) produces species which are insoluble in AN and therefore precipitate onto the electrode surfaces to give thin insulating films. It is pleasing that the coated electrodes contained nickel since this is consistent with the proposal that dipyridylnickel(II) species are produced and that they are stable to spontaneous reductive elimination.

7.6.6 General Conclusions

The work presented in this chapter deals with two areas. Firstly, the electrochemical deposition of PPy based on the 2,5-Br$_2$Py/[Ni$^{(II)}$(bpy)$_3$(ClO$_4$)$_2$]/TEAP/AN system and secondly, the properties of the resultant electrode deposits. In this section, conclusions about the polymerisation mechanism and the nature of the electrode deposits are drawn.

Preliminary investigations into the the relationship between the relative concentration of the two reactants and the polymerisation charge

led to the hypothesis that the initial steps of the polymerisation process are consistent with a second order ECE mechanism in which the reactant stoichiometry is 1 : 1 and the maximum charge consumed is four electrons per nickel. The hypothesis was rigorously tested using a specially formulated kinetic model for second order ECE processes at a RDE. It is clear from the analysis of the limiting current responses that the mechanism of PPy electrosynthesis closely conforms to the theory. Electroreductive polymerisation of (XVI) leads to the deposition of films which are essentially indistinguishable from those prepared from the $2,5\text{-Br}_2\text{Py}/[\text{Ni}^{(II)}(\text{bpy})_3(\text{ClO}_4)_2]/\text{TEAP/AN}$ system. Consequently, it is proposed that (XVI) is common to both polymerisation processes and in the latter case, (XVI) is the product of the homogeneous chemical step between $[\text{Ni}^{(0)}(\text{bpy})_2]$ and $2,5\text{-Br}_2\text{Py}$. Therefore it can be concluded that the mechanism of polymerisation has been successfully described in terms of a second order ECE theory and that the nature of the reactive intermediate has been determined. Once again it should be mentioned that a DISP1 mechanism cannot be ruled out unequivocally.

Investigations into the nature of the polymer films has led to the tentative conclusion that the pristine films are "organonickel strings" which are highly charged in their conducting state. Although the electrosynthesis of a metallised conducting polymer in which the metal is an integral part of the polymer backbone is very unusual, the experimental results strongly indicate such a structure. In particular, it can be clearly seen that exposure of the pristine films to oxygen or anodic potentials results in the polymer films undergoing dramatic structural changes. These changes are reconciled with the reductive elimination of nickel from a $-(\text{PyNi})_n-$ polymer chain leading to a $-(\text{Py})_n-/\text{Ni}$ polymer matrix. The nickel is only loosely held within the matrix because it is rapidly and irreversibly expelled by repetitive cyclic voltammetry. It is concluded that the nickel-free polymer films are poor chelates probably due to the adjacent pyridyl units being C^2-C^5 bonded. Further

investigations into the nature of the polymer films are needed for definitive structural assignment.

Appendix 7.1

This appendix deals with the modification of the case II theory to account for the situation where the diffusion coefficients of P, R and S are different.

In case II the rate of the homogeneous chemical step is so fast that we can consider the overall reaction between P and R as a titration. Consequently in the steady state, the fluxes of the reactants must balance:

$$D_P \frac{dp}{dx} = -D_R \frac{dr}{dx} \tag{7.15}$$

therefore:

$$\frac{D_P p_\infty}{X_P} = \frac{D_R r_\infty}{X_R - x_o} \tag{7.16}$$

and hence x_o:

$$x_o = X_R - \frac{D_R r_\infty X_P}{D_P p_\infty} \tag{7.17}$$

where x_o is the location of the reaction zone within the diffusion layer.

S is produced at x_o and diffuses towards the electrode and out into the bulk solution. The sum of the fluxes of S must be balanced by the flux of P:

$$\frac{D_S s_o}{x_o} + \frac{D_S s_o}{X_S - x_o} = \frac{D_P p_\infty}{X_P} \tag{7.18}$$

and therefore:

$$s_* = \frac{D_P p_\infty}{X_P} \left(\frac{x_* (X_P - x_*)}{D_S X_S} \right)$$ (7.19)

where s_* is the concentration of S at the reaction zone. At the electrode surface the flux of S can be given by:

$$D_S \frac{ds}{dx} \bigg|_{x=0} = \frac{D_S s_*}{x_*}$$ (7.20)

Substitution for x_* and s_* into equation (7.20) gives:

$$D_S \frac{ds}{dx} \bigg|_{x=0} = \frac{D_P p_\infty}{X_P} \left(1 - \frac{X_R}{X_S} + \frac{D_R r_\infty X_P}{D_P p_\infty X_S} \right)$$ (7.20)

and for case II we know that:

$$D_S \frac{ds}{dx} \bigg|_{x=0} = \frac{D_P p_\infty}{X_P \gamma}$$ (7.21)

therefore:

$$\frac{1}{\gamma} = \left(1 - \frac{X_R}{X_S} + \frac{D_R r_\infty X_P}{D_P p_\infty X_S} \right)$$ (7.22)

and since $X = 0.643 \nu^{1/6} D^{1/3} W^{-1/2}$ [172] so that $X_R \propto (D_R)^{1/3}$ and X_S and X_P similarly then:

$$\frac{1}{\gamma} = 1 - \left(\frac{D_R}{D_S} \right)^{1/3} + \left(\frac{D_R}{D_P} \right) \left(\frac{D_P}{D_S} \right)^{1/3} \frac{r_\infty}{p_\infty}$$ (7.23)

Substitution of $1/\gamma$ into equation (6.47) yields the equation (7.24) which describes the limiting current response for case II which accounts for different diffusion coefficients of P, R and S:

$$\frac{i_L}{nFA} = \frac{D_P p_\infty}{X_P} \left\{ 2 - \left(\frac{D_R}{D_S}\right)^{1/3} + \left(\frac{D_R}{D_P}\right)\left(\frac{D_P}{D_S}\right)^{1/3} \frac{r_\infty}{p_\infty} \right\} \qquad (7.24)$$

Finally the ratio of the limiting current responses in the presence and absence of R, i_L and $i_{L, r_\infty = 0}$ respectively, is given by:

$$\frac{i_L}{i_{L, r_\infty = 0}} = 2 - \left(\frac{D_R}{D_S}\right)^{1/3} + \left(\frac{D_R}{D_P}\right)\left(\frac{D_P}{D_S}\right)^{1/3} \frac{r_\infty}{p_\infty} \qquad (7.25)$$

CHAPTER 8

ELECTROREDUCTIVE POLYMERISATION OF NOVEL REDUCED STATE CONDUCTING POLYMERS

8.1 Introduction

Azines have similar chemical reactivity to pyridine[180,181]. For example, they are both π-deficient heterocycles which are readily protonated and resistant to electrophilic substitution. They both undergo oxidation at large anodic potentials and reduction at small cathodic potentials when compared to typical monomers of oxidised state conducting polymers such as pyrrole. On the basis of these considerations, we chose to attempt the syntheses of poly(azines), PAzs, because we postulated that they would also be conducting in their reduced state. We also postulated that azines, which are *para*-substituted with bromine, would behave in a similar fashion to $2,5\text{-}B_2Py$. That is, they would undergo nickel catalysed electroreductive polymerisation to yield electrode deposits of PAzs.

In this chapter we present our preliminary investigations into the syntheses of poly(pyridazine), poly(phthalazine) and poly (bromophthalazine) from 3,6-dibromopyridazine, 1,4-dibromo-phthalazine and 2,3,5-tribromopyrazine respectively. We begin by describing the conditions for the electrodeposition of all the PAzs. Next we report the electrosynthesis and some properties of each polymer. Finally, we compare and contrast the electropolymerisation and electrochemistry of PPy with that of the PAzs.

The experimental conditions for the electrodeposition of the PAzs were chosen to be as close as possible to the optimum conditions for the electrodeposition of PPy. Therefore, the electrosyntheses are all based on the electroreductive polymerisation of dibromoazines utilising the $[Ni^{(II)}(bpy)_3(ClO_4)_2]$/TEAP/AN system. The growth solutions all contain equimolar quantities (or nearly so) of $[Ni^{(II)}(bpy)_3(ClO_4)_2]$ and the dibromoazine. As with the PPy system we found that the rigorous exclusion of oxygen was essential for polymer deposition.

If the initial stages of the electrosyntheses are to be similar to that of PPy, then the potentials for the electrodeposition of the PAzs should be chosen so that the direct electrochemistry of the brominated monomers is avoided and so that $[Ni^{(III)}(bpy)_3]^{2+}$ undergoes a two-electron reduction. The first reduction waves of 3,6-dibromopyridazine, 1,4-dibromophthalazine and 2,3,5-tribromopyrazine are observed at $ca.$ -1.55, -1.35 and -1.59 V respectively (section 4.4). Therefore in order to mimic the PPy system the corresponding cathodic limits for electrodeposition should not exceed -1.55, -1.35 and -1.59 V. However, the two-electron reduction of $[Ni^{(II)}(bpy)_3(ClO_4)_2]$ does not begin until $ca.$ -1.5 V (section 4.3). This means that in order for sufficient nickel to be in the appropriate oxidation state to catalyse the polymerisations, direct electroreduction of the brominated momomers is probable, and in the case of 1,4-dibromophthalazine cannot be avoided. This is in direct contrast to the PPy system where diffusion controlled reduction of the two reactants is separated by 0.5 V so reductive electrochemistry of 2,5-Br$_2$Py is readily avoided.

Electrodeposition was attempted for each polymer by either repetitive cyclic voltammetry over a potential range whose upper limit lay within 0 to -1.2 V and whose lower limit extended beyond the first

reductive wave of $[Ni^{(II)}(bpy)_3]^{2+}$ (< -1.5 V), but did not exceed -2.0 V; or by stepping the potential from the solution's resting potential to a potential within the range -1.5 V to -2.0 V. In contrast to PPy, the eletrodeposition of all the PAzs is very sensitive to the choice of growth potential. The electrodeposition was found to be most successful when the cathodic limit exceeded the reduction potential of the brominated monomer.

The electrochemical behaviour of the coated electrodes was investigated in AN solutions containing TEAP. The coated electrodes were transferred from the growth solutions to the AN/TEAP solutions in air and no measures were taken to avoid exposure of the pristine films to oxygen. The removal of nickel from the polymer films was initially attempted by soaking the coated electrodes in aqueous EDTA (0.1 mol dm^{-3}, pH 9.2) for up to 30 mins. However, this method is not very satisfactory because the films tended to crack and flake off the electrode. In order to overcome this problem the polymer films were gradually conditioned to an aqueous environment by soaking the coated electrodes in serial dilutions of AN/water prior to transfer to the EDTA solution. This method was found to be satisfactory for poly(pyridazine), but poly(phthalazine) and poly(bromophthalazine) still flaked off the electrodes.

8.2.1 Poly(pyridazine)

We found that poly(pyridazine) may be grown by either repetitive cyclic voltammetry or potential step. Figures 8.1 and 8.2 show typical growth responses. The former method produces the best electrode coats when the lower limit is -1.78 V and the upper limit lies between 0 and -1.0 V. The first cyclic voltammogram shows an irreversible reduction wave located at E_{pc} = -1.68 V. There is a decrease in the charge enclosed by the first five successive voltammograms and thereafter each

Figure 8.1:

Thirty successive cyclic voltammograms at Pt/KV in an AN solution containing $[Ni^{(II)}(bpy)_3(ClO_4)_2]$ (5 mmol dm^{-3}), 3,6-dibromopyridazine (5 mmol dm^{-3}) and TEAP (0.1 mol dm^{-3}). Sweep rate = 100 mV s^{-1}. Potentials with respect to Ag/Ag$^+$ (AgClO$_4$, 0.01 mol dm^{-3} in AN).
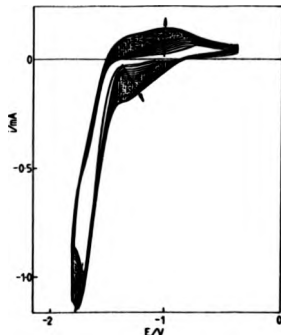
Figure 8.2:

Typical current-time curve at Pt/KV for an AN solution containing $[Ni^{(II)}(bpy)_3(ClO_4)_2]$ (5 mmol dm^{-3}), 3,6-dibromopyridazine (5 mmol dm^{-3}) and TEAP (0.1 mol dm^{-3}) for a potential step from -0.4 to -1.68 V. Potentials with respect to Ag/Ag$^+$ (AgClO$_4$, 0.01 mol dm^{-3} in AN).
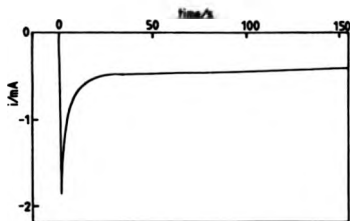
voltammogram encloses more charge than its predecessor. We observe the gradual growing in of broad redox processes at $E_{Pc} = -1.25$ V and $E_{Pa} = -1.00$ V. Orange films are clearly visible on the electrode after 10 scans. We can infer from these observations that a conducting film is being deposited on the electrode surface. Cathodic limits more negative than -1.78 V cause the reduction wave to shift cathodically on each subsequent cycle, and examination of the electrode surface showed thin yellow patchy films. An increase in the reductive overpotential is probably due to the electrodeposition of a more resistive film.

Electrodeposition by the latter potentiostatic method gives the best results when the stepped potential is -1.68 V. The current-time transients show an initial double-layer charging spike followed by a plateau. Once again we observed orange deposits on the electrode surface. Stepped-potentials more negative than -1.68 V give current-time transients which rapidly diminish in a non-Cotterell fashion to zero current and any films are very thin.

Figure 8.3(a) shows a typical response of the as-grown coated electrode in background electrolyte. There is a broad region of electroactivity lying between the potentials -0.7 to -1.8 V. Extension of the cathodic switching potential reveals another better defined redox process centred at ca. -2.0 V. Repeated cyclic voltammetry shows that the response of the coated electrodes is stable; a loss of less than 10% redox activity is observed after 25 cycles. There is no preferential loss of electroactivity between the two centres of redox activity, instead we observe an overall decrease in the charge enclosed by the cyclic voltammogram.

Figure 8.3(b) shows a typical response of an EDTA-treated coated electrode in background electrolyte. In this case there is a single sharp redox process centred at -1.9 V. A comparison between the

Figure 8.3:

Typical cyclic voltammograms of polymer coated Pt/KV in an AN
solution containing TEAP (0.1 mol dm^{-3}). The polymer films were grown
potentiostatically at -1.68 V in an AN solution containing
[Ni$^{(II)}$(bpy)$_3$(ClO$_4$)$_2$] (5 mmol dm^{-3}), 3,6-dibromopyridazine (5 mmol
dm^{-3}) and TEAP (0.1 mol dm^{-3}) for 8 min. The polymer films are (a)
as-grown and (b) treated with EDTA after preconditioning to an aqueous
environment by soaking in serial dilutions of AN/water. Potentials with
respect to Ag/Ag$^+$ (AgClO$_4$, 0.01 mol dm^{-3} in AN). Sweep rate = 100
mV s^{-1}.
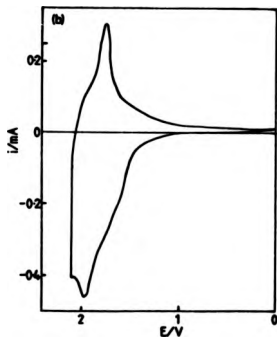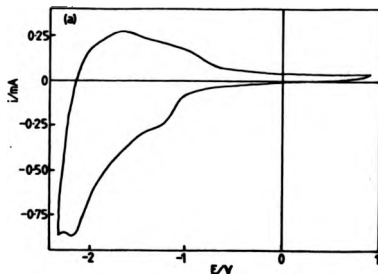
electrochemistry of the as-grown and EDTA-treated coated electrodes, allows us to propose that the broad electroactivity can be attributed to the nickel bound within the polymer films, and the redox process located at -2.0 V to the oxidation and reduction of the polymer backbone itself.

The peak heights of the redox processes of the treated and untreated polymer films all vary linearly with sweep rate. This is as expected for surface bound redox couples.

The polymer films are soluble in inorganic acids such as sulphuric acid (3 mol dm^{-3}) and yield clear orange solutions.

8.2.2 Poly(phthalazine)

Attempts to grow conducting films of poly(phthalazine) by repetitive cyclic voltammetry were unsuccessful. We varied the lower potential limits between the ranges -1.5 to -2.6 V and the upper limits between 0 to -1.2 V, and tried a variety of substrate concentrations (2.5 to 25 mmol dm^{-3}). Typically the first cyclic voltammogram shows two irreversible reduction waves located at E_{p_c} = -1.46 and -2.23 V. On successive sweeps the peak height of the first wave diminishes and shifts to more negative potentials (E_{p_c} = -1.9 V on the 15th cycle) whereas the peak current of the second reduction wave gradually increases and E_{p_c} remains essentially unaltered with each successive cycle. Figures 8.4 shows typical current-voltage curves obtained when attempting electrodeposition of poly(phthalazine) by cyclic voltammetry. In each attempt, no visible film was observed on the surface of the working electrode and cyclic voltammetry in background electrolyte confirmed that electrodeposition had failed because the current-voltage curves were typical of a clean platinum electrode.

Polymer films were successfully grown potentiostatically; the optimum stepped potential was found to be -2.0 V. As with

Figure 8.4:

Fifteen successive cyclic voltammograms at Pt/KV in an AN solution containing $[Ni^{(II)}(bpy)_3(ClO_4)_2]$ (2.5 mmol dm^{-3}), 1,4-dibromophthalazine (2.5 mmol dm^{-3}) and TEAP (0.1 mol dm^{-3}). Potentials with respect to Ag/Ag^+ ($AgClO_4$, 0.01 mol dm^{-3} in AN). Sweep rate = 100 mV s^{-1}.


Figure 8.5:

Typical current-time curve at Pt/KV for an AN solution containing $[Ni^{(II)}(bpy)_3(ClO_4)_2]$ (5 mmol dm^{-3}), 1,4-dibromophthalazine (5 mmol dm^{-3}) and TEAP (0.1 mol dm^{-3}) for a potential step from -0.4 to -2.0 V. Potentials with respect to Ag/Ag^+ (0.01 mol dm^{-3}, $AgClO_4$ in AN).

poly(pyridazine), the current-time transients show an initial double-layer charging spike followed by a plateau, figure 8.5. Following a potential step, smooth orange/yellow films uniformly cover the surface of the working electrode.

Figure 8.6 shows a typical response of the as-grown coated electrode in background electrolyte. We observe a single reasonably well defined reduction peak at -1.85 V with an associated oxidation peak at -1.75 V. Interestingly, this cyclic voltammogram has the same general form as the EDTA-treated polymers poly(pyridine) and poly(pyridazine). Unfortunately, a comparison between the as-grown and EDTA-treated poly(phthalazine) films is not possible because the films broke up and flaked off the electrode on soaking in either aqueous EDTA or AN/water mixtures.

The as-grown polymer films are soluble in inorganic acids.

8.2.3 Poly(bromopyrazine)

We found that poly(bromophthalazine) may be grown by either repetitive cyclic voltammetry or potential step. Both methods of deposition result in the uniform coverage of the working electrode, but the films appear much thinner than observed for the other polymers. Examination of the growth patterns of poly(bromopyrazine) indicate that the thickness of the electrode deposits are indeed limited. This is because the growth currents gradually diminish during the polymerisation processes, figures 8.7 and 8.8. This behaviour is typical of a film-forming process in which the film tends to block further electrochemistry.

Figure 8.9 shows a typical response of a coated electrode in background electrolyte. There are no well defined redox couples, rather we observe a broad region of electroactivity extending between 0 and -2.0 V. The polymer films are not very stable to repetitive cyclic voltammetry

Typical cyclic voltammogram of as-grown poly(phthalazine) coated Pt/KV in an AN solution containing TEAP (0.1 mol dm^{-3}). The polymer films were grown potentiostatically at -2.0 V in an AN solution containing [Ni$^{(II)}$(bpy)$_3$(ClO$_4$)$_2$] (5 mmol dm^{-3}), 1,4-dibromophthalazine (5 mmol dm^{-3}) and TEAP (0.1 mol dm^{-3}) for 4.5 min. Potentials with respect to Ag/Ag$^+$ (0.01 mol dm^{-3}, AgClO$_4$ in AN). Sweep rate = 100 mV s^{-1}.
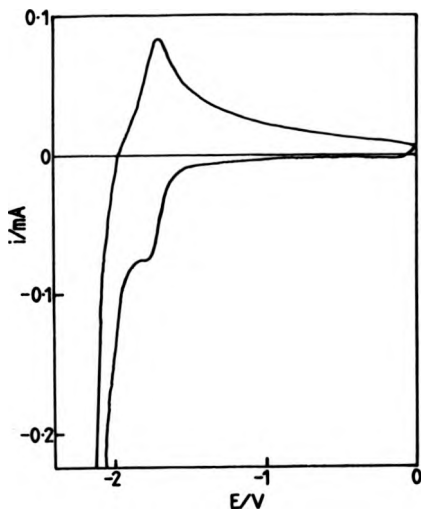
Twenty successive cyclic voltammograms at Pt/KV in an AN solution containing [Ni$^{(II)}$(bpy)$_3$(ClO$_4$)$_2$] (5 mmol dm^{-3}), 2,3,5-tribromopyrazine (4.3 mmol dm^{-3}) and TEAP (0.1 mol dm^{-3}). Potentials with respect to Ag/Ag$^+$ (0.01 mol dm^{-3}, AgClO$_4$ in AN). Sweep rate = 100 mV s^{-1}.
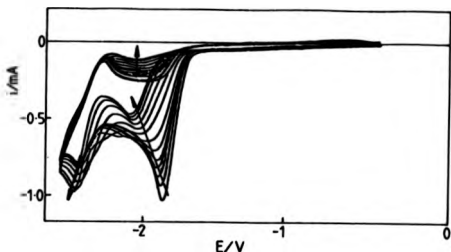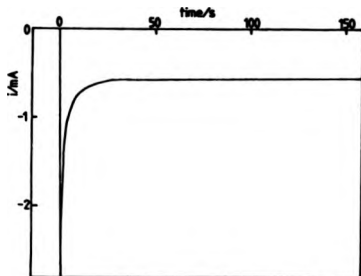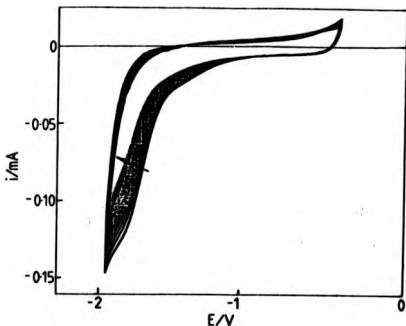

Figure 8.8:

Typical current-time curve at Pt/KV for an AN solution containing [Ni$^{(II)}$(bpy)$_3$(ClO$_4$)$_2$] (5 mmol dm^{-3}), 2,3,5-tribromopyrazine (4.3 mmol dm^{-3}) and TEAP (0.1 mol dm^{-3}) for a potential step from -0.4 to -2.0 V. Potentials with respect to Ag/Ag$^+$ (0.01 mol dm^{-3}, AgClO$_4$ in AN).
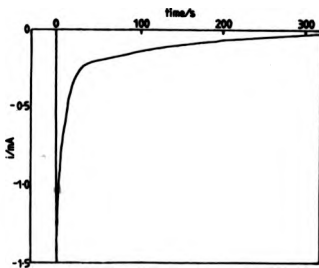
Typical cyclic voltammogram of as-grown poly(bromophthalazine) coated Pt/KV in an AN solution containing TEAP (0.1 mol dm^{-3}). The polymer film was grown potentiostatically at -2.0 V in an AN solution containing $[Ni^{(II)}(bpy)_3(ClO_4)_2]$ (5 mmol dm^{-3}), 2,3,5-tribromopyrazine (4.3 mmol dm^{-3}) and TEAP (0.1 mol dm^{-3}) for 8 min. Potentials with respect to Ag/Ag$^+$ (0.01 mol dm^{-3}, AgClO$_4$ in AN). Sweep rate = 100 mV s^{-1}.
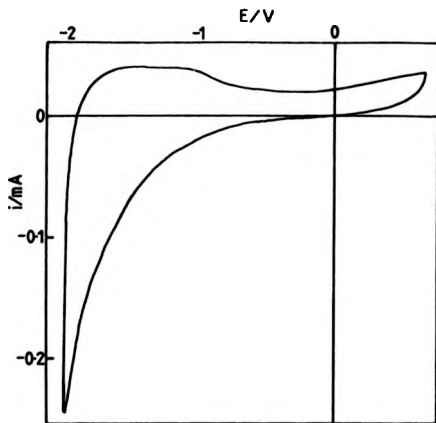
and like the poly(phthalazine) films, they flake off the electrode when transferred to aqueous solutions. The polymer films are soluble in inorganic acids.

8.3 Comparison between PPy and the PAzs

The results presented in this chapter are on the whole qualitative and the conditions for growth and treatment of the PAz films should not be regarded as definitive. Nevertheless the results clearly demonstrate that the *para*-dibromoaryl/[Ni$^{(II)}$(bpy)$_3$(ClO$_4$)$_2$]/TEAP/AN system can be used to prepare a variety of reduced state conducting polymers. The results also show that the diazyl and pyridyl polymers display a number of common features. In this section we compare and contrast the four reduced state conducting polymers prepared by this technique and suggest a set of criteria which need to be fulfilled to optimize the chances of preparing other such polymers.

The preferred growth potentials for PPy and PAz films are all more negative than -1.65 V. This means that in all cases the two-electron reduction of [Ni$^{(II)}$(bpy)$_3$]$^{2+}$ is diffusion controlled. The electrosynthesis of PPy is relatively insensitive to growth potential whereas each PAz film can only be grown over a narrow potential band. We propose that the difference in sensitivity arises because the reduction potentials of [Ni$^{(II)}$(bpy)$_3$]$^{2+}$ and the brominated azines are similar, whereas the reduction of 2,5-Br$_2$Py occurs at much more negative potentials. This means that in the PAz cases, when the nickel reduction is diffusion controlled, the processes occurring at the electrode surface will be complicated by the direct reduction of the dibromoazine. It is reasonable to suppose that this will restrict suitable growth potentials. In the case of PPy the electroreduction of 2,5-Br$_2$Py does not occur until -2.15 V, so there are no comparable complicating reactions which may disrupt the polymerisation process and thereby limit the range of suitable growth

-289-

potentials.

A comparison between the electrochemistry of poly(pyridazine) and PPy reveals that they have a number of common features: Firstly, the as-grown polymer films are electroactive in the cathodic region. Each polymer film has two centres of electroactivity; the first is broad with poorly defined redox peaks and the second, situated at more cathodic potentials, is sharper. Secondly, treatment of the polymer films with EDTA results in the loss of the broad electroactive couple and improves the definition of the remaining couple. In both cases we assign the broad electroactive couple to the reduction and oxidation of the nickel within the films, and the better defined couple to the reduction and oxidation of pyridyl or diazyl moieties. Thirdly, the peak heights of the redox processes of both polymers vary linearly with sweep rate.

One notable difference between the as-grown oxygen-exposed polymers of PPy and poly(pyridazine) is their response to repeated cyclic voltammetry in background electrolyte. The PPy films rapidly lose the broad redox couple centred at -1.5 V, and the redox couple centred at -2.10 V sharpens and stabilizes. We believe that these changes are due to the expulsion of nickel from the polymer films. By contrast, poly(pyridazine) films are reasonably stable to repeated cyclic voltammetry and the loss in electroactivity is distributed over the whole region of electroactivity. Consequently we propose that the nickel remains bound within the poly(pyridazine) films. The different behaviour of these two polymers can be explained by considering their relative abilities to coordinate metals. In section 7.6 it is suggested that PPy is a poor ligand because the pyridyl moieties are C^2-C^5 linked, figure 8.10(a). Now, if we assume that the mechanism of polymerisation of these polymers is similar, then the diazyl moieties will be C^3-C^6 linked and therefore suitably orientated for metal chelation, figure 8.10(b).

A comparison between the as-grown polymer films of poly(phthalazine), poly(pyridazine) and PPy shows the former to be markedly different. Although it shows reduced state conductivity, the broad region of electroactivity typical of the other two polymers is absent. Instead we observe a single redox couple whose shape is reminiscent of EDTA-treated PPy and poly(pyridazine) films. We can infer from the absence of the broad redox process that the as-grown poly(phthalazine) films contain negligible amounts of nickel. Ostensibly it is surprising that poly(phthalazine) films do not show the same ability to bind nickel as poly(pyridazine). However, we propose that the difference arises because coordination of the nickel to the polymer is sterically hindered by the benzo moieties, figure 8.11.

There are a number of differences between the electrosynthesis and electrochemistry of poly(bromophthalazine) compared to the other reduced state conducting polymers investigated in this project. Firstly, all attempts at the electrosynthesis of poly(bromophthalazine) led to the deposition of thin electrode coatings irrespective of growth time or reactant concentration. Secondly, the growth currents fall to zero during electrosyntheses. This is in direct contrast to the other polymers where the growth currents either remain constant or increase with time. Thirdly, the cyclic voltammetry of electrodes coated with poly(bromophthalazine) do not display any of the characteristics common to the other three polymers. Finally, these polymer films are particularly unstable to repeated cyclic voltammetry. We can infer from these results that the poly(bromophthalazine) films are unstable and much more resistive than either PPy or the other PAz films. A possible explanation for the decrease in conductivity is that a significant number of the bromopyrizyl moieties are C^2-C^3 or C^3-C^6 linked, figure 8.12. The reduction of a poly(bromophthalazine) polymer containing such linkages would result in a polymer unable to configure the extensive π conjugation needed for electronic conduction. It should be stressed that this is only a

Figure 8.10:

Proposed structures of poly(pyridine) and poly(pyridazine)

(a) Poly(pyridine)   (b) Poly(pyridazine)
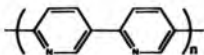
Poor ability to coordinate
metals
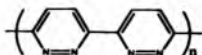
Good ability to coordinate
metals

Figure 8.11:

Proposed structure of poly(phthalazine)
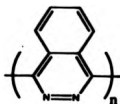
Figure 8.12:

Proposed structure of poly(bromopyrazine)
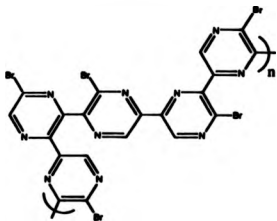
tentative proposal as the experimental results are only preliminary.

8.4 Conclusions

The electroreductive polymerisation of all three brominated azines was successful. In each case the electrode deposit is novel and the poly(pyidazine) and poly(phthalazine) films show redox activity consistent with reduced state conductivity. This is a very pleasing result because these new polymers make a significant contribution to the number of reduced state conducting polymers which can be prepared by electrochemical polymerisation. However more importantly, we have demonstrated that the bromoaryl/$[Ni^{(II)}(bpy)_3(ClO_4)_2]$/TEAP/AN system can be exploited for the successful preparation of a variety of stable reduced state conducting polymers.

CHAPTER 9

CONCLUDING REMARKS

The central theme of this thesis deals with reduced state conducting polymers and in particular with poly(pyridine). Also presented in this thesis is a detailed investigation into the electrochemistry of $[Ni(bpy)_3(ClO_4)_2]$ and the derivation of a theoretical model describing the limiting current responses of a second order ECE process at a RDE.

The synthesis of poly(pyridine) is based on the nickel catalysed electroreductive polymerisation of 2,5-dibromopyridine. The results obtained clearly show that the nature of the so called "innocent ligands" of the nickel species play an important role in determining the mechanism and properties of the resultant electrode deposits.

The initial steps of the electrosynthesis of PPy based on the $[Ni(bpy)_3(ClO_4)_2]$ system at a RDE are analysed as an ECE process. The homogeneous rate constant is extracted from this analysis. The ECE theory has been exclusively used to analyse the polymerisation data. However the theory has a much broader application than demonstrated in this thesis.

The general usage of the $[Ni(bpy)_3(ClO_4)_2]$ system to produced reduced state conducting polymers from electron deficient bromoaromatics has been successfully demonstrated. Further research in this area will almost certainly lead to the synthesis of many more reduced state conducting polymers. The copolymerisation of brominated aromatics is also a potentially fruitful area of research.

The synthesis and characterisation of the organonickel polymer precursors has been proven to be a useful aid in elucidating the

polymerisation mechanisms. Indeed this approach has conclusively demonstrated that the polymer precursor of the $[Ni(PPh_3)_4]/2,5\text{-}Br_2Py$ system is dinuclear rather than mononuclear.

Attempts to electrosynthesis conducting films from the platinum and palladium phosphine adducts proved unsuccessful It is possible that using a different ligand such as bpy, phen of a bidentate phosphine may be better.

The investigations into the nature of the electrode deposits yielded some interesting results. The suggestion that the pristine electrode deposits are organonickel strings warrants further attention.

References

1. C. P. Andrieux and J. M. Savéant, *J. Electroanal. Chem.*, **93**, (1978) 166.

2. C. P. Andrieux, J. M. Dumas-Bouchait and J. M. Savéant, *J. Electroanal. Chem.*, **159**, (1980) 159.

3. C. P. Andrieux, J. M. Dumas-Bouchait and J. M. Savéant, *J. Electroanal. Chem.*, **131**, (1980) 159.

4. C. P. Andrieux and J. M. Savéant, *J. Electroanal. Chem.*, **134**, (1982) 163.

5. F. C. Anson, *J. Phys. Chem.*, **84**, (1980) 253.

6. R. D. Rocklin and R. W. Murray, *J. Phys. Chem.*, **85**, (1981) 2104.

7. R. W. Murray, *Phil. Trans. R. Soc.*, **302**, (1981) 253.

8. W. J. Albery and A. R. Hillman, *J. Electroanal. Chem.*, **170**, (1984) 27.

9. W. J. Albery and A. R. Hillman, *R. S. C. Ann. Rep. C*, (1981) 377

10. P. R. Moses, L. Weir and R. W. Murray, *Anal. Chem.*, **45**, (1975) 1882.

11. P. R. Moses and R. W. Murray, *J. Am. Chem. Soc.*, **98**, (1976) 7435.

12. P. R. Moses and R. W. Murray, *J. Electroanal. Chem.*, **77**, (1977) 343.

13. M. M. Labes, P. Love and L. F. Nichols, *Chem. Rev.*, **79**, (1979) 1.

14. T. A. Skotheim (Ed), *Handbook of Conducting Polymers*, Marcel Dekker, New York, 1986.

15. H. Munstedt, in *Electronic Properties of Polymers and Related Compounds*, H. Kuzmany, M. Mehring, and S. Roth (Eds.),

Springer series in Solid Sate Science, **63**, (1985) 8.

16. R. L. Green and G. B. Street, *Science*, **226**, (1984) 651.

17. G. Wegner, in *Contempory Topics in Polymer Science*, E. J. Vandenberg (Ed.), **5**, (1984) 281.

18. W. J. Feast in *Chemical Sensors*, T. E. Edmonds (Ed.), Blackie Publishing Group, Glasgow (1988) 115.

19. S. Roth, Siegmar, Bleier, Hartmut, Pukacki and Wojciech, *Faraday Discuss. Chem. Soc.* **88**, (1989) 223.

20. H. Lethely, *J. Chem. Soc.*, **15**, (1862) 161.

21. A. Angeli, *Gazz. Chim. Ital.*, **46 II**, (1916) 279.

22. A. Angeli and L. Alessandri, *Gazz. Chim. Ital.*, **46 II**, (1916) 283.

23. A. Dall' Olio, Y. Dascola, V. Varana and V. Bocchi, *Comptes. Rendus.*, C **267**, (1968) 433.

24. G. K. Chandler and D. Pletcher in *Electrochemistry*, vol 10, Royal Society of chemistry, D. Pletcher (Ed.), London (1985) chapter 3, pp 117.

25. A. O. Patil, A. L. J. Heeger and F. Wudl, *Chem. Rev.*, **88**, (1988) 183.

26. T. Yamamoto, Y. Hayashi and A. Yamamoto, *Bull. Chem, Soc, Jpn.*, **51**, (1978) 2091.

27. T. Yamamoto, T. Ito, K. Kubota, *Chem. Lett.*, (1988) 153.

28. T. Yamamoto, Z. Zhou, T. Kanbara and T. Maruyama, *Chem. Lett.*, (1990) 223.

29. T. Yamamoto, T. Maruyama, T. Ikeda and M. Sisidp. *J. Chem. Soc. Chem, Commun.*, (1990) 1306.

30. G. Schiavon, G. Zotti and G. Bontempelli, *J. Electroanal. Chem.*, **194**, (1985) 327.

31. G. Schiavon, G. Zotti, G. Bontempelli and F. L. Coco, *J. Electroanal. Chem.*, **242**, (1988) 131.

32. H. Shirakawa, E. J. Louis, A.G. MacDiarmid, C-K. Chiang and A. J. Heeger, *J. Chem. Soc., Chem. Commun.*, (1977) 578.

33. H. Naarmann, *Synth. Met.*, **17**, (1987) 2233.

34. J. L. Bredas, *Mol. Cryst. Liq. Cryst.*, **118**, (1985) 49.

35. J. C. Scott, M. T. Kroubi, P. Pflunger and G. B. Street, *Phys. Rev. B*, **28**, (1983) 2140.

36. H. W. Gibson and J. M. Pochan in *Encyclopedia of Polymer Science and Engineering*, vol. 1, 2nd ed., John Wiley, New York, (1984) 87.

37. G. Zotti and G. Schiavon, *J. Electroanal. Chem.*, **163**, (1984) 385.

38. Z. Xu, G. Horowitz and F. Garnier, *J. Electroanal. Chem.*, **246**, (1988) 467.

39. R. Tomat, S. Zecchin, G. Schiavon and G. Zotti, *J. Electroanal. Chem.*, **252**, (1988) 215.

40. G. Zotti, G. Schiavon, N. Comisso, A. Berlin and G. Pagani, *Synth. Metals*, **36**, (1990) 337.

41. T. Ohsawa, K. Kaneto and K. Yoshino, *Jpn. J. Appl. Phys.*, **23**, (1984) 663.

42. G. Tourillon and F. Garnier, *J. Electroanal. Chem.*, **135**, (1982) 173.

43. E. P. Goodings *Chem. Soc. Rev.*, **5**, (1976) 95.

44. A. F. Diaz, K. K. Kanazawa and G. P. Gardini, *J. Chem. Soc.*

Commun., (1979) 635.

45. A. F. Diaz, and J. I. Castillo, *J. Chem Soc. Commun.,* (1980) 397.

46. A. F. Diaz, J. M. Vasquez and A. M. Duran, *IBM Res. Develop.,* **25.** (1981) 42.

47. A. J. Downard, D. Pletcher, *J. Electroanal. Chem.,* **206,** (1986) 139.

48. P. G. Pickup, *J. Electroanal. Chem.,* **225,** (1987) 273.

50. M. Takakuno, *Synth. Metals,* **18,** (1987) 273.

51. K. Kaneto, Y. Kohno, K. Yoshimo and Y. Inishi, *J. Chem. Soc., Chem. Commun.,* (1983) 713.

52. R. J. Waltman, J. Bargon and A. F. Diaz, *J. Phys. Chem.,* (1983) 1459.

53. A. R. Hillman and E. F. Mallen, *J. Electroanal. Chem.,* **220,** (1987) 351.

54. P. Marque, J. Roncali and F. Garnier, *J. Electroanal. Chem.,* **218,** (1987) 107.

55. A. R. Hillman and A. Hammett, *J. Electrochem Soc.,* **135,** (1988) 2517.

56. C. J. Neilsen, R. Stotz, G. T. Cheek and R. F. Nelson, *J. Electroanal. Chem.,* **90,** (1978) 127.

57. G. Tourillon and F. Garnier, *J. Electroanal. Chem.,* **135,** (1982) 173.

58. R. J. Waltman, A. F. Diaz, J. Bargon, *J. Phys. Chem.,* **88,** (1984) 434.

59. A. F. Diaz and J. A. Logan, *J. Electroanal. Chem.,* **111,** (1980) 111.

60. E. M. Genies and C. Tsintavis, *J. Electroanal. Chem.,* **195,** (1985) 109.

61. E. M. Genies, M. Lapowski and J. F. Penneau, *J. Electroanal. Chem.*, **249**, (1988) 97.

62. S. Kaplan, E. M. Conwell, A. F. Richter and A. G. MacDiarmid, *J. Am. Chem. Soc.*, **110**, (1988) 7647.

63. G. Brilmyer and R. Jasinski, *J. Electroanal. Chem.*, **129**, (1982) 1950.

64. C-F. Hsing, J. Khoury, M. D. Bezoari and P. Kovacic, *J. Polym. Sci. Polym. Chem.* **20**, (1982) 3313.

65. Y. Cao and S. Li, *J. Chem. Soc., Chem. Commun.*, (1988) 937.

66. A. J. Bard and H. Lund, (Eds) *Encyclopedia of Electrochemisrty of the Elements, Organic Section*, Marcel Dekker, New York, (1984) vol XV, pp 243.

67. J. E. O'Reilly and P. J. Elving, *J. Am. Chem. Soc.*, **94**, (1972) 7941.

68. K. B. Wiberg and T. P. Lewis, *J. Am. Chem. Soc.*, **92**, (1970) 7154.

69. C. Gosden, K.P. Healy and D. Pletcher, *J. Chem. Soc. Dalton*, (1978) 972.

70. K.P. Healy and D. Pletcher, *J. Organomet. Chem.*, **161**, (1978) 109.

71. C. Gosden and D. Pletcher, *J. Organomet. Chem.*, **186**, (1980) 401.

72. M. Troupel, Y. Rollin, C. Chevrot, F. Pfluger and J-F. Fauvarque, *J. Chem. Research (S)*, (1979) 50.

73. M. Troupel, Y. Rollin, S. Sibille, J-F. Fauvarque and J. Perichon, *J. Chem. Research (S)*, (1980) 24.

74. S. Sibille, M. Troupel, J-F. Fauvarque and J. Perichon, *J. Chem. Research (S)*, (1980) 147.

75. M. Troupel, Y. Rollin, S. Sibille, J-F. Fauvarque and J. Perichon, *J.*

Chem. Research (S), (1980) 26.

76. S. Sibille, J-C Folest, J. Coulombeix, M. Troupel, J-F. Pauvarque and J. Perichon, *J. Chem. Research (S)*, (1980) 268.

77. G. Bontempelli, S. Danielle and M. Fiorani, *J. Electroanal. Chem.*, **160**, (1984) 249.

78. M. F. Semmelhack, P. M. Helquist and L. D. Jones, *J. Am. Chem. Soc.*, **93**, (1971) 5908.

79. T.T. Tsuo and J. K. Kochi, *J. Am. Chem. Soc.*, **101**, (1979) 7547.

80. M. Mori, Y. Hashimoto and Y. Ban, *Tet. Lett.*, **21**, (1980) 631.

81. A. Nakamura and S. Otsuka, *Tet. Lett.*, **5**, (1974) 463.

82. M. Almemark and B. Akermark, *J. Chem. Soc. Chem. Comm.*, (1978) 66.

83. K. Takagi, H. Mimura and S. Inokawa, *J. Bull. Chem. Soc. Jpn.*, **57**, (1984) 3517.

84. T. Yamamoto, T. Kohara, K. Oskakada and A. Yamamoto, *Bull. Chem. Soc. Jpn.*, **56**, (1983) 2147.

85. P. W. Jennings, D. G. Pillsbury, J. L. Hall and V. T. Brice, *J. Organomet. Chem.*, **41**, (1976) 719.

86. S. Mabrouk, S. Pellegrini, J-C. Folest, Y. Rollin and J. Perichin, *J. Organomet. Chem.*, **301**, (1986) 391.

87. M. Troupel, Y. Rollin, S. Sibille and J. Perichon, *J. Organomet. Chem.*, **202**, (1980) 435.

88. Y. Rollin, M. Troupel, D.G. Tuck and J. Perichon, *J. Organomet. Chem.*, **303**, (1986) 131.

89. G. Meyer, Y. Rollin and J. Perichon, *J. Organomet. Chem.*, **333**,

(1987) 263.

90.   G. Schiavon, G. Bontempelli, M. de Nobili and B. Corain, *Inorg. Chim. Acta*, **42**, (1980) 211.

91.   G. Schiavon, G. Bontempelli and B. Corain, *J. Chem. Soc. Dalton*, (1981) 1074.

92.   Y. Rollin, M. Troupel, J. Perichon and J-F. Fauvarque, *J. Chem. Research (S)*, (1981) 322.

93.   K. Takagi, N. Hayama and K. Sasaki, *J. Organomet. Chem.*, **57**, (1984) 1887.

94.   H. Zollinger, in Azo and Diazo Chemistry, Aliphatic and Aromatic Compounds, (1961) Interscience, New York, chapter 12.

95.   W. Smith and Y-M. Kuo, *J. Electroanal. Chem.*, **188**, (1985) 189.

96.   B. Akerman, H. Johnsen, B. Roos and U. Wahlgren, *J. Am. Chem. Soc.*, **101**, (1979) 5876.

97.   G. Bontempelli, F. Mango, B. Corain and G. Schiavon, *J. Electroanal. Chem.*, **103**, (1979) 243.

98.   J-F. Fauvarque, M-A. Petit, F. Pfluger, A. Jutland and C. Cheverot, *Makromol. Chem., Rapid Commun.*, **4**, (1983) 455.

99.   J-M. Fauvarque, A. Digua, M-A. Petit and J. Savard, *Makromol. Chem.*, **186**, (1985) 2415.

100.   G. Schiavon, G. Zotti and G. Bontempelli, *J. Electroanal. Chem.*, **161**, (1984) 323.

101.   G. Schiavon, G. Zotti and G. Bontempelli, *J. Electroanal. Chem.*, **186**, (1985) 191.

102.   S. Zecchin, G. Schiavon, R. Tomat and G. Zotti, *J. Electroanal.*

Chem., **215**, (1986) 377.

103. G. M. Sheldrick, *SHELXTL PLUS* user manuel, Nicolet XRD Corporation, Madison, Wisconison, (1983).

104. *International Tables for X-ray crystallography*, Kynoch Press, Birmingham, IV, (1974).

105. P. Coad, R.A. Coad, S. Clough, J. Hyepock, R. Salisbury and C. Wilkins, *J. Org. Chem.*, **28**, (1963) 218.

106. A. Hirsch and D. Orphanos, *Can. J. Chem.*, **43**, (1965) 2708.

107. R. C. Ellingson and R. L. Henry, *J. Am. Chem. Soc.*, **71**, (1949) 2798.

108. L. C. Craig, *J. Am. Chem. Soc.*, **56**, (1934) 231.

109. R. Schunn, *Inorg. synth.*, **XV**, (1974) 5.

110. D. Coulson, *Inorg. synth.*, **XIII**, (1974) 121.

111. R. Ugo, F. Cariati and G. LaMaria, *Inorg. synth.*, **XI**, (1968) 105.

112. S. Ittel, *Inorg. synth.*, **28**, (1990) 99.

113. R. A. Schunn, *Inorg. Chem.*, **15**, (1976) 208.

114. S. Ittel, *Inorg. synth.*, **28**, (1990) 102.

115. Southampton Electrochemistry Group, *Instrumental Methods in Electrochemistry*, John Wiley and Sons, Chichester, (1985).

116. A. J. Bard and L. R. Faulkner, *Electrochemical Methods Fundementals and Applications*, John Wiley and Sons, New York, (1980).

117. W. J. Albery and M. L. Hitchman, *Ring-Disc Electrodes*, Claraendon Press, Oxford, (1971).

118. C. Amatore, M. Azzabi, P. Calas, A. Jutland, C. Lefrou and Y.

Rollin, *J. Electroanal. Chem.*, **228**, (1990) 45.

119. D. R. Fahey, *J. Am. Chem. Soc.*, **92**, (1970) 402.

120. P. Fitton and E. A. Rick, *J. Organomet. Chem.*, **28**, (1971) 287.

121. M. Hidai, T. Kashiwagi, T. Ikeuchi and Y. Uchida, *J. Organomet. Chem.*, **30**, (1971) 279.

122. K. Isobe, Y. Nakamura and S. Kawaguchi, *Chem. Lett.*, (1977) 1383.

123. T. T. Tsou and J. K. Kochi, *J. Am. Chem. Soc.*, **100**, (1978) 1633.

124. K. Nakatsu, K. Kinoshita, H. Kanda, K. Isobe, Y. Nakamura and S. Kawaguchi, *J. Chem. Soc. Jpn., Chem. Lett.*, (1980) 913.

125. K. Isobe, E. Kai, Y. Nakamura, K. Nishimoto, T. Miwa and S. Kawaguchi, *J. Am. Chem. Soc.*, **102**, (1980) 2475.

126. K. Isobe, Y. Nakamura and S. Kawaguchi, *J. Chem. Soc. Jpn.*, **53**, (1980) 139.

127. K. Isobe and S. kawaguchi, *Heterocycles*, **16**, (1981) 1603.

128. A. Mantovani and B. Crociani, *J. Organomet. Chem.*, **236**, (1982) C37.

129. B. Crociani, F. Dibianca, A. Giovenco and A. Scrivanti, *J. Organomet. Chem.*, **269**, (1984) 295.

130. B. Crociani, F. Dibianca, A. Giovenco and A. Scrivanti, *J. Organomet. Chem.*, **291**, (1985) 259.

131. R. Bertani, A. Berton, F. Dibianca and B. Crociani, *J. Organomet. Chem.*, **303**, (1986) 283.

132. B. Crociani, F. Dibianca, A. Giovenco, A. Berton and R. Bertani, *J. Organomet. Chem.*, **361**, (1989) 255.

133. M. Uchino, K. Asagi, A. Yamamoto and S. Ikeda, *J. Organomet.*

Chem., **84**, (1975) 93.

134. A.G. Orpen, L. Brammer, F. H. Allen, O. Kennard, D. G. Watson and R. Taylor, *J. Chem. Soc., Dalton Trans.*, (1989) S1.

135. G. Schiavon, S. Zecchin, G. Cogni and G. Bontempelli, *J. Electroanal. Chem.*, **48**, (1973) 425.

136. B. Henne and D. Bartak, *Inorg. Chem.*, **23**, (1984) 369.

137. N. Tanaka and Y. Sato, *Inorg. Nucl. Letts.*, **4**, (1968) 487.

138. N. Tanaka, T. Ogata and S. Niizuma, *Inorg. Nucl. Letts.*, **8**, (1972) 965.

139. R. Prasad and D. Scaife, *J. Electroanal. Chem.*, **84**, (1977) 373.

140. C. Amatore, M. Azzabi, P. Calas, A. Jutland, C. Lefrou and Y. Rollin, *J. Electroanal. Chem.*, **228**, (1990) 45.

141. reference 115, chapter 1, pp 31.

142. W. R. McWhinnie and J. D. Miller, *Adv. Inorg. Chem. Radiochem.*, **12**, (1969) 135.

143. reference 116, chapter 8, pp 287.

144. V. G. Levich, *Physiochemical Hydrodynamics*, Prentice Hall, Eaglewood, (1962).

145. reference 117, chapter 3, pp 17.

146. reference 117, chapters 6, 7 and 8.

147. C. P. Andrieux, C. Blocman, J-M. Dumus-Bouchiat and J-M. Savéant, *J. Am. Chem. Soc.*, **101**, (1979) 3431.

148. J. Casado, I. Gallardo and M. Moreno, *J. Electroanal. Chem.*, **219** (1987) 197.

149. C. P. Andrieux, P. Hapiot and J-M. Savéant, *Chem. Rev.*, **90** (1990)

732.

150. A.J. Bard (Ed) *Encyclopedia of Electrochemistry of the Elements*, Marcel Dekker, New York, (1973) vol I, pp 80.

151. reference 115, chapter 6, 183.

152. S. Torri, H. Tanka, T Katch and K. Morisaki, *Tet. Lett.*, **25**, (1984) 3207.

153. S. Torii, H. Tanka and K. Morisaki, *Tet. Letts.*, **26**, (1985) 1655.

154. T. T. Tsou and J. K. Kochi, *J. Am. Chem Soc.*, **100**, (1978) 1634.

155. R. M. Silverstein, G. C. Bassler and T. C. Morrill, *Spectrometric Identification of Organic Compounds*, John Wiley and Sons, New York, 4th ed., (1981): (a) chapter 3 pp 134, (b) chapter 6, pp 326.

156. P. A. Malachesky, L. S. Marcoux and R. N. Adams, *J. Phys. Chem.*, **70**, (1966) 4068.

157. G. S. Ailberts and I. Shian, *Anal. Chem.*, **35**, (1963) 1859.

158. S. Karp, *J. Phys. Chem.*, **71**, (1967) 1082.

159. R. G. Compton and P. R. Unwin, *J. Chem. Soc., Faraday Trans.*, *I*, **85**, (1989) 1821.

160. Personal communication R. G. Compton.

161. L. S. Marcoux, R. N. Adams and S. W. Feldberg, *J. Phys. Chem.*, **73**, (1969) 2611.

162. G. Manning, V. D. Parker and R. N. Adams, *J. Am. Chem. Soc.*, **91**, (1969) 4584.

163. K. B. Prater and A. J. Bard, *J. Electrochem. Soc.*, **117**, (1970) 1517.

164. J. M. Savéant, *Electrochim. Acta*, **12**, (1967) 753.

165. M. Mastragostino, L. Nadjo and J. M. Savéant, *Electrochim. Acta*,

13, (1968) 721.

166. L. Nadjo and J. M. Savéant, *J. Electroanal. Chem.*, **48**, (1978) 113.

167. R. G. Compton, M. J. Day, M. E. Laing, R. J. Northing, J. I. Pennman and A. M. Walker, *J. Chem. Soc., Faraday Trans., I*, **84**, (1988) 2013.

168. G. Denualt, M. Fleischmand, D. Pletcher and O. R. Tutty, *J. Electroanal. Chem.*, **280**, (1990) 243.

169. R. G. Compton and A. R. Hillman, *Chem. Br.*, **22**, (1986) 1088.

170. R. G. Compton, R. G. Harland, P. R. Unwin and A. M. Walker, *J. Chem. Soc., Faraday Trans., I*, **83**, (1987) 1261.

171. R. G. Compton, D. Manson and P. R. Unwin, *J. Chem. Soc., Faraday Trans., I*, **84**, (1988) 2057.

172. Reference 117, chapter 1, pp 13.

173. M. Abramowitz and I. A. Stegun, (Ed.), *Handbook of Mathematical Functions*, Dover Publication Inc., 9th edn., (1972) pp 446 10.4.1.

174. Reference 173, pp 446 10.4.10.

175. R. C. Weast (Ed.), *Handbook of Chemistry and Physics*, CRC Press, Cleveland, 56th ed., (1975) pp F50.

176. R. J. Waltman, J. Bargon and A. F. Diaz, *J. Phys. Chem.*, **87**, (1983) 1459.

177. L. J. Bellamy, *J. Chem, Soc.*, (1988) 2818.

178. G. Wilkinson (Ed.), *Comprehensive Organometallic Chemistry*, Permagon Press, New York, **6**, (1982) pp49.

179. J. Burgess, *Metal Ions in Solution*, Ellis Horwood, New York, (1978)

180. D. J. Brown, (Ed) *The Chemistry of Heterocyclic Compounds, The*

Pyrimidines, John Wiley and Sons, New York, (1962) Chapter 1 pp
1.

180. R. N. Castle, (Ed) *The Chemistry of Heterocyclic Compounds, The
Pyridazines*, John Wiley and Sons, New York, (1973) Chapter 1 pp
1.